UNIVERSITY OF CALIFORNIA SAN DIEGO

Microbial Ecology of the California Current Ecosystem

A dissertation submitted in partial satisfaction of the requirements for the degree Doctor of Philosophy

in

Oceanography

by

Sara Renee Rivera

Committee in charge:

Professor Lihini I. Aluwihare, Chair
Professor Andrew Allen
Professor Farooq Azam
Professor Katherine Barbeau
Professor Kaustuv Roy

2020

The Dissertation of Sara Renee Rivera is approved, and it is acceptable in quality and form for publication on microfilm and electronically:

_____

_____

_____

_____

_____
Chair

University of California San Diego

2020

DEDICATION

TO MY PARENTS,

Sharon and Paul,

who offered unconditional love and support as I followed my childhood dreams,

AND MY SIBLINGS,

Bethany and David,

who were there for the wild ride that's perhaps best summarized with a quote from

Pirates of the Caribbean,

"This is either madness or brilliance."

EPIGRAPH

“If you don't like bacteria, you're on the wrong planet.”

-Stewart Brand

TABLE OF CONTENTS

Signature Page iii

Dedication iv

Epigraph v

Table of Contents vi

List of Abbreviations xi

List of Figures xiv

List of Tables xvii

Acknowledgments xviii

Vita xxii

Abstract of the Dissertation xxiii

Introduction 1

Background 1

Thesis Organization 4

References 6

Chapter 1: Temporal and spatial variability of microbial abundance in the southern California Current System 11

Abstract 11

1.1. Introduction 12

1.2. Methods 14

1.2.1 Study region and sampling periods 14

1.2.2 Hydrographic conditions 17

1.2.3 Chlorophyll and Primary Production measurements 18

1.2.4 Supporting chemical measurements 18

1.2.5 Heterotrophic Bacterial Abundance (BA) by Flow Cytometry (FCM) and Bacterial Production (BP) 19

1.2.6 Statistical comparison 20

1.3. Results 22

1.3.1 Defining regional characteristics of the sCCS 22

1.3.1.1 Interannual variability by region for the CCE-LTER program 24

1.3.2 Seasonal and regional variability of HBac, Pro, Syn, and PEuk along CalCOFI Line 80 25

1.3.2.1 Picoplankton variability at 10m along CalCOFI Line 80 26

1.3.2.2 Picoplankton abundance anomalies corresponded with a shift in the PDO 27

1.3.2.3 Picoplankton abundance and Chl concentration relationships 28

1.3.3 Top-down controls on picoplankton and testing the enhanced microbial loop hypothesis 29

1.3.4 Bottom-up controls on heterotrophic bacterial abundance in the sCCS 31

1.3.5 Comparison of FCM data from of CalCOFI Line 80 and CCE-LTER cruises 32

1.4. Discussion 34

1.4.1 Regional designations are robust in the sCCS 35

1.4.1.1 CalCOFI Line 80 Seasonal and regional variability of HBac, Pro, Syn, and PEuk 35

1.4.1.2 Picoplankton community shifts along CalCOFI Line 80 consistent with PDO phase shift 38

1.4.1.3 Regional Comparison of CalCOFI Line 80 and CCE LTER 40

1.4.2 Top-down controls of picoplankton and testing of the enhanced microbial loop 42

1.4.3 Bottom-up controls of heterotrophic bacterial abundance in the CCE 44

1.5. Conclusions 45

1.6 Acknowledgements 46

1.7 Figures and Tables 47

1.8 Appendix 59

1.9 References 98

Chapter 2: Imbalance of carbon production and removal processes in the offshore California Current Ecosystem 107

Abstract 107

2.1. Introduction 108

2.2. Methods 110

2.2.1 Study region and sampling periods 110

2.2.2 Hydrographic conditions 111

2.2.3 Chlorophyll and Primary Production measurements 111

2.2.4 Supporting chemical measurements 112

2.2.5 Export of sinking POC 112

2.2.6 Heterotrophic bacterial abundance (BA) and bacterial biomass (BB) by Flow Cytometry (FCM) 113

2.2.7 Bacterial Production (BP) 113

2.2.8 Microzooplankton and mesozooplankton grazing rates on phytoplankton 115

2.3. Results 115

2.3.1 Biomass and Production Indices 115

2.3.2 Calculated Bacterial Carbon Demand (BCD) 118

2.3.3 Food Web Dynamics of the CCE 119

2.4. Discussion 121

2.4.1 Multiple lines of evidence suggest that the offshore CCE region is net heterotrophic 121

2.4.2 Insights on microbially mediated transitions from net autotrophy to net heterotrophy from the biomass and productivity indices 122

2.4.3 Mass balance of carbon flow in the CCE microbial food web 126

2.4.3.1 Mass balance of carbon flow in the CCE microbial food web within a westward propagating filament 129

2.4.4 Anomalously warm conditions may lead to increasing net heterotrophy in the CCE 130

2.5. Conclusions 132

2.6 Acknowledgements 133

2.7 Figures and Tables 134

2.8 Appendix 141

2.9 References 151

Chapter 3: Control of heterotrophic bacterial production in the southern California Current System 161

Abstract 161

3.1. Introduction 162

3.2. Methods 165

3.2.1 Study region and sampling periods 165

3.2.2 Hydrographic conditions 166

3.2.3 Chlorophyll and Primary Production measurements 166

3.2.4 Supporting chemical measurements 166

3.2.5 Heterotrophic BA and BB by Flow Cytometry (FCM, FCM*) 167

3.2.5.1 Heterotrophic BA and BB by Epifluorescence Microscopy (EFM) 168

3.2.6 Bacterial Production (BP) 169

3.2.7 Statistical comparison 170

3.2.8 Bottom-up and temperature control indices and bacterial-phytoplankton coupling 171

3.2.9 Microzooplankton grazing rates on phytoplankton 171

3.3. Results 172

3.3.1 Method comparison of EFM, FCM, FCM* for heterotrophic BA 172

3.3.2 Depth Profiles of Heterotrophic BA and BP in the sCCS 173

3.3.3 Relationships between Bacterial Abundance (BA) and Bacterial Production (BP) 175

3.3.4 Controls on heterotrophic bacteria 175

3.3.5 Relationships between BP and phytoplankton processes 179

3.3.6 Relationships between BP and Organic Carbon 180

3.3.7 Temperature in the sCCS 182

3.4. Discussion 183

3.4.1 Lessons learned from cross-dataset analyses 183

3.4.2 Bottom-up and top down controls of Heterotrophic Bacteria 185

3.4.3 Organic carbon concentrations as predictors of heterotrophic bacterial production 187

3.4.4 Increasing stratification in the sCCS may decrease bacterial production and abundance 189

3.4.5 Temperature control related to upwelling and nutrient conditions, not metabolic rates 192

3.5. Conclusions 194

3.6 Acknowledgements 195

3.7 Figures and Tables 196

3.8 Appendix 204

3.9 References 220

Conclusions 230

LIST OF ABBREVIATIONS

AB	autotrophic biomass
BA	heterotrophic bacterial abundance
BB	heterotrophic bacterial biomass
BCC	bacterial carbon content per cell
BCD	bacterial carbon demand
BGE	bacterial growth efficiency
BP	heterotrophic bacterial production
CalCOFI	California Cooperative Oceanic Fisheries Investigations
CCE	California Current Ecosystem
CCE-LTER	California Current Ecosystem Long Term Ecological Research
CCS	California Current System
Chl max	depth at which chlorophyll *a* concentration is at a maximum
Chl	chlorophyll *a*
CTD	Conductivity Temperature Depth sensor
DOC	dissolved organic carbon
EFM	epifluorescence microscopy
ENSO	El Niño Southern Oscillation
e-ratio	ratio of export production to net primary production
EZ	euphotic zone
Fa	Fall
FCM	flow cytometry with samples preserved with paraformaldehyde

FCM*	flow cytometry with samples preserved with glutaraldehyde
GLM	generalized linear model
GPP	gross primary production
HBac	heterotrophic bacteria
Means*	estimated marginal means
NCP	net community production
NP	new production
NPGO	North Pacific Gyre Oscillation
NPP	net primary production
NS	nearshore
OLS	ordinary least square
ONI	Oceanic Niño Index
OS	offshore
PAR	photosynthetically active radiation
PDO	Pacific Decadal Oscillation
PEuk	picoeukaryotes
PEW	Pacific Equatorial Water
POC	particulate organic carbon
Pro	*Prochlorococcus*
PSUW	Pacific Subarctic Upper Water
sCCS	southern California Current System
Sp	Sprint
SST	sea surface temperature

Su	Summer
SW	sea water
Syn	*Synechococcus*
TOC	total organic carbon
Trends*	estimated marginal trends
TS	transition
Wi	Winter

LIST OF FIGURES

CHAPTER 1

Figure 1.1: Seasonality of microbial abundance measured along CalCOFI Line 80 by oceanic region 47

Figure 1.2: Temporal and spatial trends of HBac, Pro, Syn, and PEuk at 10m 49

Figure 1.3: 10m cube root anomalies with PDO phase (1/2) 50

Figure 1.3: 10m cube root anomalies with PDO phase (continued, 2/2) 52

Figure 1.4: Trends of HBac, Pro, Syn, and PEuk abundance with Chl concentration 53

Figure 1.5: Increasing chlorophyll concentration led to an increase in BP and picoplankton 54

Figure 1.6: Trends of BP and picoplankton with Chl 55

Figure 1.7: Relationships of phytoplankton and organic carbon pools to bacteria abundance in the sCCS 56

Figure S1.1: Satellite derived Chl concentration and SST with CCE-LTER cycle tracks 59

Figure S1.2: CCE-LTER regional classifications with CalCOFI Line 80 hydrography 60

Figure S1.3: Phytoplankton and organic carbon in the sCCS 61

Figure S1.4: Temporal depth profiles of Pro abundance along Line 80 62

Figure S1.5: Temporal depth profiles of Syn abundance along Line 80 63

Figure S1.6: Correlation between PEuk and Syn 64

Figure S1.7: EZ integrated cube root anomalies 65

Figure S1.8: Regional and seasonal trends of HBac, Pro, Syn, and PEuk abundance with Chl concentration 66

Figure S1.9: Trends of HBac vs picoautotrophic abundances 67

Figure S1.10: Regional and seasonal trends of HBac vs picoautotrophs 68

Figure S1.11: CalCOFI and CCE-LTER EZ integrated HBac abundance 69

Figure S1.12: CalCOFI and CCE-LTER EZ integrated Pro abundance 70

Figure S1.13: CalCOFI and CCE-LTER EZ integrated Syn abundance 71

Figure S1.14: CalCOFI and CCE-LTER EZ integrated PEuk abundance 72

Figure S1.15: CalCOFI vs CCE-LTER heterotrophic bacterial abundance by year 73

Figure S1.16: CalCOFI vs CCE-LTER Pro abundance by year 74

Figure S1.17: CalCOFI vs CCE-LTER Syn abundance by year 75

Figure S1.18: CalCOFI vs CCE-LTER PEuk abundance by year 76

CHAPTER 2

Figure 2.1: Biomass and production indices 134

Figure 2.2: The offshore region of the CCE could be net heterotrophic with local gross primary production (GPP) unable to meet local BCD 135

Figure 2.3: CCE conceptual food web with microbial loop 136

Figure S2.1: Biomass and production indices with calculated bacterial growth efficiency and carbon demand by sample 141

Figure S2.2: Microzooplankton grazing rate by oceanic region 142

Figure S2.3: Calculated growth rates from EZ integrated values 142

CHAPTER 3

Figure 3.1: BA method comparison of epifluorescent microscopy (EFM) and flow cytometry (FCM*) 196

Figure 3.2: Bacterial carbon content per cell from EFM 197

Figure 3.3: Depth profiles of Chl concentration, BA, NPP, BP, and NO3 concentration 198

Figure 3.4: Bottom-up and top-down controls on heterotrophic bacteria 200

Figure 3.5: Relationships between BP and TOC, POC, and DOC 201

Figure 3.6 Relationship between BP and low POC concentration 202

Figure 3.7 Temperature and nitrate relationship to production 203

Figure S3.1 Daily variation of bacterial abundance (BA) within a cycle 204

Figure S3.2: Relationships between bacterial production and phytoplankton properties for the sCCS 205

Figure S3.3: Daily variation of bacterial production (BP) within a cycle 206

Figure S3.4: Relationship between FCM* BA and BP by region 207

Figure S3.5: Impact of BCC choice on the bottom-up control index 208

Figure S3.6: Log transformations and linear regressions 209

Figure S3.7: Bottom-up control index calculations 210

Figure S3.8: Temperature control index calculations 211

Figure S3.9: Relationships of microzooplankton grazing rates and heterotrophic bacterial abundance 212

Figure S3.10: Chl and BP coupling calculations 213

Figure S3.11: NPP and BP coupling calculations 214

Figure S3.12: Coupling between bacterial production and phytoplankton properties by cruise-cycle 215

Figure S3.13: Relationships between BP and organic carbon pools by cruise 216

Figure S3.14: Inverse temperature and nitrate relationship to production 217

LIST OF TABLES

CHAPTER 1

Table 1.1: Mean hydrographic depths and euphotic zone integrated biogeochemical values for the oceanic regions by program 58

Table S1.1: Geographical locations and regional designations for CalCOFI Line 80 stations 77

Table S1.2: Geographical locations and regional designations for CCE-LTER process cruise stations (1/3)..... 78

Table S1.3: Hydrographic depths and euphotic zone integrated biogeochemical values for CalCOFI cruises (1/12) 81

Table S1.4: Hydrographic depths and euphotic zone integrated biogeochemical values for comparing the CCE-LTER to CalCOFI Line 80 by cruise (1/3) 93

Table S1.5: CalCOFI mean hydrographic depths and euphotic zone integrated biogeochemical values for the oceanic regions by season. 96

Table S1.6: CalCOFI vs CCE-LTER depth profile comparison 97

CHAPTER 2

Table 2.1: Average EZ depth integrated values by CCE region 137

Table 2.2: Average EZ integrated values for the CCE food web with microbial loop 138

Table 2.3: CCE regional average calculated NPP and DOC remaining..... 140

Table S2.1: Average EZ depth integrated values by Lagrangian cruise-cycle (1/3)..... 143

Table S2.2: Average EZ integrated values for the CCE food web with microbial loop by Lagrangian cruise-cycle (1/3) 146

Table S2.3: Calculated NPP and DOC remaining..... 150

CHAPTER 3

Table S3.1: BA method comparison using Kruskal-Wallis 218

Table S3.2. Flow cytometry method comparison by cruise-cycle 219

ACKNOWLEDGMENTS

Oceanography is a uniquely interdisciplinary field. Without the guidance and support of colleagues, mentors, and friends, this work would not be where it is today. I am grateful that the Scripps Institution of Oceanography (SIO) is a place of collaboration and sharing.

First, thank you to my advisor, Dr. Lihini Aluwihare, for providing me with the opportunity to pursue a doctoral degree. Lihini encouraged me to follow my research interests, even when it meant working almost entirely in other peoples' laboratories and spending months participating in research cruises. I have grown a great deal, personally and professionally, because of how Lihini challenged me. Her discussions and contributions to this work were invaluable. Lihini's commitment to supporting underrepresented minority women in science will continue to shine a light on my path forward.

Most of my laboratory-based research was completed in the laboratory of Dr. Farooq Azam. I would like thank Farooq for his time, patience, and expertise. His work on the microbial loop inspired much of this work. Farooq has been an incredible, positive mentor. I hope he continues to follow his passions in retirement. I would also like to recognize those lab members who taught me methods to complete my research, including Dr. Julie Dinasquet, Dr. Ryan Guillemette, and Dr. Byron Pedler. Julie and Ryan were always available to help me understand the protocols and processing needed for this work. Although Bryon left SIO shortly after my arrival, he was consistently available by email to provide support. I am additionally grateful for the laboratory notebooks left behind by Dr. Ty Samo, upon whose work my research built. I look forward to working more closely with Ty in my next position as a postdoctoral researcher.

I would also like to thank and acknowledge the California Current Ecosystem Long Term Ecological Research (CCE-LTER) site and those members, past and present. While I was funded as a student through the U.S. National Science Foundation Graduate Research Fellowship Program (NSF-GRFP), the CCE-LTER, funded by a different branch of the U.S. National Science Foundation, was critical to funding my research. More than that, the CCE-LTER provided a family of supportive scientists. This family made month long research cruises not only possible, but incredibly successful and delightful. I appreciated and enjoyed collaborating with numerous people who are part of the CCE-LTER. I would like to especially thank Lauren Manck, Sarah Schwenck, Dr. Brandon Stephens, Megan Roadman, Shonna Dovel, Dr. Angel Ruacho, Kiefer Forsch, Dr. Ben Whitmore, Kayleen Fulton, Stephanie Matthews, Laura Lilly, Dr. Ty Samo, Ralph Torres, and Alice Levesque.

Additionally, I would like to thank and acknowledge the phenomenal team of faculty involved in the CCE-LTER. Their involvement was a rare opportunity for a student to work closely with renowned members of the oceanography community. Thank you to Dr. Mark Ohman and Dr. Katherine (Kathy) Barbeau for stepping into the role of acting advisor during the 2017 and 2019 CCE-LTER cruises. I am grateful to Kathy for promoting self-care and understanding limits. I would also like to thank you Dr. Michael Landry and Dr. Michael Stukel for their insight, discussions, and well-maintained datasets.

I need to thank Dr. David Engelke, Dr. Dave Pai, and Dr. Chris Bass for their belief in me as an undergraduate student who wanted to pursue a research career. Also, thank you to Dr. Chris Poulsen, Dr. Nils Walter, Dr. Kacey Lohmann, and Dr. Gregory Dick for their recommendation letters over the years. I am additionally grateful for the support of many staff members over the years including, Christopher Murphy, Gilbert Bretado, Jessica Gonzalez,

Joshua Reeves, Denise Darling, Shelley Weisel, Maureen McGreevy, Maureen McCormack, and Adam Peterson.

On a personal note, I would like to thank the members of the Marine Chemistry and Geochemistry 2014 cohort (Dr. Alyssa Griffin, Kiefer Forsch, Margot White, Matthew Pendergraft, and Kenisha Shipley) for their continuous support and moral boosting. The former members of the Aluwihare lab, including Nellie Shaul, Dr. Jenan Kharbush, Dr. Neal Arakawa, Dr. Brandon Stephens, and Magali Marella, who provided guidance and friendship throughout my graduate career and the current members, Margot White, Irina Koester, Tran Nguyen, and Ralph Torres, who supported my work through numerous iterations. I owe thanks also to Aaron Ward and Dr. Petia Yanchulova for reminding me to step outside of the Scripps Institution of Oceanography (SIO) campus. Furthermore, Sarah Clark, Shae Rafferty, and Kaitlyn Mays have supported me from around the country before I even set foot on the SIO campus.

Most importantly, I need to acknowledge the love and support of my family. My husband, Mitchell Boldin, supported me through the constant ups and downs associated with research and graduate school. My parents, Sharon and Paul Rivera, who have supported and financed many of the decisions that led me to this place, including numerous trips to the beach, school field trips and campus, and traveling across the country to support my move. My siblings, David and Bethany Rivera, have been my long-term companions and research associates, albeit sometimes unwillingly. I could not have succeeded without the support from my family.

This work would not have been possible without support from various funding sources. The majority of this work was funded by the U.S. National Science Foundation

(NSF) OCE-04-17616, OCE-10-26607, OCE-16-37632, DGE-1650112. Any opinions, findings, and conclusions or recommendations expressed in this material are those of the authors and do not necessarily reflect the views of the National Science Foundation. In addition, student support was provided by the University of California San Diego's Graduate Division through the Competitive Edge and San Diego Fellowships, the Scripps Institution of Oceanography department, and the generosity of donors through the H. William Menard Memorial Fund.

Chapter 1, in part, is currently being prepared for submission for publication of the material. Rivera, S. R.; Goericke, R.; Stephens, B. M.; Dovel, S.; Roadman, M.; Kahru, M.; Landry, M. R.; Aluwihare, L. I.. The dissertation author was the primary investigator and author of this material.

Chapter 2, in part, is currently being prepared for submission for publication of the material. Rivera, S. R.; Stephens, B. M.; Samo, T. J.; Stukel, M. R.; Ohman, M.D.; Landry, M. R.; Farooq, A.; Aluwihare, L. I.. The dissertation author was the primary investigator and author of this material.

Chapter 3, in part, is currently being prepared for submission for publication of the material. Rivera, S. R.; Stephens, B. M.; Samo, T. J.; Rasina, B.; Stukel, M. R.; Landry, M. R.; Farooq, A.; Aluwihare, L. I.. The dissertation author was the primary investigator and author of this material.

VITA

2013	Bachelor of Science, Biochemistry, Geological Sciences, University of Michigan
2015	Master of Science, Oceanography, Scripps Institution of Oceanography, University of California San Diego
2020	Doctor of Philosophy, Oceanography, Scripps Institution of Oceanography, University of California San Diego

ABSTRACT OF THE DISSERTATION

Microbial Ecology of the California Current Ecosystem

by

Sara Renee Rivera

Doctor of Philosophy in Oceanography

University of California San Diego, 2020

Professor Lihini I. Aluwihare, Chair

The southern CCS (sCCS), part of the California Current Ecosystem (CCE), is home to the California Cooperative Oceanic Fisheries Investigation (CalCOFI) survey program and the California Current Ecosystem Long Term Ecological Research (CCE-LTER) program. CalCOFI, begun in 1949, was designed as a survey program, sampling the same stations each quarter; whereas, the CCE-LTER program was designed to study interactions between various

physical perturbations and ecosystem processes using Lagrangian cycles. The goal of this thesis was to examine microbial dynamics within these two programs and present a model for carbon fluxes into and out of the bacterial compartment. **Chapter 1** 'binned' findings from CCE-LTER cruises into the relevant CalCOFI climatology and hydrography allowing the mechanistic studies into microbial dynamics enabled by the CCE-LTER program to be interpreted in the context of long-term observations. For example, the underlying mechanism of the enhanced microbial loop hypothesis, originally based on CalCOFI data, was supported using bacterial production data from CCE-LTER cycles in 2017. Additionally, the picoplankton community responded to broad climate variability with increased abundances and shifts in spatial distribution following a switch to the positive phase of the Pacific Decadal Oscillation at the end of 2013. Using the binned oceanic regions designated in **Chapter 1**, **Chapter 2** showed that including the bacterial component in the food web strengthened previous conclusions that the nearshore is net autotrophic, providing excess carbon available to be laterally exported to the offshore. Examination of the westward propagating 2017 Morro Bay filament supported the hypothesis that lateral transport of organic material could support offshore, net heterotrophic communities. Bacterial production was strongly correlated to organic carbon pools, as observed in **Chapter 3**. Bottom-up control of bacterial production across the CCE was comparable to global trends, but did not scale with net primary production, perhaps due to enhanced grazing nearshore. Furthermore, the observed temperature control of bacterial production was a proxy for the role of upwelling and substrate production, not metabolic rate. Strong bottom-up controls and weak temperature controls observed during the 2014 warm anomaly suggest future warming and stratification within the sCCS could be rapidly experienced by the bacterial community.

Introduction

BACKGROUND

The southern California Current System (sCCS), is a well-studied Eastern boundary current region. Eastern boundary current regions are important sites of net primary production in the surface ocean that provide nutrients needed to support large-scale fisheries, representing less than 1% of the global ocean but 20% of the global marine fish catch (Chavez & Messie 2009). The California Cooperative Oceanic Fisheries Investigations (CalCOFI) survey program began in 1949 in response to the sardine population collapse off the coast of California. In 2004, the California Current Ecosystem Long Term Ecological Research (CCE-LTER) program began as a compliment to the existing CalCOFI program. CalCOFI aims to study the ecological aspects of the sCCS by sampling the same locations 3-4 times a year (Eulerian methods). The CCE-LTER aims to study the transitions in the ecosystem using short 2-6 day cycles following a single water parcel (short Lagrangian cycles), repeated 4-6 times with different water parcels, across the region every 1-2 years to examine mesoscale variability and conduct biological process experiments (Landry et al. 2009, Ohman et al. 2013, Goericke & Ohman 2015). The combination of these programs has led to important results regarding how warming surface waters are decreasing nutrient delivery and organism populations, particularly with respect to photosynthetic organisms and grazers. Up until now, an essential piece missing from the conversation has been the role of heterotrophic bacteria across the system.

The sCCS encompasses several different productivity regimes from upwelling driven, productive coastal waters to more stratified oligotrophic subtropical gyre waters (Chavez &

Messie 2009, Landry et al. 2009, Ohman et al. 2013, Goericke & Ohman 2015). This region is also known for its sub-mesoscale variability with numerous, eddies, filaments, and fronts developing in the region throughout the year (Nagai et al. 2015). Recent modeling suggests that offshore transport of nutrients and organic matter by mesoscale features, such as eddies and filaments, is an important process in this system (Gruber et al. 2011, Nagai et al. 2015). Increasing e-ratios from nearshore to offshore (Kelly et al. 2018) and total organic carbon (TOC) gradients in the CCE (Stephens et al. 2018) support these modeling results. The response of the heterotrophic bacterial community to potential offshore gradients in organic matter has not been examined in this system to date, but it may be anticipated that bacterial carbon demand as a fraction of local net primary production also increases offshore.

Furthermore, inter-annual variability linked to El Niño and, more recently, warm anomaly/ocean heatwave events are well documented in the region (Bond et al. 2015, Jacox et al. 2016, Gentemann et al. 2017, Gomez-Ocampo et al. 2018, Smale et al. 2019). Such dynamics can complicate our ability to extract long term trends from these studies; however, heterotrophic bacteria, because of their high abundance and fast growth rates (Burrell et al. 2017), represent an attractive and accessible component of ecosystems to study and monitor in the context of global change. For example, several climate models predict that the warming of the surface ocean will increase stratification and subsequently, decrease nutrient delivery to the surface ocean (Sarmiento et al. 2004, Polovina et al. 2008). The increase in oligotrophic ocean area may also increase regions of net heterotrophy, at least temporarily (Hoppe et al. 2002, Polovina et al. 2008, Duarte et al. 2013). Understanding the future flow of energy and nutrients within the surface ocean can thus benefit from a study of microbial dynamics across a gradient of stratification regimes.

As major recyclers of organic matter, heterotrophic bacteria play a crucial role in determining the net metabolic state of the ocean (Azam et al. 1983, Azam & Malfatti 2007, Fenchel 2008). They modulate the lateral transport of dissolved and suspended particulate organic carbon (Legendre & Lefevre 1995, del Giorgio & Duarte 2002) because their respiration decreases the concentration of organic carbon available for off-shore export (Aristegui et al. 2004). In addition, heterotrophic bacteria can convert the entrained particulate organic carbon into dissolved organic carbon (DOC) due to inefficient coupling of hydrolysis and uptake (Smith et al. 1992), which can decrease the loss of organic carbon through vertical export (Alvarez-Salgado et al. 2007). Heterotrophic bacteria recycle organic matter, but their population dynamics can also be controlled by nutrient supply, or bottom-up controls.

Overall, the role of heterotrophic bacteria in carbon turnover (i.e., bacterial productivity) can be constrained by both bottom-up and top-down controls. Evidence for bottom-up controls, which are driven by the availability of resources, such as DOC, is primarily found in the relationship of bacterial abundance and bacterial production to indices of primary production (Billen et al. 1990, Ducklow 1992, Kim & Ducklow 2016). In addition, warmer ocean temperatures can impact BP by increasing metabolic rates (White et al. 1991, Herrmann et al. 2014) throughout the microbial loop, which could enhance both bottom-up and top down controls. Previous studies have examined controls on bacterial production in particular regions of the ocean and a few studies have provided a time series context (Cole et al. 1988, Barbosa et al. 2001, Karl & Church 2014, Kim & Ducklow 2016, Viviani & Church 2017). Within the CCE-LTER, long term observations of these same controls is possible, and take place across different biomes that are hydrographically connected and influenced by similar climate forcing. Furthermore, the gradient from coastal upwelling driven regimes,

through the California Current region, which includes areas of curl driven upwelling (Rykaczewski & Checkley 2008), out to the eastern edge of the North Pacific Subtropical Gyre, expresses in a spatial gradient, the expected temporal trajectory of surface ocean conditions as the atmosphere continues to warm.

THESIS ORGANIZATION

The following dissertation chapters will place marine heterotrophic bacteria into the larger existing conversation of ecosystem dynamics within the sCCS.

Chapter 1 builds a comprehensive framework to bridge the CalCOFI and CCE-LTER programs utilizing both the time-series aspects of CalCOFI and the process studies conducted during the CCE-LTER program. First, CalCOFI data from 49 cruises (November 2004 - November 2017) along Line 80 were used to classify three distinct oceanic regions- the nearshore, transition, and offshore. Cycles from 6 CCE-LTER cruises (totaling 28 cycles), were classified into these regions. Then, two hypotheses, including the enhanced grazing hypothesis (Goericke 2011, Taylor & Landry 2018) and the picoplankton response to warming surface waters (Flombaum et al. 2013), were tested in this context.

Chapter 2 examines the trophic state of the sCCS from the heterotrophic bacterial perspective using ratios of bacterial biomass to autotrophic biomass and bacterial production to net primary production, as well as estimations of bacterial carbon demand as a fraction of net primary production. Sampling was conducted on the 6 CCE-LTER cruises previously discussed in Chapter 1. Overall, the calculated trophic state of the ecosystem in the transition and offshore region when bacteria were included in the microbial food web was often different from the trophic state calculated using a traditional (grazing) food web. Finally,

lateral transport of organic matter from the net autotrophic nearshore region was shown to be adequate as a source of supplementary material needed to support a net heterotrophic offshore system.

Chapter 3 addresses the controls of bacterial production within the sCCS, again utilizing samples from the aforementioned 6 CCE-LTER cruises. Bottom-up controls were assessed directly through correlations with organic matter stocks, as well as with correlations to net primary production and chlorophyll concentrations. Bottom-up controls were also examined indirectly through the relationship of bacterial biomass to bacterial production (Billen et al. 1990, Ducklow 1992). Top down controls were examined indirectly, using grazing on phytoplankton as a proxy for grazing on heterotrophic bacteria. Temperature control on metabolic rates was additionally assessed and found to influence bacterial production primarily because temperatures was closely related to upwelling and thus nutrient delivery and the production of substrates to support heterotrophic bacteria. Overall, the dataset also captured several different climate transitions – El Niño (Jacox et al. 2016) and different phases of the Pacific Decadal Oscillation (PDO) (Mantua et al. 1997, Di Lorenzo et al. 2008, Miller et al. 2015) and the North Pacific Gyre oscillation (NPGO) (Di Lorenzo et al. 2008) – which allowed me to further examine the response of the bacterial population to regional climate change.

REFERENCES

Alvarez-Salgado XA, Aristegui J, Barton ED, Hansell DA (2007) Contribution of upwelling filaments to offshore carbon export in the subtropical Northeast Atlantic Ocean. Limnology and Oceanography 52:1287-1292

Aristegui J, Barton ED, Tett P, Montero MF, Garcia-Munoz M, Basterretxea G, Cussatlegras AS, Ojeda A, de Armas D (2004) Variability in plankton community structure, metabolism, and vertical carbon fluxes along an upwelling filament (Cape Juby, NW Africa). Progress in Oceanography 62:95-113

Azam F, Fenchel T, Field JG, Gray JS, Meyer-Reil LA, Thingstad F (1983) THE ECOLOGICAL ROLE OF WATER COLUMN MICROBES IN THE SEA. Marine Ecology Progress Series 10:257-264

Azam F, Malfatti F (2007) Microbial structuring of marine ecosystems (vol 5, pg 782-791, 2007). Nature Reviews Microbiology 5:966-U923

Barbosa AB, Galvao HM, Mendes PA, Alvarez-Salgado XA, Figueiras FG, Joint I (2001) Short-term variability of heterotrophic bacterioplankton during upwelling off the NW Iberian margin. Progress in Oceanography 51:339-359

Billen G, Servais P, Becquevort S (1990) Dynamics of bacterioplankton in oligotrophic and eutrophic aquatic environments: bottom-up or top-down control?. Hydrobiologia:37-42

Bond NA, Cronin MF, Freeland H, Mantua N (2015) Causes and impacts of the 2014 warm anomaly in the NE Pacific. Geophysical Research Letters 42:3414-3420

Burrell TJ, Maas EW, Hulston DA, Law CS (2017) Variable response to warming and ocean acidification by bacterial processes in different plankton communities. Aquatic Microbial Ecology 79:49-62

Chavez FP, Messie M (2009) A comparison of Eastern Boundary Upwelling Ecosystems. Progress in Oceanography 83:80-96

Cole JJ, Findlay S, Pace ML (1988) BACTERIAL PRODUCTION IN FRESH AND SALTWATER ECOSYSTEMS - A CROSS-SYSTEM OVERVIEW. Marine Ecology Progress Series 43:1-10

del Giorgio PA, Duarte CM (2002) Respiration in the open ocean. Nature 420:379-384

Di Lorenzo E, Schneider N, Cobb KM, Franks PJS, Chhak K, Miller AJ, McWilliams JC, Bograd SJ, Arango H, Curchitser E, Powell TM, Riviere P (2008) North Pacific Gyre Oscillation links ocean climate and ecosystem change. Geophysical Research Letters 35

Duarte CM, Regaudie-de-Gioux A, Arrieta JM, Delgado-Huertas A, Agusti S (2013) The Oligotrophic Ocean Is Heterotrophic. In: Carlson CA, Giovannoni SJ (eds) Annual Review of Marine Science, Vol 5, Book 5. Annual Reviews, Palo Alto

Ducklow HW (1992) Factors regulating bottom-up control of bacteria biomass in open ocean plankton communities. Arch Hydrobiol Beih Ergebn Limnol:207–217

Fenchel T (2008) The microbial loop-25 years later. Journal of Experimental Marine Biology and Ecology 366:99-103

Flombaum P, Gallegos JL, Gordillo RA, Rincon J, Zabala LL, Jiao NAZ, Karl DM, Li WKW, Lomas MW, Veneziano D, Vera CS, Vrugt JA, Martiny AC (2013) Present and future global distributions of the marine Cyanobacteria Prochlorococcus and Synechococcus. Proceedings of the National Academy of Sciences of the United States of America 110:9824-9829

Gentemann CL, Fewings MR, Garcia-Reyes M (2017) Satellite sea surface temperatures along the West Coast of the United States during the 2014-2016 northeast Pacific marine heat wave. Geophysical Research Letters 44:312-319

Goericke R (2011) The structure of marine phytoplankton communities--patterns, rules, and mechanisms., Book 52, California Cooperative Oceanic Fisheries Investigations Report

Goericke R, Ohman MD (2015) Introduction to CCE-LTER: Responses of the California Current Ecosystem to climate forcing. Deep-Sea Research Part Ii-Topical Studies in Oceanography 112:1-5

Gomez-Ocampo E, Gaxiola-Castro G, Burazo R, Beier E (2018) Effects of the 2013-2016 warm anomalies on the California Current phytoplankton. Deep-Sea Research Part Ii-Topical Studies in Oceanography 151:64-76

Gruber N, Lachkar Z, Frenzel H, Marchesiello P, Munnich M, McWilliams JC, Nagai T, Plattner GK (2011) Eddy-induced reduction of biological production in eastern boundary upwelling systems. Nature Geoscience 4:787-792

Herrmann M, Estournel C, Adloff F, Diaz F (2014) Impact of climate change on the northwestern Mediterranean Sea pelagic planktonic ecosystem and associated carbon cycle. Journal of Geophysical Research-Oceans 119:5815-5836

Hoppe HG, Gocke K, Koppe R, Begler C (2002) Bacterial growth and primary production along a north-south transect of the Atlantic Ocean. Nature 416:168-171

Jacox MG, Hazen EL, Zaba KD, Rudnick DL, Edwards CA, Moore AM, Bograd SJ (2016) Impacts of the 2015-2016 El Nino on the California Current System: Early assessment and comparison to past events. Geophysical Research Letters 43:7072-7080

Karl DM, Church MJ (2014) Microbial oceanography and the Hawaii Ocean Time-series programme. Nature Reviews Microbiology 12:699-713

Kelly TB, Goericke R, Kahru M, Song H, Stukel MR (2018) CCE II: Spatial and interannual variability in export efficiency and the biological pump in an eastern boundary current upwelling system with substantial lateral advection. Deep-Sea Research Part I-Oceanographic Research Papers 140:14-25

Kim H, Ducklow HW (2016) A Decadal (2002-2014) Analysis for Dynamics of Heterotrophic Bacteria in an Antarctic Coastal Ecosystem: Variability and Physical and Biogeochemical Forcings. Frontiers in Marine Science 3

Landry MR, Ohman MD, Goericke R, Stukel MR, Tsyrklevich K (2009) Lagrangian studies of phytoplankton growth and grazing relationships in a coastal upwelling ecosystem off Southern California. Progress in Oceanography 83:208-216

Legendre L, Lefevre J (1995) MICROBIAL FOOD WEBS AND THE EXPORT OF BIOGENIC CARBON IN OCEANS. Aquatic Microbial Ecology 9:69-77

Mantua NJ, Hare SR, Zhang Y, Wallace JM, Francis RC (1997) A Pacific interdecadal climate oscillation with impacts on salmon production. Bulletin of the American Meteorological Society 78:1069-1079

Miller AJ, Song H, Subramanian AC (2015) The physical oceanographic environment during the CCE-LTER Years: Changes in climate and concepts. Deep-Sea Research Part Ii-Topical Studies in Oceanography 112:6-17

Nagai T, Gruber N, Frenzel H, Lachkar Z, McWilliams JC, Plattner GK (2015) Dominant role of eddies and filaments in the offshore transport of carbon and nutrients in the California Current System. Journal of Geophysical Research-Oceans 120:5318-5341

Ohman MD, Barbeau K, Franks PJS, Goericke R, Landry MR, Miller AJ (2013) Ecological Transitions in a Coastal Upwelling Ecosystem. Oceanography 26:210-219

Polovina JJ, Howell EA, Abecassis M (2008) Ocean's least productive waters are expanding. Geophysical Research Letters 35:5

Rykaczewski RR, Checkley DM (2008) Influence of ocean winds on the pelagic ecosystem in upwelling regions. Proceedings of the National Academy of Sciences of the United States of America 105:1965-1970

Sarmiento JL, Slater R, Barber R, Bopp L, Doney SC, Hirst AC, Kleypas J, Matear R, Mikolajewicz U, Monfray P, Soldatov V, Spall SA, Stouffer R (2004) Response of ocean ecosystems to climate warming. Global Biogeochemical Cycles 18:35

Smale DA, Wernberg T, Oliver ECJ, Thomsen M, Harvey BP, Straub SC, Burrows MT, Alexander LV, Benthuysen JA, Donat MG, Feng M, Hobday AJ, Holbrook NJ, Perkins-Kirkpatrick SE, Scannell HA, Sen Gupta A, Payne BL, Moore PJ (2019) Marine heatwaves threaten global biodiversity and the provision of ecosystem services. Nature Climate Change 9:306-312

Smith DC, Simon M, Alldredge AL, Azam F (1992) INTENSE HYDROLYTIC ENZYME-ACTIVITY ON MARINE AGGREGATES AND IMPLICATIONS FOR RAPID PARTICLE DISSOLUTION. Nature 359:139-142

Stephens BM, Porrachia M, Dovel S, Roadman M, Goericke R, Aluwihare LI (2018) Nonsinking Organic Matter Production in the California Current. Global Biogeochemical Cycles 32:1386-1405

Taylor AG, Landry MR (2018) Phytoplankton biomass and size structure across trophic gradients in the southern California Current and adjacent ocean ecosystems. Marine Ecology Progress Series 592:1-17

Viviani DA, Church MJ (2017) Decoupling between bacterial production and primary production over multiple time scales in the North Pacific Subtropical Gyre. Deep-Sea Research Part I-Oceanographic Research Papers 121:132-142

White PA, Kalff J, Rasmussen JB, Gasol JM (1991) THE EFFECT OF TEMPERATURE AND ALGAL BIOMASS ON BACTERIAL PRODUCTION AND SPECIFIC GROWTH-RATE IN FRESH-WATER AND MARINE HABITATS. Microbial Ecology 21:99-118

Chapter 1: Temporal and spatial variability of microbial abundance in the southern California Current System

Sara R. Rivera, Ralf Goericke, Brandon M. Stephens, Shonna Dovel, Megan Roadman, Mati Kahru, Michael R. Landry, Lihini I. Aluwihare

ABSTRACT

The southern California Current System (sCCS) is a uniquely well studied, highly dynamic Eastern boundary current. Both the California Cooperative Oceanic Fisheries Investigations (CalCOFI) survey program, begun in 1949, and the California Current Ecosystem Long Term Ecological Research (CCE-LTER) program, begun in 2005, are situated in this region, with some overlap in their study domain. The CalCOFI program was designed primarily as a survey program, sampling the same stations each quarter; whereas, the CCE-LTER program was designed to study interactions between various physical perturbations and ecosystem processes. From the perspective of long-term observations, however, it is important to be able to 'bin' findings from various CCE-LTER cruises into the relevant CalCOFI climatology and hydrography to allow the discoveries enabled by the CCE-LTER program to be interpreted in a longer-term context. As a first step, biogeochemical parameters were used to separate the two datasets into regions designated as nearshore, transition and offshore. Within these regions the variability in heterotrophic bacteria (HBac) and picoautotrophs (*Synechococcus, Prochlorococcus* and picoeukaryotes) was evaluated to determine the overlap between CCE-LTER and CalCOFI datasets. The sampling design of CCE-LTER cruises sometimes made it difficult to overlay these data on the CalCOFI timeseries, but the differences were informative. Seasonal variations in picoplankton

abundance as recorded by CalCOFI cruises provided a framework to compare CCE-LTER cruises that were conducted in different seasons with one another, which was helpful for examining interannual variations within the CCE-LTER dataset. Our data also support previous studies in the region that invoked the importance of microzooplankton grazing triggered by increases in HBac, for controlling the abundance of picoplankton, particularly in the nearshore. Using the CCE-LTER data, underlying mechanisms were tested and support for this hypothesis, previously coined the enhanced microbial loop, was found during a "normal" year. When comparing a warm year (2016) to the normal year (2017), however, it appeared that the abundances of picoautotrophs and HBac in the nearshore during the warm year were controlled by different processes. Furthermore, the CalCOFI time series identified a significant shift in abundance and spatial distribution of picoplankton following the switch to a positive Pacific Decadal Oscillation (PDO) phase at the end of 2013, with higher abundances of HBac and Prochlorococcus, in particular, persisting through the 2015/2016 El Niño event to the end of our study period (November 2017).

1.1. INTRODUCTION

The southern California Current System (sCCS), is a well-studied Eastern boundary current region with two active monitoring programs: the California Cooperative Oceanic Fisheries Investigations (CalCOFI) survey program, which samples 3-4 times a year using Eulerian methods, and the California Current Ecosystem Long Term Ecological Research (CCE-LTER) program, which uses short Lagrangian cycles to examine mesoscale variability and conduct biological process experiments. The sCCS encompasses several different productivity regimes from upwelling driven, productive coastal waters to more stratified

oligotrophic subtropical gyre waters (Chavez & Messie 2009, Landry et al. 2009, Ohman et al. 2013, Goericke & Ohman 2015). This region is also known for its sub-mesoscale variability with numerous, eddies, filaments, and fronts developing in the region throughout the year (Nagai et al. 2015). Furthermore, inter-annual variability linked to El Niño and, more recently, warm anomaly/ocean heatwave events are well documented in the region (Jacox et al. 2016, Gentemann et al. 2017, Gomez-Ocampo et al. 2018, Smale et al. 2019). Such dynamics can complicate our ability to extract long term trends from these studies. Here, we build upon existing classification schemes using physical and biological parameters, to provide a framework for retrospective comparison between the two programs.

One important goal of the CCE-LTER dataset is to document interannual changes in ecological and biogeochemical processes in the sCCS. However, because there are seasonal differences in the timing of CCE-LTER cruises it is necessary to identify any seasonal patterns in the parameters of interest before attributing observed variations to forcing that occurs on longer time scales. Luckily, the CalCOFI program, which is conducted quarterly in the region, allows us to examine potential seasonal variations in relevant microbial parameters. Any seasonality can then be compared with CCE-LTER cruises to identify seasonal biases that would preclude us from comparing between CCE-LTER cruises. First, this was addressed this by examining seasonality in the CalCOFI dataset for comparable parameters. Second, CCE-LTER cruise measurements were compared to contemporaneous CalCOFI data collected nearby to identify any short-term variability in the region. Typically, a CalCOFI cruise occurred during the same month as a CCE-LTER cruise, and CalCOFI Line 80 was the focus of our comparison because the CCE-LTER sampling domain often overlapped with the spatial extent of this line (Appendix Figure S1.1). Finally, flow

cytometer-based abundance data (heterotrophic bacteria, *Prochlorococcus*, *Synechococcus*, and picoeukaryotes) were utilized to assess seasonal and interannual variability in the microbial response of the sCCS. The focus was solely on these populations because seasonal and regional patterns have been previously identified for these organisms (Olson et al. 1990, Partensky et al. 1999a, Collier & Palenik 2003, Linacre et al. 2010, Tai et al. 2011, Connell et al. 2017). Previous studies in the region have also linked the abundances of these organisms, particularly in the nearshore, suggesting that bacterial activity catalyzed by the release of dissolved organic carbon (DOC) from larger autotrophs results in a grazing response that affects picoplankton abundance (Goericke 2011, Taylor & Landry 2018). Furthermore, small autotrophic and heterotrophic microorganisms are expected to respond most rapidly to interannual variations in environmental parameters.

1.2. METHODS

1.2.1 Study region and sampling periods

This study focuses on a subregion of the California Current System (CCS) that extends from the upwelling waters off Point Conception to the edge of the oligotrophic gyre (a total distance of 500 km offshore; Appendix Figure S1.1, Tables S1.1 and S1.2). Samples for this study were collected either during quarterly CalCOFI cruises between 2004 and 2017 (n=49) or during 6 CCE-LTER cruises between 2006 and 2017. The CalCOFI cruises included in this study were conducted in November 2004; January, April, July, November 2005; February, April 1-18 (specific dates are included when a CalCOFI cruise served as a comparison to a CCE-LTER cruise), July, October 2006; January, March 28-April 29, June, November 2007; January, March 28-April 29, August, October 14-30 2008; January, March,

July, November 2009; January, April, July, October 2010; January, April, July, October 2011; January, March, October 2012; January, April, July, November 2013; March, July 6-22, November 2014; January, April 2015; January, April 1-23, July, November 2016; January, March 29-April 20, August, November 2017. Samples were collected on CCE-LTER cruises from May 8-June 7 2006 (P0605), April 2-21 2007 (P0704), September 30-October 29 2008 (P0810), August 6-September 4 (P1408), April 19-May 12 2016 (P1604), and June 1-July 2 2017 (P1706). The CCE-LTER cruises from 2010 and 2012 were excluded from this analysis due to their strict focus on frontal features.

Ecosystem conditions during 2004-2013 (Miller et al. 2015) and 2017 were El Niño-neutral and 2014-2016 were warm with a warm anomaly encountered during 2014 (Bond et al. 2015, Gentemann et al. 2017) and an El Niño event during 2015-2016 (Di Lorenzo & Mantua 2016, Jacox et al. 2016). Moderately positive North Pacific Gyre Oscillation (NPGO) conditions were encountered in 2007 while strongly positive NPGO conditions prevailed in 2008. The remaining cruises – 1408, 1604 and 1706 – took place during weakly or moderately negative NPGO conditions (see Di Lorenzo et al. (2008) and Miller et al. (2015)) for a description of oceanographic conditions during positive and negative NPGO phases). During 2008, the Pacific Decadal Oscillation (PDO) index was also strongly negative, but during 2014 (moderate), 2016 (strong) and 2017 (moderate) the PDO index was positive (e.g., Mantua et al. (1997) for a definition of the PDO index); whereas the 2006 and 2007 cruises took place during neutral PDO conditions. Several recent studies have suggested that variations in salinity, nutrients and chlorophyll more closely follow ENSO or NPGO in the sCCS (Di Lorenzo et al. 2008). Bograd et al. (2019) noted that both the lower salinity, and cooler Pacific Subarctic Upper Water (PSUW, which dominates the California Current down

to ~200 m) and the saltier and warmer Pacific Equatorial Water (PEW) could be found in the upper water column along Line 80, with the latter dominating inshore of the former. Seasonal variability in the strength of each water mass was observed, with PSUW dominating even surface waters closer to shore during the winter and spring, while PEW was more prominent along Line 80 in the summer (>30% of the water mass contribution) and fall (25-30%) (Bograd et al. 2019). However, interannual variability appeared to dominate the spatial extent of each water mass, with ENSO events being particularly relevant, and a consistently lower composition of PSUW <50 m at station 80 during 2014, 2016 and 2017.

CalCOFI samples as many of their 66 stations, down to ~500 m, per cruise as possible. Whereas the CCE-LTER uses a Lagrangian framework to follow a water mass for several days in a 'cycle.' The location of each cycle and its duration was determine based on the research framework for that specific CCE-LTER cruise. The CalCOFI stations examined in this study are restricted to CalCOFI Line 80 because they most closely aligned with the study area sampled by the CCE-LTER. Within the CalCOFI dataset, sampling locations were designated nearshore (n=98 locations, stations 51 and 55), transition (n=147 locations, stations 60, 70, and 80), and offshore (n=98 locations, stations 90 and 100) based on previous work (Munro et al. 2013, Taylor et al. 2015, Stephens et al. 2018). The sampling framework for the CCE-LTER is well described (Landry et al. 2009, Ohman et al. 2013, Stukel et al. 2013). Typically, water masses with the appropriate characteristics for the planned sampling design are pre-identified using surveys collected by a Moving Vessel Profiler or a SeaSoar (Ohman et al. 2012) and then followed for several days to study the evolution of communities and material fluxes. Chosen water parcels represent various physical features, such as

oceanographic fronts and filaments, and biological gradients, from eutrophic to oligotrophic environments.

1.2.2 Hydrographic conditions

The nitracline depth is defined here as the depth where only 1 µM of nitrate remains. In cases, where the 1 µM depth was not sampled, a linear extrapolation between the relevant measurements was made in order to estimate the appropriate depth (Georicke et al. 2007). In this way, the nitracline depth during CCE-LTER cruises was calculated for each day of a given cycle and then averaged over the entire cycle (typically 3-4 days). Regional averages were then computed from all of the cycles that fell within a designated region, as discussed in the Results section (i.e., offshore, transition, and nearshore regional designations). Whereas for CalCOFI cruises the nitracline depth was estimated as above, and the relevant stations that corresponded to either nearshore, transition or offshore (see above) were averaged to provide a regional comparison with the CCE-LTER dataset.

The chlorophyll maximum was determined from a CTD rosette-mounted fluorometer, using chlorophyll fluorescence measured on the downcast. For CCE-LTER cruises, cycle days were averaged to give a chlorophyll max depth for each cycle. Regional averages were computed as described above for nitracline depth.

In this study, the euphotic zone (EZ) depth is defined as the 1% surface irradiance depth. CCE-LTER cruises utilized photosynthetically active radiation (PAR) measurements using a 4-π Licor PAC sensor in the water column and a 2-π Licor PAC sensor for surface measurements. The percent surface irradiance was calculated from in situ PAR recorded by the CTD downcast and surface PAR. Where possible, daily, cast by cast data were used and

then averaged to be consistent with other measured parameters. CalCOFI cruises utilized Secchi disk measurements, with the 1% surface irradiance depth being equivalent to three times the Secchi disc depth. Because CalCOFI often sampled during nighttime hours, Secchi disc measurements were not always available. Therefore, an average, seasonal 1% surface irradiance depth was calculated from each defined oceanographic region when a Secchi disc measurement was unavailable. Integrated values discussed in the paper refer to data integrated over the average EZ depth for each CCE-LTER cycle or CalCOFI Line 80 station (Appendix Tables S1.3, S1.4, S1.5).

1.2.3 Chlorophyll and Primary Production measurements

Chlorophyll a (Chl) concentrations were measured at 6-8 depths after Strickland and Parsons (1972). The depth of maximum Chl concentration (Chl max) was determined from fluorescence on the CTD downcast. Net primary production (NPP) was measured using the ^{14}C method at 6-8 depths as described by (Eppley & Holm-Hansen 1986, Morrow et al. 2018). For CCE-LTER cruise P1706, the ^{14}C-NPP samples were compromised and NPP was computed from a model that assimilated data from previous CCE-LTER cruises (Stukel et al. 2019).

1.2.4 Supporting chemical measurements

Oxidized nitrogen species were analyzed following a modification of Armstrong et al. (1967). Total organic carbon (TOC) and/or dissolved organic carbon (DOC), from at least 6 depths, were analyzed following Stephens et al. (2018). In the case of suspended particulate organic carbon (POC), two (P0605, P0704, P0810; CalCOFI) or four (P1408, P1604, P1706)

L of SW were filtered onto pre-combusted (450°C, 6 h) Whatman GF/F filters for measurements (Stephens et al. 2018).

1.2.5 Heterotrophic Bacterial Abundance (BA) by Flow Cytometry (FCM) and Bacterial Production (BP)

Preserved samples (2 ml SW + paraformaldehyde, 0.5% final) were frozen in liquid N_2, stored at -80°C, and sent to the University of Hawaii's School of Ocean and Earth Science and Technology (SOEST) Flow Cytometry Facility for analysis. Prior to analysis, samples were thawed and stained with Hoechst 33342 in the dark at room temperature for 1 hour (Monger & Landry 1993) and analyzed with a Beckman-Coulter EPICS Altra flow cytometer with dual lasers (tuned to UV [200 mW] and 488 nm [1 W] excitation) to estimate abundances of heterotrophic bacteria (HBac), *Prochlorococcus* (Pro), *Synechococcus* (Syn), pico-eukaryotes (PEuk). All samples were spiked with fluorescent beads to normalize fluorescence and scattering properties. Raw data were processed using the software FlowJo (Treestar Inc., www.flowjo.com) with correction factors of 0.95 for the preservative, 0.10 for run volume and 0.82 for coincidence.

Bacterial production (BP) measurements were only made on CCE-LTER cruises. Seawater samples were also taken from 6 depths from each mid-day CTD cast, typically at 11 a.m. BP was determined from rates of bacterial protein synthesis (Kirchman et al. 1982, Kirchman et al. 1985, Simon & Azam 1989, Smith & Azam 1992). For each sample, 1.7 mL seawater were incubated with approximately 20 nM 3H-Leucine for one hour. Incubation temperatures were either room temperature during P1604 or 9°C during P1706. The effect of incubation temperature on BP using all the available CCE-LTER BP data and found that

incubation temperature had no significant impact on BP values (linear regression, $p = 0.15$ and 0.45, respectively) in the offshore and transition regions, but was statistically significant in the nearshore ($p<0.05$); however, the nearshore was the most data limited and the resulting slope ($m=0.052$) suggests there was minimal impact of incubation temperature on BP. Samples from P1604, and P1706 were done in triplicate with single TCA-killed controls. The standard errors of all methods were comparable. After the incubation was complete, all samples were killed with an addition of 100% TCA for a final concentration of 5% TCA before processed using the centrifugation method as described in Smith et al. (1992). Samples were frozen and stored at -20°C as needed. All samples were analyzed for disintegrations per minute on a Beckan LS8000A liquid scintillation counter. Disintegrations per minute were converted to protein synthesis rates assuming 3.1 kg C mol^{-1} leucine and 24 h day^{-1} (Simon & Azam 1989).

1.2.6 Statistical comparison

Hydrographic and biogeochemical gradients along CalCOFI Line 80 were used to divide stations into three regional groupings: nearshore (n=464 samples, stations 51 and 55), transition (n=764 samples, stations 60, 70, and 80), and offshore (n=476 samples, stations 90 and 100); and four seasonal groupings: Winter (n= 400 samples, January and February), Spring (n=419 samples, March and April), Summer (n= 419 samples, June, July, and August), Fall (n= 466 samples, October and November). The effect of region and season on microbial abundance (i.e. HBac, Pro, Syn, and PEuk abundances) was evaluated using a generalized linear model (GLM) for negative binomial distributions (Pro, Syn, and PEuk abundances) or Poisson distributions (HBac abundances). In each model, depth (m) was the fixed factor and

abundance was the response variable. In each case, the response variables were log transformed prior to calculating the estimated marginal trends (trends*) and estimated marginal means (means*) using the package "emmeans," available in the free software environment in R. Both estimated marginal trends and means create reference grids based on model predicted trends or means (adjusted for interactions of variables such as region and season) within the model, and then calculate the average of the predictions within the grid. We used trends* and means* to evaluate seasonal or regional characteristics in the CCS. Tukey post-hoc analysis was done with a confidence level of 95%. Means* were transformed back to their original scales for reporting.

The CCE-LTER cruises (designated as P, year, month) were compared to CalCOFI cruises (year, month, ship initials) conducted as close to the same time as possible. The resulting pairs are as follows: P0605 and 0604JD, P0704 and 0704JD, P0810 and 0810NH, P1408 and 1407NH, P1604 and 1604SH, P1706 and 1704SH. The deepest samples that were compared from each year were 125 m in 2006, 110 m in 2007, 61 m in 2008, 126 m in 2014, 101 m in 2016, and 261 m in 2017.

ANOVA, combined with Tukey HSD post-hoc test with a confidence level of 95%, was used to evaluate statistical differences among the CCE-LTER oceanic regions for nitracline depth, Chl concentration maximum depth (Chl max), EZ depth, NPP, Chl, POC, and TOC. Additionally, a Kruskal–Wallis one-way analysis of variance with 95% confidence interval was used to compare overall CalCOFI and CCE-LTER metrics (i.e. HBac, Pro, Syn, and PEuk abundances) for each pair. Plotted trend lines were added in R using the the "geom_smooth" function within the "ggplot2" package. Displayed equations and R^2 values

were determined using the "stat_poly_eq" function within the "ggpmisc" package, while the "stat_cor" function within the "ggpubr" package was used to determine the p-values.

1.3. RESULTS

1.3.1 Defining regional characteristics of the sCCS

Each of the three oceanic regions (nearshore, transition, and offshore) have defining ecological and biogeochemical characteristics. CalCOFI stations along Line 80 were designated nearshore (stations 51 and 55), transition (stations 60, 70, and 80), and offshore (stations 90 and 100) based on previous studies (Munro et al. 2013; Stephens et al. 2018; Taylor et al. 2015). The nearshore region had a shallow nitracline, Chl max, and euphotic zone (EZ); the transition had an intermediate nitracline, Chl max, and EZ; whereas the offshore region had a deep nitracline, Chl max, and EZ depths (Table 1.1). Regional differences were more important than seasonal differences for each of these parameters (Appendix Figure S1.2).

Regional groupings for CCE-LTER (Appendix Table S1.2) were similar to Morrow et al. (2018), except that P1408-C3 was classified as transition based on the nitracline (24 ± 1 m) and P0810-C5 as nearshore based on net primary production (NPP) (95 ± 17 mmol C m^{-2} d^{-1}), which was significantly elevated in comparison to the rest of the cycles from that year (23 to 57 mmol C m^{-2} d^{-1}). Our study also included CCE-LTER cruise P1706, where P1706-C1 and P1706-C2 were classified as nearshore and P1706-C3 and P1706-C4 were classified as transition. For P1706, classification into regions was based on the EZ and Chl max depths; and no P1706 cycles were determined to be offshore. The CCE-LTER regional groupings

exhibited the same trends as the CalCOFI regions, with decreasing nitracline, chlorophyll max, and EZ depths offshore (Table 1.1, Appendix Figure S1.2).

Regional trends for integrated EZ values, from the nearshore through the transition to the offshore, showed decreasing rates of NPP, decreasing concentrations of chlorophyll a (Chl) and suspended particulate organic carbon (POC), and increasing concentrations of total organic carbon (TOC) (Table 1.1, Appendix Figure S1.3). For integrated Chl and POC concetrations, CCE-LTER cruises fell within or near to the expected range from the CalCOFI cruises, but such a close correspondence was not observed for NPP and TOC. In the nearshore during spring and summer and in the transition during the spring, NPP was higher during CCE-LTER cruises than might be predicted from CalCOFI NPP. This is not surprising because the CCE-LTER program intentionally targeted sites of active upwelling in the nearshore where production is likely to be highest, whereas CalCOFI samples fixed nearshore stations regardless of productivity. Furthermore, the NPP method differed between the two programs: CCE-LTER uses the more traditional 12 hour, ^{14}C-incubation but CalCOFI uses a 6-hour incubation due to time constraints. In the case of total organic carbon (TOC), both datasets were limited, and so, the mismatch was expected. Generally, there was good agreement between the CCE-LTER and CalCOFI regional groupings.

Regional characteristics were more defining than seasonal differences for each parameter that was tested (Appendix Figure S1.3, Table S1.5); however, there were some seasonal trends in the nearshore: for example, NPP peaked in the spring as expected based on the timing of upwelling in the region, but Chl, POC, and TOC concentrations peaked in the summer.

1.3.1.1 Interannual variability by region for the CCE-LTER program

Although CCE-LTER cruises P0605, P1604, and P1706 and their respective CalCOFI cruises 0604JD, 1604SH, and 1704SH exhibited the expected offshore decrease in nitracline, chlorophyll max, and EZ depth, CCE-LTER cruise P0704 was different. For example, during P0704, the nitracline in the nearshore and transition was much shallower but became deeper offshore, indicating strong upwelling conditions near the coast. Increased upwelling near coast would have been consistent with the return to positive NPGO conditions. The corresponding CalCOFI cruise 0704JD also showed a similar response (Appendix Table S1.4). Designation of the euphotic zone for P0704 was less precise than other years due to a problem with the PAR surface reading and may have led to erroneous designation of the depth of the EZ. For example, the nearshore P0704-C3 EZ depth was an outlier but was included in this study because the remaining parameters were commensurate with other years.

The results from P0810 had to be singled out because the cruise was designed to sample frontal zones. As such, the spatial separation of nitracline and Chl max depth typical of some of the other datasets was not as clear during this cruise. Morrow et al. (2018) did not have any of the P0810 cycles classified as nearshore upwelling, which would simplify the classification by grouping P0810-C1, C3, C4, C5 into the transition region. Here, P0810-C5 was reclassified as most representative of the nearshore region during times of subdued upwelling conditions, based primarily on a shallow nitracline depth, high NPP, and high Chl concentrations. The CalCOFI cruise 0810NH transition station 60 also had relatively high NPP and Chl concentrations but had a deeper nitracline depth (Appendix Table S1.4). Unfortunately, NPP was not measured at either nearshore station during 0810NH. During

2008 the NPGO index was strongly positive (peaking in August and September), and so, there may have been remnants of a productive summer upwelling season.

During P1408, offshore P1408-C4 and P1408-C5 did not always conform to the expected offshore trend. For example, the Chl max depth for P1408-C4 was shallower than transition cycle P1408-C2 but the same average depth as transition cycle P1408-C1. The CalCOFI cruise 1407NH, on the other hand, did conform to the expected trends (Appendix Table S1.4).

During P1706, no cycles were classified as offshore even though P1706-C3 did exhibit characteristics consistent with an oligotrophic water mass. After the "warm" CCE-LTER cruises of 2014 (warm anomaly) and 2016 (the tail end of an El Niño), P1706 signified a return to relatively "normal" conditions in the region, with the nitracline shoaling to very shallow depths for the nearshore (P1706-C1 and P1706-C2) and transition (P1706-C3) Cycles. This shoaling was also observed during CalCOFI cruise 1704SH in the nearshore (stations 51 and 55) and transition (station 60).

1.3.2 Seasonal and regional variability of HBac, Pro, Syn, and PEuk along CalCOFI Line 80

To examine the seasonal variability in picoplankton abundance by region in the sCCS, estimated marginal means, designated here as means*, were utilized with regards to FCM abundance, and estimated marginal trends (trends*) with regards to depth profiles of FCM abundance. The four populations that were examined in this study included heterotrophic bacteria (HBac), *Prochlorococcus* (Pro), *Synechococcus* (Syn), and picoeukaryotes (PEuk). Overall, there was no seasonal or regional difference in the HBac means* or trends*,

consistent with the fact that the abundance of the HBac population and their depth distribution remained fairly stable over the relevant time period (Figure 1.1a & b, panels I-III). Syn and PEuk populations, on the other hand, did exhibit significant seasonal variations across oceanic regions (Figure 1.1a & b, panels IV-XII). The PEuks exhibited the greatest seasonal variability (Figure 1.1a & b, panels X-XII) in both means* and trends* with spring cruises generally having steeper trends* and fall cruises exhibiting low means*. The more similar behavior of PEuks during the spring and winter, particularly in the nearshore and transition, may be linked to seasonal variations in Pacific Subarctic Upper water (PSUW) as observed by Bograd et al., (2019). Syn means* peaked in the transition and were lower nearshore than offshore, perhaps due to control of nearshore populations by enhanced grazing. Syn depth trends showed similar seasonal variability across the regions but exhibited the steepest gradient in the offshore during spring (Figure 1.1a & b, panels VII-IX). Pro means* increased with increasing distance from shore (Figure 1.1a, panels IV-VI), consistent with their expected dominance in oligotrophic environments (Partensky et al. 1999a, Partensky et al. 1999b), with almost no significant difference in depth trends* (Figure 1.1a, panels IV-VI).

1.3.2.1 Picoplankton variability at 10m along CalCOFI Line 80

The 10 m HBac abundances were defined by generally higher values inshore of station 80 (Bird & Kalff 1984, Cho & Azam 1990), while Pro showed the opposite distribution, with higher values offshore of station 70 (Figure 1.2a,b). The temporal variability observed in the transition for both HBac and Pro may be linked to changes in stratification and water mass characteristics (Appendix Figure S1.2a,b). Consistent with previous literature (Partensky et al. 1999a, Partensky et al. 1999b), surface Pro abundances were between 104-105. In addition to

being most prominent in the offshore, their abundances extended deeper, past the EZ, compared to Syn abundances (Gutierrez-Rodriguez et al. 2014) (Figure 1.2b,c, Appendix Figures S1.4, S1.5). Similar to what was reported in Linacre et al. (2010), Pro was likely too scarce to count in the nearshore region, leading to values close to zero in surface waters.

The Syn abundance at 10 m depth also exhibited enhanced variability in the transition region (Figure 1.2c), consistent with previously reported CalCOFI data along Lines 83 (Collier & Palenik 2003) and 93 (Tai et al. 2011). The Syn abundances reported here are the same magnitude (104-105) as those reported in the sCCS, the coast of Mexico (Linacre et al. 2015), the central Atlantic Ocean (Vazquez-Dominguez et al. 2008), and the Canary upwelling system (Partensky et al. 1996), but lower than those reported for other upwelling areas such as the Costa Rican Dome (Saito et al. 2005, Gutierrez-Rodriguez et al. 2014). PEuk abundances and Syn abundances at the surface were correlated (Appendix Figure S1.6) as predicted by Worden et al. (2004).

1.3.2.2 Picoplankton abundance anomalies corresponded with a shift in the PDO

To more directly examine interannual variations and the underlying mechanisms, the 10m cube root anomalies in picoplankton abundance, nitrate and Chl concentrations over the 2004-2017 period were computed relative to the mean from 2004-2012. The mean was restricted to the time period before 2012 to highlight the shift that occurred along Line 80 at the end of 2013. The cube root anomalies uncovered certain time periods that may be linked to indices of decadal variability. For example, from about spring 2007 to summer 2008, there is variability in the transition and offshore (higher nitrate and Pro, but lower HBac, Syn and PEuks) that could be linked to positive NPGO and negative PDO conditions that prevailed

during this time in the region (Figure 1.3). Both Chl and nitrate concentrations (Figure 1.3a,b) were anomalously low in the nearshore beginning with the spring cruise in 2014. Prior to this period there was significant variability in both of these parameters throughout Line 80, and similar variability was apparent for Syn and PEuk abundances (Figure 1.3e,f) as well. Beginning at the end of 2013, when the PDO shifted to positive values, and until 2017, the anomalous patterns in picoplankton abundance became more prominent and spatially restricted. Positive HBac anomalies closer to shore and positive Pro abundances farther offshore appeared more frequently in the time series after 2013, with station 70 acting as the 'barrier.' The EZ integrated Pro stocks reflected the same overall temporal shift (Appendix Figures S1.7). During this same period, anomalously high PEuk and Syn abundances became more spatially restricted to the nearshore, and the interannual variability of integrated PEuk stocks increased inshore of and including station 60 (Appendix Figure S1.7).

1.3.2.3 Picoplankton abundance and Chl concentration relationships

Consistent with previous studies in the region, picoplankton (Pro, Syn, and PEuks together) abundances peaked at relatively low Chl concentrations (Goericke 2011, Taylor & Landry 2018) and then decreased rapidly, despite increasing Chl concentrations, and in some cases, reached a minimum threshold value (Figure 1.4). As others have noted previously for picoplankton biomass, Pro peaked at lower Chl concentrations than Syn and PEuk (Figure 1.4b). In this dataset Syn reached its highest abundance at slightly lower Chl concentrations than PEuk and their overall abundances were similar. Even though abundance and not biomass was used, peaks in picoplankton abundance occurred at very similar Chl concentrations to those previously reported (e.g., Taylor & Landry 2018). Furthermore, the

modeled fits proposed by Goericke (2011) mirrored the relationship plotted here for all groups from both the CalCOFI and CCE-LTER datasets (Figure 1.4), which supported the hypothesis that Chl is a useful proxy for phytoplankton size distributions and dynamics in the region (Appendix Figure S1.8). Also consistent with earlier observations, this expanded dataset showed that HBac continued to increase with Chl concentration. The slope of this relationship, however, was low compared to the initial rapid increase in picoautotrophic abundance with Chl concentration because heterotrophic bacterial are always present throughout the water column (Figure 4). It is likely that the positive relationship between Chl concentration and HBac is partially driven by the fact that both parameters are low at depth and increase closer to the surface.

1.3.3 Top-down controls on picoplankton and testing the enhanced microbial loop hypothesis

The relationship between picoplankton biomass and Chl concentration has been previously attributed to enhanced grazing pressure (Goericke 2011). The hypothesis states that as HBac biomass increases in response to the release of DOC by larger phytoplankton that dominate at high Chl concentrations, grazers are stimulated and non-selectively graze on the picoplankton size class, resulting in the observed relationships. This hypothesis has been coined the enhanced microbial loop by Taylor and Landry (2018). For both CCE-LTER and CalCOFI datasets, HBac abundances were significantly positively correlated with the sum of Pro, Syn, and PEuk abundances (Appendix Figure S1.9), but the CalCOFI dataset had a more positive slope. The positive correlation between HBac abundances and the summed

picophytoplankton abundances was maintained across all regions and seasons (Appendix Figure S1.10).

To further explore the enhanced microbial loop concept, the abundance of picophytoplankton and bacterial production (BP) measurements for the two CCE-LTER datasets where we measured both on the same samples (P1604 and P1706, the latter serving as a comparison dataset) were compared. BP was not measured on CalCOFI cruises. For both years, relatively rapid increases in Syn and PEuk cell abundance over a relatively small range of increasing BP were observed (Figure 1.5). If it is assumed that heterotrophic bacteria take up carbon at the rate that it is released, then BP may be a reasonable proxy for the enhanced microbial loop. During 2016, BP continued to increase, nearly linearly, with Chl concentration, after Pro abundances had decreased and Syn and PEuk abundances had plateaued (Figure 1.5). In contrast, during the more normal 2017 cruise, Syn and PEuk abundances first peaked as BP increased and then BP, Syn and PEuk abundances showed a similar relationship at higher Chl concentrations, when BP and picoplankton abundances stabilized. The parallel relationship between HBac, Syn and PEuk abundances at higher Chl concentrations, observed in 2017, suggested a similar control on their abundance, such as microzooplankton grazing. During 2016, the continued rapid increase in BP, even at low Chl concentrations, suggested that picophytoplankton and HBac populations were decoupled. Moreover, the BP versus Chl concentration pattern was distinct in the two years, with much higher BP per Chl concentration in 2016 (Figure 1.5). The observed differences between the two years cannot be attributed to seasonal differences (April versus June) because PEuk abundance would be expected to show the greatest seasonal difference in the nearshore (Figure 1.1) but instead behaves similarly in 2016 and 2017.

Looking at the difference between P1706 and P1604 further, the picophytoplankton abundance threshold was higher in 2016, but this was only robustly observed for Syn abundances in the nearshore, and to some extent in the transition (Figure 1.6). In the offshore region, where Chl concentrations were low, Pro abundance increased linearly with BP and then begins to plateau. Whereas in the transition region, where Chl concentration was elevated, first a rapid increase was observed followed immediately by a rapid decrease in Pro abundance just as Syn and PEuk abundance began to stabilize (Figure 1.6). Overall, the slope of the BP versus picoplankton abundance relationships changed nearly synchronously, supporting a link between these parameters.

1.3.4 Bottom-up controls on heterotrophic bacterial abundance in the sCCS

The role of NPP, Chl , TOC, POC, or DOC concentrations in controlling HBac abundance in the sCCS was also explored. The HBac abundance was significantly ($p<0.05$) positively correlated with NPP, Chl, TOC, POC, and DOC concentrations, with the exception of the offshore relationship between DOC concentrations and HBac abundance, which was not significant (Figure 1.7). The DOC concentration relationships are based only on CCE-LTER cruises (P1408, P1604, and P1706) because DOC concentration was not measured during CalCOFI cruises. However, it is well established that in the offshore region TOC concentration primarily reflects DOC concentration (Stephens et al. 2018), whereas in the transition and nearshore when NPP is elevated, TOC concentration will include some suspended POC. The correlation of HBac abundance with POC or DOC concentrations, regionally, had higher explanatory power than with Chl concentrations, NPP, or TOC concentrations. HBac abundance was more strongly correlated with Chl concentration and

NPP in the nearshore than in the transition and offshore areas, whereas the most significant correlation with TOC concentration was observed in the transition region. During P1604, HBac abundance was exceptionally elevated when compared with all parameters. In fact, high HBac abundance at relatively low Chl (Figure 1.7a) and POC concentrations (Figure 1.7d) in the nearshore implied an active microbial loop during this time.

1.3.5 Comparison of FCM data from of CalCOFI Line 80 and CCE-LTER cruises

The same FCM method was used to estimate cell abundance on both CCE-LTER and CalCOFI cruises, which allowed us to compare CCE-LTER data with CalCOFI stations sampled during the same time period. Restricting our analyses to CalCOFI Line 80 allowed us to focus only on stations that intersected water masses sampled by the CCE-LTER. Picoplankton abundance, when integrated over the EZ, was similar for both programs, except in 2016 when nearshore and transition abundances sampled by the CCE-LTER were higher for PEuks, and Syn and HBac abundances were also elevated but only in the nearshore (Appendix Figures S1.11-S1.14). The comparison of integrated stocks between programs indicated that the CCE-LTER dataset adequately reflected the means state along Line 80 for most overlapping time points. However, when depth profiles were compared, a different picture emerged. A comparison of depth profiles between programs showed that HBac and Pro abundances were generally more variable than Syn and PEuk abundances between the CCE-LTER and CalCOFI sampling (Appendix Table S1.6, Figures S1.15-S18), although Syn abundances were often significantly different in the nearshore.

No consistent patterns of variability in the depth profiles collected by the two programs were determined. For example, in 2006, in the offshore region, all picoplankton

groups had higher deep maxima during the CCE-LTER, but only HBac and Pro abundances were significantly different. Whereas in 2007, all groups were significantly different; Pro and PEuk abundances sampled by the CCE-LTER were lower but HBac and Syn abundances were higher. It was only in 2014 that both programs showed good agreement in the offshore and transition. Unfortunately, none of the CCE-LTER cycles from 2014 were classified as nearshore, even though geographically they were in similar locations as other nearshore sites, so it was not possible to determine whether the pattern persisted into the nearshore region. Once exception in 2014 was a single CalCOFI Pro profile from the transition region (station 80), that showed a depth distribution that was more similar to CCE-LTER cycles and CalCOFI stations classified as offshore. This may be consistent with the observed interannual variability in the amount of PSUW found at station 80, which showed a decrease during the 2014-2018 period (Bograd et al. 2019). In support of this hypothesis, the transition HBac profile from the same CalCOFI cruise also appeared to fit better with offshore profiles.

Like 2008, the 2016 datasets showed some significant mismatches in the transition and nearshore regions, but in contrast to 2008, they showed good agreement in the offshore region. Overall, in 2016, HBac and Pro cells were significantly less abundant and PEuk cells significantly more abundant, in the transition during CCE-LTER. Whereas HBac, Syn and PEuks cells were all significantly more abundant in the nearshore during the CCE-LTER cruise. Also, in 2016, the deep maximum in HBac, Syn and PEuk abundance was deeper in the water column in the offshore during the CCE-LTER cruise, but such a shift was more difficult to discern for Pro. The 2017 CalCOFI data were significantly different from CCE-LTER datasets of the same year. In general, some CCE-LTER datapoints exceeded CalCOFI measurements in the nearshore for Syn and PEuk. Also of note was the deep peak of Pro

abundance in the transition, but this could be a result of offshore water influencing this CCE-LTER cycle that was classified as transition (evidence to support an offshore influence at this cycle is also found in the relationship of PEuk and Syn to BP as seen in Figure 1.6).

1.4. DISCUSSION

As has been consistently demonstrated for the region, wind driven coastal upwelling supplies nitrate to the nearshore region (Rykaczewski & Checkley 2008, Stephens et al. 2018). As a result, the nearshore through the transition to the offshore had increasing nitracline, Chl max, and EZ depths (Table 1.1, Appendix Figure S1.2). Several properties integrated over the EZ, such as NPP, Chl and POC concentrations, decreased offshore, but integrated TOC inventories increased offshore (Table 1.1, Appendix Figure S1.3).

The goal of this study was to provide a context and rationale for retrospective comparisons between the long-term time series data available from the CalCOFI program and the process studies that are typical of the CCE-LTER program. Furthermore, data available through quarterly CalCOFI cruises, conducted in the same region, was capitalized to constrain seasonal variations in bacterial and picoautotroph abundances. This provided data to more robustly compare CCE-LTER cruises that were conducted during different times of year in this notoriously dynamic region. It was shown that seasonal variability was of little concern for HBac and Pro abundances in the sCCS, enabling a robust comparison of these parameters across CCE-LTER cruises. By comparing contemporaneous CCE-LTER and CalCOFI cruises, we were able to confirm our regional designations for CCE-LTER cruises as nearshore, transition and offshore, and determine which CCE-LTER cruises were most

representative of the system at the time and thus, most relevant, for examining interannual variability in the sCCS.

1.4.1 Regional designations are robust in the sCCS

The hydrography of the sCCS (nitracline, Chl max, and EZ depths) enabled us to designate three oceanic regions (offshore, transition, and nearshore) that were generally consistent with regional designations in previous studies (Munro et al. 2013, Taylor et al. 2015, Morrow et al. 2018, Stephens et al. 2018). Seasonal variability was low within each oceanic region, whereas the variability between regions appropriately reflected the spatial segregation of water mass characteristics and the region-specific mechanisms of nutrient delivery to the surface ocean. Inventories of NPP, Chl, POC and TOC in the EZ provided additional evidence that regional differences were most prominent. This gave us confidence that potential temporal variability within a region could be examined from the relevant CCE-LTER cruises (Table 1.1, Appendix Figures S1.2, S1.3).

1.4.1.1 CalCOFI Line 80 Seasonal and regional variability of HBac, Pro, Syn, and PEuk

The lack of seasonal differences in HBac and Pro means* within the CalCOFI dataset gave us some confidence that our regional CCE-LTER designations, which combined different seasons, were reasonable (Figure 1.1). In contrast, both the Syn and PEuk populations exhibited seasonal changes in abundance and depth distribution within a region, and this observation must be taken into consideration when comparing the ecology of these organisms across CCE-LTER cruises.

Variations in the seasonal stability of picoplankton are likely a result of their adaptations to particular nutrient and oceanographic conditions. For example, HBac abundance may be stable across seasons due to their higher diversity and metabolic plasticity (Chen & Liu 2011), dormancy (Stevenson, 1978; Smith and del Giorgio, 2003) and/or because of top-down limits set by grazing pressures (Li et al. 2004). *Prochlorococcus* is ubiquitous in the euphotic zones of the tropical and subtropical oceans (Biller et al. 2015), and consistent with this expectation, Pro means* exhibited little seasonal variability. Furthermore, their high diversity (Kashtan et al. 2014) could allow them to respond rapidly to changing ecosystem conditions. In contrast, Syn abundances varied seasonally, with regional maxima occurring during different seasons: fall maxima were observed in the nearshore, summer maxima in transition, and winter and spring maxima in the offshore region. The seasonality of PEuk was interesting in that all three regions showed similar seasonality, where spring and winter had higher mean abundances overall. This variability may be linked to the seasonal meandering of Pacific Subarctic Upper Water (PSUW) along Line 80, where maximum contributions of this water mass in the transition and nearshore region was observed in spring and winter (Bograd et al. 2019). In general, the observed seasonal trends align well with previous work by Taylor et al. (2015) in the sCCS and in the oligotrophic northwestern Mediterranean (Massana 2011).

Overall, the three regions along CalCOFI Line 80 were distinct in terms of the abundance and depth distribution of HBac, Pro, Syn, and PEuk populations. In the nearshore, their distributions declined more sharply with depth than in the transition region, which is consistent with the typically shallower mixed layer nearshore that results from enhanced upwelling conditions. The offshore profiles maintained elevated biomass to deeper depths,

consistent with the deep EZ in this region. As previously shown for the sCCS, the mean* abundances for Pro and Syn were differentiated by region, with Syn often found in cooler, mesotrophic waters while Pro dominated offshore in warm oligotrophic waters (Partensky et al. 1999a, Taylor et al. 2012, Kent et al. 2019), increasing in abundance from the nearshore through the transition to the offshore where these organisms can compete more effectively for nutrients (Chisholm et al. 1988, Partensky et al. 1999b, Biller et al. 2015). For example, Pro has a large genomic diversity that is hypothesized to make it particularly well suited for oligotrophic environments (Chisholm et al. 1988, Partensky et al. 1999b, Biller et al. 2015) and Syn and Pro may use different N sources as has been previously demonstrated (Moore et al. 2002).

Syn abundances are also impacted by the interplay of ecotypes that vary across time and space in the sCCS (Collier & Palenik 2003, Tai & Palenik 2009, Paerl et al. 2011, Tai et al. 2011, Paerl et al. 2012, Gutierrez-Rodriguez et al. 2014, Sudek et al. 2015, Nagarkar et al. 2018). Although potential Syn nitrate or iron limitation (Landry & Kirchman 2002), could be alleviated by upwelling, the cold temperatures associated with upwelling waters can also limit Syn growth (Collier & Palenik 2003). The interplay between nutrient availability and optimum growth temperatures could explain why Syn abundance in the nearshore peaks in the fall when upwelling has lessened. For example, (Paerl et al. 2011) reported that Syn peaked in the fall because of the combination of increasing sea surface temperatures and decreased mixing, in what they termed the coastal transition. The transition region, however, would be expected to have a more stable water column, with warmer waters and residual nutrients transported there by Ekman transport, and this could explain the summer Syn peak in this region. In the offshore region, a spring peak in Syn may be supported by nutrient exported

from the nearshore in offshore propagating filaments of upwelled water, whereas a winter peak may be fueled by local mixing. In the offshore region, both PEuk and Syn abundances may be controlled by similar processes, whereas in the summer and fall, grazing pressure or susceptibility to virus infection may limit abundance (Bec et al. 2005, Massana 2011).

1.4.1.2 Picoplankton community shifts along CalCOFI Line 80 consistent with PDO phase shift

The sCCS was expected to be in an upwelling regime between 2007-2012 due to the strongly positive NPGO values (Miller et al. 2015). Whereas from 2014 through 2017, the Pacific Decadal Oscillation (PDO) index (Mantua et al. 1997) was at its highest positive, warm phase, values since 1997. Positive PDO condition are similar to El Niño conditions in the region, with decreased transport of PSUW from the north and increased input of PEW along the coast, from the south. Water mass designations are to be consistent with Bograd et al., (2019), who showed that the contribution of PSUW to Line 80, station 80 has decreased since 2013, consistent with positive PDO values. The excessively warm sea surface temperature (SST) anomalies during this time in the eastern North Pacific Ocean, may have contributed to the high positive PDO values observed (Appendix Figure S1.1b). Additionally, the Oceanic Niño Index (ONI), indicated a strong El Niño in 2016 of a similar magnitude to that in 1997-1998, although its direct impact on the sCCS appears to have been muted compared to the 1997-1998 event (Jacox et al. 2016).

Overall, PEuk and HBac abundances were lower offshore beginning in 2014 and increased nearshore. This shoreward shift of PEuk abundance may have important implications for food web dynamics because PEuk populations could play an outsized role in

trophic transfer (Worden et al. 2004). Our data also showed an increase in Syn abundances during the warm anomaly in 2014. Some studies have shown that Syn growth rates increase in warmer seawater (Agawin et al. 1998) and this could explain the observed trend in our timeseries. Because Syn and PEuk populations tended to exhibit similar trends and are correlated (Appendix Figure S1.4) the results are consistent with increasing oligotrophic conditions throughout the region beginning in 2014. Such a finding is supported by the observed timeseries of Pro, which increased in the offshore during the same time period as well. In line with other studies (Saito et al. 2005), Syn abundances decreased during El Niño conditions and were outpaced by Pro abundances in the transition and offshore regions.

Pro abundances offshore and in the transition increased over the course of the time series (Figures 1.2b and 1.3d). Summer peaks in Pro abundances in the offshore could be linked to increased stratification and low new production (Olson et al. 1990, Bustillos-Guzman et al. 1995, Lindell & Post 1995). Similar to Linacre et al. (2010), Pro abundances were likely too scarce to count in the nearshore region, leading to values close to or equal to zero.

Ecotypes of Pro and Syn were not assessed, but many studies have indicated that ecotypes are spatially (Paerl et al. 2011, Tai et al. 2011) and temporally (Tai & Palenik 2009, Paerl et al. 2011) conserved. Global niche modeling predicts an increase in both Syn and Pro abundances in response to climate changes, with particular emphasis on forcing from sea surface temperature and increased stratification (Flombaum et al. 2013). Observed increases of Pro abundance during the warm anomaly may signify an overall shift in picoplankton communities in response to repeated warm and stratified upper ocean conditions. The sustained increase in Pro abundances through the end of 2017, and the prolonged shore-ward

shift of HBac and PEuk abundances, require continued monitoring to assess if this represents a regime shift or a temporary response.

1.4.1.3 Regional Comparison of CalCOFI Line 80 and CCE LTER

A direct comparison of CCE-LTER data with CalCOFI data identified significant differences between the programs that could sometimes be explained by the design of the CCE-LTER cruise and at other times likely reflected by the inherent, short-term variability in the climatology and hydrography of each region. For example, mesoscale features such as filaments, fronts, and eddies are common and often targeted by CCE-LTER cruises (Ohman et al. 2012, Samo et al. 2012, Taylor et al. 2012, Ohman et al. 2013, Nagai et al. 2015). Our comparison of these datasets confirmed that hydrographic properties are likely a better aggregate variable than strict geographic boundaries for timeseries comparisons in the CCE because biomes are relatively fluid (Hayward & Venrick 1998, Mantyla et al. 2008), especially in the nearshore and transition region.

The differential response of HBac, PEuk, Syn, and Pro between cruises also suggested that the different microbial food web components responded to changes on different timescales. Yet, often when Hbac was significantly different between programs, Pro was also significantly different (although not in the same manner), whereas Syn and PEuk were more likely to exhibit similar patterns. In general, the 2017 CCE-LTER cruise was the least representative of the corresponding CalCOFI data by region. Only one nearshore PEuk depth profile was not statistically different between the two programs (Appendix Table S1.6). These cruises were the least contemporaneous, and so, higher variability was attributed to this temporal offset. The datasets from 2014 showed the least variability between programs. This

may be due to the fact that submesoscale variability had been significantly reduced due to the strongly stratified conditions that prevailed in the sCCS during both the CCE-LTER and CalCOFI cruises in 2014. As such, the 2014 data from the CCE-LTER cruise are likely representative of the biogeochemical response of the sCCS to warm anomaly events. During 2016, the most variability was encountered in the nearshore. The CalCOFI cruise captured conditions more typical of the El Niño whereas the CCE-LTER cruise encountered a system in recovery, with a productive ecosystem. For example, the CCE-LTER cruise detected higher abundances of PEuk in both the nearshore and transition regions, and high Hbac and Syn abundances in the nearshore (Appendix Figures S1.15-S1.18). Although different from the response observed in the CalCOFI data, the nearshore 2016 data from the CCE-LTER cruise provide the opportunity to examine the response of the picoplankton community to nutrient inputs following a period of prolonged upper ocean warming and stratification. Overall, the picoplankton community sampled during the 2016 CCE-LTER cruise appeared to respond rapidly to upwelling in the nearshore region, which may have identified a phytoplankton community response that paralleled observations for zooplankton, where warm water species that had been transported into the region during the 2014-2015 warm anomaly, persisted and flourished when upwelling conditions returned to normal (Peterson et al. 2017). The persistence of a picoautotrophic dominated phytoplankton community was consistent with the 10 m anomaly time series data which showed that Syn and PEuk abundances in the nearshore region increased between 2013-2017 (Figure 1.3) following the return of the positive PDO phase. These communities also appeared to have a unique impact on the overall microbial community as discussed in Section 1.4.2.

1.4.2 Top-down controls of picoplankton and testing of the enhanced microbial loop

Our extended timeseries for the region confirmed previous observations of the relationship between picoplankton abundance (biomass in the caser of previous studies; (Goericke 2011, Taylor & Landry 2018) and Chl. Even though abundance and not biomass was used, peaks in abundance occurred at very similar Chl values to those previously reported for picoplankton biomass (e.g., Taylor & Landry 2018) and then continued to decrease or maintain at higher Chl. The modeled fits proposed by Goericke (2011) mirror the relationship plotted here for all groups (Figure 1.4).

One important goal of this study was to ensure that CCE-LTER data fit within the CalCOFI framework. Good agreement for Syn and PEuk patterns with Chl concentrations between CalCOFI and CCE-LTER datasets were found, and although Pro and HBac abundances showed comparable patterns across both datasets, their abundance-Chl concentration relationship was the most variable. However, this may be an artifact of the limited collection period for CCE-LTER data used in this study. For example, the 10 m abundances of Pro and Hbac are greater during the latter part of the CalCOFI timeseries (Figures 1.2a,b and 1.3c,d) and 50% of our CCE-LTER dataset was collected during that time period.

Studies in the sCCS (Goericke 2011, Nagarkar et al. 2018, Taylor & Landry 2018) have demonstrated that the picoplankton mean* abundance in the nearshore is effectively controlled by microzooplankton grazing. The hypothesis, coined the enhanced microbial loop by Taylor and Landry (2018), states that in the nearshore region, an increase in heterotrophic bacterial abundance catalyzed by DOC release from growing autotrophic biomass, increases the grazing response by microzooplankton, which consume plankton in the pico size class

with little selectivity. In support of this hypothesis, HBac abundances were significantly positively correlated with the sum of Pro, Syn, and PEuk abundances (Appendix Figure S1.9) that was maintained across all regions and seasons (Appendix Figure S1.10).

Another goal of this work was to identify ways in which the process-oriented studies conducted through the CCE-LTER program, could provide mechanistic insights into the larger dataset available through the CalCOFI timeseries. For example, bacterial production (BP) was measured during some CCE-LTER cruises, but not CalCOFI cruises. If heterotrophic bacteria are assumed take up carbon at the rate that it is released by phytoplankton then it would suggest that BP is an underlying driver of the enhanced microbial loop (Goericke 2011, Taylor & Landry 2018). During P1604 and P1706, both BP and picoplankton abundance were measured on the same samples. Based on our previous discussions, the spatial distribution of the P1706 response was more typical for the region, whereas during P1604 picoplankton and HBac abundance in the nearshore region was significantly elevated relative to Chl and POC concentrations compared to P1706.

The Syn populations reached higher abundances at the same Chl concentration in 2016 than in 2017. BP, however, continued to increase with Chl in 2016 despite a slow-down in Syn and PEuk growth (Figure 1.5). Both of these observations suggested that nonselective grazing on the picoplakton size class may not have been the dominant mortality process. Based on relationships to BP, we instead propose that in 2016 viral lysis of *Synechococcus* may have played an important role, primarily in the nearshore. Such a mechanism would also explain the potential continued supply of DOC to maintain BP (Suttle 2007) in the absence of large autotrophs. Studies have suggested that cyanophages that target specific strains of Syn require a specific host density before they begin to propagate (Suttle & Chan 1994), and this

threshold may have been reached in the sCCS nearshore during the 2016 CCE-LTER cruise. Passive or active release of DOC from picoplankton would be consistent with recent reports of DOC production by picoautotrophs (Zhao et al. 2017, Organelli & Claustre 2019). Overall, in 2017, BP provided added evidence in support of the role of enhanced bacterial activity in catalyzing the growth of microzooplankton grazers particularly at the higher Chl concentrations reached during P1706, that then impacted the abundance of both heterotrophic bacteria and autotrophic picoplankton. However, coastal upwelling following prolonged upper ocean warming in 2016, elicited what appeared to be a different relationship between HBac and picoeukaryotes, particularly in the nearshore, suggesting a shift in the microbial loop hypothesis where viral lysis may have impacted Syn populations while potentially enhancing HBac.

1.4.3 Bottom-up controls of heterotrophic bacterial abundance in the CCE

Significant positive correlations between bacterial abundance and Chl, NPP, TOC, POC, and DOC were observed throughout the sCCS (Figure 1.7). However, most of these relationships have relatively low explanatory power. The HBac abundance was strongly correlated with POC concentration. This result could be driven by particles acting as hot spots for microbial growth and reproduction (Paerl 1975, Ploug & Grossart 1999, Ploug et al. 1999, Grossart & Ploug 2001) and because POC is likely a good proxy for the freshly available organic matter that is necessary for supporting bacterial growth. For example, labile DOC accumulation in the nearshore region can lag NPP because upwelling contributes a high background of refractory DOC to the upper ocean (Halewood et al. 2012, Stephens et al.

2018), making suspended POC concentration a more reliable indicator of new organic matter production in marine environments.

The nearshore generally had the strongest correlations indicating that a greater proportion of the organic pool, potentially derived from local NPP, was either unavailable to heterotrophic bacteria or that bacterial activity was being limited in the offshore and transition regions. Interestingly, the slope of the relationships in the nearshore varied between years (Figure 1.7a-e, panels III), suggesting that the flux of carbon through heterotrophic bacteria could not be easily predicted or inferred based on these relationships.

1.5. CONCLUSIONS

The California Current System (CCS) is a dynamic Eastern boundary, which can complicate timeseries studies. However, the presence of two long term research programs the California Cooperative Oceanic Fisheries Investigations (CalCOFI) survey program and the California Current Ecosystem Long Term Ecological Research (CCE-LTER) program also make the area one of the most well-studied in the ocean. In this study, we propose a framework to combine the data from both programs to strengthen the interpretations that can be made from either dataset alone. Our results support the use of hydrographic properties - nitracline, Chl max, and EZ depths - as defining variables for binning data from each program into subregions. By observing the biological response of the picoplankton community, which responds quickly to changing ocean conditions, we provide further support for this classification scheme. Temporal variations in the abundance of picoplankton showed a consistent shift in regional distributions following the 2014 warm anomaly and the switch to a positive PDO phase. This year also stood out because it showed the closest agreement

between sampling programs indicating that submesocale variations were muted in the region as a result of the widespread upper ocean warming and associated stratification. Moreover, we were also able to further examine potential controls on picoplankton abundance in the nearshore by utilizing CCE-LTER data to test the enhanced microbial loop hypothesis derived from CalCOFI data. We propose using hydrographic properties to classify future CCE-LTER cruise cycles for retrospective analysis involving CalCOFI datasets.

1.6 ACKNOWLEDGEMENTS

Chapter 1, in part, is currently being prepared for submission for publication of the material. Rivera, S. R.; Goericke, R.; Stephens, B. M.; Dovel, S.; Roadman, M.; Kahru, M.; Landry, M. R.; Aluwihare, L. I.. The dissertation author was the primary investigator and author of this material.

1.7 FIGURES AND TABLES

Figure 1.1: Seasonality of microbial abundance measured along CalCOFI Line 80 by oceanic region

Estimated marginal means (a) and estimated marginal trends (b) of CalCOFI Line 80 by season (spring =Sp, summer = Su, fall = Fa, winter = Wi, grey shading) for heterotrophic bacteria (I-III), *Prochlorococcus* (IV-VI), *Synechococcus* (VII-IX), and picoeukaryotes (X-XII). Different italic letters (*a-c*) designate significantly ($p < 0.05$) different seasonal means (a) or slopes (b) by region.

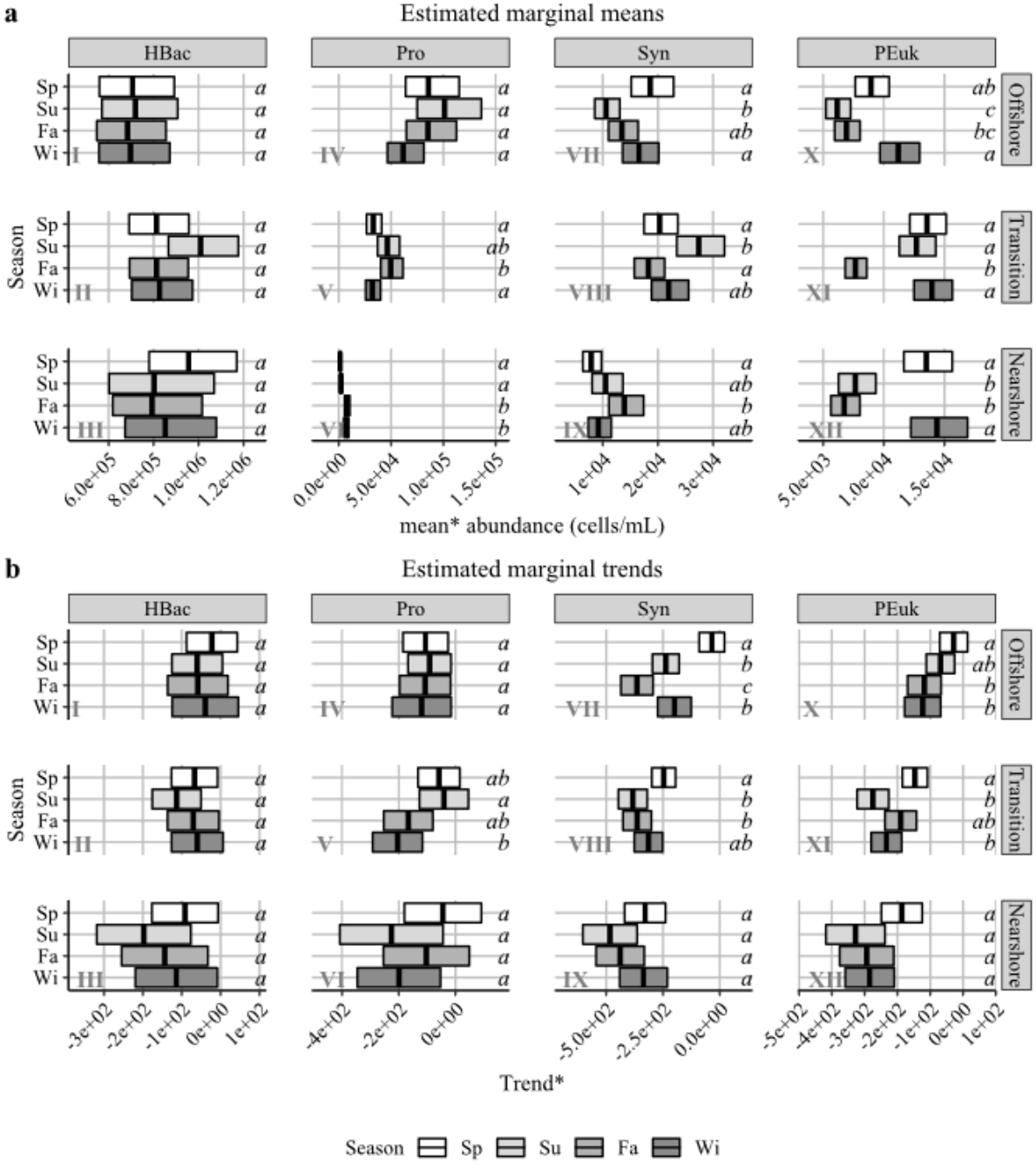
a
Estimated marginal means
HBac
Pro
Syn
PEuk
Offshore
Transition
Nearshore
Season
Sp
Su
Fa
Wi
I
II
III
IV
V
VI
VII
VIII
IX
X
XI
XII
mean* abundance (cells/mL)
b
Estimated marginal trends
Trend*
Season Sp Su Fa Wi

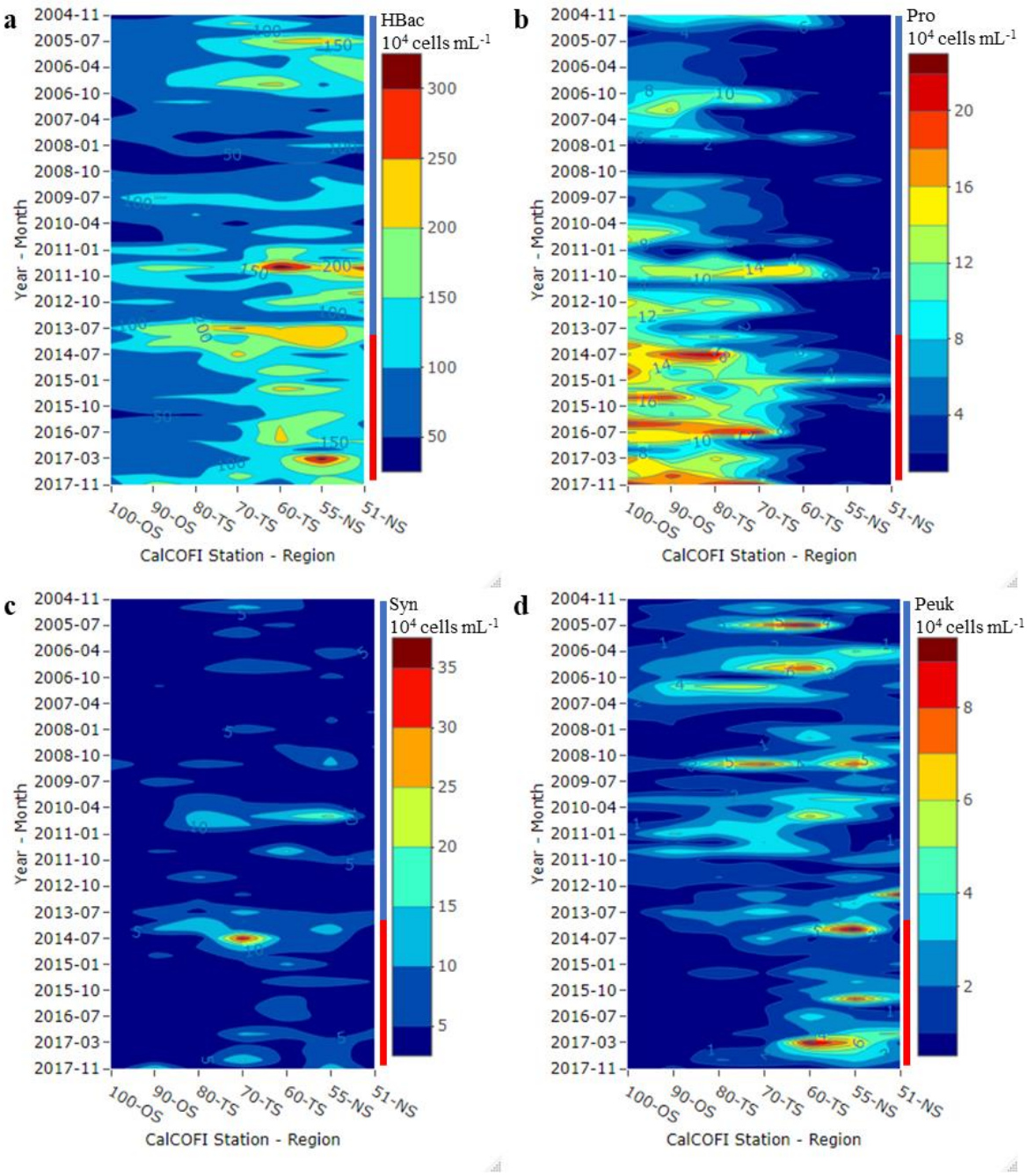

Figure 1.2: Temporal and spatial trends of HBac, Pro, Syn, and PEuk at 10m

Data from 10m depths across CalCOFI Line 80 for HBac (a), Pro (b), Syn (c), and PEuk (d) abundances. The thin bar between the plot and the legend corresponds to the PDO phase with blue representing the negative, "cool" phase and red representing the positive, "warm" phase.

Figure 1.3: 10m cube root anomalies with PDO phase (1/2)

Cube root anomalies of Chl (a), nitrate (b), HBac (c), Pro (d), Syn (e), and PEuk (f) concentrations along Line 80 from nearshore (NS, stations 51 and 55), through the transition (TS, stations 60, 70, and 80), to the offshore (OS, stations 90 and 100) from November 2014 through November 2017. Zero values of Pro abundance were removed prior to transformation. The thin bar between the plot and the legend corresponds to the PDO phase with blue representing the negative, “cool” phase and red representing the positive, “warm” phase.

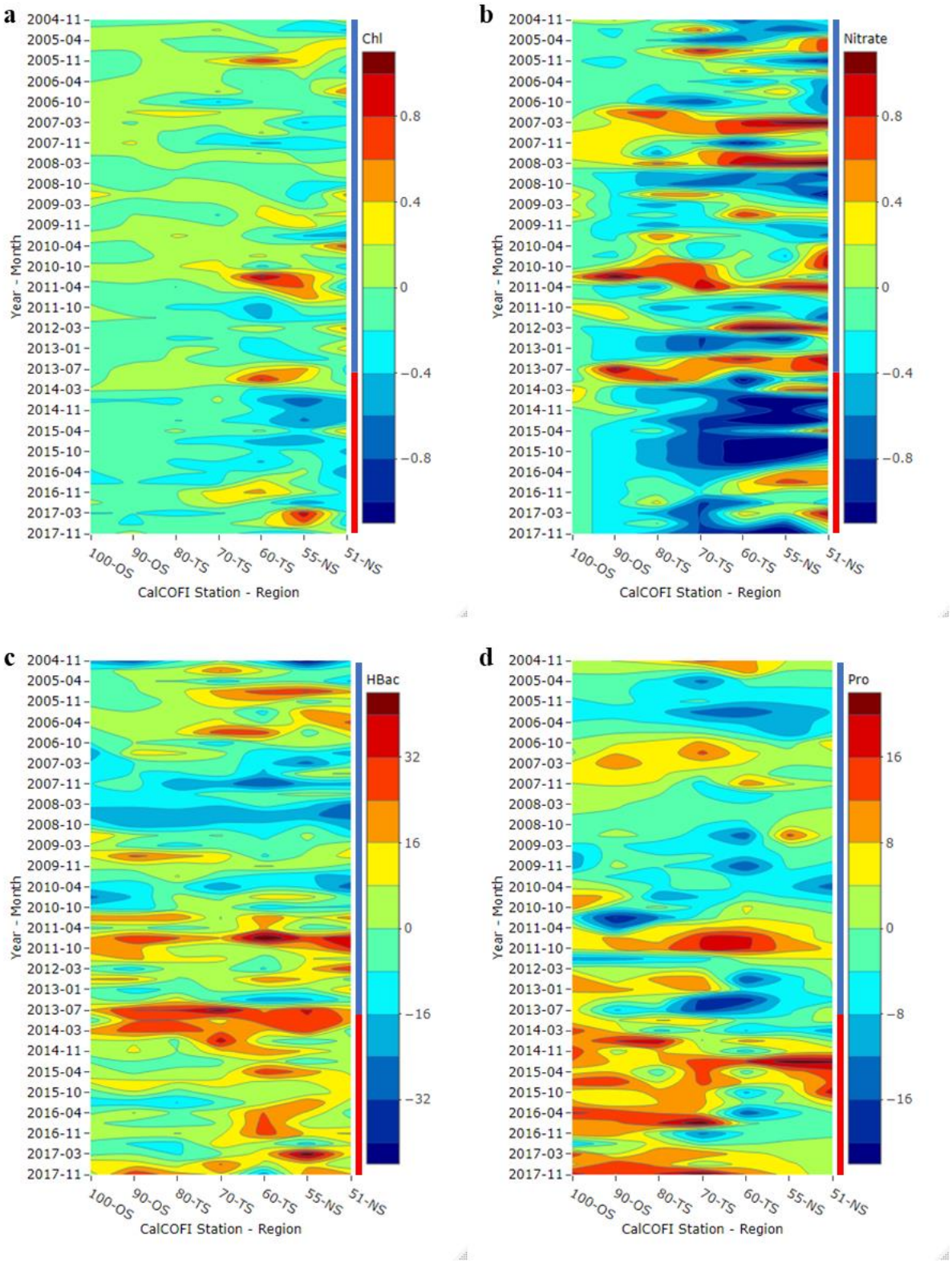
a
Chl
0.8
0.4
0
−0.4
−0.8
b
Nitrate
0.8
0.4
0
−0.4
−0.8
c
HBac
32
16
0
−16
−32
d
Pro
16
8
0
−8
−16
Year - Month
2004-11
2005-04
2005-11
2006-04
2006-10
2007-03
2007-11
2008-03
2008-10
2009-03
2009-11
2010-04
2010-10
2011-04
2011-10
2012-03
2013-01
2013-07
2014-03
2014-11
2015-04
2015-10
2016-04
2016-11
2017-03
2017-11
100-OS
90-OS
80-TS
70-TS
60-TS
55-NS
51-NS
CalCOFI Station - Region

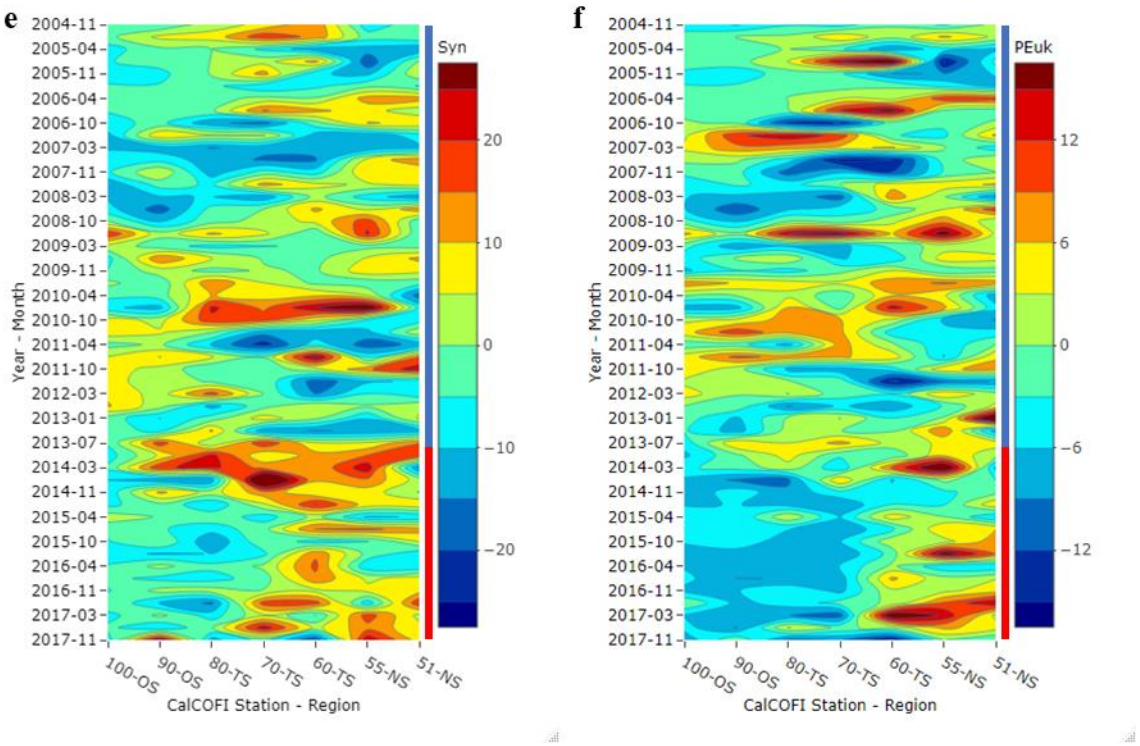

Figure 1.3: 10m cube root anomalies with PDO phase (continued, 2/2)

Cube root anomalies of Chl (a), nitrate (b), HBac (c), Pro (d), Syn (e), and PEuk (f) concentrations along Line 80 from nearshore (NS, stations 51 and 55), through the transition (TS, stations 60, 70, and 80), to the offshore (OS, stations 90 and 100) from November 2014 through November 2017. Zero values of Pro abundance were removed prior to transformation. The thin bar between the plot and the legend corresponds to the PDO phase with blue representing the negative, "cool" phase and red representing the positive, "warm" phase.

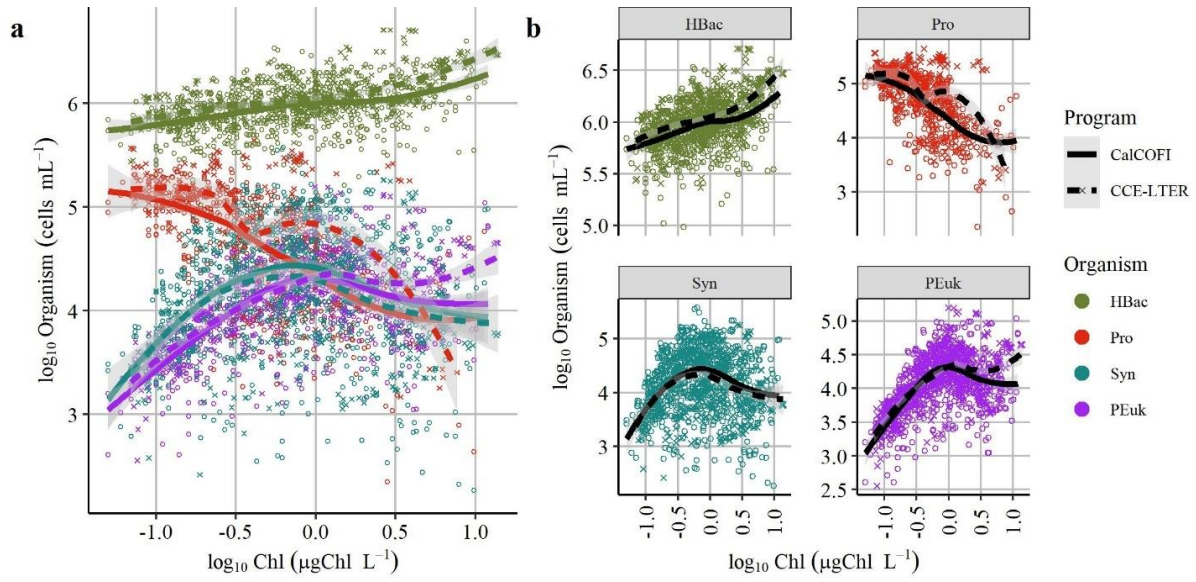

Figure 1.4: Trends of HBac, Pro, Syn, and PEuk abundance with Chl concentration

Trends Chl concentrations *vs* HBac (pink), Pro (green), Syn (blue), and PEuk (purple) abundances from the top 30m for both CalCOFI (solid lines) and CCE-LTER (dashed lines) programs. Zero values of Pro were removed prior to log transformation.

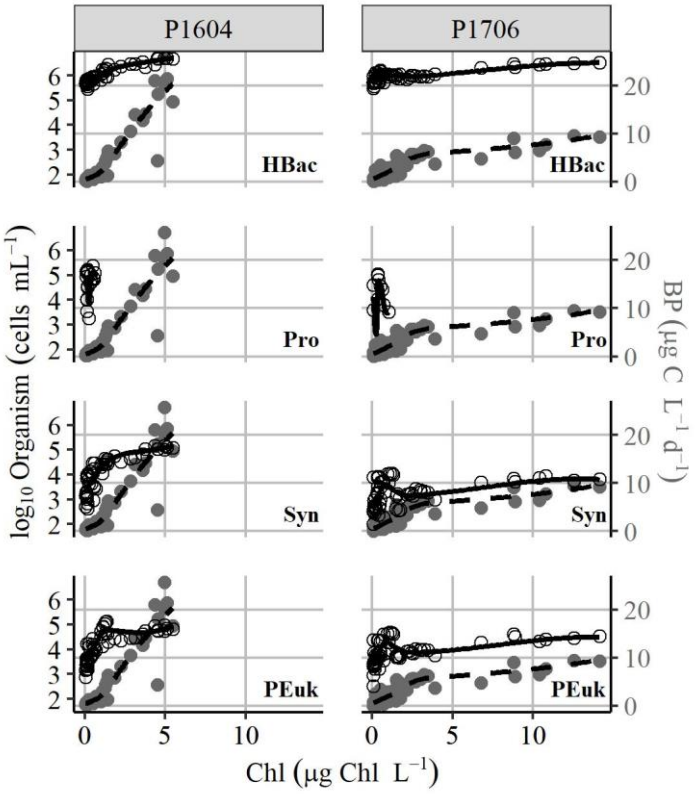

Figure 1.5: Increasing chlorophyll concentration led to an increase in BP and picoplankton

Trends of Chl concentration with HBac, Pro, Syn, and PEuk (open circles) and BP (closed circles) with plotted trend lines (picoplankton- solid, BP- dashed). Zero values of Pro were removed prior to log transformation.

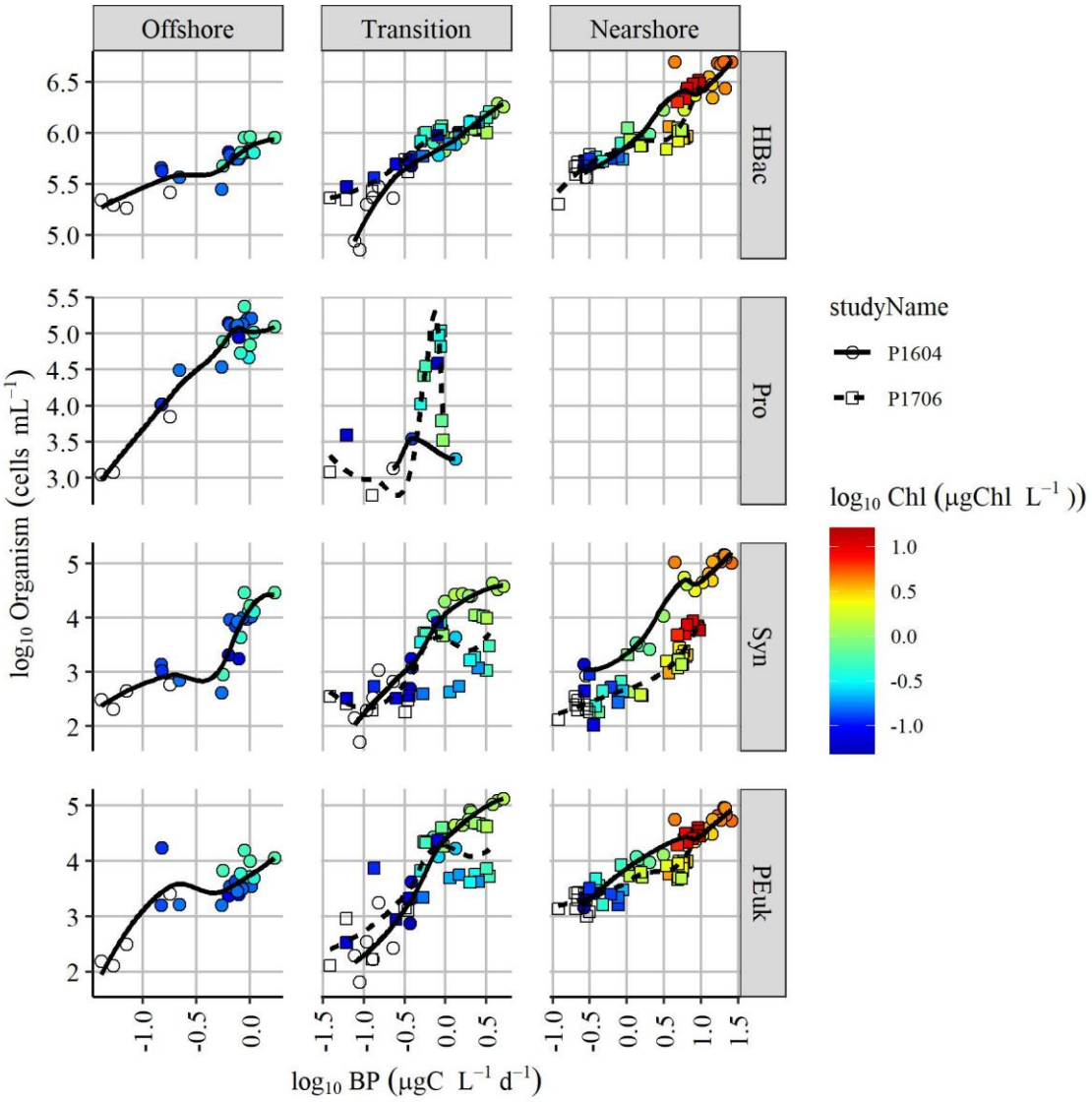

Figure 1.6: Trends of BP and picoplankton with Chl

Trends of BP *vs* HBac, Pro, Syn, or PEuk abundance, colored by Chl concentration for 2016 (P1604) and 2017 (P1706). Zero values of Pro were removed prior to log transformation.

Figure 1.7: Relationships of phytoplankton and organic carbon pools to bacteria abundance in the sCCS

The linear relationships of phytoplankton properties (Chl a and PP) and organic carbon pools (TOC, POC, and DOC) to bacterial abundance (HBac) by FCM for each region of the sCCS with CalCOFI cruise data plotted in grey and CCE-LTER data plotted in blue (normal years) or red (warm years). All are significant ($p<0.05$) except the relationship between offshore DOC and BA (e, I, $p=0.17$).

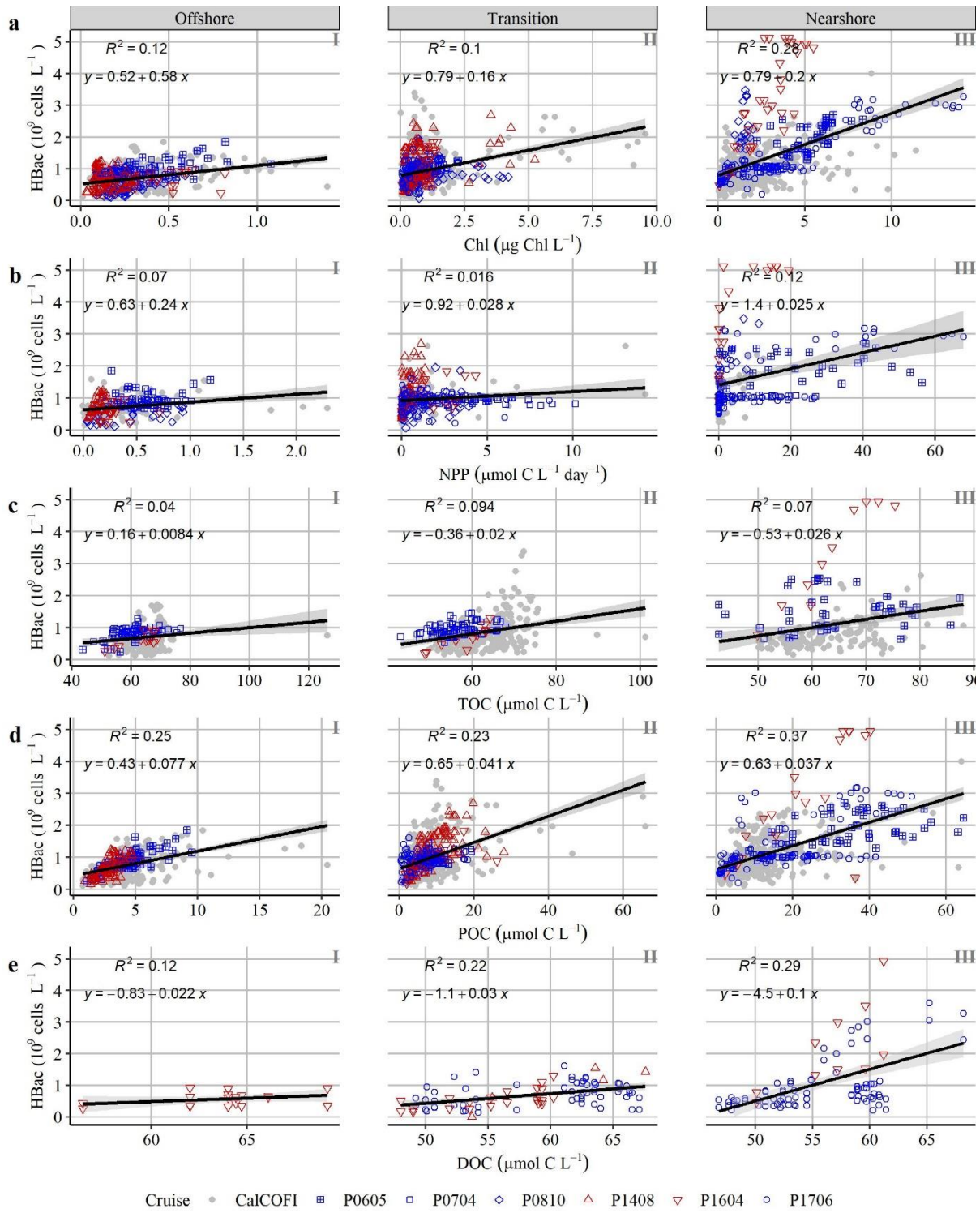
a
Offshore
Transition
Nearshore
I
II
III
R^2 = 0.12
y = 0.52 + 0.58 x
R^2 = 0.1
y = 0.79 + 0.16 x
R^2 = 0.28
y = 0.79 + 0.2 x
HBac (10^9 cells L^{-1})
Chl (µg Chl L^{-1})
b
R^2 = 0.07
y = 0.63 + 0.24 x
R^2 = 0.016
y = 0.92 + 0.028 x
R^2 = 0.12
y = 1.4 + 0.025 x
NPP (µmol C L^{-1} day^{-1})
c
R^2 = 0.04
y = 0.16 + 0.0084 x
R^2 = 0.094
y = −0.36 + 0.02 x
R^2 = 0.07
y = −0.53 + 0.026 x
TOC (µmol C L^{-1})
d
R^2 = 0.25
y = 0.43 + 0.077 x
R^2 = 0.23
y = 0.65 + 0.041 x
R^2 = 0.37
y = 0.63 + 0.037 x
POC (µmol C L^{-1})
e
R^2 = 0.12
y = −0.83 + 0.022 x
R^2 = 0.22
y = −1.1 + 0.03 x
R^2 = 0.29
y = −4.5 + 0.1 x
DOC (µmol C L^{-1})
Cruise
CalCOFI
P0605
P0704
P0810
P1408
P1604
P1706

Table 1.1: Mean hydrographic depths and euphotic zone integrated biogeochemical values for the oceanic regions by program

Mean biogeochemical parameters integrated over the euphotic zone (1% surface irradiance) depth plus/minus the standard error.

Region	Program	Nitracline	Chl max	Euphotic Zone	NPP	Chl	POC	TOC
		m			mmol C m^{-2} d^{-1}	mg Chl m^{-2}	mmol C m^{-2}	
Offshore	CCE-LTER	72 ± 5, N = 9	63 ± 7, N = 9	63 ± 4, N = 9	21 ± 43, N = 9	10 ± 1, N = 9	206 ± 14, N = 9	3427 ± 539, N = 3
	CalCOFI	71 ± 3, N = 89	59 ± 2, N = 91	68 ± 3, N = 43	26 ± 4, N = 26	17 ± 1, N = 100	221 ± 10, N = 99	3980 ± 152, N = 23
Transition	CCE-LTER	12 ± 4, N = 12	29 ± 3, N = 12	35 ± 3, N = 12	62 ± 12, N = 12	25 ± 4, N = 12	290 ± 17, N = 12	1638 ± 321, N = 5
	CalCOFI	31 ± 2, N = 141	34 ± 2, N = 140	48 ± 2, N = 72	53 ± 8, N = 42	34 ± 4, N = 153	284 ± 16, N = 153	2581 ± 131, N = 42
Nearshore	CCE-LTER	1 ± 1, N = 7	14 ± 1, N = 7	22 ± 5, N = 7	292 ± 63, N = 7	69 ± 12, N = 7	426 ± 55, N = 7	1070 ± 229, N = 5
	CalCOFI	5 ± 1, N = 96	14 ± 1, N = 96	28 ± 2, N = 35	126 ± 14, N = 14	59 ± 4, N = 104	325 ± 19, N = 104	1602 ± 115, N = 30

1.8 APPENDIX

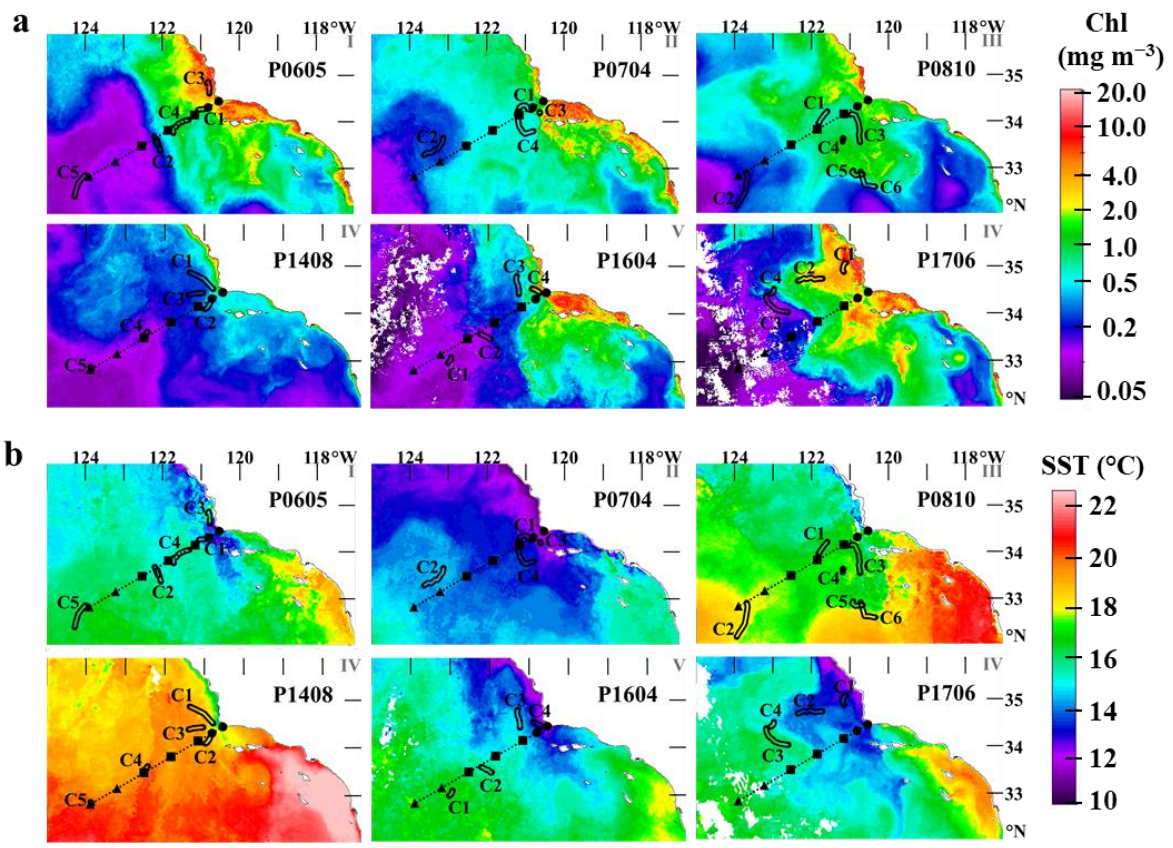

Figure S1.1: Satellite derived Chl concentration and SST with CCE-LTER cycle tracks

Sea surface chlorophyll *a* concentrations (a) and sea surface temperature, SST, (b) from satellite data for all CCE-LTER cruises that are part of this study. Each map (I-IV) is a single CCE-LTER cruise with cycle tracks (open lines) labeled by Cycle number (C#). CalCOFI Line 80 (dashed line) stations are designated for nearshore (circles), transition (squares), and offshore (triangles). P1408 and P1604 are considered "warm" years.

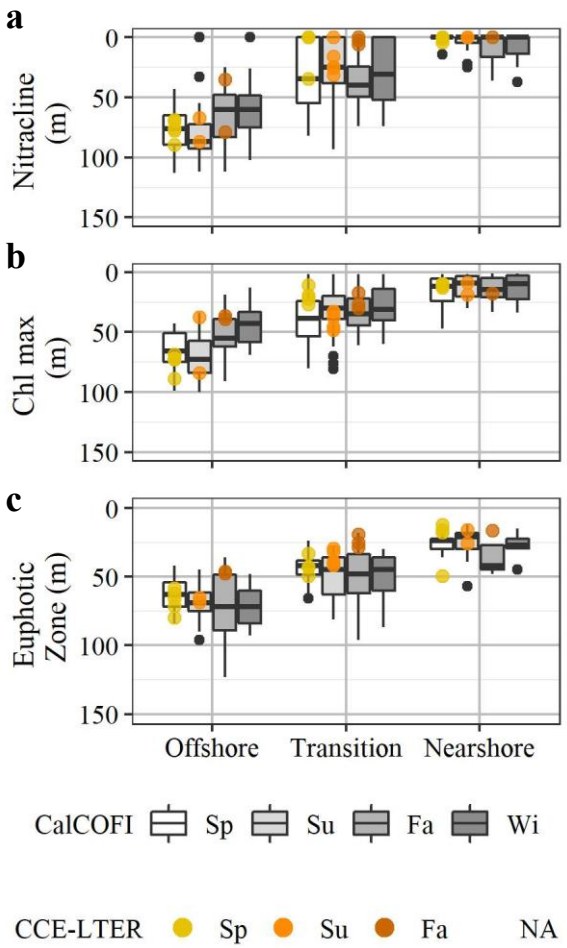

Figure S1.2: CCE-LTER regional classifications with CalCOFI Line 80 hydrography

Box and whisker plots showing the nitracline depth (a), chlorophyll a max depth (b), and euphotic zone depth (c) ranges by season (grey shading, spring=Sp, summer=Su, fall=Fa, winter=Wi) and region (x-axis) across CalCOFI Line 80 with black points designating outliers. The CCE-LTER cruises took place during spring (P0605, P0704, P1604), summer (P1408, P1706), and fall (P0810). Overlying colored points (Sp-yellow, Su-orange, Fa-brown) are the mean cycle values for CCE-LTER cruises.

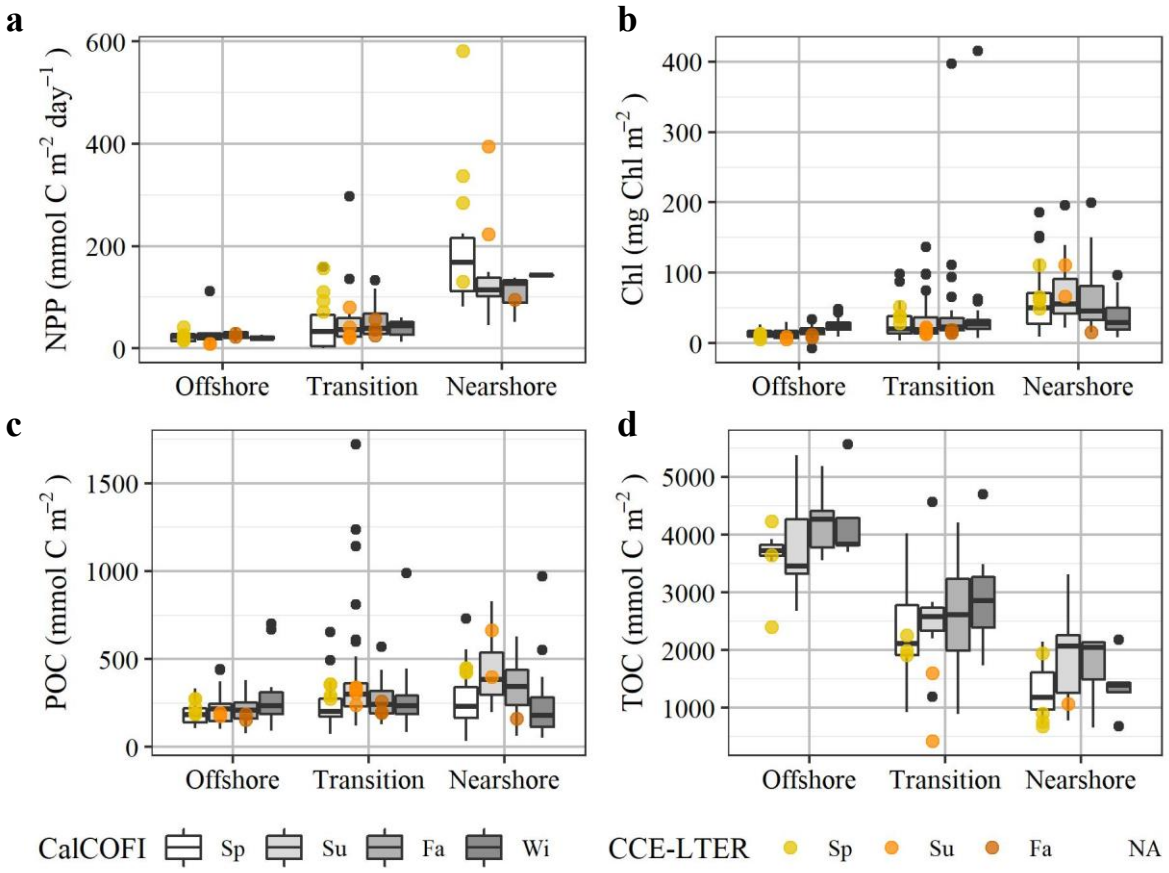

Figure S1.3: Phytoplankton and organic carbon in the sCCS

Box and whisker plots showing net primary production (a), chlorophyll a concentration (b), suspended particulate organic carbon (c) and total organic carbon (d), integrated over the euphotic zone, ranges by season (grey shading, spring=Sp, summer=Su, fall=Fa, winter=Wi) and region (x-axis) across CalCOFI Line 80 with black points designating outliers. The CCE-LTER cruises took place during spring (P0605, P0704, P1604), summer (P1408, P1706), and fall (P0810). Overlying colored points (Sp-yellow, Su-orange, Fa-brown) are the mean integrated cycle values for CCE-LTER cruises.

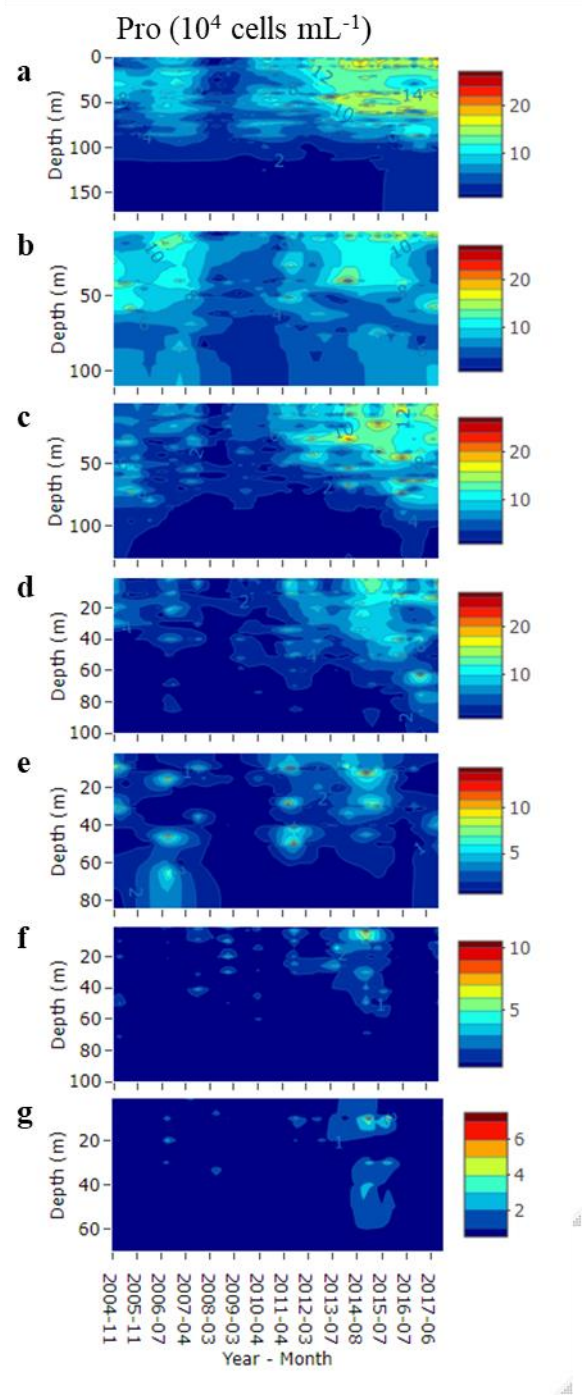

Figure S1.4: Temporal depth profiles of Pro abundance along Line 80

Depth plots of Pro abundance from 2004-2017 along Line 80 at stations 51 (a), 55 (b), 60 (c), 70 (d), 80 (e) ,90 (f), and 100 (g).

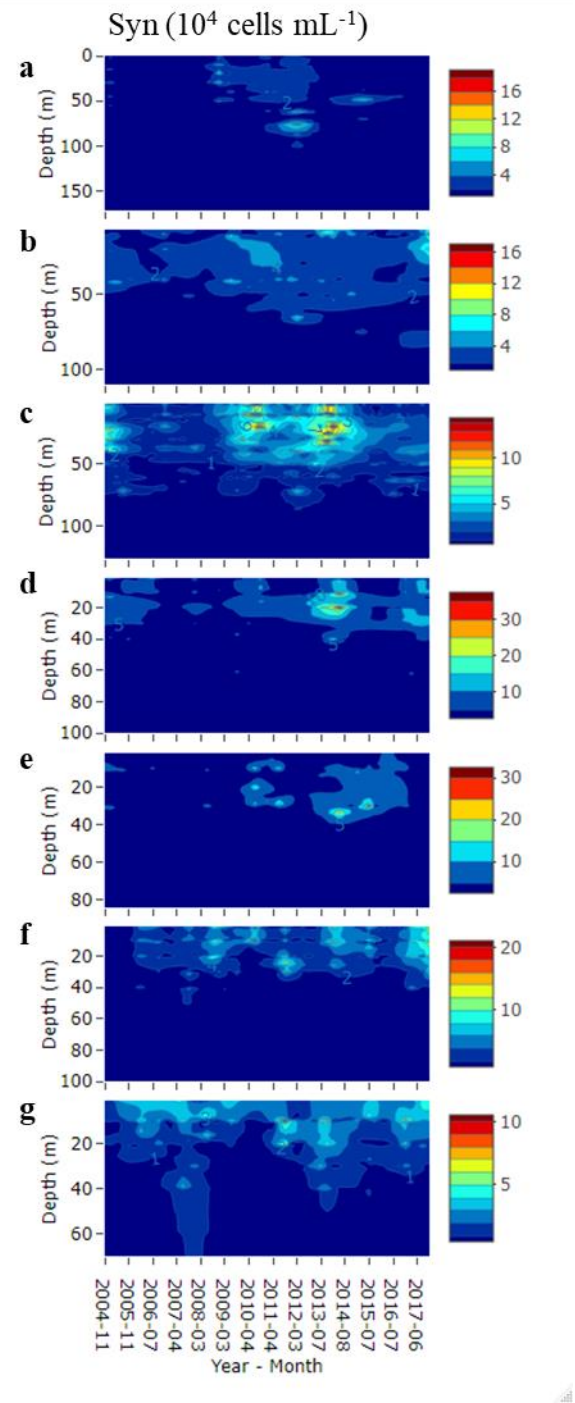

Figure S1.5: Temporal depth profiles of Syn abundance along Line 80

Depth plots of Syn abundance from 2004-2017 along Line 80 at stations 51 (a), 55 (b), 60 (c), 70 (d), 80 (e) ,90 (f), and 100 (g).

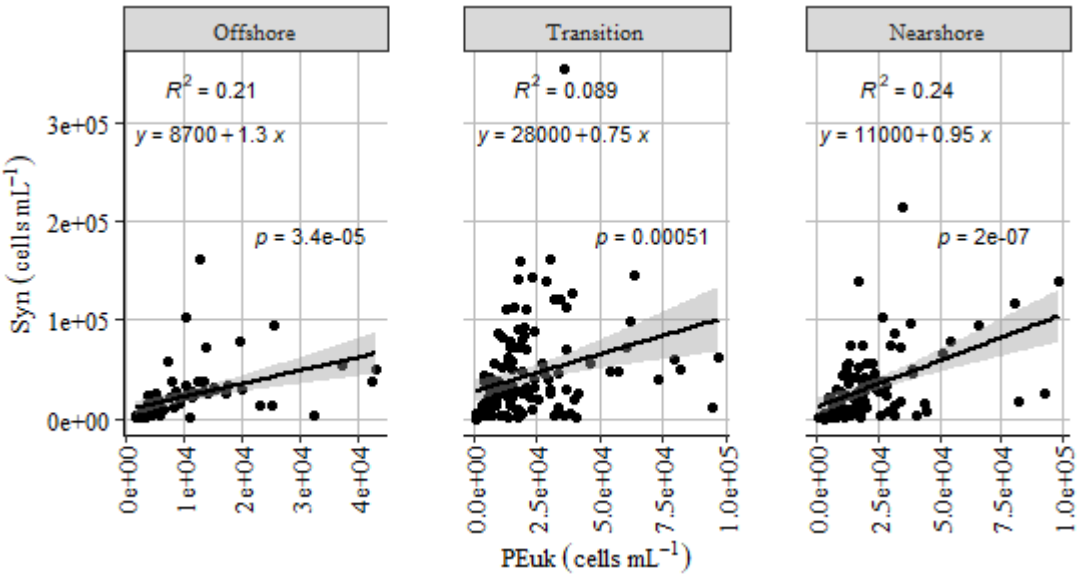

Figure S1.6: Correlation between PEuk and Syn

Linear regression of PEuk abundance *vs* Syn abundance CalCOFI data from 10m depth, grouped by region.

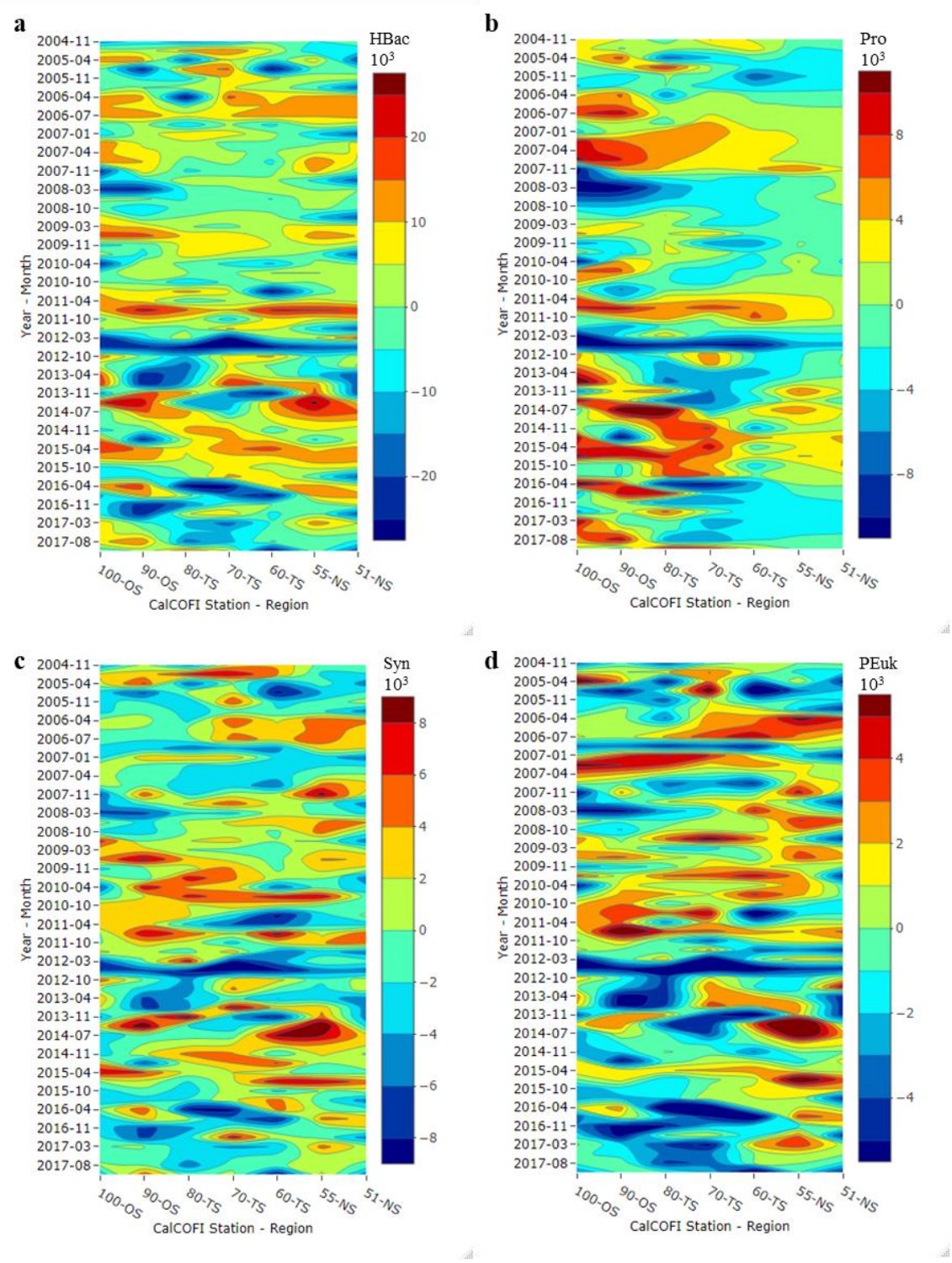

Figure S1.7: EZ integrated cube root anomalies

EZ integrated cube root anomalies calculated from a 2004-2012 mean for HBac (a), Pro (b), Syn (c), and PEuk (d) abundances.

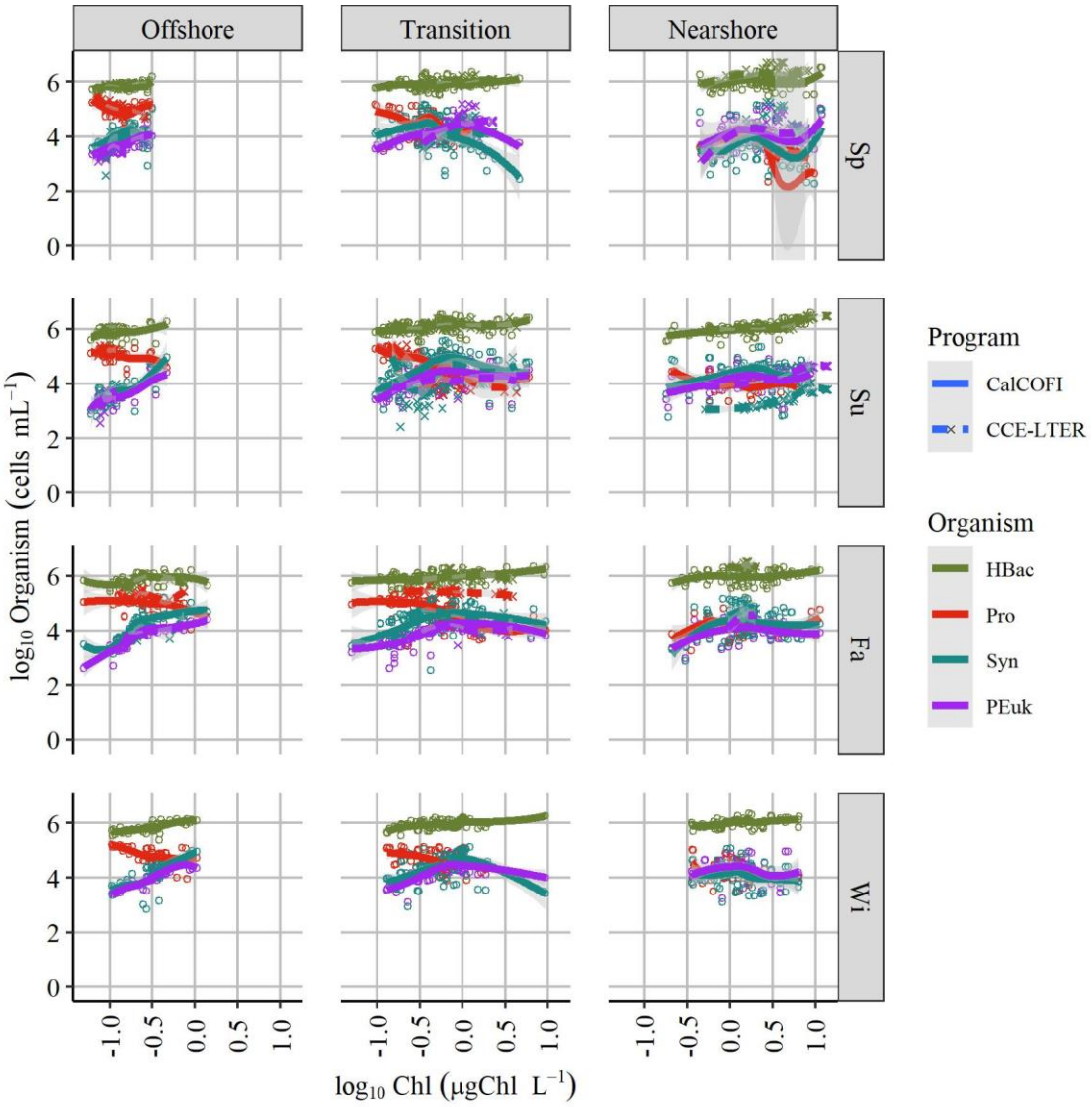

Figure S1.8: Regional and seasonal trends of HBac, Pro, Syn, and PEuk abundance with Chl concentration

Trends Chl concentrations *vs* HBac (pink), Pro (green), Syn (blue), and PEuk (purple) abundances for both CalCOFI (solid lines) and CCE-LTER (dashed lines) programs by region and season.

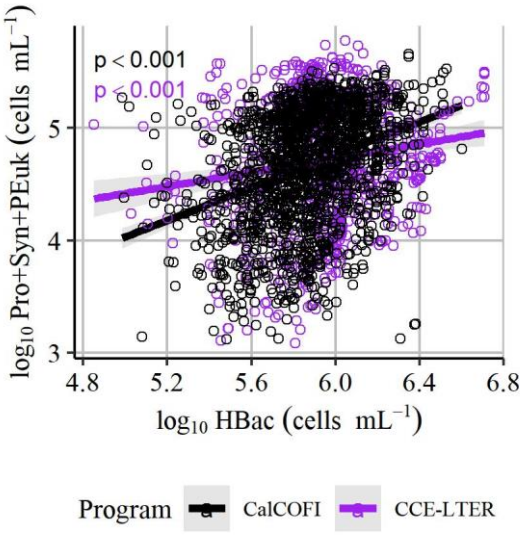

Figure S1.9: Trends of HBac vs picoautotrophic abundances

Linear relationships of HBac *vs* all picoautotrophs (Pro, Syn, and PEuk) abundances for CalCOFI (black) and CCE-LTER (purple) datasets.

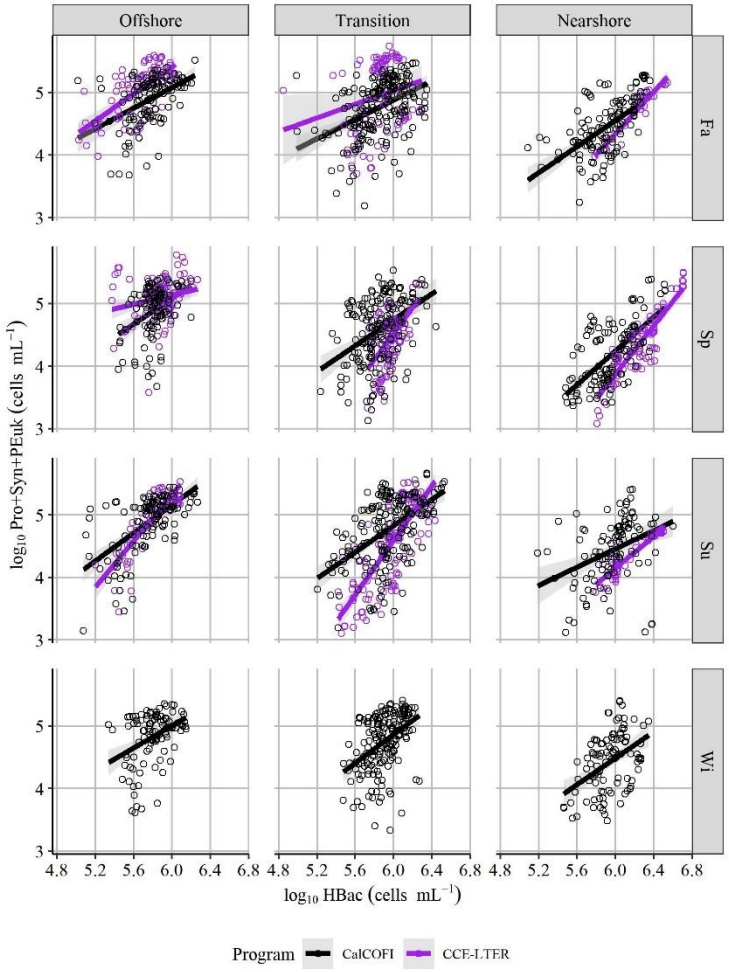

Figure S1.10: Regional and seasonal trends of HBac vs picoautotrophs

Linear relationships of HBac *vs* PEuk abundances for CalCOFI (black) and CCE-LTER (purple) datasets by region and season.

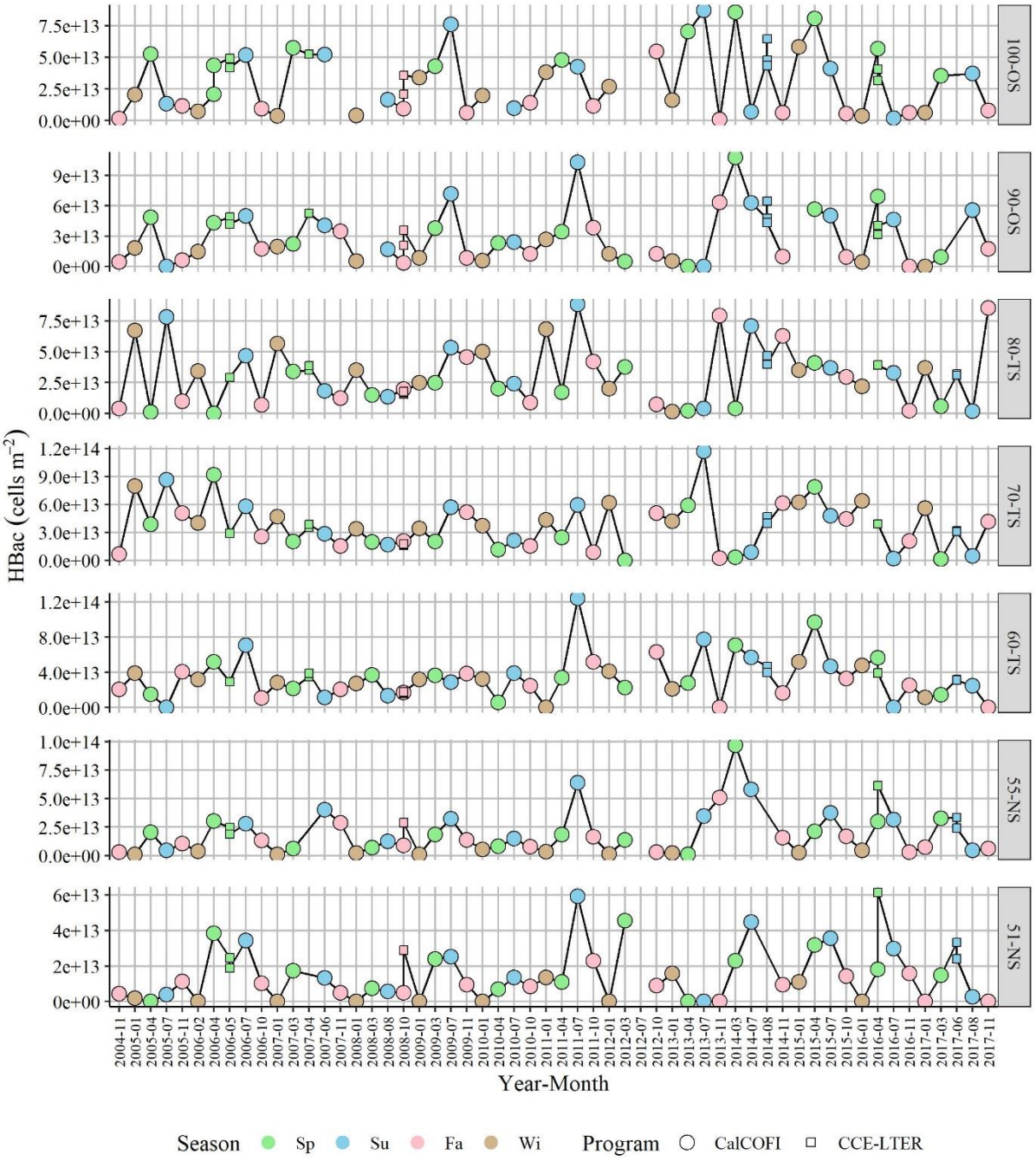

Figure S1.11: CalCOFI and CCE-LTER EZ integrated HBac abundance

CalCOFI cruise data (circles) plotted by station with overlying CCE-LTER data (squares) for the corresponding region (OS = offshore, TS = transition, NS = nearshore), when available. The CCE-LTER data per region is repeated for each CalCOFI station. Colors correspond to season of sampling.

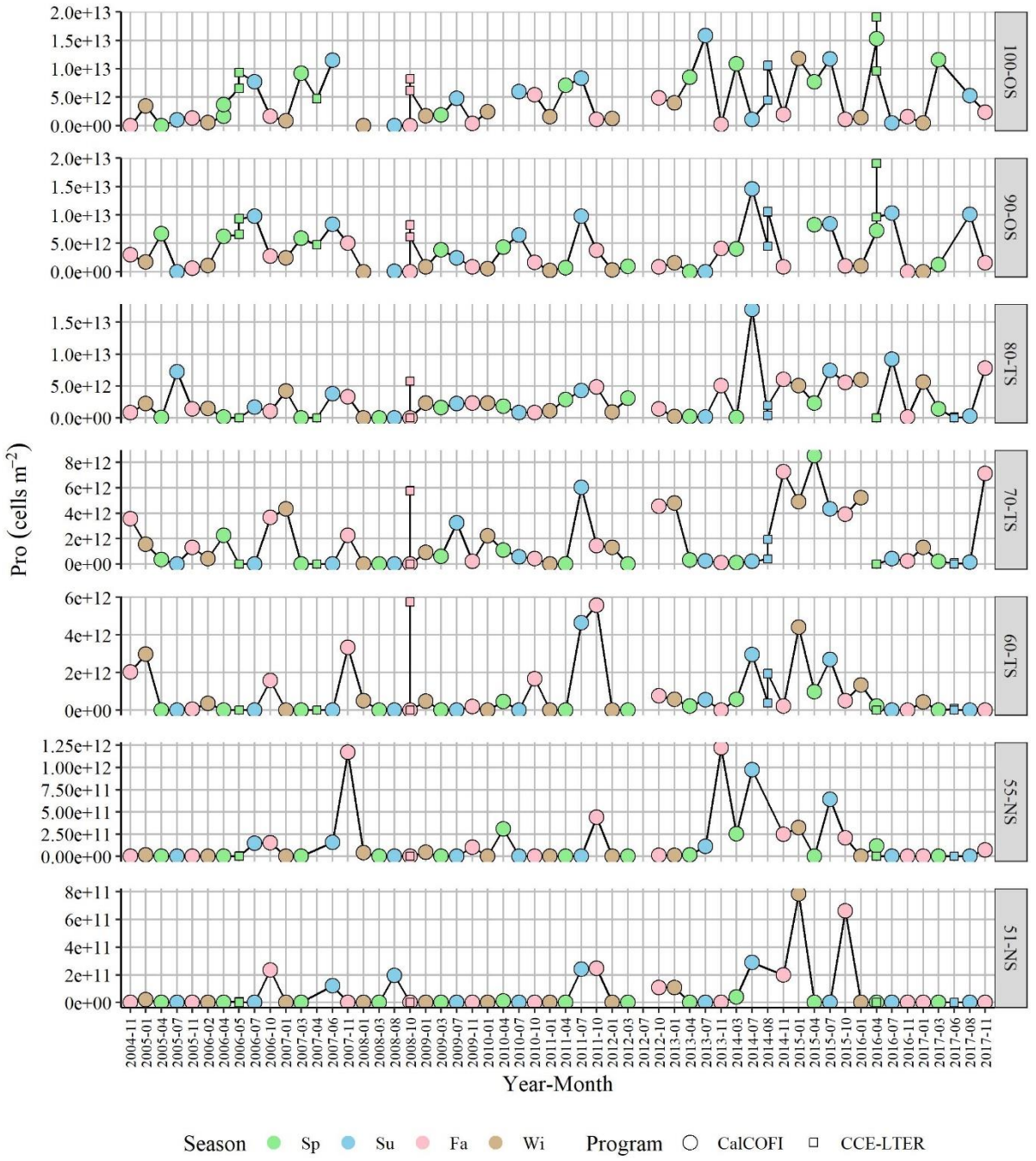

Figure S1.12: CalCOFI and CCE-LTER EZ integrated Pro abundance

CalCOFI cruise data (circles) plotted by station with overlying CCE-LTER data (squares) for the corresponding region (OS = offshore, TS = transition, NS = nearshore), when available. The CCE-LTER data per region is repeated for each CalCOFI station. Colors correspond to season of sampling.

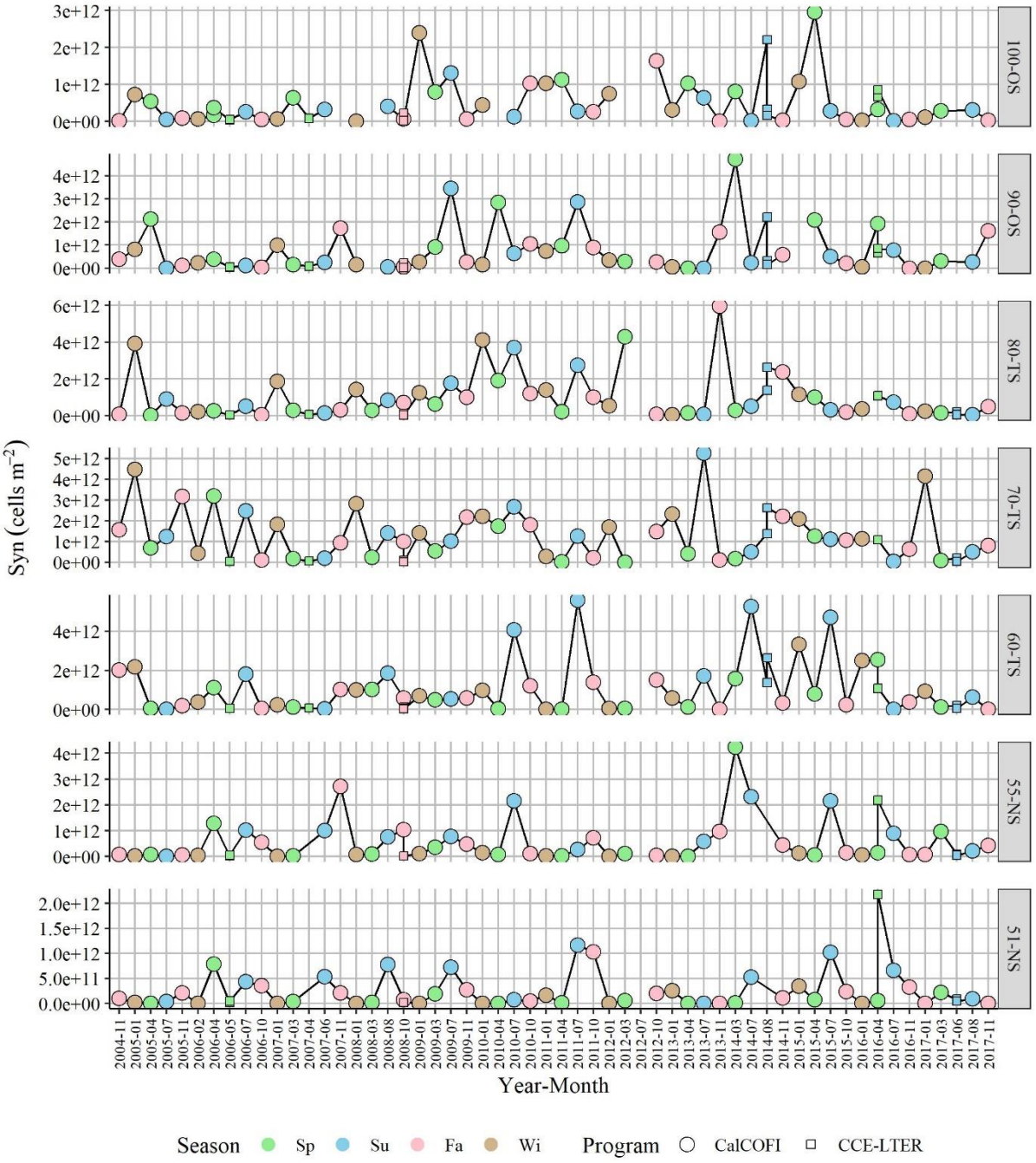

Figure S1.13: CalCOFI and CCE-LTER EZ integrated Syn abundance

CalCOFI cruise data (circles) plotted by station with overlying CCE-LTER data (squares) for the corresponding region (OS = offshore, TS = transition, NS = nearshore), when available. The CCE-LTER data per region is repeated for each CalCOFI station. Colors correspond to season of sampling.

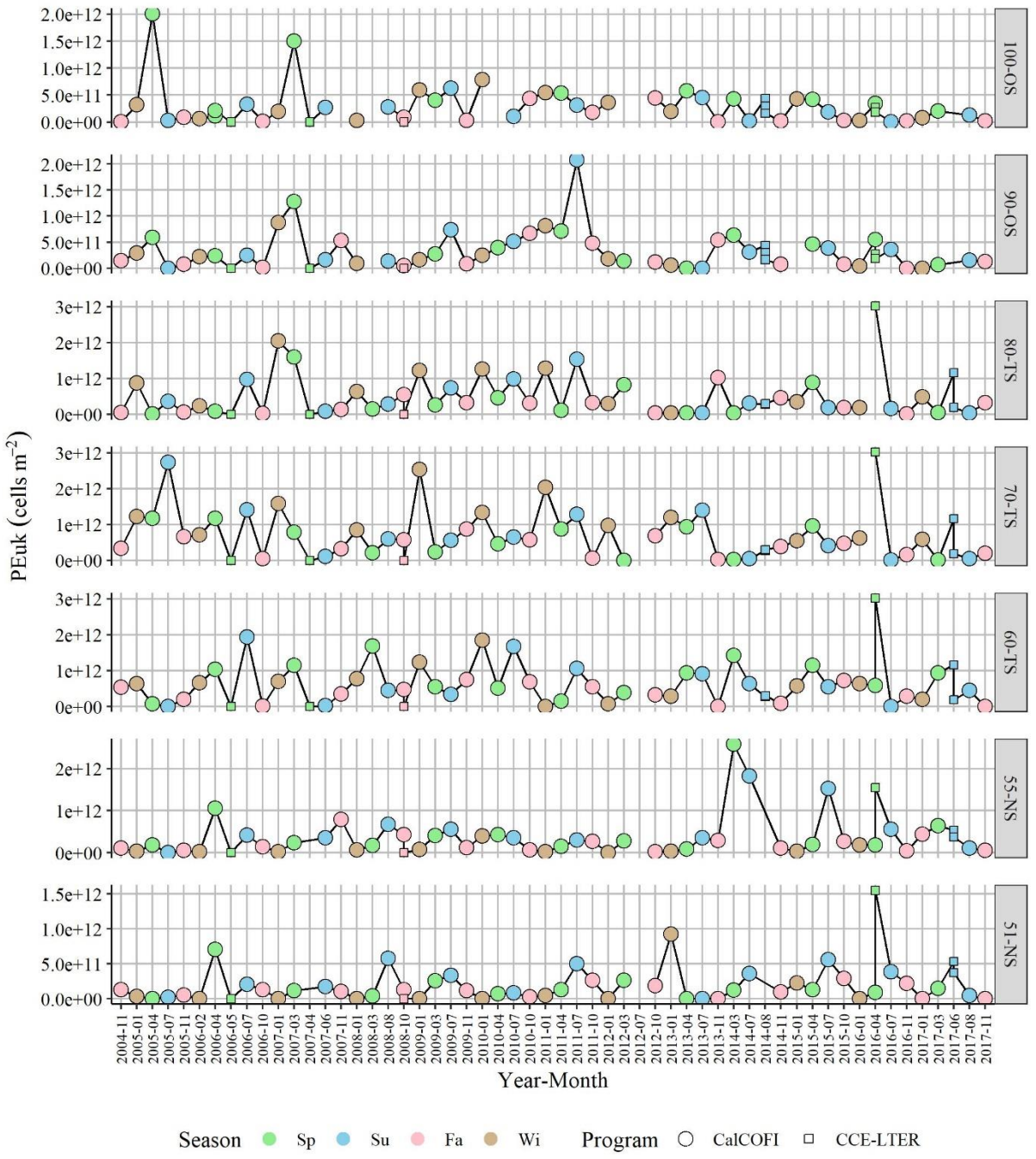

Figure S1.14: CalCOFI and CCE-LTER EZ integrated PEuk abundance

CalCOFI cruise data (circles) plotted by station with overlying CCE-LTER data (squares) for the corresponding region (OS = offshore, TS = transition, NS = nearshore), when available. The CCE-LTER data per region is repeated for each CalCOFI station. Colors correspond to season of sampling.

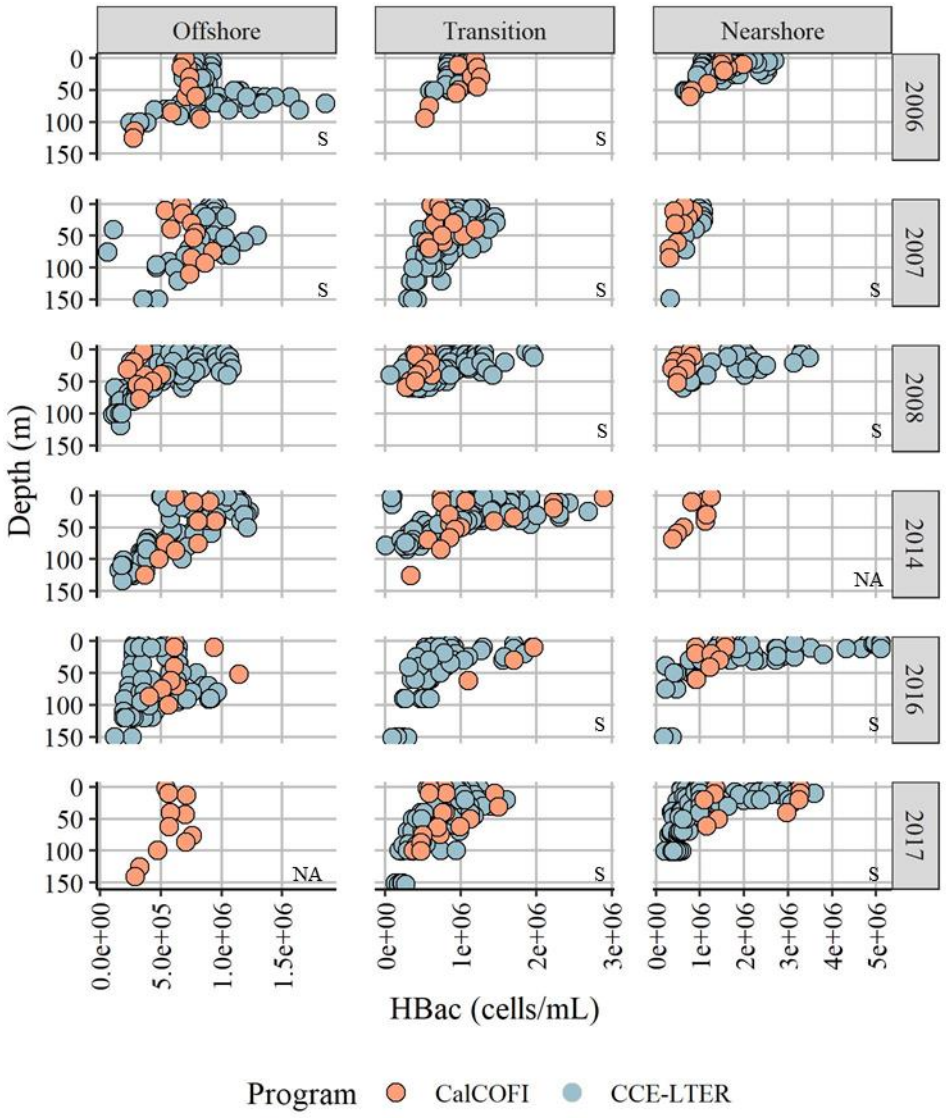

Figure S1.15: CalCOFI vs CCE-LTER heterotrophic bacterial abundance by year

CalCOFI cruise data (pink) plotted over CCE-LTER data (blue) by depth. When the data was significantly different between programs, the panel is designated by an "S." If the statistically difference could not be determined, the panel is marked by an "NA."

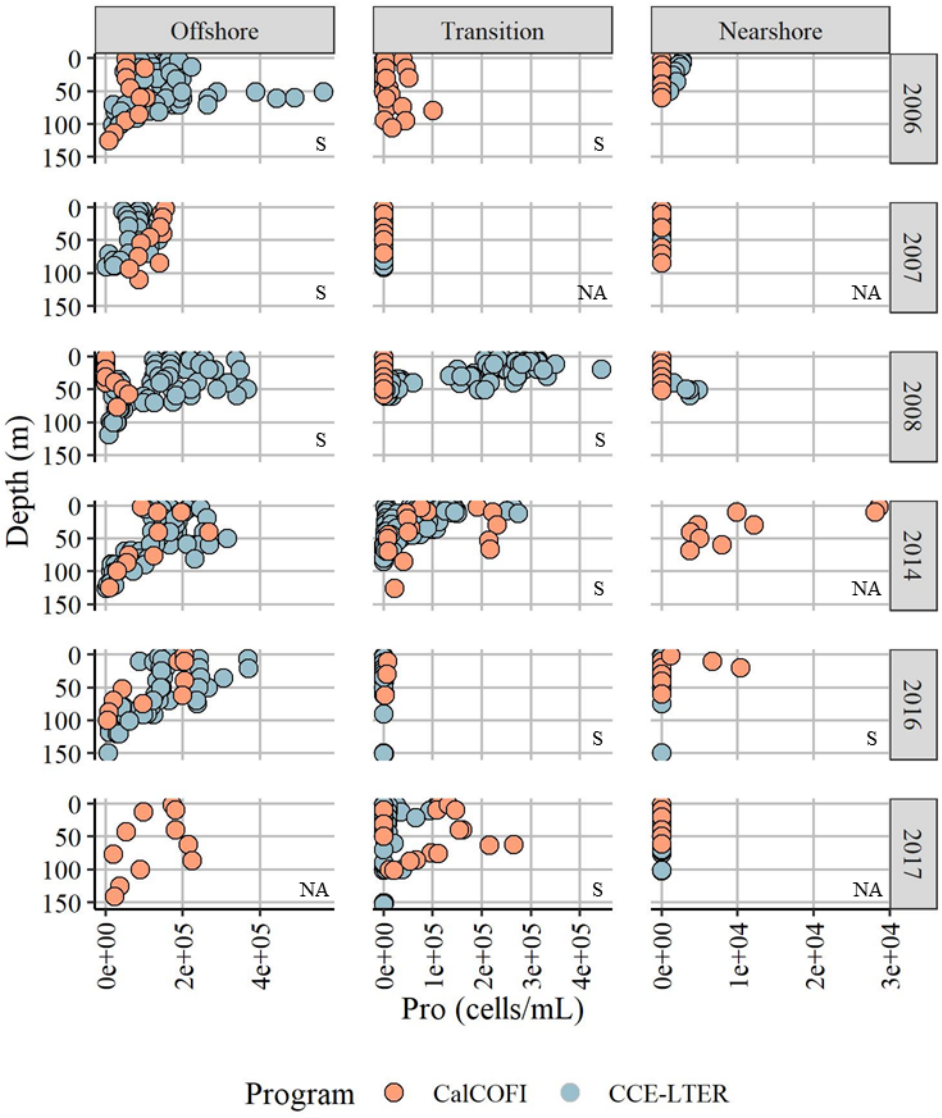

Figure S1.16: CalCOFI vs CCE-LTER Pro abundance by year

CalCOFI cruise data (pink) plotted over CCE-LTER data (blue) by depth. When the data was significantly different between programs, the panel is designated by an "S." If the statistically difference could not be determined, the panel is marked by an "NA."

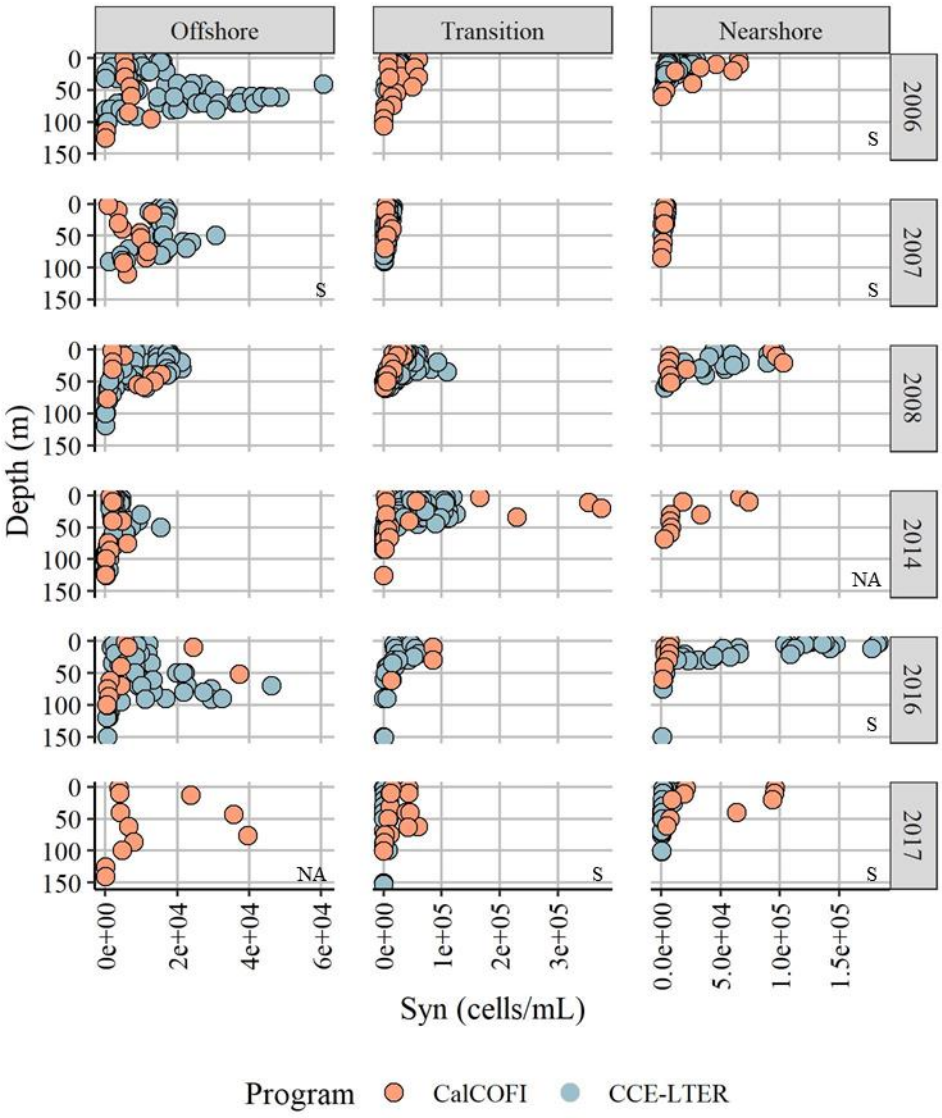

Figure S1.17: CalCOFI vs CCE-LTER Syn abundance by year

CalCOFI cruise data (pink) plotted over CCE-LTER data (blue) by depth. When the data was significantly different between programs, the panel is designated by an "S." If the statistically difference could not be determined, the panel is marked by an "NA."

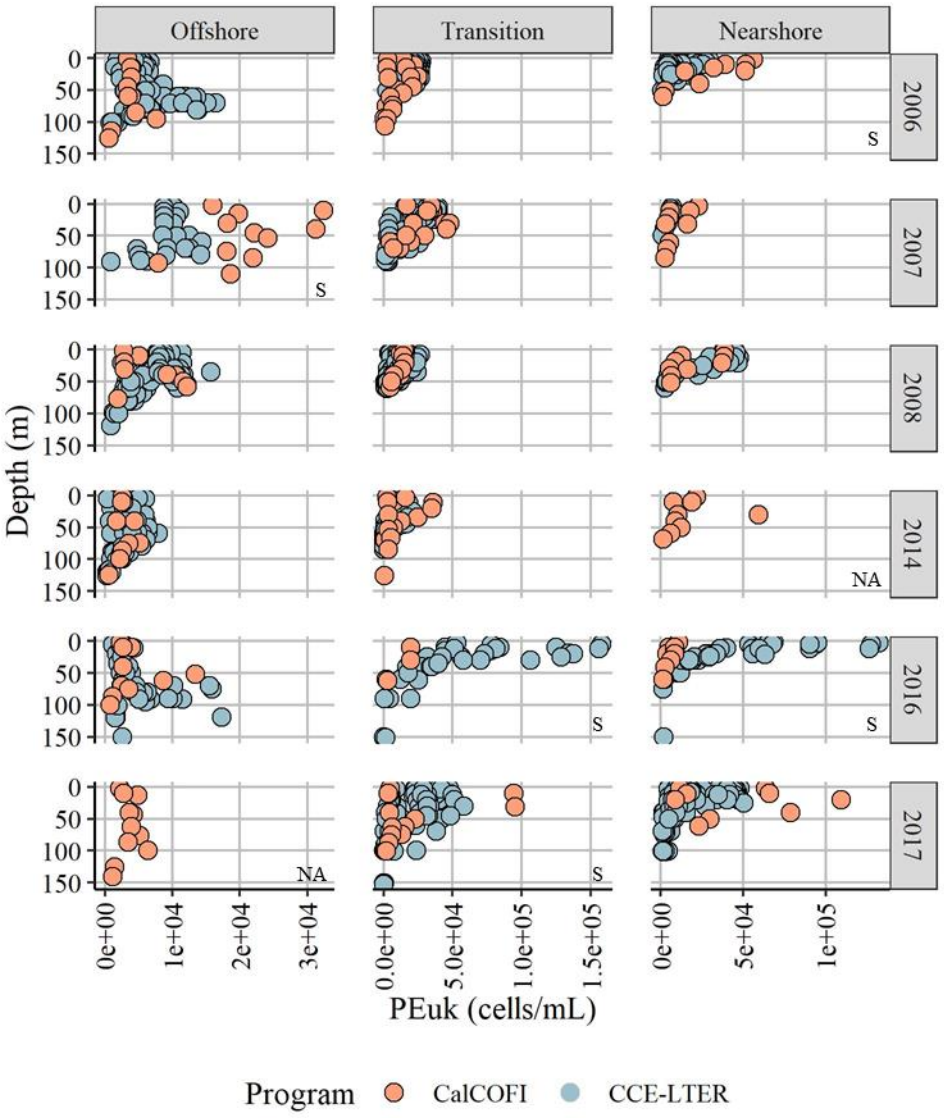

Figure S1.18: CalCOFI vs CCE-LTER PEuk abundance by year

CalCOFI cruise data (pink) plotted over CCE-LTER data (blue) by depth. When the data was significantly different between programs, the panel is designated by an "S." If the statistically difference could not be determined, the panel is marked by an "NA."

Table S1.1: Geographical locations and regional designations for CalCOFI Line 80 stations

Cruise	Line	Station	Region	Latitude (°)	Longitude (°)
CalCOFI	80	51	Nearshore	34.45	-120.52
CalCOFI	80	55	Nearshore	34.32	-120.80
CalCOFI	80	60	Transition	34.15	-121.15
CalCOFI	80	70	Transition	33.82	-121.84
CalCOFI	80	80	Transition	33.48	-122.53
CalCOFI	80	90	Offshore	33.15	-123.22
CalCOFI	80	100	Offshore	32.82	-123.91

Table S1.2: Geographical locations and regional designations for CCE-LTER process cruise stations (1/3)

Cruise	Cycle	Cycle Day	Region	Latitude (°)	Longitude (°)
P0605	1	1	Nearshore	34.33	-120.80
P0605	1	2	Nearshore	34.29	-120.84
P0605	1	4	Nearshore	34.27	-121.04
P0605	1	5	Nearshore	34.26	-121.06
P0605	2	1	Offshore	33.68	-122.20
P0605	2	2	Offshore	33.50	-122.11
P0605	2	3	Offshore	33.62	-122.13
P0605	2	4	Offshore	33.49	-122.09
P0605	2	5	Offshore	33.36	-122.04
P0605	3	1	Nearshore	34.61	-120.77
P0605	3	2	Nearshore	34.75	-120.77
P0605	3	3	Nearshore	34.86	-120.80
P0605	3	4	Nearshore	34.84	-120.83
P0605	4	1	Transition	34.05	-121.30
P0605	4	2	Transition	34.02	-121.43
P0605	4	3	Transition	33.96	-121.57
P0605	4	4	Transition	33.89	-121.65
P0605	4	5	Transition	33.87	-121.72
P0605	4	6	Transition	33.76	-121.71
P0605	5	1	Offshore	32.85	-124.00
P0605	5	2	Offshore	32.78	-124.09
P0605	5	3	Offshore	32.67	-124.19
P0605	5	4	Offshore	32.49	-124.25
P0605	5	5	Offshore	32.38	-124.28
P0704	1	1	Transition	34.26	-120.84
P0704	1	2	Transition	34.28	-120.91
P0704	1	3	Transition	34.33	-120.95
P0704	1	4	Transition	34.36	-121.05
P0704	1	5	Transition	34.31	-121.15
P0704	2	1	Offshore	33.55	-123.16
P0704	2	2	Offshore	33.41	-123.28
P0704	2	3	Offshore	33.33	-123.45
P0704	2	4	Offshore	33.28	-123.64
P0704	3	1	Nearshore	34.22	-120.62
P0704	4	1	Transition	34.23	-121.19
P0704	4	2	Transition	33.92	-121.16
P0704	4	3	Transition	33.82	-121.08
P0704	4	4	Transition	33.74	-121.00

Table S1.2: Geographical locations and regional designations for CCE-LTER process cruise stations (continued 2/3)

Cruise	Cycle	Cycle Day	Region	Latitude (°)	Longitude (°)
P0704	4	5	Transition	33.80	-120.78
P0810	1	1	Transition	34.13	-120.98
P0810	1	2	Transition	34.11	-120.84
P0810	1	3	Transition	33.97	-120.77
P0810	1	4	Transition	33.78	-120.73
P0810	1	5	Transition	33.53	-120.73
P0810	2	1	Offshore	32.89	-123.69
P0810	2	2	Offshore	32.80	-123.66
P0810	2	3	Offshore	32.71	-123.68
P0810	2	4	Offshore	32.45	-123.73
P0810	2	5	Offshore	32.29	-123.84
P0810	2	6	Offshore	32.15	-123.95
P0810	3	1	Transition	33.95	-121.81
P0810	3	2	Transition	34.02	-121.76
P0810	3	3	Transition	34.11	-121.68
P0810	3	4	Transition	34.20	-121.58
P0810	4	1	Transition	33.61	-121.16
P0810	4	2	Transition	33.61	-121.16
P0810	4	3	Transition	33.55	-121.18
P0810	5	1	Nearshore	32.92	-120.90
P0810	5	2	Nearshore	32.82	-120.84
P0810	5	3	Nearshore	32.84	-120.65
P0810	6	1	Offshore	32.90	-120.71
P0810	6	2	Offshore	32.59	-120.47
P0810	6	3	Offshore	32.57	-120.33
P1408	1	1	Transition	34.51	-120.77
P1408	1	2	Transition	34.72	-121.00
P1408	1	3	Transition	34.81	-121.22
P1408	1	4	Transition	34.87	-121.36
P1408	2	1	Transition	34.27	-120.82
P1408	2	2	Transition	34.17	-120.87
P1408	2	3	Transition	34.12	-120.92
P1408	2	4	Transition	34.09	-120.97
P1408	3	1	Transition	34.39	-121.39
P1408	3	2	Transition	34.41	-121.28
P1408	3	3	Transition	34.43	-121.15
P1408	3	4	Transition	34.43	-121.02
P1408	4	1	Offshore	33.52	-122.56

Table S1.2: Geographical locations and regional designations for CCE-LTER process cruise stations (continued 3/3)

Cruise	Cycle	Cycle Day	Region	Latitude (°)	Longitude (°)
P1408	4	2	Offshore	33.54	-122.51
P1408	4	3	Offshore	33.60	-122.44
P1408	4	4	Offshore	33.64	-122.40
P1408	5	1	Offshore	32.88	-123.90
P1408	5	2	Offshore	32.84	-123.87
P1408	5	3	Offshore	32.81	-123.87
P1408	5	4	Offshore	32.77	-123.87
P1604	1	1	Offshore	32.98	-123.03
P1604	1	2	Offshore	33.09	-122.94
P1604	2	1	Offshore	33.59	-122.21
P1604	2	2	Offshore	33.52	-122.06
P1604	2	3	Offshore	33.47	-121.97
P1604	3	1	Transition	34.80	-121.28
P1604	3	2	Transition	34.67	-121.28
P1604	3	3	Transition	34.50	-121.22
P1604	4	1	Nearshore	34.44	-120.70
P1604	4	2	Nearshore	34.50	-120.78
P1604	4	3	Nearshore	34.53	-120.87
P1706	1	1	Nearshore	35.07	-121.09
P1706	1	2	Nearshore	35.05	-121.14
P1706	1	3	Nearshore	34.95	-121.18
P1706	1	4	Nearshore	34.87	-121.15
P1706	2	1	Nearshore	34.73	-121.71
P1706	2	2	Nearshore	34.72	-121.92
P1706	2	3	Nearshore	34.72	-122.14
P1706	2	4	Nearshore	34.71	-122.28
P1706	2	5	Nearshore	34.68	-122.35
P1706	3	1	Transition	34.37	-123.18
P1706	3	2	Transition	34.20	-123.11
P1706	3	3	Transition	34.09	-122.95
P1706	3	4	Transition	34.02	-122.60
P1706	4	1	Transition	34.40	-123.07
P1706	4	2	Transition	34.45	-122.99
P1706	4	3	Transition	34.51	-122.97

Table S1.3: Hydrographic depths and euphotic zone integrated biogeochemical values for CalCOFI cruises (1/12)

Mean biogeochemical parameters integrated over the calculated euphotic zone (1% surface irradiance) when available or the average seasonal euphotic zone depth by region (designated by *) when Secchi disc measurements were unavailable for CalCOFI cruises.

Cruise	Station	Season	Region	Nitracline	Chl max	Euphotic Zone	NPP	Chl	POC	TOC
				m			mmol C m^{-2} d^{-1}	mg Chl m^{-2}	mmol C m^{-2}	
A0411	51	Fa	Nearshore	0	19	38*	n.d.	86	469	n.d.
A0411	55	Fa	Nearshore	0	17	42	n.d.	67	282	n.d.
A0411	60	Fa	Transition	41	34	39	23	41	439	n.d.
A0411	70	Fa	Transition	32	45	50*	n.d.	20	287	n.d.
A0411	80	Fa	Transition	31	33	50*	n.d.	18	295	n.d.
A0411	90	Fa	Offshore	48	39	90	13	21	156	n.d.
A0411	100	Fa	Offshore	76	62	99	n.d.	21	267	n.d.
A0501	51	Wi	Nearshore	2	19	28*	n.d.	19	130	n.d.
A0501	55	Wi	Nearshore	15	2	28*	n.d.	28	162	n.d.
A0501	60	Wi	Transition	42	21	50*	n.d.	31	195	n.d.
A0501	70	Wi	Transition	0	13	36	61	32	236	n.d.
A0501	80	Wi	Transition	40	33	30	n.d.	30	295	n.d.
A0501	90	Wi	Offshore	45	15	71*	n.d.	26	216	n.d.
A0501	100	Wi	Offshore	69	48	71*	n.d.	19	196	n.d.
A0504	51	Sp	Nearshore	0	8	26*	n.d.	95	310	n.d.
A0504	55	Sp	Nearshore	0	3	24	n.d.	46	305	n.d.
A0504	60	Sp	Transition	9	18	33	54	47	195	n.d.
A0504	70	Sp	Transition	48	44	39	n.d.	20	135	n.d.
A0504	80	Sp	Transition	64	56	44*	n.d.	7	100	n.d.
A0504	90	Sp	Offshore	62	72	72	24	20	176	n.d.
A0504	100	Sp	Offshore	71	51	66	n.d.	15	202	n.d.
A0507	51	Su	Nearshore	2	2	31*	n.d.	104	729	n.d.
A0507	55	Su	Nearshore	0	28	31*	n.d.	140	198	n.d.
A0507	60	Su	Transition	0	30	49*	n.d.	68	283	n.d.
A0507	70	Su	Transition	0	30	48	41	20	312	n.d.
A0507	80	Su	Transition	90	76	54	n.d.	8	171	n.d.
A0507	90	Su	Offshore	88	93	70*	n.d.	6	182	n.d.
A0507	100	Su	Offshore	88	94	70*	n.d.	7	157	n.d.
A0511	51	Fa	Nearshore	27	26	38*	n.d.	81	600	n.d.
A0511	55	Fa	Nearshore	17	3	38*	n.d.	123	627	n.d.
A0511	60	Fa	Transition	0	6	18	117	111	349	n.d.
A0511	70	Fa	Transition	40	22	30	n.d.	36	192	n.d.
A0511	80	Fa	Transition	65	60	50*	n.d.	14	135	n.d.

Table S1.3: Hydrographic depths and euphotic zone integrated biogeochemical values for CalCOFI cruises (continued 2/12)

Mean biogeochemical parameters integrated over the calculated euphotic zone (1% surface irradiance) when available or the average seasonal euphotic zone depth by region (designated by *) when Secchi disc measurements were unavailable for CalCOFI cruises.

Cruise	Station	Season	Region	Nitracline	Chl max	Euphotic Zone	NPP	Chl	POC	TOC
				m			mmol C m^{-2} d^{-1}	mg Chl m^{-2}	mmol C m^{-2}	
A0511	90	Fa	Offshore	60	40	71*	n.d.	28	260	n.d.
A0511	100	Fa	Offshore	51	56	69	24	22	247	n.d.
A0602	51	Wi	Nearshore	0	24	28*	n.d.	32	340	n.d.
A0602	55	Wi	Nearshore	0	34	28*	n.d.	63	280	n.d.
A0602	60	Wi	Transition	0	29	66	54	30	160	n.d.
A0602	70	Wi	Transition	44	50	50*	n.d.	29	193	n.d.
A0602	80	Wi	Transition	66	47	50*	n.d.	11	92	n.d.
A0602	90	Wi	Offshore	57	63	71*	n.d.	30	212	n.d.
A0602	100	Wi	Offshore	n.d.	n.d.	84	19	20	191	n.d.
A0604	51	Sp	Nearshore	0	12	24	n.d.	66	554	n.d.
A0604	55	Sp	Nearshore	14	39	26*	n.d.	20	252	n.d.
A0604	60	Sp	Transition	27	30	44*	n.d.	33	246	n.d.
A0604	70	Sp	Transition	58	60	51	12	38	239	n.d.
A0604	80	Sp	Transition	81	80	66	n.d.	10	192	n.d.
A0604	90	Sp	Offshore	106	92	63*	n.d.	9	106	n.d.
A0604	100	Sp	Offshore	72	65	63*	n.d.	7	133	n.d.
A0604	100	Sp	Offshore	90	86	63*	n.d.	7	133	n.d.
A0607	51	Su	Nearshore	11	8	18	n.d.	53	548	n.d.
A0607	55	Su	Nearshore	3	8	31*	n.d.	50	369	n.d.
A0607	60	Su	Transition	0	28	49*	n.d.	49	294	n.d.
A0607	70	Su	Transition	16	5	49*	n.d.	38	295	n.d.
A0607	80	Su	Transition	28	37	72	44	33	280	n.d.
A0607	90	Su	Offshore	87	73	70*	n.d.	7	134	n.d.
A0607	100	Su	Offshore	97	59	70*	n.d.	8	176	n.d.
A0610	51	Fa	Nearshore	13	4	38*	n.d.	38	363	n.d.
A0610	55	Fa	Nearshore	32	1	38*	n.d.	53	517	n.d.
A0610	60	Fa	Transition	74	61	50*	n.d.	9	147	n.d.
A0610	70	Fa	Transition	64	57	96	25	19	210	n.d.
A0610	80	Fa	Transition	48	53	50*	n.d.	13	160	n.d.
A0610	90	Fa	Offshore	93	76	71*	n.d.	8	112	n.d.
A0610	100	Fa	Offshore	102	58	123	32	34	380	n.d.
A0701	51	Wi	Nearshore	n.d.	n.d.	28*	n.d.	31	116	n.d.
A0701	55	Wi	Nearshore	n.d.	n.d.	28*	n.d.	45	286	n.d.

Table S1.3: Hydrographic depths and euphotic zone integrated biogeochemical values for CalCOFI cruises (continued 3/12)

Mean biogeochemical parameters integrated over the calculated euphotic zone (1% surface irradiance) when available or the average seasonal euphotic zone depth by region (designated by *) when Secchi disc measurements were unavailable for CalCOFI cruises.

Cruise	Station	Season	Region	Nitracline	Chl max	Euphotic Zone	NPP	Chl	POC	TOC
				m			mmol C m^{-2} d^{-1}	mg Chl m^{-2}	mmol C m^{-2}	
A0701	60	Wi	Transition	n.d.	n.d.	50*	n.d.	63	446	n.d.
A0701	70	Wi	Transition	n.d.	n.d.	36	n.d.	31	171	n.d.
A0701	80	Wi	Transition	n.d.	n.d.	45	39	32	295	n.d.
A0701	90	Wi	Offshore	n.d.	n.d.	71*	n.d.	44	296	n.d.
A0701	100	Wi	Offshore	n.d.	n.d.	71*	n.d.	29	327	n.d.
A0704	51	Sp	Nearshore	0	17	24	n.d.	27	156	n.d.
A0704	55	Sp	Nearshore	0	27	26*	n.d.	17	57	n.d.
A0704	60	Sp	Transition	0	32	44*	n.d.	55	223	n.d.
A0704	70	Sp	Transition	0	16	42	n.d.	24	182	n.d.
A0704	80	Sp	Transition	0	39	42	1	53	272	n.d.
A0704	90	Sp	Offshore	87	43	42	n.d.	12	220	n.d.
A0704	100	Sp	Offshore	67	57	63*	n.d.	14	231	n.d.
A0707	51	Su	Nearshore	0	2	31*	n.d.	58	198	n.d.
A0707	55	Su	Nearshore	0	18	21	122	42	322	n.d.
A0707	60	Su	Transition	0	13	36	n.d.	75	440	n.d.
A0707	70	Su	Transition	0	27	49*	n.d.	12	223	n.d.
A0707	80	Su	Transition	68	62	49*	n.d.	5	121	n.d.
A0707	90	Su	Offshore	91	73	78	17	18	236	n.d.
A0707	100	Su	Offshore	96	84	90	n.d.	13	303	n.d.
A0711	51	Fa	Nearshore	0	2	38*	n.d.	43	286	n.d.
A0711	55	Fa	Nearshore	0	30	48	51	28	313	n.d.
A0711	60	Fa	Transition	50	35	51	n.d.	19	324	n.d.
A0711	70	Fa	Transition	40	38	50*	n.d.	14	202	n.d.
A0711	80	Fa	Transition	52	37	50*	n.d.	14	245	n.d.
A0711	90	Fa	Offshore	51	30	36	26	23	234	n.d.
A0711	100	Fa	Offshore	n.d.	n.d.	71*	n.d.	n.d.	n.d.	n.d.
A0801	51	Wi	Nearshore	0	2	28*	n.d.	36	100	n.d.
A0801	55	Wi	Nearshore	0	1	27	n.d.	34	182	n.d.
A0801	60	Wi	Transition	0	13	33	61	46	311	n.d.
A0801	70	Wi	Transition	0	7	50*	n.d.	36	378	n.d.
A0801	80	Wi	Transition	25	38	60	26	26	245	n.d.
A0801	90	Wi	Offshore	93	32	72	n.d.	28	221	n.d.
A0801	100	Wi	Offshore	77	47	71*	n.d.	21	288	n.d.

Table S1.3: Hydrographic depths and euphotic zone integrated biogeochemical values for CalCOFI cruises (continued 4/12)

Mean biogeochemical parameters integrated over the calculated euphotic zone (1% surface irradiance) when available or the average seasonal euphotic zone depth by region (designated by *) when Secchi disc measurements were unavailable for CalCOFI cruises.

Cruise	Station	Season	Region	Nitracline	Chl max	Euphotic Zone	NPP	Chl	POC	TOC
				m			mmol C m^{-2} d^{-1}	mg Chl m^{-2}	mmol C m^{-2}	
A0804	51	Sp	Nearshore	0	12	33	n.d.	64	196	1111
A0804	55	Sp	Nearshore	0	21	26*	n.d.	56	105	1252
A0804	60	Sp	Transition	0	49	44*	n.d.	48	368	2630
A0804	70	Sp	Transition	0	49	44*	n.d.	15	183	2116
A0804	80	Sp	Transition	0	2	44*	n.d.	19	149	1876
A0804	90	Sp	Offshore	n.d.	n.d.	63*	n.d.	n.d.	n.d.	n.d.
A0804	100	Sp	Offshore	n.d.	n.d.	63*	n.d.	n.d.	n.d.	n.d.
A0808	51	Su	Nearshore	10	18	18	100	47	295	1221
A0808	55	Su	Nearshore	0	28	21	n.d.	39	272	1385
A0808	60	Su	Transition	32	2	49*	n.d.	39	362	2203
A0808	70	Su	Transition	36	34	49*	n.d.	11	307	2745
A0808	80	Su	Transition	38	36	39	23	16	299	2574
A0808	90	Su	Offshore	62	57	57	n.d.	13	193	2682
A0808	100	Su	Offshore	55	49	70*	n.d.	21	364	4345
A0810	51	Fa	Nearshore	0	13	38*	n.d.	42	364	2136
A0810	55	Fa	Nearshore	15	2	38*	n.d.	39	571	1961
A0810	60	Fa	Transition	20	24	33	86	47	160	1524
A0810	70	Fa	Transition	36	44	33	n.d.	23	367	2050
A0810	80	Fa	Transition	24	26	50*	n.d.	44	339	3234
A0810	90	Fa	Offshore	68	55	71*	n.d.	13	n.d.	3646
A0810	100	Fa	Offshore	83	56	87	33	18	79	5187
0901NH	51	Wi	Nearshore	16	16	45	n.d.	86	972	2176
0901NH	55	Wi	Nearshore	0	12	28*	n.d.	22	192	1244
0901NH	60	Wi	Transition	0	14	50*	n.d.	59	385	2388
0901NH	70	Wi	Transition	0	18	45	50	25	292	2344
0901NH	80	Wi	Transition	8	14	39	n.d.	14	166	1732
0901NH	90	Wi	Offshore	53	44	71*	n.d.	29	702	3702
0901NH	100	Wi	Offshore	39	13	71*	n.d.	48	667	4288
0903JD	51	Sp	Nearshore	0	29	26*	n.d.	74	552	n.d.
0903JD	55	Sp	Nearshore	0	5	26*	n.d.	38	289	n.d.
0903JD	60	Sp	Transition	0	21	44*	n.d.	87	493	n.d.
0903JD	70	Sp	Transition	56	53	48	1	23	245	n.d.
0903JD	80	Sp	Transition	82	41	44*	n.d.	13	204	n.d.

Table S1.3: Hydrographic depths and euphotic zone integrated biogeochemical values for CalCOFI cruises (continued 5/12)

Mean biogeochemical parameters integrated over the calculated euphotic zone (1% surface irradiance) when available or the average seasonal euphotic zone depth by region (designated by *) when Secchi disc measurements were unavailable for CalCOFI cruises.

Cruise	Station	Season	Region	Nitracline	Chl max	Euphotic Zone	NPP	Chl	POC	TOC
				m			mmol C m^{-2} d^{-1}	mg Chl m^{-2}	mmol C m^{-2}	
0903JD	90	Sp	Offshore	92	81	63*	n.d.	10	169	n.d.
0903JD	100	Sp	Offshore	72	60	84	26	18	242	n.d.
0907MZ	51	Su	Nearshore	0	2	31*	n.d.	105	375	2102
0907MZ	55	Su	Nearshore	0	10	31*	n.d.	69	449	2029
0907MZ	60	Su	Transition	0	15	39	136	97	276	1193
0907MZ	70	Su	Transition	39	39	49*	n.d.	11	349	2656
0907MZ	80	Su	Transition	40	38	49*	n.d.	15	280	2669
0907MZ	90	Su	Offshore	33	39	45	29	15	245	2695
0907MZ	100	Su	Offshore	71	66	63	n.d.	21	227	4264
0911NH	51	Fa	Nearshore	0	15	27	n.d.	30	242	1341
0911NH	55	Fa	Nearshore	0	23	38*	n.d.	151	524	2138
0911NH	60	Fa	Transition	40	25	50*	n.d.	66	206	1987
0911NH	70	Fa	Transition	3	20	27	52	39	143	892
0911NH	80	Fa	Transition	74	49	51	n.d.	21	166	2613
0911NH	90	Fa	Offshore	56	19	71*	n.d.	21	172	4425
0911NH	100	Fa	Offshore	103	87	71*	n.d.	10	119	4172
1001NH	51	Wi	Nearshore	21	3	28*	n.d.	15	128	1354
1001NH	55	Wi	Nearshore	0	3	28*	n.d.	16	89	1433
1001NH	60	Wi	Transition	0	2	50*	n.d.	36	250	2862
1001NH	70	Wi	Transition	24	32	42	43	25	258	2435
1001NH	80	Wi	Transition	0	31	50*	n.d.	39	426	3486
1001NH	90	Wi	Offshore	42	41	71*	n.d.	24	234	3826
1001NH	100	Wi	Offshore	n.d.	n.d.	60	27	23	233	3829
1004MF	51	Sp	Nearshore	0	5	26*	n.d.	186	730	1492
1004MF	55	Sp	Nearshore	0	11	26*	n.d.	48	202	897
1004MF	60	Sp	Transition	0	3	44*	n.d.	12	128	930
1004MF	70	Sp	Transition	53	28	30	n.d.	16	280	1986
1004MF	80	Sp	Transition	70	58	44*	n.d.	9	185	1961
1004MF	90	Sp	Offshore	79	67	63*	n.d.	19	321	3922
1004MF	100	Sp	Offshore	n.d.	n.d.	63*	n.d.	n.d.	n.d.	n.d.
1008NH	51	Su	Nearshore	0	8	21	149	80	268	1201
1008NH	55	Su	Nearshore	0	18	18	n.d.	22	235	783
1008NH	60	Su	Transition	0	20	49*	n.d.	71	600	2201

Table S1.3: Hydrographic depths and euphotic zone integrated biogeochemical values for CalCOFI cruises (continued 6/12)

Mean biogeochemical parameters integrated over the calculated euphotic zone (1% surface irradiance) when available or the average seasonal euphotic zone depth by region (designated by *) when Secchi disc measurements were unavailable for CalCOFI cruises.

Cruise	Station	Season	Region	Nitracline	Chl max	Euphotic Zone	NPP	Chl	POC	TOC
				m			mmol C m^{-2} d^{-1}	mg Chl m^{-2}	mmol C m^{-2}	
1008NH	70	Su	Transition	12	10	49*	n.d.	29	303	2462
1008NH	80	Su	Transition	11	26	45	56	25	320	2550
1008NH	90	Su	Offshore	62	54	70*	n.d.	17	239	3325
1008NH	100	Su	Offshore	102	93	70*	n.d.	6	131	3431
1011NH	51	Fa	Nearshore	0	14	38*	n.d.	28	219	n.d.
1011NH	55	Fa	Nearshore	0	13	38*	n.d.	91	428	n.d.
1011NH	60	Fa	Transition	2	38	50*	n.d.	25	289	n.d.
1011NH	70	Fa	Transition	0	15	33	61	34	293	n.d.
1011NH	80	Fa	Transition	0	11	50*	n.d.	30	328	n.d.
1011NH	90	Fa	Offshore	25	35	71*	n.d.	33	298	n.d.
1011NH	100	Fa	Offshore	63	54	51	24	19	215	n.d.
1101NH	51	Wi	Nearshore	0	26	30	144	84	380	n.d.
1101NH	55	Wi	Nearshore	3	8	15	n.d.	64	255	n.d.
1101NH	60	Wi	Transition	0	3	50*	n.d.	415	990	n.d.
1101NH	70	Wi	Transition	0	44	50*	n.d.	39	278	n.d.
1101NH	80	Wi	Transition	7	29	50*	n.d.	22	240	n.d.
1101NH	90	Wi	Offshore	0	19	48	n.d.	28	117	n.d.
1101NH	100	Wi	Offshore	26	31	71*	n.d.	43	310	n.d.
1104SH	51	Sp	Nearshore	0	25	26*	n.d.	19	115	n.d.
1104SH	55	Sp	Nearshore	0	8	26*	n.d.	152	494	n.d.
1104SH	60	Sp	Transition	0	8	24	160	98	293	n.d.
1104SH	70	Sp	Transition	0	31	45	n.d.	26	256	n.d.
1104SH	80	Sp	Transition	64	67	44*	n.d.	6	75	n.d.
1104SH	90	Sp	Offshore	43	44	51	34	21	217	n.d.
1104SH	100	Sp	Offshore	92	75	48	n.d.	5	140	n.d.
1108NH	51	Su	Nearshore	0	2	31*	n.d.	90	663	2133
1108NH	55	Su	Nearshore	0	21	31*	n.d.	196	827	2295
1108NH	60	Su	Transition	3	23	49*	n.d.	22	376	2837
1108NH	70	Su	Transition	35	38	39	32	11	240	2339
1108NH	80	Su	Transition	29	41	49*	n.d.	13	340	2738
1108NH	90	Su	Offshore	85	54	70*	n.d.	21	440	3454
1108NH	100	Su	Offshore	97	74	72	112	17	232	n.d.
1110NH	51	Fa	Nearshore	15	17	38*	n.d.	81	569	n.d.

Table S1.3: Hydrographic depths and euphotic zone integrated biogeochemical values for CalCOFI cruises (continued 7/12)

Mean biogeochemical parameters integrated over the calculated euphotic zone (1% surface irradiance) when available or the average seasonal euphotic zone depth by region (designated by *) when Secchi disc measurements were unavailable for CalCOFI cruises.

Cruise	Station	Season	Region	Nitracline	Chl max	Euphotic Zone	NPP	Chl	POC	TOC
				m			mmol C m^{-2} d^{-1}	mg Chl m^{-2}	mmol C m^{-2}	
1110NH	55	Fa	Nearshore	36	25	38*	n.d.	23	296	n.d.
1110NH	60	Fa	Transition	42	50	60	29	19	241	n.d.
1110NH	70	Fa	Transition	58	51	69	n.d.	18	242	n.d.
1110NH	80	Fa	Transition	42	40	50*	n.d.	18	157	n.d.
1110NH	90	Fa	Offshore	41	46	48	18	-7	205	n.d.
1110NH	100	Fa	Offshore	48	51	48	n.d.	11	205	n.d.
1202NH	51	Wi	Nearshore	10	13	27	n.d.	22	176	n.d.
1202NH	55	Wi	Nearshore	0	12	28*	n.d.	77	400	n.d.
1202NH	60	Wi	Transition	0	60	50*	n.d.	20	188	n.d.
1202NH	70	Wi	Transition	52	4	50*	n.d.	16	176	n.d.
1202NH	80	Wi	Transition	55	40	45	13	15	183	n.d.
1202NH	90	Wi	Offshore	62	36	71*	n.d.	31	339	n.d.
1202NH	100	Wi	Offshore	56	42	71*	n.d.	24	322	n.d.
1203SH	51	Sp	Nearshore	0	20	30	224	150	340	n.d.
1203SH	55	Sp	Nearshore	0	32	30	122	56	94	n.d.
1203SH	60	Sp	Transition	0	35	39	n.d.	58	300	n.d.
1203SH	70	Sp	Transition	n.d.	n.d.	44*	n.d.	n.d.	n.d.	n.d.
1203SH	80	Sp	Transition	49	47	44*	n.d.	14	192	n.d.
1203SH	90	Sp	Offshore	68	61	63*	15	11	141	n.d.
1203SH	100	Sp	Offshore	n.d.	72	63*	n.d.	15	225	n.d.
1207OS	51	Su	Nearshore	n.d.	n.d.	27	46	92	683	n.d.
1207OS	55	Su	Nearshore	n.d.	n.d.	12	n.d.	131	674	n.d.
1207OS	60	Su	Transition	n.d.	n.d.	49*	n.d.	20	514	n.d.
1207OS	70	Su	Transition	n.d.	n.d.	49*	n.d.	36	1721	n.d.
1207OS	80	Su	Transition	n.d.	n.d.	27	66	15	185	n.d.
1207OS	90	Su	Offshore	n.d.	n.d.	69	n.d.	10	236	n.d.
1207OS	100	Su	Offshore	n.d.	n.d.	70*	n.d.	23	372	n.d.
1210NH	51	Fa	Nearshore	0	2	38*	n.d.	48	164	n.d.
1210NH	55	Fa	Nearshore	22	11	38*	n.d.	38	291	n.d.
1210NH	60	Fa	Transition	39	18	42	38	20	351	n.d.
1210NH	70	Fa	Transition	32	31	57	n.d.	23	262	n.d.
1210NH	80	Fa	Transition	61	46	50*	n.d.	11	158	n.d.
1210NH	90	Fa	Offshore	41	28	71*	n.d.	17	205	n.d.

Table S1.3: Hydrographic depths and euphotic zone integrated biogeochemical values for CalCOFI cruises (continued 8/12)

Mean biogeochemical parameters integrated over the calculated euphotic zone (1% surface irradiance) when available or the average seasonal euphotic zone depth by region (designated by *) when Secchi disc measurements were unavailable for CalCOFI cruises.

Cruise	Station	Season	Region	Nitracline	Chl max	Euphotic Zone	NPP	Chl	POC	TOC
				m			mmol C m^{-2} d^{-1}	mg Chl m^{-2}	mmol C m^{-2}	
1210NH	100	Fa	Offshore	35	41	57	40	20	260	n.d.
1301SH	51	Wi	Nearshore	0	6	21	n.d.	96	552	n.d.
1301SH	55	Wi	Nearshore	0	30	28*	n.d.	8	109	n.d.
1301SH	60	Wi	Transition	21	27	50*	n.d.	20	84	n.d.
1301SH	70	Wi	Transition	53	21	50*	n.d.	25	224	n.d.
1301SH	80	Wi	Transition	54	39	48	26	18	205	n.d.
1301SH	90	Wi	Offshore	82	64	71*	n.d.	12	179	n.d.
1301SH	100	Wi	Offshore	73	66	71*	n.d.	16	181	n.d.
1304SH	51	Sp	Nearshore	0	2	26*	n.d.	39	50	n.d.
1304SH	55	Sp	Nearshore	0	26	26*	n.d.	20	33	n.d.
1304SH	60	Sp	Transition	0	25	54	69	41	165	n.d.
1304SH	70	Sp	Transition	0	47	42	n.d.	12	143	n.d.
1304SH	80	Sp	Transition	54	34	44*	n.d.	17	265	n.d.
1304SH	90	Sp	Offshore	83	85	63*	n.d.	14	161	n.d.
1304SH	100	Sp	Offshore	113	74	57	10	10	131	n.d.
1307NH	51	Su	Nearshore	0	2	31*	n.d.	28	298	n.d.
1307NH	55	Su	Nearshore	0	5	21	n.d.	87	305	n.d.
1307NH	60	Su	Transition	0	24	27	297	137	610	n.d.
1307NH	70	Su	Transition	0	19	36	n.d.	20	206	n.d.
1307NH	80	Su	Transition	0	17	49*	n.d.	29	1143	n.d.
1307NH	90	Su	Offshore	0	34	70*	n.d.	30	441	n.d.
1307NH	100	Su	Offshore	93	71	69	23	13	212	n.d.
1311NH	51	Fa	Nearshore	11	8	38*	n.d.	63	134	n.d.
1311NH	55	Fa	Nearshore	14	21	27	138	200	418	n.d.
1311NH	60	Fa	Transition	25	13	50*	n.d.	397	571	n.d.
1311NH	70	Fa	Transition	0	2	50*	n.d.	29	190	n.d.
1311NH	80	Fa	Transition	0	32	45	28	18	128	n.d.
1311NH	90	Fa	Offshore	42	33	36	n.d.	19	127	n.d.
1311NH	100	Fa	Offshore	112	72	71*	n.d.	11	123	n.d.
1404OS	51	Sp	Nearshore	0	19	30	n.d.	94	450	1987
1404OS	55	Sp	Nearshore	0	47	36	214	46	240	2142
1404OS	60	Sp	Transition	14	15	42	n.d.	21	176	1483
1404OS	70	Sp	Transition	42	42	44*	n.d.	17	296	2930

Table S1.3: Hydrographic depths and euphotic zone integrated biogeochemical values for CalCOFI cruises (continued 9/12)

Mean biogeochemical parameters integrated over the calculated euphotic zone (1% surface irradiance) when available or the average seasonal euphotic zone depth by region (designated by *) when Secchi disc measurements were unavailable for CalCOFI cruises.

Cruise	Station	Season	Region	Nitracline	Chl max	Euphotic Zone	NPP	Chl	POC	TOC
				m			mmol C m^{-2} d^{-1}	mg Chl m^{-2}	mmol C m^{-2}	
1404OS	80	Sp	Transition	42	37	44*	n.d.	19	178	2801
1404OS	90	Sp	Offshore	54	49	57	36	22	215	3719
1404OS	100	Sp	Offshore	56	51	54	n.d.	16	197	3543
1407NH	51	Su	Nearshore	25	21	39	n.d.	53	484	2321
1407NH	55	Su	Nearshore	22	30	57	n.d.	38	396	3309
1407NH	60	Su	Transition	30	34	54	32	24	360	n.d.
1407NH	70	Su	Transition	25	18	49*	n.d.	26	810	n.d.
1407NH	80	Su	Transition	93	70	81	20	16	194	4566
1407NH	90	Su	Offshore	77	77	96	n.d.	19	220	5378
1407NH	100	Su	Offshore	91	89	70*	n.d.	7	105	4225
1411NH	51	Fa	Nearshore	0	14	38*	n.d.	15	63	660
1411NH	55	Fa	Nearshore	30	33	38*	n.d.	19	100	2137
1411NH	60	Fa	Transition	36	28	50*	n.d.	41	412	3130
1411NH	70	Fa	Transition	45	37	69	41	30	270	4208
1411NH	80	Fa	Transition	47	51	63	n.d.	20	197	3321
1411NH	90	Fa	Offshore	59	56	71*	n.d.	20	221	3559
1411NH	100	Fa	Offshore	100	91	71*	n.d.	8	116	4353
1501NH	51	Wi	Nearshore	25	3	28*	n.d.	18	68	680
1501NH	55	Wi	Nearshore	37	28	28*	n.d.	9	51	1428
1501NH	60	Wi	Transition	32	32	51	45	27	231	2974
1501NH	70	Wi	Transition	44	43	78	n.d.	33	308	4699
1501NH	80	Wi	Transition	47	40	50*	n.d.	14	199	3271
1501NH	90	Wi	Offshore	n.d.	52	71*	n.d.	n.d.	n.d.	n.d.
1501NH	100	Wi	Offshore	60	57	93	17	22	242	5564
1504NH	51	Sp	Nearshore	0	18	18	n.d.	53	224	992
1504NH	55	Sp	Nearshore	0	4	26*	n.d.	24	200	730
1504NH	60	Sp	Transition	25	62	44*	n.d.	60	653	2765
1504NH	70	Sp	Transition	54	60	63	n.d.	24	275	4027
1504NH	80	Sp	Transition	49	38	44*	n.d.	20	264	n.d.
1504NH	90	Sp	Offshore	76	75	63*	n.d.	10	128	n.d.
1504NH	100	Sp	Offshore	85	50	78	12	20	249	n.d.
1507OC	51	Su	Nearshore	n.d.	n.d.	30	144	76	502	n.d.
1507OC	55	Su	Nearshore	n.d.	n.d.	31*	n.d.	43	403	n.d.

Table S1.3: Hydrographic depths and euphotic zone integrated biogeochemical values for CalCOFI cruises (continued 10/12)

Mean biogeochemical parameters integrated over the calculated euphotic zone (1% surface irradiance) when available or the average seasonal euphotic zone depth by region (designated by *) when Secchi disc measurements were unavailable for CalCOFI cruises.

Cruise	Station	Season	Region	Nitracline	Chl max	Euphotic Zone	NPP	Chl	POC	TOC
				m			mmol C m^{-2} d^{-1}	mg Chl m^{-2}	mmol C m^{-2}	
1507OC	60	Su	Transition	n.d.	n.d.	49*	n.d.	17	254	n.d.
1507OC	70	Su	Transition	n.d.	n.d.	63	n.d.	21	320	n.d.
1507OC	80	Su	Transition	n.d.	n.d.	66	21	15	123	n.d.
1507OC	90	Su	Offshore	n.d.	n.d.	70*	n.d.	14	296	n.d.
1507OC	100	Su	Offshore	n.d.	n.d.	70*	n.d.	7	172	n.d.
1511OC	51	Fa	Nearshore	n.d.	n.d.	38*	n.d.	23	216	n.d.
1511OC	55	Fa	Nearshore	n.d.	n.d.	45	127	61	362	n.d.
1511OC	60	Fa	Transition	n.d.	n.d.	63	n.d.	36	323	n.d.
1511OC	70	Fa	Transition	n.d.	n.d.	50*	n.d.	28	257	n.d.
1511OC	80	Fa	Transition	n.d.	n.d.	50*	n.d.	14	181	n.d.
1511OC	90	Fa	Offshore	n.d.	n.d.	75	29	20	221	n.d.
1511OC	100	Fa	Offshore	n.d.	n.d.	93	n.d.	16	182	n.d.
1601RL	51	Wi	Nearshore	0	4	28*	n.d.	27	159	n.d.
1601RL	55	Wi	Nearshore	16	2	28*	n.d.	33	209	n.d.
1601RL	60	Wi	Transition	58	35	50*	n.d.	22	202	n.d.
1601RL	70	Wi	Transition	74	53	78	17	19	197	n.d.
1601RL	80	Wi	Transition	72	54	50*	n.d.	8	108	n.d.
1601RL	90	Wi	Offshore	85	69	71*	n.d.	11	93	n.d.
1601RL	100	Wi	Offshore	102	63	71*	n.d.	9	96	n.d.
1604SH	51	Sp	Nearshore	0	3	26*	n.d.	9	200	n.d.
1604SH	55	Sp	Nearshore	0	5	26*	n.d.	54	341	n.d.
1604SH	60	Sp	Transition	51	10	44*	n.d.	26	303	n.d.
1604SH	70	Sp	Transition	n.d.	n.d.	44*	n.d.	n.d.	n.d.	n.d.
1604SH	80	Sp	Transition	n.d.	n.d.	44*	n.d.	n.d.	n.d.	n.d.
1604SH	90	Sp	Offshore	55	48	63*	n.d.	27	331	n.d.
1604SH	100	Sp	Offshore	63	63	63	n.d.	9	190	n.d.
1607OS	51	Su	Nearshore	0	11	31*	n.d.	33	375	n.d.
1607OS	55	Su	Nearshore	0	21	33	106	45	405	n.d.
1607OS	60	Su	Transition	0	NA	49*	n.d.	99	1237	n.d.
1607OS	70	Su	Transition	53	60	49*	n.d.	7	134	n.d.
1607OS	80	Su	Transition	81	81	72	12	10	170	n.d.
1607OS	90	Su	Offshore	77	84	70*	n.d.	9	140	n.d.
1607OS	100	Su	Offshore	87	79	70*	n.d.	5	122	n.d.

Table S1.3: Hydrographic depths and euphotic zone integrated biogeochemical values for CalCOFI cruises (continued 11/12)

Mean biogeochemical parameters integrated over the calculated euphotic zone (1% surface irradiance) when available or the average seasonal euphotic zone depth by region (designated by *) when Secchi disc measurements were unavailable for CalCOFI cruises.

Cruise	Station	Season	Region	Nitracline	Chl max	Euphotic Zone	NPP	Chl	POC	TOC
				m			mmol C m^{-2} d^{-1}	mg Chl m^{-2}	mmol C m^{-2}	
1611SR	51	Fa	Nearshore	0	3	38*	n.d.	34	230	n.d.
1611SR	55	Fa	Nearshore	0	23	38*	n.d.	77	326	n.d.
1611SR	60	Fa	Transition	0	17	39	133	94	325	n.d.
1611SR	70	Fa	Transition	36	22	36	n.d.	43	202	n.d.
1611SR	80	Fa	Transition	49	22	50*	n.d.	21	220	n.d.
1611SR	90	Fa	Offshore	76	55	71*	n.d.	16	255	n.d.
1611SR	100	Fa	Offshore	83	66	81	18	18	214	n.d.
1701RL	51	Wi	Nearshore	0	7	28*	n.d.	29	233	n.d.
1701RL	55	Wi	Nearshore	0	24	28*	n.d.	10	54	n.d.
1701RL	60	Wi	Transition	36	4	50*	n.d.	33	280	n.d.
1701RL	70	Wi	Transition	31	22	33	45	32	268	n.d.
1701RL	80	Wi	Transition	57	49	87	n.d.	25	175	n.d.
1701RL	90	Wi	Offshore	71	39	71*	n.d.	19	160	n.d.
1701RL	100	Wi	Offshore	52	34	71*	n.d.	22	310	n.d.
1704SH	51	Sp	Nearshore	0	11	21	82	29	225	n.d.
1704SH	55	Sp	Nearshore	0	11	18	n.d.	120	438	n.d.
1704SH	60	Sp	Transition	0	14	36	n.d.	24	184	n.d.
1704SH	70	Sp	Transition	66	67	44*	n.d.	7	137	n.d.
1704SH	80	Sp	Transition	71	75	44*	n.d.	4	84	n.d.
1704SH	90	Sp	Offshore	89	73	66	21	10	165	n.d.
1704SH	100	Sp	Offshore	107	99	78	n.d.	6	167	n.d.
1708SR	51	Su	Nearshore	5	3	31*	n.d.	37	283	n.d.
1708SR	55	Su	Nearshore	11	4	31*	n.d.	117	673	n.d.
1708SR	60	Su	Transition	17	21	27	n.d.	38	263	n.d.
1708SR	70	Su	Transition	33	39	49*	n.d.	17	361	n.d.
1708SR	80	Su	Transition	42	43	49*	n.d.	13	190	n.d.
1708SR	90	Su	Offshore	112	100	66	6	5	122	n.d.
1708SR	100	Su	Offshore	85	66	60	n.d.	9	144	n.d.
1711SR	51	Fa	Nearshore	0	21	38*	n.d.	102	415	n.d.
1711SR	55	Fa	Nearshore	31	17	38*	n.d.	37	363	n.d.
1711SR	60	Fa	Transition	46	40	50*	n.d.	21	194	n.d.
1711SR	70	Fa	Transition	57	43	60	28	25	282	n.d.
1711SR	80	Fa	Transition	68	39	90	n.d.	27	225	n.d.

Table S1.3: Hydrographic depths and euphotic zone integrated biogeochemical values for CalCOFI cruises (continued 12/12)

Mean biogeochemical parameters integrated over the calculated euphotic zone (1% surface irradiance) when available or the average seasonal euphotic zone depth by region (designated by *) when Secchi disc measurements were unavailable for CalCOFI cruises.

Cruise	Station	Season	Region	Nitracline	Chl max	Euphotic Zone	NPP	Chl	POC	TOC
				m			mmol C m^{-2} d^{-1}	mg Chl m^{-2}	mmol C m^{-2}	
1711SR	90	Fa	Offshore	27	22	71*	n.d.	24	263	n.d.
1711SR	100	Fa	Offshore	79	67	71*	n.d.	13	192	n.d.

Table S1.4: Hydrographic depths and euphotic zone integrated biogeochemical values for comparing the CCE-LTER to CalCOFI Line 80 by cruise (1/3)

Nitracline, chlorophyll max, and euphotic zone depths with mean biogeochemical parameters integrated over the euphotic zone depth (1% surface irradiance). The average seasonal euphotic zone (designated by *) was used when Secchi disc data was unavailable. Data is available from the Datazoo site (https://oceaninformatics.ucsd.edu/datazoo/catalogs/ccelter/datasets).

Region	Condition	Cruise	Cycle or Station	Nitracline	Chl max	Euphotic Zone	PP	Chl	POC	TOC
				m			mmol C m^{-2} d^{-1}	mg Chl m^{-2}	mmol C m^{-2}	
Offshore - Nutrient Limited	Normal	P0605	2	76	72	62	22 ± 10, N = 4	9 ± 1, N = 10	275 ± 10, N = 5	n.d.
		P0605	5	69	68	58	26 ± 3, N = 4	6 ± 0, N = 9	189 ± 9, N = 5	n.d.
		0604JD	90	106	92	63*	n.d.	9	106	n.d.
		0604JD	100	72	65	63*	n.d.	7	133	n.d.
		P0704	2	78	73	66	41 ± 2, N = 3	14 ± 1, N = 8	276 ± 12, N = 8	3647 ± 172, N = 11
		0704JD	90	87	43	42	n.d.	12	220	n.d.
		0704JD	100	67	57	63*	n.d.	14	231	n.d.
		P0810	2	78	39	47	29 ± 2, N = 4	8 ± 1, N = 9	154 ± 15, N = 9	n.d.
		P0810	6	35	36	46	23 ± 2, N = 2	12 ± 0, N = 5	185 ± 7, N = 5	n.d.
		0810NH	90	68	55	71*	n.d.	13	n.d.	3646
		0810NH	100	83	56	87	33	18	79	5187
	Warm	P1408	4	67	38	65	9 ± 0, N = 3	9 ± 0, N = 7	194 ± 16, N = 7	n.d.
		P1408	5	87	84	68	9 ± 0, N = 3	6 ± 0, N = 7	175 ± 8, N = 7	n.d.
		1407NH	90	77	77	96	n.d.	19	220	5378
		1407NH	100	91	89	70*	n.d.	7	105	4225
	El Niño	P1604	1	70	71	72	15 ± NA, N = 1	12 ± 3, N = 4	222 ± 68, N = 3	2402 ± NA, N = 1
		P1604	2	90	89	80	18 ± 3, N = 3	10 ± 1, N = 7	187 ± 9, N = 7	4232 ± 249, N = 3
		1604SH	90	52	48	63*	n.d.	27	331	n.d.
		1604SH	100	62	63	63	n.d.	9	190	n.d.

Table S1.4: Hydrographic depths and euphotic zone integrated biogeochemical values for comparing the CCE-LTER to CalCOFI Line 80 by cruise (continued 2/3)

Nitracline, chlorophyll max, and euphotic zone depths with mean biogeochemical parameters integrated over the euphotic zone depth (1% surface irradiance). The average seasonal euphotic zone (designated by *) was used when Secchi disc data was unavailable. Data is available from the Datazoo site (https://oceaninformatics.ucsd.edu/datazoo/catalogs/ccelter/datasets).

Region	Condition	Cruise	Cycle or Station	Nitracline	Chl max	Euphotic Zone	NPP	Chl	POC	TOC
				m			mmol C m^{-2} d^{-1}	mg Chl m^{-2}	mmol C m^{-2}	
Transition	Normal	P0605	4	34	22	33	111 ± 10, N = 4	28 ± 2, N = 10	273 ± 21, N = 6	n.d.
		0604JD	60	27	30	44*	n.d.	33	246	n.d.
		0604JD	70	58	60	51	12	38	239	n.d.
		0604JD	80	81	80	66	n.d.	10	192	n.d.
		P0704	1	0	11	43	93 ± 36, N = 4	52 ± 6, N = 9	354 ± 39, N = 9	1908 ± 150, N = 13
		P0704	4	0	67	49	157 ± 25, N = 4	39 ± 3, N = 9	294 ± 16, N = 9	2260 ± 44, N = 13
		0704JD	60	0	32	44*	n.d.	55	223	n.d.
		0704JD	70	0	16	42	n.d.	24	182	n.d.
		0704JD	80	0	39	42	1	53	272	n.d.
		P0810	1	0	30	29	25 ± 5, N = 4	19 ± 6, N = 9	197 ± 34, N = 9	n.d.
		P0810	3	6	17	25	57 ± 3, N = 3	15 ± 1, N = 7	195 ± 8, N = 7	n.d.
		P0810	4	3	67	19	36 ± 2, N = 2	15 ± 5, N = 5	260 ± 40, N = 5	n.d.
		0810NH	60	20	24	33	86	47	160	1524
		0810NH	70	36	44	33	n.d.	23	367	2050
		0810NH	80	24	26	50*	n.d.	44	339	3234
	Warm	P1408	1	25	38	29	24 ± 5, N = 3	21 ± 5, N = 7	341 ± 50, N = 7	423 ± 16, N = 2
		P1408	2	31	46	32	23 ± 1, N = 3	18 ± 1, N = 7	325 ± 24, N = 7	1602 ± 332, N = 3
		P1408	3	24	33	42	20 ± 0, N = 3	13 ± 1, N = 7	238 ± 17, N = 7	n.d.
		1407NH	60	30	34	54	32	24	360	n.d.
		1407NH	70	25	18	49*	n.d.	26	810	n.d.
		1407NH	80	93	70	81	20	16	194	4566
	El Niño	P1604	3	0	20	43	71 ± 11, N = 3	38 ± 2, N = 7	359 ± 43, N = 7	1995 ± 450, N = 4
		1604SH	60	51	10	44*	n.d.	26	303	n.d.
		1604SH	70	n.d.	n.d.	44*	n.d.	n.d.	n.d.	n.d.
		1604SH	80	n.d.	n.d.	44*	n.d.	n.d.	n.d.	n.d.
	Normal	P1706	3	16	48	39	80 ± 19[‡], N = 6	23 ± 7, N = 6	308 ± 107, N = 3	n.d.
		P1706	4	0	33	40	41 ± 5[‡], N = 4	14 ± 3, N = 4	337 ± 37, N = 2	n.d.
		1704SH	60	0	14	36	n.d.	24	184	n.d.
		1704SH	70	66	67	44*	n.d.	7	137	n.d.
		1704SH	80	71	74	44*	n.d.	4	84	n.d.

Table S1.4: Hydrographic depths and euphotic zone integrated biogeochemical values for comparing the CCE-LTER to CalCOFI Line 80 by cruise (continued 3/3)

Nitracline, chlorophyll max, and euphotic zone depths with mean biogeochemical parameters integrated over the euphotic zone depth (1% surface irradiance). The average seasonal euphotic zone (designated by *) was used when Secchi disc data was unavailable. Data is available from the Datazoo site (https://oceaninformatics.ucsd.edu/datazoo/catalogs/ccelter/datasets).

Region	Condition	Cruise	Cycle or Station	Nitracline	Chl max	Euphotic Zone	NPP	Chl	POC	TOC
				m			mmol C m^{-2} d^{-1}	mg Chl m^{-2}	mmol C m^{-2}	
Nearshore - Upwelling	Normal	P0605	1	0	12	16	285 ± 63, N = 4	66 ± 8, N = 9	425 ± 71, N = 5	758 ± 85, N = 9
		P0605	3	2	10	12	337 ± 6, N = 3	61 ± 4, N = 7	431 ± 50, N = 4	677 ± NA, N = 1
		0604JD	51	0	12	24	n.d.	66	554	n.d.
		0604JD	55	14	39	26*	n.d.	20	252	n.d.
		P0704	3	0	10	49	581 ± NA, N = 1	111 ± 34, N = 2	448 ± 58, N = 2	1945 ± 541, N = 3
		0704JD	51	0	17	24	n.d.	27	156	n.d.
		0704JD	55	0	27	26*	n.d.	17	57	n.d.
		P0810	5	0	18	16	95 ± 17, N = 2	16 ± 4, N = 6	162 ± 18, N = 5	n.d.
		0810NH	51	0	13	38*	n.d.	42	364	2136
		0810NH	55	15	2	38*	n.d.	39	571	1961
	El Niño	P1604	4	4	13	18	130 ± 14, N = 3	49 ± 3, N = 7	449 ± 32, N = 7	902 ± 61, N = 3
		1604SH	51	0	3	26*	n.d.	9	200	n.d.
		1604SH	55	0	5	26*	n.d.	54	341	n.d.
	Normal	P1706	1	0	9	16	395 ± 88[i], N = 6	111 ± 14, N = 6	399 ± 69, N = 4	1067 ± NA, N = 1
		P1706	2	0	19	26	223 ± 31[i], N = 7	67 ± 7, N = 7	666 ± 88, N = 4	n.d.
		1704SH	51	0	11	21	82	29	225	n.d.
		1704SH	55	0	11	18	n.d.	120	438	n.d.

Table S1.5: CalCOFI mean hydrographic depths and euphotic zone integrated biogeochemical values for the oceanic regions by season.

Mean hydrographic depths and biogeochemical parameters integrated over the euphotic zone (1% surface irradiance) depth plus/minus the standard error for CalCOFI cruises.

Region	Season	Nitracline	Chl max	Euphotic Zone	NPP	Chl	POC	TOC
		m			mmol C m^{-2} d^{-1}	mg Chl m^{-2}	mmol C m^{-2}	
Offshore	Sp	77 ± 4, N = 23	66 ± 3, N = 24	63 ± 4, N = 13	22 ± 3, N = 8	13 ± 1, N = 24	191 ± 12, N = 24	3728 ± 190, N = 3
	Su	79 ± 5, N = 22	71 ± 4, N = 22	70 ± 4, N = 11	38 ± 19, N = 5	13 ± 1, N = 26	225 ± 19, N = 26	3756 ± 292, N = 9
	Fa	65 ± 5, N = 25	52 ± 4, N = 25	71 ± 7, N = 14	26 ± 3, N = 10	18 ± 2, N = 27	205 ± 13, N = 26	4223 ± 242, N = 6
	Wi	60 ± 6, N = 19	44 ± 4, N = 20	71 ± 8, N = 5	21 ± 3, N = 3	25 ± 2, N = 23	267 ± 31, N = 23	4242 ± 345, N = 5
Transition	Sp	31 ± 5, N = 36	39 ± 3, N = 36	44 ± 3, N = 16	50 ± 25, N = 6	28 ± 4, N = 36	229 ± 18, N = 36	2318 ± 251, N = 11
	Su	26 ± 5, N = 33	33 ± 3, N = 32	49 ± 4, N = 17	65 ± 23, N = 12	31 ± 5, N = 39	391 ± 52, N = 39	2595 ± 202, N = 13
	Fa	35 ± 4, N = 39	34 ± 2, N = 39	50 ± 5, N = 22	55 ± 11, N = 12	38 ± 9, N = 42	254 ± 25, N = 36	2551 ± 334, N = 9
	Wi	29 ± 4, N = 33	29 ± 3, N = 33	50 ± 4, N = 17	40 ± 5, N = 12	39 ± 11, N = 36	259 ± 25, N = 36	2910 ± 286, N = 9
Nearshore	Sp	1 ± 1, N = 26	16 ± 2, N = 26	26 ± 2, N = 11	160 ± 35, N = 4	62 ± 9, N = 26	275 ± 34, N = 26	1325 ± 181, N = 8
	Su	4 ± 2, N = 22	12 ± 2, N = 22	26 ± 3, N = 13	111 ± 15, N = 6	72 ± 8, N = 26	432 ± 34, N = 26	1878 ± 233, N = 10
	Fa	10 ± 2, N = 26	15 ± 2, N = 26	38 ± 5, N = 5	105 ± 27, N = 3	61 ± 8, N = 28	348 ± 29, N = 28	1729 ± 248, N = 6
	Wi	7 ± 2, N = 22	13 ± 2, N = 22	28 ± 4, N = 6	144 ± NA, N = 1	38 ± 5, N = 22=4	234 ± 41, N = 24	138y6 ± 196, N = 6

Table S1.6: CalCOFI vs CCE-LTER depth profile comparison

Kruskal–Wallis one-way analysis of variance with 95% confidence interval was used to compare the overall CalCOFI and CCE-LTER metrics (i.e. HBac, Pro, Syn, and PEuk abundances) for each pair. Significantly different comparisons ($p<0.05$) are **bold**.

Region	Organism	2006, April/May	2007, April	2008, October	2014, August	2016, April	2017, April/June
Offshore	HBac	**Chi^2 = 7.9092 p = 0.004918**	**Chi^2 =14.755 p = 0.0001224**	Chi^2 =2.702 p = 0.1002	Chi^2 =0.05625 p = 0.681	Chi^2 =0.82049 p = 0.365	NA
	Pro	**Chi^2 =9.2638 p = 0.002337**	**Chi^2 =11.533 p = 0.0006838**	**Chi^2 =13.787 p = 0.00020**	Chi^2 =0.169 p = 0.681	Chi^2 =1.64 p = 0.2003	NA
	Syn	Chi^2 =2.823 p = 0.09292	**Chi^2 =14.756 p = 0.0001223**	Chi^2 =0.77192 p = 0.3796	Chi^2 =0.18907 p = 0.6637	Chi^2 =3.282 p = 0.07005	NA
	PEuk	Chi^2 =3.1164 p = 0.07751	**Chi^2 =17.204 p = 3.358E-05**	Chi^2 =0.16311 p = 0.6863	Chi^2 =1.0241 p = 0.3116	Chi^2 =0.0351225 p = 0.8513	NA
Transition	HBac	**Chi^2 =6.6617 p = 0.00685**	**Chi^2 =13.575 p = 0.00022**	**Chi^2 =18.084 p = 2.11E-5**	Chi^2 =0.18735 p = 0.6651	**Chi^2 =4.4661 p = 0.03457**	**Chi^2 =5.4512 p =0.01955**
	Pro	**Chi^2 =39.76 p = 2.872E-10**	NA	**Chi^2 =22.68 p = 1.914E-6**	**Chi^2 =4.5665 p = 0.0326**	**Chi^2 =19.86 p = 8.333E-6**	**Chi^2 =25.673 p =4.045E-07**
	Syn	Chi^2 =0.19492 p = 0.6589	Chi^2 =1.4628 p = 0.2265	Chi^2 =6.4095 p = 0.01135	Chi^2 =0.20161 p = 0.6534	Chi^2 =1.4545 p = 0.2278	**Chi^2 =10.982 p =0.0009201**
	PEuk	Chi^2 =3.6846 p = 0.05942	Chi^2 =2.2817 p = 0.1309	Chi^2 =0.50643 p = 0.4767	Chi^2 =0.03049 p = 0.8614	**Chi^2 =5.3434 p = 0.0208**	**Chi^2 =4.8807 p =0.02716**
Nearshore	HBac	Chi^2 =1.6261 p = 0.2022	**Chi^2 =10.704 p = 0.00106**	**Chi^2 =16.668 p = 4.452E-5**	NA	**Chi^2 =15.009 p = 0.000107**	**Chi^2 =7.0312 p =0.00801**
	Pro	Chi^2 =1.2407 p = 0.2653	NA	Chi^2 =2.1245 p = 0.145	NA	**Chi^2 =6.4734 p = 0.01095**	NA
	Syn	**Chi^2 =6.9399 p = 0.00842**	**Chi^2 =5.787 p = 0.01614**	Chi^2 =0.52941 p = 0.4669	NA	**Chi^2 =15.685 p = 7.481E-5**	**Chi^2 =18.337 p =1.851E-05**
	PEuk	**Chi^2 =6.0837 p = 0.01364**	Chi^2 =0.33333 p = 0.5637	Chi^2 =1.1912 p = 0.2751	NA	**Chi^2 =17.357 p = 3.097E-5**	Chi^2 =3.409 p =0.06484

1.9 REFERENCES

Agawin NSR, Duarte CM, Agusti S (1998) Growth and abundance of Synechococcus sp. in a Mediterranean Bay: seasonality and relationship with temperature. Marine Ecology Progress Series 170:45-53

Armstrong FAJ, Stearns CR, Strickland JDH (1967) Author links open overlay panel The measurement of upwelling and subsequent biological process by means of the Technicon Autoanalyzer® and associated equipment. Deep Sea Research and Oceanographic Abrstracts 14:381-389

Bec B, Husseini-Ratrema J, Collos Y, Souchu P, Vaquer A (2005) Phytoplankton seasonal dynamics in a Mediterranean coastal lagoon: emphasis on the picoeukaryote community. Journal of Plankton Research 27:881-894

Biller SJ, Berube PM, Lindell D, Chisholm SW (2015) Prochlorococcus: the structure and function of collective diversity. Nature Reviews Microbiology 13:13-27

Bird DF, Kalff J (1984) EMPIRICAL RELATIONSHIPS BETWEEN BACTERIAL ABUNDANCE AND CHLOROPHYLL CONCENTRATION IN FRESH AND MARINE WATERS. Canadian Journal of Fisheries and Aquatic Sciences 41:1015-1023

Bograd SJ, Schroeder ID, Jacox MG (2019) A water mass history of the Southern California current system. Geophysical Research Letters 46:6690-6698

Bond NA, Cronin MF, Freeland H, Mantua N (2015) Causes and impacts of the 2014 warm anomaly in the NE Pacific. Geophysical Research Letters 42:3414-3420

Bustillos-Guzman J, Claustre H, Marty JC (1995) SPECIFIC PHYTOPLANKTON SIGNATURES AND THEIR RELATIONSHIP TO HYDROGRAPHIC CONDITIONS IN THE COASTAL NORTHWESTERN MEDITERRANEAN-SEA. Marine Ecology Progress Series 124:247-258

Chavez FP, Messie M (2009) A comparison of Eastern Boundary Upwelling Ecosystems. Progress in Oceanography 83:80-96

Chen BZ, Liu HB (2011) Temporal stability of marine phytoplankton in a subtropical coastal environment. Aquatic Ecology 45:427-438

Chisholm SW, Olson RJ, Zettler ER, Goericke R, Waterbury JB, Welschmeyer NA (1988) A NOVEL FREE-LIVING PROCHLOROPHYTE ABUNDANT IN THE OCEANIC EUPHOTIC ZONE. Nature 334:340-343

Cho BC, Azam F (1990) BIOGEOCHEMICAL SIGNIFICANCE OF BACTERIAL BIOMASS IN THE OCEANS EUPHOTIC ZONE. Marine Ecology Progress Series 63:253-259

Collier JL, Palenik B (2003) Phycoerythrin-containing picoplankton in the Southern California Bight. Deep-Sea Research Part Ii-Topical Studies in Oceanography 50:2405-2422

Connell PE, Campbell V, Gellene AG, Hu SK, Caron DA (2017) Planktonic food web structure at a coastal time-series site: II. Spatiotemporal variability of microbial trophic activities. Deep-Sea Research Part I-Oceanographic Research Papers 121:210-223

Di Lorenzo E, Mantua N (2016) Multi-year persistence of the 2014/15 North Pacific marine heatwave. Nature Climate Change 6:1042-1047

Di Lorenzo E, Schneider N, Cobb KM, Franks PJS, Chhak K, Miller AJ, McWilliams JC, Bograd SJ, Arango H, Curchitser E, Powell TM, Riviere P (2008) North Pacific Gyre Oscillation links ocean climate and ecosystem change. Geophysical Research Letters 35

Eppley RW, Holm-Hansen O (1986) Primary Production in the Southern California Bight, Vol 15. Springer-Verlag

Flombaum P, Gallegos JL, Gordillo RA, Rincon J, Zabala LL, Jiao NAZ, Karl DM, Li WKW, Lomas MW, Veneziano D, Vera CS, Vrugt JA, Martiny AC (2013) Present and future global distributions of the marine Cyanobacteria Prochlorococcus and Synechococcus. Proceedings of the National Academy of Sciences of the United States of America 110:9824-9829

Gentemann CL, Fewings MR, Garcia-Reyes M (2017) Satellite sea surface temperatures along the West Coast of the United States during the 2014-2016 northeast Pacific marine heat wave. Geophysical Research Letters 44:312-319

Georicke R, Verick E, Koslow R, Sydeman WJ, Schwing FB, Bograd SJ, Peterson WT, Emmett R, Lara Lara JRé, Gaxiola Castro G, G ómez Valdez Jé, Hyrenbach KD, Bradley RW, Weise MJ, Harvey JT, Collins C, Lo NCH (2007) The state of the California Current, 2006–2007: regional and local processes dominate. In, Book 48, California Cooperative Fisheries Investigations Report

Goericke R (2011) The structure of marine phytoplankton communities--patterns, rules, and mechanisms. In, Book 52, California Cooperative Oceanic Fisheries Investigations Report

Goericke R, Ohman MD (2015) Introduction to CCE-LTER: Responses of the California Current Ecosystem to climate forcing. Deep-Sea Research Part Ii-Topical Studies in Oceanography 112:1-5

Gomez-Ocampo E, Gaxiola-Castro G, Burazo R, Beier E (2018) Effects of the 2013-2016 warm anomalies on the California Current phytoplankton. Deep-Sea Research Part Ii-Topical Studies in Oceanography 151:64-76

Grossart HP, Ploug H (2001) Microbial degradation of organic carbon and nitrogen on diatom aggregates. Limnology and Oceanography 46:267-277

Gutierrez-Rodriguez A, Slack G, Daniels EF, Selph KE, Palenik B, Landry MR (2014) Fine spatial structure of genetically distinct picocyanobacterial populations across environmental gradients in the Costa Rica Dome. Limnology and Oceanography 59:705-723

Halewood ER, Carlson CA, Brzezinski MA, Reed DC, Goodman J (2012) Annual cycle of organic matter partitioning and its availability to bacteria across the Santa Barbara Channel continental shelf. Aquatic Microbial Ecology 67:189-209

Hayward TL, Venrick EL (1998) Nearsurface pattern in the California Current: coupling between physical and biological structure. Deep-Sea Research Part Ii-Topical Studies in Oceanography 45:1617-1638

Jacox MG, Hazen EL, Zaba KD, Rudnick DL, Edwards CA, Moore AM, Bograd SJ (2016) Impacts of the 2015-2016 El Nino on the California Current System: Early assessment and comparison to past events. Geophysical Research Letters 43:7072-7080

Kashtan N, Roggensack SE, Rodrigue S, Thompson JW, Biller SJ, Coe A, Ding HM, Marttinen P, Malmstrom RR, Stocker R, Follows MJ, Stepanauskas R, Chisholm SW (2014) Single-Cell Genomics Reveals Hundreds of Coexisting Subpopulations in Wild Prochlorococcus. Science 344:416-420

Kent AG, Baer SE, Mouginot C, Huang JS, Larkin AA, Lomas MW, Martiny AC (2019) Parallel phylogeography of Prochlorococcus and Synechococcus. Isme Journal 13:430-441

Kirchman D, Ducklow H, Mitchell R (1982) ESTIMATES OF BACTERIAL GROWTH FROM CHANGES IN UPTAKE RATES AND BIOMASS. Applied and Environmental Microbiology 44:1296-1307

Kirchman D, Knees E, Hodson R (1985) LEUCINE INCORPORATION AND ITS POTENTIAL AS A MEASURE OF PROTEIN-SYNTHESIS BY BACTERIA IN NATURAL AQUATIC SYSTEMS. Applied and Environmental Microbiology 49:599-607

Landry MR, Kirchman DL (2002) Microbial community structure and variability in the tropical Pacific. Deep-Sea Research Part Ii-Topical Studies in Oceanography 49:2669-2693

Landry MR, Ohman MD, Goericke R, Stukel MR, Tsyrklevich K (2009) Lagrangian studies of phytoplankton growth and grazing relationships in a coastal upwelling ecosystem off Southern California. Progress in Oceanography 83:208-216

Li WKW, Head EJH, Harrison WG (2004) Macroecological limits of heterotrophic bacterial abundance in the ocean. Deep-Sea Research Part I-Oceanographic Research Papers 51:1529-1540

Linacre L, Lara-Lara R, Camacho-Ibar V, Herguera JC, Bazan-Guzman C, Ferreira-Bartrina V (2015) Distribution pattern of picoplankton carbon biomass linked to mesoscale dynamics in the southern gulf of Mexico during winter conditions. Deep-Sea Research Part I-Oceanographic Research Papers 106:55-67

Linacre LP, Landry MR, Lara-Lara JR, Hernandez-Ayon JM, Bazan-Guzman C (2010) Picoplankton dynamics during contrasting seasonal oceanographic conditions at a coastal upwelling station off Northern Baja California, Mexico. Journal of Plankton Research 32:539-557

Lindell D, Post AF (1995) ULTRAPHYTOPLANKTON SUCCESSION IS TRIGGERED BY DEEP WINTER MIXING IN THE GULF-OF-AQABA (EILAT), RED-SEA. Limnology and Oceanography 40:1130-1141

Mantua NJ, Hare SR, Zhang Y, Wallace JM, Francis RC (1997) A Pacific interdecadal climate oscillation with impacts on salmon production. Bulletin of the American Meteorological Society 78:1069-1079

Mantyla AW, Bograd SJ, Venrick EL (2008) Patterns and controls of chlorophyll-a and primary productivity cycles in the Southern California Bight. Journal of Marine Systems 73:48-60

Massana R (2011) Eukaryotic Picoplankton in Surface Oceans. Annual Review of Microbiology, 65:91-110

Miller AJ, Song H, Subramanian AC (2015) The physical oceanographic environment during the CCE-LTER Years: Changes in climate and concepts. Deep-Sea Research Part Ii-Topical Studies in Oceanography 112:6-17

Monger BC, Landry MR (1993) FLOW CYTOMETRIC ANALYSIS OF MARINE-BACTERIA WITH HOECHST 33342. Applied and Environmental Microbiology 59:905-911

Moore LR, Post AF, Rocap G, Chisholm SW (2002) Utilization of different nitrogen sources by the marine cyanobacteria Prochlorococcus and Synechococcus. Limnology and Oceanography 47:989-996

Morrow RM, Ohman MD, Goericke R, Kelly TB, Stephens BM, Stukel MR (2018) CCE V: Primary production, mesozooplankton grazing, and the biological pump in the California Current Ecosystem: Variability and response to El Nino. Deep-Sea Research Part I-Oceanographic Research Papers 140:52-62

Munro DR, Quay PD, Juranek LW, Goericke R (2013) Biological production rates off the Southern California coast estimated from triple O-2 isotopes and O-2 : Ar gas ratios. Limnology and Oceanography 58:1312-1328

Nagai T, Gruber N, Frenzel H, Lachkar Z, McWilliams JC, Plattner GK (2015) Dominant role of eddies and filaments in the offshore transport of carbon and nutrients in the California Current System. Journal of Geophysical Research-Oceans 120:5318-5341

Nagarkar M, Countway PD, Yoo YD, Daniels E, Poulton NJ, Palenik B (2018) Temporal dynamics of eukaryotic microbial diversity at a coastal Pacific site. Isme Journal 12:2278-2291

Ohman MD, Barbeau K, Franks PJS, Goericke R, Landry MR, Miller AJ (2013) Ecological Transitions in a Coastal Upwelling Ecosystem. Oceanography 26:210-219

Ohman MD, Powell JR, Picheral M, Jensen DW (2012) Mesozooplankton and particulate matter responses to a deep-water frontal system in the southern California Current System. Journal of Plankton Research 34:815-827

Olson RJ, Chisholm SW, Zettler ER, Altabet MA, Dusenberry JA (1990) SPATIAL AND TEMPORAL DISTRIBUTIONS OF PROCHLOROPHYTE PICOPLANKTON IN THE NORTH-ATLANTIC OCEAN. Deep-Sea Research Part a-Oceanographic Research Papers 37:1033-1051

Organelli E, Claustre H (2019) Small Phytoplankton Shapes Colored Dissolved Organic Matter Dynamics in the North Atlantic Subtropical Gyre. Geophysical Research Letters 46:12183-12191

Paerl HW (1975) Microbial Attachment to Particles in Marine and Freshwater Ecosystems. Microbial Ecology 2:73-83

Paerl RW, Johnson KS, Welsh RM, Worden AZ, Chavez FP, Zehr JP (2011) Differential distributions of Synechococcus subgroups across the California current system. Frontiers in Microbiology 2:59

Paerl RW, Turk KA, Beinart RA, Chavez FP, Zehr JP (2012) Seasonal change in the abundance of Synechococcus and multiple distinct phylotypes in Monterey Bay determined by rbcL and narB quantitative PCR. Environmental Microbiology 14:580-593

Partensky F, Blanchot J, Lantoine F, Neveux J, Marie D (1996) Vertical structure of picophytoplankton at different trophic sites of the tropical northeastern Atlantic Ocean. Deep-Sea Research Part I-Oceanographic Research Papers 43:1191-1213

Partensky F, Blanchot J, Vaulot D (1999a) Differential distribution and ecology of Prochlorococcus and Synechococcus in oceanic waters: a review. Bulletin of the Oceanographic Institute of Monaco 19:457-475

Partensky F, Hess WR, Vaulot D (1999b) Prochlorococcus, a marine photosynthetic prokaryote of global significance. Microbiology and Molecular Biology Reviews 63:106-127

Peterson WT, Fisher JL, Strub PT, Du XN, Risien C, Peterson J, Shaw CT (2017) The pelagic ecosystem in the Northern California Current off Oregon during the 2014-2016 warm anomalies within the context of the past 20 years. Journal of Geophysical Research-Oceans 122:7267-7290

Ploug H, Grossart HP (1999) Bacterial production and respiration in suspended aggregates - a matter of the incubation method. Aquatic Microbial Ecology 20:21-29

Ploug H, Grossart HP, Azam F, Jorgensen BB (1999) Photosynthesis, respiration, and carbon turnover in sinking marine snow from surface waters of Southern California Bight: implications for the carbon cycle in the ocean. Marine Ecology Progress Series 179:1-11

Rykaczewski RR, Checkley DM (2008) Influence of ocean winds on the pelagic ecosystem in upwelling regions. Proceedings of the National Academy of Sciences of the United States of America 105:1965-1970

Saito MA, Rocap G, Moffett JW (2005) Production of cobalt binding ligands in a Synechococcus feature at the Costa Rica upwelling dome. Limnology and Oceanography 50:279-290

Samo TJ, Pedler BE, Ball GI, Pasulka AL, Taylor AG, Aluwihare LI, Azam F, Goericke R, Landry MR (2012) Microbial distribution and activity across a water mass frontal zone in the California Current Ecosystem. Journal of Plankton Research 34:802-814

Simon M, Azam F (1989) PROTEIN-CONTENT AND PROTEIN-SYNTHESIS RATES OF PLANKTONIC MARINE-BACTERIA. Marine Ecology Progress Series 51:201-213

Smale DA, Wernberg T, Oliver ECJ, Thomsen M, Harvey BP, Straub SC, Burrows MT, Alexander LV, Benthuysen JA, Donat MG, Feng M, Hobday AJ, Holbrook NJ, Perkins-Kirkpatrick SE, Scannell HA, Sen Gupta A, Payne BL, Moore PJ (2019) Marine heatwaves threaten global biodiversity and the provision of ecosystem services. Nature Climate Change 9:306-312

Smith DC, Azam F (1992) A simple, economical method for measuring bacterial protein synthesis in seawater using 3H-leucine. In, Book 6, Mar. Microb. Food Webs

Stephens BM, Porrachia M, Dovel S, Roadman M, Goericke R, Aluwihare LI (2018) Nonsinking Organic Matter Production in the California Current. Global Biogeochemical Cycles 32:1386-1405

Strickland JDH, Parsons TR (1972) A Practical Handbook of Seawater Analysis. In, Book 157. Fisheries Research Board of Canada Bulletin

Stukel, Michael, Goericke R, Landry M (2019) Predicting primary production in the southern California Current Ecosystem from chlorophyll, nutrient concentrations, and irradiance. bioRxiv 590240

Stukel MR, Ohman MD, Benitez-Nelson CR, Landry MR (2013) Contributions of mesozooplankton to vertical carbon export in a coastal upwelling system. Marine Ecology Progress Series 491:47-65

Sudek S, Everroad RC, Gehman ALM, Smith JM, Poirier CL, Chavez FP, Worden AZ (2015) Cyanobacterial distributions along a physico-chemical gradient in the Northeastern Pacific Ocean. Environmental Microbiology 17:3692-3707

Suttle CA (2007) Marine viruses - major players in the global ecosystem. Nature Reviews Microbiology 5:801-812

Suttle CA, Chan AM (1994) DYNAMICS AND DISTRIBUTION OF CYANOPHAGES AND THEIR EFFECT ON MARINE SYNECHOCOCCUS SPP. Applied and Environmental Microbiology 60:3167-3174

Tai V, Burton RS, Palenik B (2011) Temporal and spatial distributions of marine Synechococcus in the Southern California Bight assessed by hybridization to bead-arrays. Marine Ecology Progress Series 426:133-U164

Tai V, Palenik B (2009) Temporal variation of Synechococcus clades at a coastal Pacific Ocean monitoring site. Isme Journal 3:903-915

Taylor AG, Goericke R, Landry MR, Selph KE, Wick DA, Roadman MJ (2012) Sharp gradients in phytoplankton community structure across a frontal zone in the California Current Ecosystem. Journal of Plankton Research 34:778-789

Taylor AG, Landry MR (2018) Phytoplankton biomass and size structure across trophic gradients in the southern California Current and adjacent ocean ecosystems. Marine Ecology Progress Series 592:1-17

Taylor AG, Landry MR, Selph KE, Wokuluk JJ (2015) Temporal and spatial patterns of microbial community biomass and composition in the Southern California Current Ecosystem. Deep-Sea Research Part II-Topical Studies in Oceanography 112:117-128

Vazquez-Dominguez E, Duarte CM, Agusti S, Jurgens K, Vaque D, Gasol JM (2008) Microbial plankton abundance and heterotrophic activity across the Central Atlantic Ocean. Progress in Oceanography 79:83-94

Worden AZ, Nolan JK, Palenik B (2004) Assessing the dynamics and ecology of marine picophytoplankton: The importance of the eukaryotic component. Limnology and Oceanography 49:168-179

Zhao Z, Gonsior M, Luek J, Timko S, Ianiri H, Hertkorn N, Schmitt-Kopplin P, Fang XT, Zeng QL, Jiao NZ, Chen F (2017) Picocyanobacteria and deep-ocean fluorescent dissolved organic matter share similar optical properties. Nature Communications 8

Chapter 2: Imbalance of carbon production and removal processes in the offshore California Current Ecosystem

Sara R. Rivera, Brandon M. Stephens, Ty J. Samo, Michael R. Stukel, Mark Ohman, Michael R. Landry, Farooq Azam, Lihini I. Aluwihare

ABSTRACT

Several existing studies suggest that lateral export of nutrients, organic matter, and organisms connects nearshore upwelling regions to offshore oligotrophic environments in the California Current Ecosystem (CCE). Using data from cruises conducted in the CCE between 2006-2017, we compare indices of heterotrophic bacterial abundance and activity to indices of primary production to test the hypothesis that the offshore CCE is a net heterotrophic environment. Bacterial abundance increased as a ratio of autotrophic biomass from the nearshore (0.11 ± 0.05) to the offshore (0.61 ± 0.07). The fraction of local net primary production (NPP) represented by bacterial production also increased from the nearshore (0.08 ± 0.03) to the offshore (0.26 ± 0.05). Furthermore, calculated bacterial carbon demand (BCD) could be satisfied in excess by NPP nearshore but exceeded local NPP offshore. Together these data support the hypothesis that oligotrophic offshore environments of the CCE are net heterotrophic. A first order food web incorporating the microbial loop indicated that lateral transport from a net autotrophic nearshore could support zooplankton grazing in the net heterotrophic offshore, with an overall net NPP surplus of roughly 67 mmol C m^{-2} d^{-1}, but that estimated DOC released by phytoplankton and zooplankton processes was insufficient to support BCD in much of the CCE. We propose that excess NPP from the nearshore is transported laterally in mesoscale features, such as westward propagating filaments, to

differentially support bacterioplankton and zooplankton communities and explain the observed imbalance in the offshore. This is supported by a close examination of a westward propagating filament in the CCE.

2.1. INTRODUCTION

Several studies have debated the net metabolic state of the upper ocean (Duarte et al. 2013, Ducklow & Doney 2013, Williams et al. 2013). In this debate, oligotrophic subtropical gyres have emerged as potential regions of net heterotrophy, fueled by the lateral advection of organic carbon from productive coastal regions, particularly Eastern Boundary Current Upwelling systems (Alvarez-Salgado et al. 2007, Nagai et al. 2015).

The California Current Ecosystem (CCE) is a moderately productive Eastern Boundary Current that flows equatorward along the coast of the western United States (Chavez & Messie 2009). The biological productivity of the CCE is supported by both wind driven coastal upwelling and Ekman pumping (Ohman et al. 2013). The CCE hosts the California Current Ecosystem Long Term Ecological Research (CCE-LTER) program, which uses short Lagrangian cycles to examine mesoscale variability and conduct biological process experiments (Goericke & Ohman 2015). Recent modeling suggests that offshore transport of nutrients and organic matter by mesoscale features, such as eddies and filaments, is an important process in this system (Gruber et al. 2011, Nagai et al. 2015). Increasing e-ratios from nearshore to offshore (Kelly et al. 2018) and total organic carbon (TOC) gradients in the CCE (Stephens et al. 2018) support these modeling results. The response of the heterotrophic bacterial community to potential offshore gradients in organic matter has not been examined

in this system to date, but it may be anticipated that bacterial carbon demand (BCD) as a fraction of local net primary production (NPP) also increases offshore.

Heterotrophic bacteria, because of their high abundance and fast growth rates (Moran et al. 2015, Burrell et al. 2017), represent an attractive and accessible component of ecosystems to study and monitor in the context of global change. For example, several climate models predict that the warming of the surface ocean will increase stratification and subsequently, decrease nutrient delivery to the surface ocean (Sarmiento et al. 2004, Polovina et al. 2008). The increase in oligotrophic ocean area may also increase regions of net heterotrophy, at least temporarily (Hoppe et al. 2002, Polovina et al. 2008, Duarte et al. 2013). Understanding the future flow of energy and nutrients within the surface ocean can thus benefit from a study of microbial dynamics across a gradient of stratification regimes.

As major recyclers of organic matter, heterotrophic bacteria play a crucial role in determining the net metabolic state of the ocean (Azam et al. 1983, Azam & Malfatti 2007, Fenchel 2008). They modulate the lateral transport of dissolved and suspended particulate organic carbon (Legendre & Lefevre 1995, del Giorgio & Duarte 2002) because their respiration decreases the concentration of organic carbon available for off-shore export (Aristegui et al. 2004). In addition, heterotrophic bacteria can convert the entrained particulate organic carbon (POC) into dissolved organic carbon (DOC) due to inefficient coupling of hydrolysis and uptake (Smith et al. 1992), which can decrease the loss of organic carbon through vertical export (Alvarez-Salgado et al. 2007).

Here, we examine the metabolic state of the ocean across three biogeographic regimes within the CCE through a comparison of heterotrophic and autotrophic parameters. By including bacterial production (BP) along with other pathways of carbon exchange in the

microbial loop, our data support the hypothesis that in the CCE, excess organic carbon is available for export from the nearshore. Whereas in the oligotrophic offshore environment, the deficits or sometimes close balance of fluxes together with the potential uncertainties around the parameters of bacterial growth efficiency (BGE) and DOC release, supports that hypothesis that the offshore can be net heterotrophic. This pattern was also implied by the heterotrophic bacterial: phytoplankton biomass or productivity ratios. Finally, we use the warm anomaly data from 2014 to examine how the metabolic state of the CCE may respond to future marine heatwaves *sensu* Frolicher and Laufkotter (2018).

2.2. METHODS

2.2.1 Study region and sampling periods

Data for this study were collected in the southern California Current System that encompasses typical springtime upwelling dominated waters nearshore of Point Conception and extends to the edge of the oligotrophic gyre, up to 500 km offshore. Samples for this study were collected on CCE-LTER cruises from May 8–June 7 2006 (P0605), April 2–21, 2007 (P0704), September 30–October 29 2008 (P0810), August 6–September 4 (P1408), April 19–May 12 2016 (P1604), and June 1–July 2 2017 (P1706) (see Sections 1.3.1 and 1.4.1, Kelly et al. 2018, Morrow et al. 2018 for details). Ecosystem conditions during 2004-2013 and 2017 were El Niño-neutral ("normal") and 2014-2016 were warm, with a warm anomaly encountered during P1408 (Bond et al. 2015, Gentemann et al. 2017) and the tail of end of El Niño conditions encountered during P1604 (Di Lorenzo & Mantua 2016, Jacox et al. 2016). The sampling framework for the CCE-LTER is well described (Landry et al. 2009, Ohman et al. 2012, Stukel et al. 2013) and is only briefly described here. During CCE-LTER

cruises, a Moving Vessel Profiler or a SeaSoar (Ohman et al. 2012) was used to identify particular physical and biological conditions for further process studies. Depending on the cruise, the sampling sites were chosen to represent various hydrographic regimes including, California Current waters, active coastal upwelling, oligotrophic gyre regions, or (sub)mesoscale features such as frontal zones and filaments. Regional groupings of cruise-cycles were delineated according to water column properties such as nitracline depth, chlorophyll maximum depth, and euphotic zone depth (see Sections 1.3.1 and 1.4.1).

2.2.2 Hydrographic conditions

In this study, the euphotic zone (EZ) depth is defined as the 0.1% surface irradiance depth. A 0.1% surface irradiance depth was used instead of the more common 1% to most accurately approximate the depth of the light compensation point, or the point where net photosynthesis is zero (Eppley & Holm-Hansen 1986, Karl & Church 2017). Photosynthetically active radiation (PAR) was measured using a 4-π Licor PAC sensor in the water column and a 2-π Licor PAC sensor for surface measurements, and percent surface irradiance was calculated from in situ PAR recorded by the CTD downcast and surface PAR. Where possible, daily, cast by cast data were used and then averaged to be consistent with other measured parameters. Integrated values discussed in this paper refer to data integrations performed over the average EZ depth, as defined here, for each cycle.

2.2.3 Chlorophyll and Primary Production measurements

Chlorophyll a (Chl) concentrations were measured at 6-8 depths after Strickland and Parsons (1972) and converted to autotrophic biomass (AB) using a modeled carbon (mg):Chl

(mg) calculated from the method described in Li et al. (2010). NPP was measured at 6-8 depths using the ^{14}C method after Strickland and Parsons (1972) and as detailed in Morrow et al. (2018), but because ^{14}C-NPP samples were compromised for P1706, NPP was computed from a model that assimilated data from previous CCE-LTER cruises (Stukel et al. 2019a).

2.2.4 Supporting chemical measurements

Approximately 40 mL of seawater (SW) was collected from at least 6 depths for TOC (P0704, P1408, P1604) and/or DOC (P1408, P1604, P1706) analysis following Stephens et al. (2018). Two (P0605, P0704, P0810) or four (P1408, P1604, P1706) L of SW were filtered and processed for suspended POC measurements following Stephens et al. (2018).

2.2.5 Export of sinking POC

Export of sinking POC was measured using VERTEX-style, surface-tethered drifting particle interceptor traps (PIT). Briefly, traps were deployed with a formaldehyde-brine for 2.5 to 5.5 days with PIT cross-pieces typically positioned near the base of the euphotic zone and at one to two deeper depths. After recovery, swimming mesozooplankton were carefully removed under a stereomicroscope and samples were split and filtered for multiple analyses, including particulate organic carbon and nitrogen. Detailed methods are available in Stukel et al. (2019b) and Stukel & Barbeau (2020).

Sinking POC flux was normalized to the base of the EZ, averaged over each Cycle, using: $f_{EZ}=f_{sedtrap}\times\gamma\Delta d$, where γ is the remineralization length coefficient and Δd is the difference between the depth of the euphotic zone and the depth of the sediment trap (Kelly et al. 2018). An average γ value of 0.0063 m^{-1} was used based on previous work (Stukel et al

2015). During P0605 sediment traps were not deployed, and so, 234Th:238U disequilibria integrated to a depth of 1% surface irradiance was used, after Kelly et al. (2018).

2.2.6 Heterotrophic bacterial abundance (BA) and bacterial biomass (BB) by Flow Cytometry (FCM)

Bacterial abundance and biomass were determined from preserved samples (2 ml SW + paraformaldehyde, 0.5% final) that had been flash frozen in liquid N2, stored at -80°C, and sent to the University of Hawaii's School of Ocean and Earth Science and Technology (SOEST) Flow Cytometry Facility. Prior to analysis, samples were thawed and stained with Hoechst 33342 in the dark, at room temperature, for 1 hour (Monger & Landry 1993) and heterotrophic bacterial abundance was quantified with a Beckman-Coulter EPICS Altra flow cytometer with dual lasers (tuned to UV [200 mW] and 488 nm [1 W] excitation). All samples were spiked with fluorescent beads to normalize fluorescence and scattering properties. Raw data were processed using the software FlowJo (Treestar Inc., www.flowjo.com) with correction factors of 0.95 for preservative, 0.10 run volume and 0.82 coincidence. To estimate heterotrophic bacterial biomass (BB), flow cytometry (FCM) based bacterial abundance (BA) measurements were multiplied using a uniform heterotrophic bacterial cell carbon content of 11 fg C $cell^{-1}$ (Garrison et al. 2000).

2.2.7 Bacterial Production (BP)

Seawater samples were also taken from 6 depths from each mid-day CTD cast, typically at 11 a.m., to estimate rates of bacterial protein synthesis (Kirchman et al. 1982, Kirchman et al. 1985, Simon & Azam 1989, Smith & Azam 1992). Over the course of the

CCE-LTER program, these measurements were made by different investigators, which has resulted in some method discrepancies between cruises.

For each sample, 1.7 mL seawater, or 1.8 mL seawater during P1408, were incubated with approximately 20 nM 3H-Leucine for one hour. Incubation temperatures varied depending on the cruise: 10°C (samples collected from 75 to 200 m) and 12°C (samples collected from surface to 70 m) during P0704; *in situ* temperature during P0810; 12°C during P1408; room temperature during P1604; and 9°C during P1706. Incubation temperature in the offshore and transition regions had no significant impact on BP values ($p = 0.15$ and 0.45, respectively), but was statistically significant in the nearshore ($p<0.05$); however, the nearshore was the most data limited and the resulting slope ($m = 0.052$) suggests there was minimal impact of incubation temperature on BP. Samples from P0704 and P0810 were done in triplicate with duplicate TCA-killed controls. Samples from P1408 were done in quadruplicate with duplicate TCA-killed controls. Samples from P1604, and P1706 were done in triplicate with single TCA-killed controls. The standard errors of all methods were comparable. After the incubation was complete, all samples were killed with an addition of 100% TCA for a final concentration of 5% TCA. The P0704 and P0810 samples were filtered on 0.2 µm pore size polycarbonate filters and three additions of 1 mL 5% TCA were made. The filters were dried in individual scintillation vials at room temperature before scintillation cocktail was added and analyzed. The P1408, P1604, and P1706 samples were processed using the centrifugation method as described in Smith et al. (1992). Samples were frozen and stored at -20°C as needed. All samples were analyzed for disintegrations per minute on a Beckman LS6000A liquid scintillation counter. Disintegrations per minute were converted to protein synthesis rates assuming 3.1 kg C mol^{-1} leucine and 24 h day^{-1} (Simon & Azam 1989).

Bacterial growth efficiency (BGE) was calculated from bacterial production per hour (BP) using the equation $BGE = \frac{0.037 + 0.65 \times BP}{1.8 + BP}$ as described by del Giorgio and Cole (1998). Bacterial carbon demand (BCD) was calculated from EZ integrated BP per day and the calculated EZ integrated BGE using $BCD = \frac{BP}{BGE}$.

2.2.8 Microzooplankton and mesozooplankton grazing rates on phytoplankton

Microzooplankton grazing rates were assessed from rates of phytoplankton community growth in dilution experiments as described in Landry et al. (2009). The percent of NPP grazed by microzooplankton was calculated as the phytoplankton growth rate divided by the microzooplankton grazing rate (Landry et al. 2009).

Mesozooplankton grazing rates were determined from gut pigment samples taken from twice daily oblique bongo net tows (late morning and near midnight tows with a target depth of 210 using a 0.71 m diameter net with 202 µm mesh) as described in Morrow et al. (2018). The grazing rate, determined from the sum of chlorophyll and phaeopigment, was converted to carbon units using the previously described carbon (mg):Chl (mg) calculated from the method described in Li et al. (2010) and integrated to the EZ depth.

2.3. RESULTS

2.3.1 Biomass and Production Indices

The metabolic state of a region was assessed from the ratio of EZ integrated heterotrophic bacterial biomass (BB) to EZ integrated autotrophic biomass (AB). In this case, BB was estimated from FCM and AB was calculated from Chl (Table 2.1, Appendix Table

S2.1). This ratio of BB:AB will be referred to as the "biomass index." We also calculated the ratio of EZ integrated bacterial production (BP) to EZ integrated net primary production (NPP), herein referred to as the "productivity index." We examined both these indices because we did not measure BP on every CCE-LTER cruise presented here.

The biomass index (Figure 2.1a) increased from the nearshore (average of cycles: 0.21 ± 0.07), through the transition (0.57 ± 0.12), to the offshore (0.97 ± 0.18), even though the amount of BB and AB decreased from nearshore to the offshore (Table 2.1). Non-integrated values were also highest in the offshore and transition regions in comparison to the nearshore (Appendix Figure S2.1a). The highest BB:AB values were found at low NPP values, whereas the BB:AB was always low at the highest NPP values, indicating that AB and BB did not scale similarly with NPP. An analogous relationship is observed for the productivity index, with nearshore (0.08 ± 0.03) increasing through the transition (0.15 ± 0.03) to the offshore (0.26 ± 0.05) (Figure 2.1b; Appendix Figure S2.1b). Although there is good agreement between the regional averages ($Production\ index = 4.17(Biomass\ index) - 0.10$, R^2 = 0.99), there is no clear relationship between the biomass index and the productivity index by Lagrangian cycle. For example, the highest biomass indices and production indices were not observed on the same cruises. Overall, the productivity index occupies half the range of the biomass index, but without direct estimates of bacterial carbon content (BCC), it is difficult to ascertain whether the biomass index is representative of the environment. However, BCC of offshore and transition regions would have to be lower than 11 fg C $cell^{-1}$ to bring biomass index values below 1, and biomass indices exceeding 1 are not unusual for oligotrophic environments (Fuhrman et al. 1989, Cho & Azam 1990). Production indices for the CCE were similar to those calculated in upwelling coastal (0.04-0.22) and oceanic (0.19-0.28) regions

off central Chile (Cuevasa et al. 2004). Lagrangian studies off the NW Iberian margin reported production indices within the EZ that were similar to the CCE nearshore: 0.06 ± 0.01 and 0.07 ± 0.01 at the shelf-edge and off-shelf, respectively (Barbosa et al. 2001). Biomass indices from the same study were 0.15 ± 0.01 along the shelf-edge, not much different from the CCE nearshore, and 0.39 ± 0.04 off-shelf in an upwelling filament, which falls between the CCE nearshore and transition.

To further examine these patterns of high biomass indices at low NPP, which suggest net heterotrophy, Cole (1999) attempted to constrain the ratio of bacterial respiration (BR) to NPP. When BR is close to or exceeds NPP, the system must be net heterotrophic. We did not directly measure BR or BGE in this study, and so, we used the relationship of del Giorgio and Cole (1998) to calculate BGE. Although we realize that these are dependent estimates, the patterns we observe are consistent with our expectations and previous studies. When the relationship between our calculated BGE and the production index is examined in the context of the BR:NPP relationship (following Cole, (1999); Figure 2.2a), we see that the nearshore is mostly autotrophic. However, most of our transition and offshore cycles fall well outside the range of net autotrophy. The 2014 cruise stood out because all regions had high production indices but low BGE, which suggested that net heterotrophy dominated the system during this time. Similar patterns were observed for offshore cycles from 2016.

Our BGE values are on the low end but we have confidence in these values for reasons outlined below. It has been suggested that high BGEs may be more typical of longer incubations and that short term respiration experiments give lower BGEs (del Giorgio et al. (2011). BGEs for marine bacteria have been previously calculated to be between 10-30% (Lancelot & Billen 1984, Billen & Fontigny 1987), with values as low as 1% in the

oligotrophic ocean and as high as 61% in eutrophic estuaries (Coffin et al. 1993) and coastal bloom conditions (Wear et al. 2015). Finally, our calculated values are nearly identical to the values and trend calculated from BR and BP along an inshore-offshore transect off the coast of Oregon (del Giorgio et al. 2011). The latter study observed BGEs that were <15%, and which generally decreased offshore. However, when longer term incubations were examined, that is, when filtered samples were incubated for 24 hours or more and then tested for BP using the standard methods described here, the relationship to concurrent BR measurements yielded much higher BGE values. Our data are most similar to the initial BP measurements reported in del Giorgio et al (2011), which all fall below a BGE of 20% (see Figure 2.2a).

Since we used BP to calculate BGE, our measurements may be biased to respond more sensitively to variations in NPP, for example, especially given evidence that BP responds more strongly to resource availability (including substrate quality and quantity) whereas BR may not (del Giorgio & Cole 1998, Lopez-Urrutia & Moran 2007). However, our data in regions of low NPP (i.e., when BP is >20% of NPP) would require BGEs >15-30% in order to approach BR:NPP = 1, especially for offshore cycles from 2014 and 2016.

2.3.2 Calculated Bacterial Carbon Demand (BCD)

Bacterial carbon demand (BCD) was estimated from BGE (Figure 2b) and increased from nearshore (135 ± 10 mmol C m^{-2} d^{-1}) through the transition (143 ± 9 mmol C m^{-2} d^{-1}) and to the offshore (150 ± 16 mmol C m^{-2} d^{-1}) regions, but these differences were not significant (ANOVA, $p = 0.74$)and indicated marked variability with NPP. Values to the right of the 1:1 line (Figure 2.2b) indicated that only in nearshore cycles did NPP exceed BCD (Table 2.2, Appendix Table S2.2). Measured BCD:NPP has been shown in the nearshore

Santa Barbara Channel to have a wide range of 20 to 180% (Halewood et al. 2012), consistent with the nearshore range of 19-109% observed for this study. All cycles from 2007 were also close to the 1:1 line identifying a system that was likely close to balance during this time. Gross primary production (GPP, designated by the 3:1 line based on rounding up the average $GPP_{O2/Ar}$:NPP_{14C} of 2.4 from Kranz et al. [2020]) generally exceeded BCD in the transition region, but still indicated a deficit in PP for the offshore.

The BCD as a percentage of NPP were highest in offshore cycles during P1408 and P1604 (Appendix Table S2.2) and required unreasonable extracellular DOC release relative to NPP to satisfy the calculated BCD. To put this in the context of a "missing carbon flux", calculated BCD exceeded NPP by 125 ± 18 mmol C L^{-1} d^{-1} in the offshore (Appendix Table S2.2; where NPP was 25 ± 5 mmol C L^{-1} d^{-1}). It is possible that our calculation of BGE and then BCD provides unreasonable values (see discussion above), but BCD would have to be approximately 10 fold lower and therefore, BGE ~50%, based on the measured BP:NPP. However, this high BCD could be satisfied by supplements from the nearshore.

2.3.3 Food Web Dynamics of the CCE

Food web dynamics of the CCE domain are complicated by changing community structure and mesoscale features, but we attempt to simplify this by using the previously defined oceanic regions. In this preliminary food web analysis, we include loss terms for NPP including micro- and mesozooplankton grazing (terms B and C, respectively, in Figure 2.3) and eventually export through sinking POC (D in Figure 2.3). Additionally, we estimated DOC release including both phytoplankton extracellular excretion not accounted for in NPP measurements (H in Figure 2.3) (e.g. Halewood et al. 2012), DOC release from viral lysis (I

in Figure 2.3) (Nagata 2000), and potential DOC production from NPP as micro- and mesozooplankton grazing and excretion (J and K, respectively, in Figure 2.3) (Stukel et al. 2013, Steinberg et al. 2017, Morrow et al. 2018). The amount of microzooplankton carbon supplied to mesozooplankton was determined by assuming that the vertically exported carbon (D in Table 2.2) represented 30% of zooplankton carbon demand (Conover 1966) and that carbon was supplied to mesozooplanton from both phytoplankton (measured grazing rates, B in Table 2.2) and microzooplankton (G in Table 2.2).

Overall, BP was of similar magnitude to phytoplankton extracellular release, export production, and mesozooplankton grazing on NPP (A, C, D and H in Table 2.2) throughout the region but considerably lower than microzooplankton grazing on NPP. BP satisfies the greatest proportion of microzooplankton carbon demand in the transition region (95 ± 4%) and is a negligible component of the microzooplankton diet in the nearshore at 11 ± 7% (A in Table 2.2). Although the rate of microzooplankton grazing on phytoplankton did not vary much by region, with a mean of 0.27 d^{-1} in the nearshore and transition regions and an almost identical mean of 0.28 d^{-1} offshore (Appendix Figure S2.2), the average percentage of NPP consumed by microzooplankton increased from a mean of 60 ± 9% nearshore to 82 ± 10% in the transition and 95 ± 10% offshore (B in Table 2.2). In the offshore, this left little NPP for mesozooplankton grazing, and the percentage of either NPP or microzooplankton carbon channeled through mesozooplankton (C and G, respectively, in Table 2.2) peaked in the transition region.

Using existing literature, we estimated the DOC released by phytoplankton (extracellular release + viral lysis), microzooplankton (protozoan), and mesozooplankton (metazoan) (H, I, J, and K in Table 2.2). If the percentage of DOC that is estimated to be

released by microzooplankton is robust (after (Steinberg et al. 2017), then bacteria derive as much DOC (ultimately from NPP) from microzooplankton grazing as they do from phytoplankton extracellular release. The DOC released locally (Table 2.3; 154 ± 32 mmol C m^{-2} d^{-1}) in the nearshore exceeded the calculated BCD (F in Table 2.2) on average by 12 ± 55 mmol C m^{-2} d^{-1}. However, if two nearshore samples from P0704 and P1706 were excluded then BCD exceeded the DOC released (Appendix Table S2.2, S2.3). The transition and offshore regions (Table 2.3) did not have enough local DOC release to support the calculated BCD, which exceeded release by 95 ± 13 mmol C m^{-2} d^{-1} (373 ± 50% of DOC released utilized) or 138 ± 17 mmol C m^{-2} d^{-1} (1,760 ± 330% of DOC released utilized), respectively. In these environments, the flux balance suggests that the system is net heterotrophic. These trends were superimposed on an overall decrease in the amount of NPP, sinking export flux, and BP moving from nearshore to the offshore (Table 2.2).

2.4. DISCUSSION

2.4.1 Multiple lines of evidence suggest that the offshore CCE region is net heterotrophic

Several studies have suggested that oligotrophic subtropical gyres are net heterotrophic (Duarte et al. 2013, Ducklow & Doney 2013, Williams et al. 2013), fueled by the lateral movement of organic carbon from coastal areas (Duarte & Agusti 1998, del Giorgio & Duarte 2002, Duarte et al. 2013, Lovecchio et al. 2017). Eastern boundary currents, such as the CCE, are particularly productive upwelling regions that have been called upon as sources of this organic carbon (Alvarez-Salgado et al. 2007, Nagai et al. 2015). In this study, we examined the ratio of bacterial biomass to autotrophic biomass (biomass index), the ratio of BP to NPP (productivity index), and the relationship of bacterial carbon demand (BCD) to

other fluxes within the microbial loop and found that all of these perspectives support the hypothesis that net heterotrophy is commonplace in the offshore CCE. To satisfy this net heterotrophy, lateral export of carbon from the nearshore to the offshore is invoked.

2.4.2 Insights on microbially mediated transitions from net autotrophy to net heterotrophy from the biomass and productivity indices

The largest dataset that was available for comparing autotrophic and heterotrophic processes in the CCE was the biomass index: the ratio of BB:AB. From the regional averages of the biomass index (Figure 2.1a), we conclude that local AB in the nearshore and transition regions could feasibly support local BB. However, it is unlikely that, on average, the offshore local AB could support measured local BB. We note that we are considering the regional averages here because the biomass index varied interannually in the offshore and transition (Figure 2.1a). Still, the relationship of the biomass index with NPP is striking (Figure 2.1a), showing that indices close to or exceeding 1 are all found in regions of very low NPP, whereas the opposite is true at very high NPP. We would expect AB and NPP to be correlated, and low relative BB at high NPP may be related to enhanced microzooplankton grazing on bacteria in regions of high autotrophic production (Goericke 2011, Taylor & Landry 2018); however, we can posit how relatively high BB is maintained at low local NPP.

Going a step further, we compared the biomass index for each individual sample (Appendix Figure S2.1) and found that nearshore results continue to support the conclusion that local AB can support local BB. The transition region becomes more variable, as does the offshore region, likely reflecting the complex mesoscale dynamics common in the region and subsequent effects on physiochemical gradients. Some sites in the offshore exhibited a

biomass index that exceeded 1, which indicated that local AB was insufficient to support local BB even at the individual sample level.

The biomass trend described here has been previously reviewed and values exceeding one have been linked to detritus serving as an additional source of carbon for heterotrophic microbial communities in the offshore (Gasol et al. 1997). However, standing stocks of suspended POC are also low in the offshore (see Sections 1.3.1 and 1.4.1, Stephens et al. 2018). Furthermore, the biomass index is likely underestimated because BB was calculated using an assumed bacterial carbon content of 11 fg C $cell^{-1}$, which sometimes underestimates the bacterial carbon content in the CCE (see Sections 3.3.1 and 3.4.1, Samo et al. 2012, Pedler et al. 2014). We conclude that despite some of these caveats, the biomass index supports the hypothesis that heterotrophic production in the offshore region of the CCE cannot be supported by local primary production. This hypothesis is consistent with our analyses of the production index and recent reports from Station ALOHA, which was found to be net heterotrophic (Martinez-Garcia & Karl 2015) and serves as an adequate CCE offshore analog.

The production index – BP:NPP (Figure 2.1b) - was examined in this study because a comparison of carbon fluxes into microbial biomass may be more accurate than the steady state standing stocks biomass which can be influenced by additional factors such as input from lateral transport and removal through grazing or viral loss. One caveat is that the production index dataset is significantly smaller. The average production index for marine systems is 0.20-0.30 (Cole et al. 1988, Ducklow et al. 1993, Ducklow 1999), with 0.10 reported at the Scripps Pier (Fuhrman & Azam 1980). Our results are consistent with previous work – offshore values (0.26 ± 0.05) are closer to the marine average and nearshore values (0.08 ± 0.03) similar to the Scripps Pier, with the transition region values (0.15 ± 0.03) in

between those (Figure 2.1b). We interpret increasing values from nearshore to offshore as indicators of increasingly net heterotrophy offshore (Cole 1999, Lee & Bong 2008).

This trend of increasing production index values from nearshore to offshore was primarily a result of a disproportionate decrease in NPP relative to BP. Redistribution of carbon among food web compartments, such as higher BGEs offshore, a relative increase in the partitioning of primary production to DOC or increased production of DOC from grazing/grazers or viral lysis, may be able to maintain the relative increase in BB offshore. BGE values decreased offshore (Figure 2.2a) but since BP was used to calculate BGE (after del Giorgio and Cole, (1998), their autocorrelation prevents our ability to consider how they together influence the nearshore to offshore trends. We instead examined these relationships in the context of a model developed by Cole (1999), which contextualizes the production index versus BGE within a net autotrophy or net heterotrophy standpoint as defined by the ratios of bacterial respiration to NPP (Figure 2.2a).

This examination indicated that much higher BGEs than those calculated here (and in some cases unreasonably high BGEs for an oligotrophic environment) would be required to move many of our offshore datapoints out of the net heterotrophic space (2007 is an exception). Furthermore, a number of studies have shown that BGE decreases in oligotrophic environments (del Giorgio & Cole 1998, Biddanda et al. 2001, Eiler et al. 2003), most relevantly by a study off the coast of Oregon wherein, the magnitude and pattern of BGE from nearshore to offshore followed the same trend that we observed in our calculated BGE dataset (del Giorgio et al. 2011). This study did not measure extracellular DOC production, but a previous study in the region indicated that the partitioning of primary production to DOC decreased offshore (Stephens et al. 2018). Still, we are unable to definitively rule out the

possibility that partitioning of photosynthate to DOC increased offshore during our study. Grazing rates remained relatively constant throughout the region, but a greater proportion of phytoplankton biomass was grazed by microzooplankton in the offshore (Table 2.2). Even with these potential shifts in carbon flow, the BCD (Figure 2.2b, Table 2.2) in the offshore region, determined from a calculated BGE, cannot be satisfied.

We considered that methodology played a role in our observations, reflecting on the work of Hill et al. (2013) and their suggestion that in oligotrophic environments, the addition of saturating concentrations of ^{3}H-Leu would overestimate BP, which would decrease production indices and calculated BGE in the offshore. Although we did not attempt to examine BP under different added leucine concentrations, the observed trends for the production index presented here were consistent with the biomass index, which was independent of BP measurements (Figure 2.1b).

We suggest instead that the increase in BB:AB and BP:NPP offshore is indicative of an additional supply of organic carbon to the offshore (Carlson et al. 2007). One potential source of this allochthonous carbon is the lateral transport of organic matter from the nearshore to the offshore (Alvarez-Salgado et al. 2001, Barbosa et al. 2001, Stukel et al. 2011, Kelly et al. 2018). For example, Stephens et al. (2018), estimated that 10 ± 7 mmol C m^{-2} d^{-1} of passively moving organic carbon (i.e., non-sinking reservoirs) may be exported from the nearshore by lateral advection during productive, upwelling periods. Furthermore, strong mesoscale features in the region, such as offshore moving filaments and eddies have been shown to entrain organic matter and are common features of the CCE (Gruber et al. 2011, Ohman et al. 2013, Davis & Di Lorenzo 2015, Nagai et al. 2015). In fact, during P1706, a westward propagating coastal filament was examined to more directly assess the lateral

transport of nutrients, biomass and carbon reservoirs within these mesoscale features by comparing two sites that intersected the same water mass 8 days apart. The site sampled at the beginning of the 8 days period had low biomass and production indices, whereas after 8 days we encountered higher biomass and production indices consistent with a delayed response of the microbial community and change in metabolic state (Figure 2.1b). There was also a clear shift from a nearly net autotrophic system nearshore to a strongly net heterotrophic system in the transition region (Figure 2.2a,b), showing that the local primary production was insufficient to support the local bacterial production demand.

2.4.3 Mass balance of carbon flow in the CCE microbial food web

Although several other components of the CCE-LTER food web have been extensively described in the literature, this is the first report to place the bacterial compartment in context. By calculating bacterial carbon demand using our BP data and inserting that value into the food web (Figure 2.3; F in Table 2.2), we are better able to assess the metabolic balance within the CCE.

Assuming local NPP supports local populations, we would expect each region to utilize approximately 100% of the NPP. Our calculations assume that the ^{14}C method approximates NPP (Marra 2002) and is available to satisfy trophic transfer through microzooplankton and mesozooplankton grazing. Recent studies in the CCE have estimated gross oxygen production (GOP) using the triple oxygen isotope method and found that GOP converted to carbon units (gross primary production, GPP) exceeded ^{14}C estimated NPP by approximately 2-3 times (Munro et al. 2013, Haskell et al. 2017, Manning et al. 2017), which is consistent with work from other regions (Bender et al. 1992, Fasham et al. 1999, Marra

2002, Hendricks et al. 2005). The *in situ* O_2/Ar based method, used on the P1604 and P1706 cruises, found an average GPP:NPP of 2.4 (Kranz et al. 2020). As such, GPP represents the upper limit of carbon supply to the food web in the region and overall, provided ample carbon to satisfy the grazing processes identified in Figure 2.3, but were not sufficient to meet the calculated BCD in the offshore (Figure 2.2b). Relative to GPP then, the CCE is net autotrophic, until reaching the offshore region. However, autotrophic respiration cannot be ignored and can be between 30-55% of GPP (Duarte & Cebrian 1996, Fasham et al. 1999, Haskell et al. 2017, Kranz et al. 2020).

In support of our expectation that local NPP supplied much of the carbon to the rest of the food web, our results based on the traditional (grazing) food web showed that about 18 ± 5% (or 66 ± 25 mmol C m^{-2} d^{-1}) of nearshore NPP was not utilized in the nearshore region (Table 2.3). Haskell et al. (2016) estimated that 12% of NPP was lost through horizontal transport, enough to satisfy the our offshore regions which require an additional 11 ± 7% (or 3 ± 3 mmol C m^{-2} d^{-1}) of local NPP on average. A similar result was determined in Stephens et al. (2018) where new production (NP) or net community production (NCP) was found to exceed loss processes (sinking and TOC production) in the nearshore whereas loss processes approximated and sometimes exceeded NP or NCP offshore. Across the entire CCE region ($NPP_{remaining}$ from nearshore + $NPP_{remaining}$ from transition + $NPP_{remaining}$ from offshore), roughly 67 mmol C m^{-2} d^{-1} was needed to satisfy the grazing loss processes considered here. Examination of the traditional (grazing) food web supports the hypothesis that excess carbon produced in the net autotrophic nearshore would be sufficient to support the carbon demand of the offshore, net heterotrophic region.

While BCD exceeded NPP in both the transition and nearshore (F, Table 2.2), our BCD calculations may be overestimated due to underestimated BGEs (relative to values of 10-30% that are often measured). However, the BGE adjustment that would be required to bring BCD closer in line with NPP offshore would make BGE higher than is typically observed (~50%), especially in offshore oligotrophic regions (del Giorgio et al. 2011). Although some studies compare BCD to NPP directly (e.g. Halewood et al. 2012), the heterotrophic bacterial component can also utilize substantial DOC pools released through multiple mechanisms.

The nearshore DOC released (Table 2.3) exceeded BCD (F in Table 2.2) by 12 ± 55 mmol C m^{-2} d^{-1}, but the transition and offshore required an additional 95 ±13 mmol C m^{-2} d^{-1} and 138 ± 17 mmol C m^{-2} d^{-1}, respectively. If we doubled our calculated BGE, thereby halving BCD ($\frac{1}{2}F$ from Table 2.2), the nearshore would have ~ 80 ± 51 mmol C m^{-2} d^{-1} of excess DOC. Maintaining these lower BCD estimates throughout the region would allow us to export enough DOC from the nearshore to satisfy BCD in the transition and nearly achieve balance in the offshore (deficit of 7 mmol C m^{-2} d^{-1} which is within the margin of error). We recognize that the local DOC release could be increased if we quantified viral lysis of heterotrophic bacteria and remineralization of detritus as additional local sources of DOC, but these mechanisms were not explored in this analysis. Stephens et al. (2018) used standing stocks of carbon to estimate that 10 ± 7 mmol C m^{-2} d^{-1} would be laterally transported offshore from the nearshore region, setting an upper limit of 17 mmol C m^{-2} d^{-1}. Therefore, conservatively applying our laterally transported carbon flux of 17 mmol C m^{-2} d^{-1}, the transition region would approach balance, but there would be no excess DOC to be transported to the offshore and net heterotrophy would be maintained in the offshore region.

2.4.3.1 Mass balance of carbon flow in the CCE microbial food web within a westward propagating filament

To further test the hypothesis that the CCE domain progressed from net autotrophy in the nearshore to net heterotrophy in the offshore, we took advantage of a water mass sampled twice during 2017 initially in the nearshore and 8 days later in the transition region. In the nearshore cycle, 34 mmol C m^{-2} d^{-1} of NPP remaining after grazing (84% of local NPP utilized by grazing), which would satisfy the 10 mmol C m^{-2} d^{-1} deficit (124% of local NPP utilized by grazing) in the transition cycle, even with the 17 mmol C m^{-2} d^{-1} upper limit (Table 2.3). However, when considering the microbial food web, the nearshore cycle had a deficit of 28 mmol C m^{-2} d^{-1} of DOC released and the transition cycle BCD needed an additional 168 mmol C m^{-2} d^{-1} of DOC. If the BGE was twice that calculated, then BCD would have been easily met from DOC released ($DOC_{remaining} = \frac{1}{2}F - H - I - J - K$ from Table 2.2) in the nearshore cycle with an additional 46 mmol C m^{-2} d^{-1} remaining. The transition cycle would have a deficit of DOC (68 mmol C m^{-2} d^{-1}) that could not be met by lateral transport from the more nearshore cycle. If we assume an upper limit of 17 mmol C m^{-2} d^{-1} for lateral transport and all 7 mmol C m^{-2} d^{-1} of excess laterally transported NPP was converted to DOC with no loss, then the transition region would still not have enough carbon to support grazing and the heterotrophic bacterial carbon demand.

One potential explanation of the observed net heterotrophy of the microbial food web, but not the traditional (grazing) food web, is the possibility of another unquantified source of particulate or dissolved organic matter. During the 2017 cruise, the *e*-ratio (found in column D, Table 2.2) was found to be 0.80 in the transition cycle compared to 0.02 in the nearshore

cycle, even though the total amount of export was similar. Furthermore, the measured vertical export exceeded microzooplankton grazing rates in the transition region, suggesting significant transport of carbon offshore, through biotic or abiotic factors, prior to sinking. Additionally, the most nearshore cycle of P1706 (cycle 1) had an excess of 131 mmol C m^{-2} d^{-1} from NPP after grazing and 178 mmol C m^{-2} d^{-1} from estimated DOC released after accounting for BCD (Appendix Table S2.3), which if laterally transported, would be more than enough to support the calculated deficit of released DOC in the transition cycle. Together, these results indicate that lateral transport of excess organic material from the production nearshore region within a westward propagating filament could support the net heterotrophic regions farther offshore.

Another possible set of explanations is that our calculated BCD were overestimated and/or our estimates of DOC released were underestimated. Neither BGE nor DOC release were quantified in this study, and both can strongly influence the observed trends of net heterotrophy offshore. As such, these terms should be prioritized for further study in this region.

2.4.4 Anomalously warm conditions may lead to increasing net heterotrophy in the CCE

During the 2014 warm anomaly, we found that the production index was elevated because NPP decreased disproportionately offshore (Figure 2.1b) relative to BP, despite low growth rates for both heterotrophic bacteria and phytoplankton (calculated as NPP/AB or BP/BB from Appendix Tables S2.1 and S2.2, Appendix Figure S2.3). In fact, every cycle from P1408 had a deficit of carbon in terms of NPP utilized by the traditional (grazing) food web and of DOC released compared to the calculated BCD (microbial food web) (Appendix

Table S2.3). Even if BCD was halved from doubling the BGE, the deficit prevailed, indicating the CCE, especially offshore, may become increasingly net heterotrophic under the surface stratification conditions imposed by warm anomaly events. Because none of the P1408 cycles could be classified as nearshore for this analysis (even though geographically, many of the sampling stations would be considered close to the coast), we were unable to determine whether excess NPP was available to supplement offshore heterotrophic demand.

If lateral export was not available to supplement this net heterotrophy then another explanation must be considered. The warm anomaly in 2014 had strongly stratified, warm waters in the upper 100 m (Bond et al. 2015, Gentemann et al. 2017) not unlike the typical conditions at Station ALOHA in the North Pacific Gyre. Seasonal decoupling between NPP and BP, with elevated NPP from May through August and elevated BP from August through October, has been observed at Station ALOHA (Viviani & Church 2017), and such a temporal decoupling of autotrophy from heterotrophy could explain the elevated production indices, slow bacterial growth rates, and the imbalance of NPP and BCD. If the CCE experienced the same seasonal decoupling, we would have expected to then see similar results between only cruises P0810 and P1408; however, we found similar production indices during P1604 in the offshore region as well (Figure 2.1b).

Instead, the stratified conditions experienced in August 2014 and in the offshore during the tail end of El Niño in April 2016 may explain the mismatch. The DOC released to support BCD was insufficient across all regions during these years (Appendix Tables S2.2 and S2.3). NPP was enough in the nearshore and transition to support grazing in 2008 and 2016, in contrast to 2014 (Appendix Table S2.3). Because the DOC release was estimated and heavily relied on assumed percentages, the NPP comparison was more reliable. These results

support the conclusion that the warm anomaly of 2014 had a unique impact on the CCE domain.

2.5. CONCLUSIONS

Here we used a heterotrophic-bacteria centered view to examine organic carbon exchange in the CCE. For example, several recent studies have suggested that the lateral export of carbon from the nearshore CCE to the offshore is needed to explain the imbalance of new production and export production in the nearshore. Here, we show using three different comparisons – biomass index, production index, and carbon exchange in the microbial loop - that net heterotrophy in the offshore is likely and common, and provide a different perspective on the need for laterally exported carbon to support the observed imbalances in the offshore. Our data from the nearshore add to the mounting evidence that the nearshore CCE is net autotrophic and underscores the importance of quantifying the bacterial component of the CCE carbon flux due to their role as major players in the biogeochemistry of the CCE. In the same vein, we also identified several data deficiencies, such as accurate estimates of bacterial growth efficiency (BGE) to robustly constrain bacterial carbon demand (BCD), direct estimates of the fraction of primary production partitioned into DOC by extracellular release and viral lysis, the role of grazing related DOC production, and the total amount of carbon ingested by mesozooplankton, that preclude accurate estimates of the balance between autotrophy and heterotrophy in the region. Further, it will be important to test whether saturating concentrations of 3H-Leucine overestimate/underestimate BP in the offshore/nearshore and more assuredly contribute to production index calculations. Future work should aim to quantify additional primary production loss terms, such as viral mortality,

and the interdependence of primary production loss terms across the CCE-LTER domain to better constrain the first order food web analysis presented in this study. This work exemplifies the importance of considering heterotrophic bacteria not simply as recyclers of organic matter, but as dynamic contributors to the trophic state of the ecosystem.

2.6 ACKNOWLEDGEMENTS

Chapter 2, in part, is currently being prepared for submission for publication of the material. Rivera, S. R.; Stephens, B. M.; Samo, T. J.; Stukel, M. R.; Ohman, M.D.; Landry, M. R.; Farooq, A.; Aluwihare, L. I.. The dissertation author was the primary investigator and author of this material.

2.7 FIGURES AND TABLES

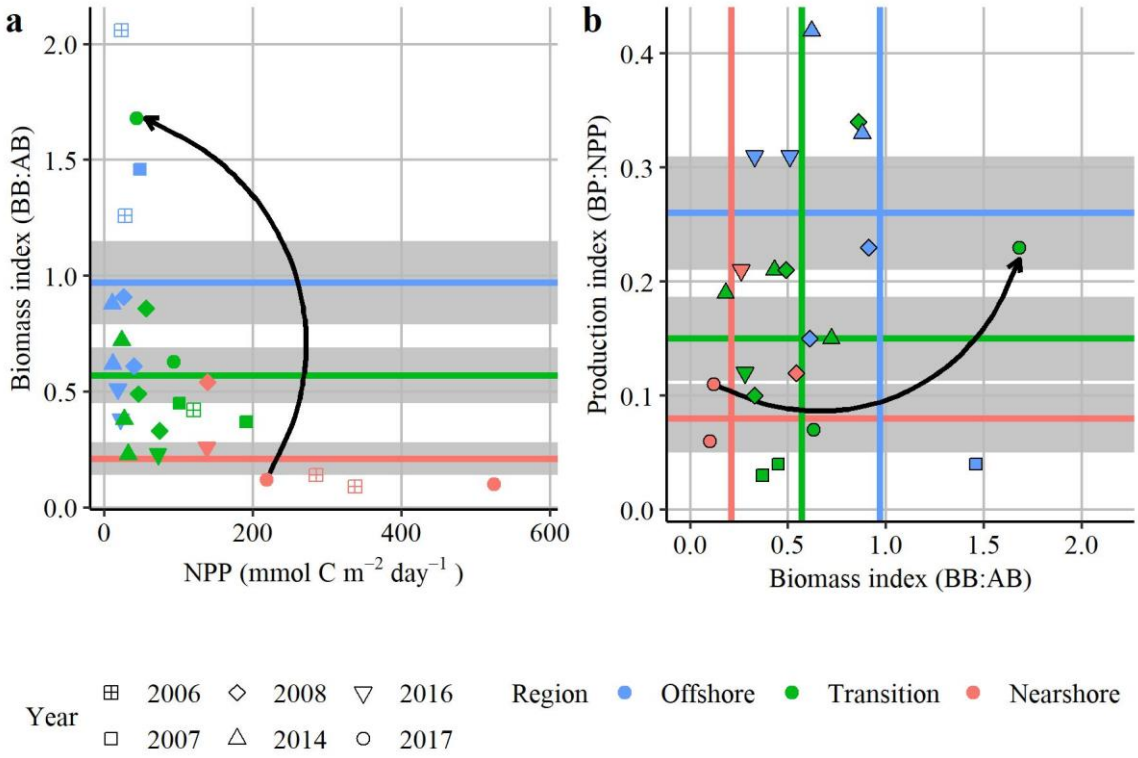

Figure 2.1: Biomass and production indices

(a) Euphotic zone integrated ratios of calculated bacterial biomass (BB) to calculated autotrophic biomass (AB) or the biomass index plotted relative to similarly integrated NPP. (b) Euphotic zone integrated ratios of bacterial production (BP) to primary production (NPP) or the production index and its relationship to the biomass index. Mean per region (colored horizontal lines) and standard error (grey shading) per mean also shown. The curved arrows connect nearshore cycle P1706-C2 to transition cycle P1706-C4.

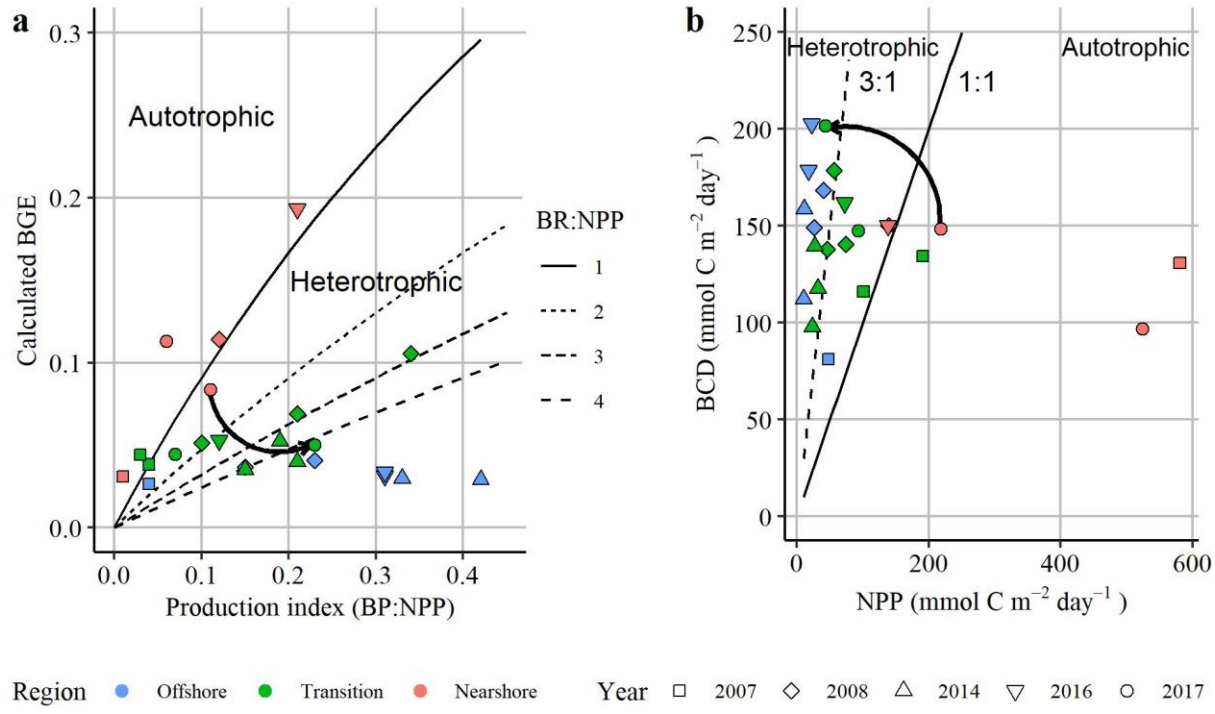

Figure 2.2: The offshore region of the CCE could be net heterotrophic with local gross primary production (GPP) unable to meet local BCD

(a) The ratio of EZ integrated BP:NPP (production index) compared to BGE calculated using BP per hour. Assumed values of BP:NPP and BGE were used to calculate the isolines for values of the ratio of BR:NPP (designated by line type) as presented by Cole (1999). Points above the solid black line (BR:NPP = 1) indicate net autotrophy, while those below indicate net heterotrophy. (b) The calculated BCD from the calculated BGE and BP per day compared to local NPP. The solid line designates the 1:1 line, the dashed line designates the 3:1 line or the high estimate of GPP for the system. The curved arrows connect nearshore cycle P1706-C2 to transition cycle P1706-C4.

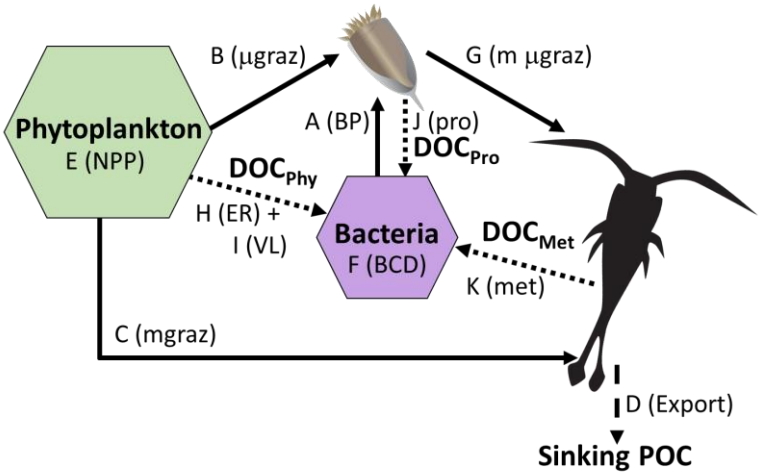

Figure 2.3: CCE conceptual food web with microbial loop

A first order food web incorporating the microbial loop (sizes are not meant to be proportional).

Letter designations: A = measured bacterial production (BP), B = measured microzooplankton grazing of phytoplankton (µgraz), C = measured mesozooplankton grazing of phytoplankton (mgraz), D = measured export of sinking particulate organic carbon (POC), E = measured net primary production (NPP), F = calculated bacterial carbon demand (BCD), G = calculated mesozooplankton grazing on microzooplankton based on an assumed total mesozooplankton grazing rate equal to 30% of the export rate (m µgraz), H = estimated extracellular release of DOC by phytoplankton (ER), I = estimated DOC released by viral lysis of phytoplankton (VL), J = estimated DOC released by microzooplankton (protozoan, pro), K = estimated DOC released by mesozooplankton (metazoan, met). DOC_{Phy} represents the total estimated DOC released from phytoplankton. DOC_{Pro} represents the total estimated DOC released from protozoan. DOC_{Pet} represents the total estimated DOC released from metazoan.

Source: Table 2.2 for average regional values and Appendix Table S2.2 for average Lagrangian cycle values by region and cruise.

Table 2.1: Average EZ depth integrated values by CCE region

Average EZ depth integrated values by CCE region. Values for AB and BB were converted from Chl concentration and BA prior to integration and averaging (see Section 2.2 Methods for details).

	EZ depth	**Chl**	**AB**	**BA**	**BB**
	m	**mg Chl m^{-2}**	**mmol C m^{-2}**	**cells m^{-2}**	**mmol C m^{-2}**
Offshore	98 ± 3, N = 9	21 ± 1, N = 9	69 ± 10, N = 9	6.16E+13 ± 6.14E+12, N = 9	55.1 ± 5.4, N = 9
Transition	63 ± 4, N = 12	47 ± 4, N = 12	131 ± 19, N = 12	5.39E+13 ± 3.94E+12, N = 12	61.7 ± 8.5, N = 12
Nearshore	38 ± 8, N = 7	106 ± 18, N = 7	340 ± 79, N = 7	4.91E+13 ± 8.36E+12, N = 7	53.6 ± 8.0, N = 7

Table 2.2: Average EZ integrated values for the CCE food web with microbial loop

Average EZ depth integrated values by CCE region. Values per cruise-cycle were integrated and averaged per Lagrangian cycle prior to averaging per region. The percentages within parenthesis for columns A-G were calculated from cruise-cycle averages. The percentages within parenthesis for columns H-K were derived from the literature as cited.

	A[a]	B[a]	C[a]	D[a]	E[a]	F[b]	G[c]	H [d,e]	I[f]	J[f]	K[g]
	BP ("A":"B" as %)	Microzoo grazing on phyto ("B":"E" as %)	Mesozoo grazing on phyto ("C":"E" as %)	Export (e-ratio)	NPP	BCD ("F":"E" as %)	Mesozoo grazing on microzoo ("G":("A"+"B") as %)	Extracellular release of DOC by phyto ("H":"E" as %)	Release of DOC from phytoby viral lysis ("I":"E" = 10%)	Release of DOC by microzoo ("I":"B" = 20-30%)	Release of DOC by mesozoo ("K": ("D"/0.3 – "C") = 10-30%)
	mmol Carbon m^{-2} d^{-1}										
Regional averages											
Offshore	5 ±1, N = 7 (31 ± 6%, N = 7)	25 ± 6, N = 9 (95 ± 10%, N = 9)	3 ± 1, N = 8 (14 ± 5%, N = 8)	5 ± 1, N = 9 (0.23 ± 0.03, N = 9)	25 ± 5, N = 9	150 ± 16, N = 7 (806 ± 166%, N = 7)	12 ± 2, N = 6 (45 ± 10%, N = 6)	1.5 (5%)	2.5	5.0 – 7.5	0.3 – 0.8
Transition	8 ± 1, N = 11 (95 ± 4%, N = 11)	52 ± 7, N = 12 (82 ± 10%, N = 12)	17 ± 4, N = 12 (31 ± 8%, N = 12)	14 ± 2, N = 12 (0.26 ± 0.07, N = 12)	73 ± 14, N = 12	143 ± 9, N = 11 (287 ± 45%, N = 11)	32 ± 8, N = 12 (61 ± 19%, N = 11)	14 – 21 (20-30%)	7.3	10.4 – 15.6	1.7 – 5.0
Nearshore	15 ± 4, N = 6 (11 ± 7%, N = 4)	202 ± 42, N = 6 (60 ± 9%, N = 6)	34 ± 7, N = 5 (12 ± 2%, N = 5)	27 ± 5, N = 4 (0.13 ± 0.03, N = 4)	317 ± 68, N = 7	135 ± 10, N = 5 (65 ± 20%, N = 5)	72 ± 10, N = 3 (32 ± 17%, N = 2)	38 – 64 (12-20%)	31.7	40.4 – 60.6	3.4 – 10.1
Westward propagating filament											
Nearshore P1706-C2	12.4 ± 1.3, N = 4 (8%)	164 (75 ± 9%, N = 4)	20.1 ± 2.6, N = 8 (9%)	32.1 ± 5.8, N = 3 (0.06)	218 ± 35[i], N = 8	148.4 ± 14.3, N = 4 (68%)	87 (49%)	26 – 44 (12-20%)	21.8	32.7 – 49.1	2.0 – 6.0
Transition P1706-C4	10.1 ± 2.2, N = 2 (33%)	31 (72 ± 5%, N = 2)	50.6 ± 0.9, N = 4 (52%)	34.3 ± 3.5, N = 3 (0.80)	43 ± 4, N = 5	201.7 ± 24.2, N = 2 (469%)	92 (224%)	9 – 13 (20-30%)	4.3	6.2 – 9.3	2.2 – 6.7

[a]From this study (see Section 2.2 Methods for details)
[b]Calculated from calculated BGE (BGE calculated as described by del Giorgio and Cole (1998), see Section 2.2 Methods for details)
[c]Export assumed to be 30% of total mesozooplankton grazing, calculated as ("D"/0.3 – "C")
[d]Offshore (5%), transition (20-30%), and nearshore (12%) from Stephens et al. (2018)
[e]Nearshore (20%) from Halewood et al. (2012)
[f]From Nagata (2000)
[g]Steinberg and Landry (2017)

Table 2.3: CCE regional average calculated NPP and DOC remaining

Values for each Lagrangian cycle were calculated using values (designated by letters) from Appendix Table S2.2 and averaged by region.

	$NPP_{remaining}$ (%NPP utilized)	DOC released	$DOC_{remaining}$ (%DOC utilized)
	= E - B - C	= H + I + J + K	= F - H - I - J - K
	mmol Carbon m^{-2} d^{-1}		
Regional averages			
Offshore	-3.2 ± 2.7, N = 8 (111 ± 7%, N = 8)	11.7 ± 3.0, N = 8	-138 ± 17, N = 8 (1,760 ± 330%, N = 8)
Transition	4.7 ± 8.6, N = 12 (113 ± 15%, N = 12)	49.8 ± 7.7, N = 12	-95 ± 13, N = 12 (373 ± 50%, N = 12)
Nearshore	65.5 ± 25.3, N = 4 (82 ± 5%, N = 4)	154.4 ± 32.4, N = 4	12 ± 55, N = 4 (155 ± 54%, N = 4)
Westward propagating filament			
Nearshore P1706-C2	34 (84%)	120.5	-28 (123%)
Transition P1706-C4	-10 (124%)	33.2	-168 (607%)

2.8 APPENDIX

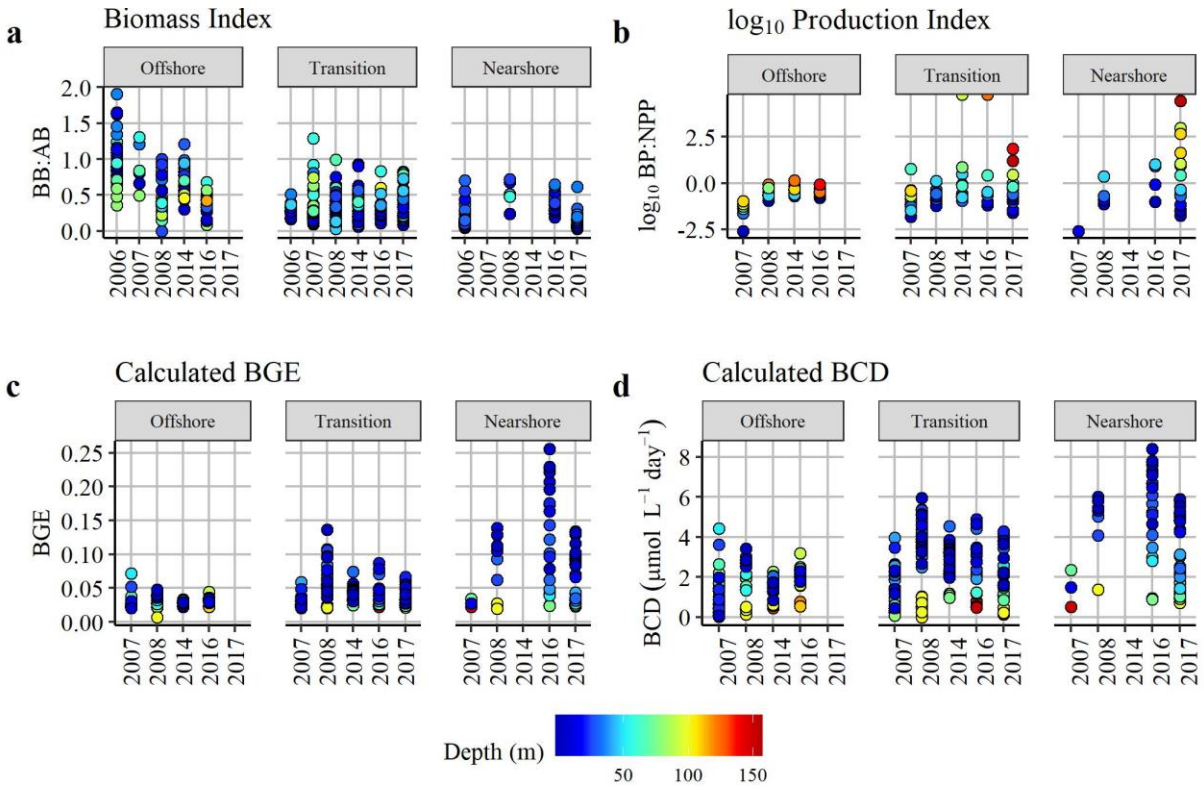

Figure S2.1: Biomass and production indices with calculated bacterial growth efficiency and carbon demand by sample

(a) The biomass index calculated by FCM, (b) log of the production index, (c) calculated BGE, and (d) calculated BCD colored by sample depth.

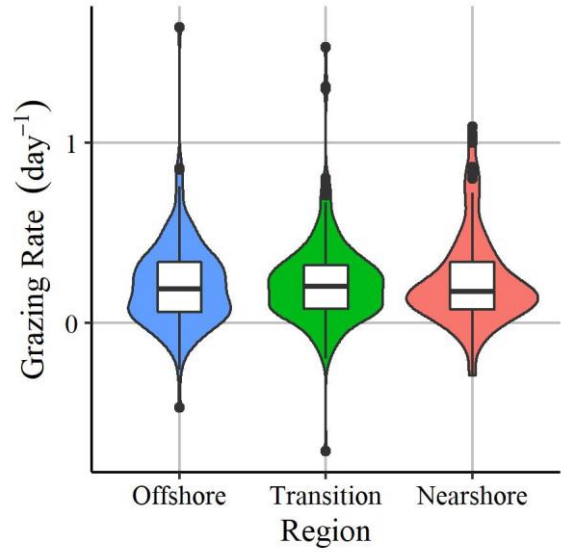

Figure S2.2: Microzooplankton grazing rate by oceanic region

The microzooplankton grazing rate by region. Overlaid box plots show the statistical distribution and means per region.

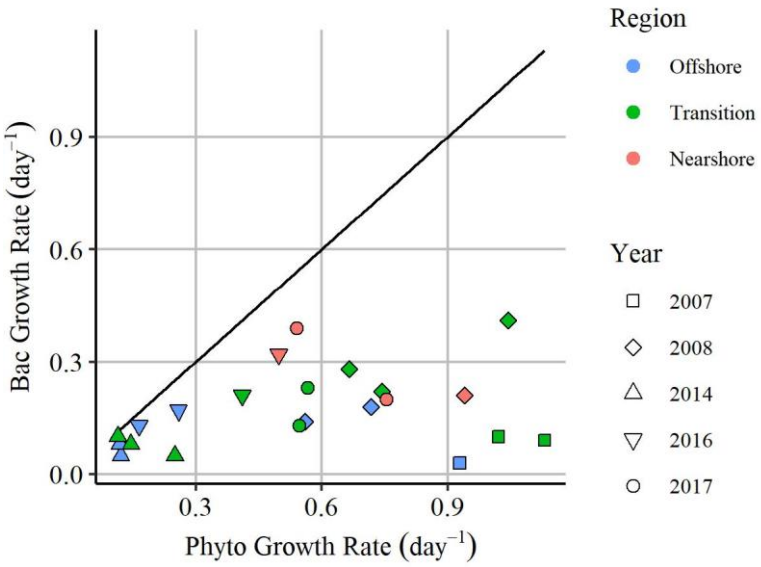

Figure S2.3: Calculated growth rates from EZ integrated values

Growth rates calculated as NPP/AB (phyto growth rate) or BP/BB (bac growth rate) from Appendix Tables S2.1 and S2.2, colored by region and shape by year. The solid line is the 1:1 line.

Table S2.1: Average EZ depth integrated values by Lagrangian cruise-cycle (1/3)

Average EZ depth integrated values by Lagrangian cruise-cycle and separated by CCE region. Values for AB and BB were converted from Chl concentration and BA prior to integration and averaging (see Section 2.2 Methods for details).

Region	Cruise	Cycle	EZ depth	Chl	AB	BA (FCM)	BB
			m	mg Chl m^{-2}	mmol C m^{-2}	cells m^{-2}	mmol C m^{-2}
Offshore	P0605	2	104 ± 3, N = 6	24 ± 1, N = 10	33 ± 14, N = 4	7.43E+13 ± 1.30E+12, N = 5	68.1 ± 1.2, N = 5
	P0605	5	82 ± 2, N = 8	21 ± 2, N = 9	54 ± 4, N = 4	7.48E+13 ± 4.42E+12, N = 5	68.5 ± 4.0, N = 5
	P0704	2	100 ± NA, N = 1	29 ± 2, N = 8	52 ± NA, N = 1	8.25E+13 ± 2.52E+12, N = 4	75.6 ± 2.3, N = 4
	P0810	2	88 ± 6, N = 6	18 ± 1, N = 9	56 ± 7, N = 3	3.82E+13 ± 4.31E+12, N = 6	34.1 ± 4.4, N = 6
	P0810	6	97 ± 11, N = 3	21 ± 1, N = 5	46 ± 5, N = 2	4.38E+13 ± 1.83E+12, N = 3	42.3 ± 4.1, N = 3
	P1408	4	99 ± NA, N = 1	17 ± 1, N = 7	83 ± 5, N = 3	8.19E+13 ± 2.80E+12, N = 4	72.6 ± 1.1, N = 3
	P1408	5	103 ± NA, N = 1	16 ± 1, N = 7	93 ± 9, N = 3	6.52E+13 ± 2.67E+12, N = 4	57.4 ± 0.6, N = 3
	P1604	1	103 ± NA, N = 1	24 ± 3, N = 4	70 ± NA, N = 1	3.65E+13 ± 1.55E+13, N = 2	33.2 ± 14.0, N = 2
	P1604	2	108 ± NA, N = 1	22 ± 1, N = 7	134 ± 7, N = 3	5.70E+13 ± 3.49E+11, N = 3	52.1 ± 0.2, N = 3

Table S2.1: Average EZ depth integrated values by Lagrangian cruise-cycle (continued, 2/3)

Average EZ depth integrated values by Lagrangian cruise-cycle and separated by CCE region. Values for AB and BB were converted from Chl concentration and BA prior to integration and averaging (see Section 2.2 Methods for details).

Region	Cruise	Cycle	EZ depth	Chl	AB	BA (FCM)	BB
			m	mg Chl m^{-2}	mmol C m^{-2}	cells m^{-2}	mmol C m^{-2}
Transition	P0605	4	57 ± 6, N = 6	46 ± 2, N = 10	105 ± 5, N = 4	4.76E+13 ± 2.46E+12, N = 6	44.4 ± 1.9, N = 6
	P0704	1	70 ± NA, N = 1	67 ± 7, N = 9	99 ± 4, N = 3	4.90E+13 ± 2.27E+12, N = 5	44.9 ± 2.1, N = 5
	P0704	4	80 ± NA, N = 1	67 ± 4, N = 9	169 ± 17, N = 4	6.80E+13 ± 5.78E+12, N = 5	62.3 ± 5.3, N = 5
	P0810	1	62 ± 6, N = 5	54 ± 14, N = 9	69 ± 19, N = 4	3.72E+13 ± 1.85E+12, N = 5	34.2 ± 1.7, N = 5
	P0810	3	55 ± 3, N = 5	37 ± 1, N = 7	100 ± 5, N = 3	3.58E+13 ± 6.13E+12, N = 4	32.6 ± 5.5, N = 4
	P0810	4	40 ± 1, N = 2	51 ± 8, N = 5	54 ± 20, N = 2	4.62E+13 ± 5.50E+12, N = 3	46.3 ± 4.9, N = 3
	P1408	1	47 ± NA, N = 1	67 ± 9, N = 7	282 ± 82, N = 3	6.91E+13 ± 7.72E+12, N = 4	64.0 ± 10.0, N = 3
	P1408	2	61 ± NA, N = 1	44 ± 3, N = 7	186 ± 1, N = 3	7.62E+13 ± 7.10E+12, N = 4	70.8 ± 9.2, N = 3
	P1408	3	72 ± NA, N = 1	28 ± 1, N = 7	92 ± 3, N = 3	7.06E+13 ± 4.66E+12, N = 4	66.2 ± 5.7, N = 3
	P1604	3	77 ± NA, N = 1	46 ± 1, N = 7	175 ± 3, N = 3	4.58E+13 ± 4.43E+12, N = 3	41.7 ± 4.2, N = 3
	P1706	3	65 ± 10, N = 3	42 ± 8, N = 7	170 ± 50, N = 3	5.37E+13 ± 3.49E+12, N = 4	49.2 ± 3.2, N = 4
	P1706	4	75 ± 9, N = 2	18 ± 3, N = 5	76 ± 0, N = 2	4.70E+13 ± 8.18E+12, N = 3	43.1 ± 7.5, N = 3

Table S2.1: Average EZ depth integrated values by Lagrangian cruise-cycle (continued, 3/3)

Average EZ depth integrated values by Lagrangian cruise-cycle and separated by CCE region. Values for AB and BB were converted from Chl concentration and BA prior to integration and averaging (see Section 2.2 Methods for details).

Region	Cruise	Cycle	EZ depth	Chl	AB	BA (FCM)	BB
			m	mg Chl m^{-2}	mmol C m^{-2}	cells m^{-2}	mmol C m^{-2}
Nearshore	P0605	1	23 ± 3, N = 11	105 ± 8, N = 9	241 ± 38, N = 4	3.72E+13 ± 5.54E+12, N = 5	34.1 ± 5.1, N = 5
	P0605	3	17 ± ,2 N = 14	83 ± 6, N = 7	272 ± 28, N = 3	2.68E+13 ± 2.20E+12, N = 4	24.5 ± 2.0, N = 4
	P0704	3	80 ± NA, N = 1	136 ± 22, N = 2	n.d.	4.86E+13 ± NA, N = 1	44.5 ± NA, N = 1
	P0810	5	44 ± ,1 N = 2	49 ± 10, N = 6	148 ± NA, N = 1	8.75E+13 ± 1.50E+13, N = 3	80.0 ± 13.2, N = 3
	P1604	4	30 ± NA, N = 1	86 ± 3, N = 7	278 ± 17, N = 3	1.11E+14 ± NA, N = 3	90.4 ± 9.6, N = 3
	P1706	1	28 ± 1, N = 3	196 ± 21, N = 7	695 ± 196, N = 3	5.99E+13 ± 6.36E+12, N = 4	54.9 ± 5.8, N = 4
	P1706	2	44 ± 4, N = 4	85 ± 9, N = 8	404 ± 52, N = 4	3.44E+13 ± 3.18E+12, N = 5	31.5 ± 2.9, N = 5

Table S2.2: Average EZ integrated values for the CCE food web with microbial loop by Lagrangian cruise-cycle (1/3)

Average EZ depth integrated values integrated and averaged per Lagrangian cycle, by CCE region. The percentages within parenthesis for columns A-G are the value within the column of interest as a percentage of the columns designated within the parentheses. The percentages within parenthesis for columns H-K were derived from the literature as cited.

			A[a]	B[a]	C[a]	D[a]	E[a]	F[b]	G[c]	H[d,e]	I[f]	J[f]	K[g]
Region	Cruise	Cycle	BP ("A":"B" as %)	Microzoo grazing on phyto ("B":"E" as %)	Mesozoo grazing on phyto ("C":"E" as %)	Export (e-ratio)	NPP	BCD ("F":"E" as %)	Mesozoo grazing on microzoo ("G":("A"+"B") as %)	Extracellular release of DOC by phyto ("H":"E" as %)	Release of DOC from phytoby viral lysis ("I":"E" = 10%)	Release of DOC by microzoo ("I":"B" = 20-30%)	Release of DOC by mesozoo ("K": ("D"/0.3 – "C") = 10-30%)
			mmol Carbon m^{-2} d^{-1}										
Offshore	P0605	2	n.d. (n.d.)	16 (69 ± 26%, N = 4)	2.1 ± 0.4, N = 11 (9%)	6.0* (0.26)	23 ± 12, N = 4	n.d. (n.d.)	18 (n.d.)	1.2 (5%)	2.3	3.2 – 4.8	0.2 – 0.6 (10-30%)
	P0605	5	n.d. (n.d.)	43 (154 ± 13%, N = 4)	1.0 ± 0.2, N = 8 (4%)	6.3* (0.23)	38 ± 6, N = 4	n.d. (n.d.)	20 (n.d.)	1.4 (5%)	3.8	8.6 – 12.9	0.1 – 0.3 (10-30%)
	P0704	2	2.1 ± 0.6, N = 4 (3%)	62 (129 ± 27%, N = 3)	2.0 ± 0.3, N = 8 (4%)	2.6 ± NA, N = 1 (0.05)	48 ± 4, N = 3	81.1 ± 18.9, N = 4 (169%)	7 (10%)	2.4 (5%)	4.8	12.4 – 18.6	0.2 – 0.6 (10-30%)
	P0810	2	6.2 ± 0.9, N = 3 (18%)	34 (86 ± 17%, N = 4)	6.2 ± 0.8, N = 7 (16%)	6.2 ± NA, N = 1 (0.16)	40 ± 1, N = 4	168.5 ± 18.2, N = 3 (421%)	14 (36%)	2.0 (5%)	4.0	6.9 – 10.3	0.6 – 1.9 (10-30%)
	P0810	6	6.1 ± 0.1, N = 2 (35%)	17 (66 ± 7%, N = 2)	n.d. (n.d.)	8.3 ± 0.8, N = 2 (0.32)	26 ± 2, N = 2	149.2 ± 5.2, N = 2 (574%)	n.d. (n.d.)	1.3 (5%)	2.6	3.4 – 5.1	n.d. (10-30%)
	P1408	4	3.3 ± 0.5, N = 3 (38%)	9 (89 ± 14%, N = 3)	2.8 ± 0.4, N = 6 (28%)	3.4 ± 0.1, N = 3 (0.34)	10 ± 0, N = 3	112.1 ± 13.7, N = 3 (1,121%)	9 (70%)	0.5 (5%)	1.0	1.8 – 2.7	0.3 – 0.8 (10-30%)
	P1408	5	4.6 ± 0.9, N = 3 (45%)	10 (92 ± 3%, N = 3)	3.7 ± 0.7, N = 6 (34%)	3.0 ± 0.1, N = 3 (0.27)	11 ± 0, N = 3	158.7 ± 25.1, N = 3 (1,443%)	9 (43%)	0.6 (5%)	1.1	2.0 – 3.0	0.4 – 1.1 (10-30%)
	P1604	1	5.6 ± NA, N = 1 (43%)	13 (72 ± NA%, N = 1)	22.0 ± 0.5, N = 2 (11%)	4.7 ± 1.2, N = 2 (0.26)	18 ± NA, N = 1	178.7 ± NA, N = 1 (993%)	14 (74%)	0.9 (5%)	1.8	2.6 – 3.9	0.2 – 0.6 (10-30%)
	P1604	2	6.8 ± 0.6, N = 3 (31%)	22 (99 ± 17%, N = 3)	1.4 ± 0.3, N = 6 (6%)	3.9 ± 0.5, N = 2 (0.18)	22 ± 3, N = 3	202.8 ± 11.0, N = 3 (922%)	12 (41%)	1.1 (5%)	2.2	4.4 – 6.5	0.1 – 0.4 (10-30%)

[a]From this study (see Section 2.2 Methods for details)
[b]Calculated from calculated BGE (BGE calculated as described by del Giorgio and Cole (1998), see Section 2.2 Methods for details)
[c]Export assumed to be 30% of total mesozooplankton grazing, calculated as ("D"/0.3 – "C")
[d]Offshore (5%), transition (20-30%), and nearshore (12%) from Stephens et al. (2018)
[e]Nearshore (20%) from Halewood et al. (2012)
[f]From Nagata (2000)
[g]Steinberg and Landry (2017)

Table S2.2: Average EZ integrated values for the CCE food web with microbial loop by Lagrangian cruise-cycle (continued, 2/3)

Average EZ depth integrated values integrated and averaged per Lagrangian cycle, by CCE region. The percentages within parenthesis for columns A-G are the value within the column of interest as a percentage of the columns designated within the parentheses. The percentages within parenthesis for columns H-K were derived from the literature as cited.

			A[a]	B[a]	C[a]	D[a]	E[a]	F[b]	G[c]	H[d,e]	I[f]	J[f]	K[g]
Region	Cruise	Cycle	BP ("A":"B" as %)	Microzoo grazing on phyto ("B":"E" as %)	Mesozoo grazing on phyto ("C":"E" as %)	Export (e-ratio)	NPP	BCD ("F":"E" as %)	Mesozoo grazing on microzoo ("G":("A"+" B") as %)	Extracellular release of DOC by phyto ("H":"E" as %)	Release of DOC from phytoby viral lysis ("I":"E" = 10%)	Release of DOC by microzoo ("I":"B" = 20-30%)	Release of DOC by mesozoo ("K": ("D"/0.3 – "C") = 10-30%)
			mmol Carbon m^{-2} d^{-1}										
Transition	P0605	4	n.d. (n.d.)	80 (67 ± 19%, N = 4)	27.1 ± 1.4, N = 7 (5%)	11.1* (0.09)	120 ± 10, N = 4	n.d. (n.d.)	31 (n.d.)	24 – 36 (20-30%)	12.0	16.1 – 24.1	0.6 – 1.9 (10-30%)
	P0704	1	4.5 ± 1.1, N = 5 (7%)	68 (67 ± 8%, N = 4)	17.7 ± 7.1, N = 8 (48%)	14.5 ± NA, N = 1 (0.14)	101 ± 35, N = 4	116.0 ± 17.2, N = 5 (115%)	0 (0%)	20 – 30 (20-30%)	10.1	13.5 – 20.3	4.9 – 14.6 (10-30%)
	P0704	4	5.9 ± 3.6, N = 4 (6%)	103 (54 ± 5%, N = 4)	30.2 ± 4.4, N = 8 (9%)	16.1 ± NA, N = 1 (0.08)	191 ± 38, N = 4	134.4 ± 52.9, N = 4 (70%)	36 (33%)	38 – 57 (20-30%)	19.1	20.6 – 30.9	1.8 – 5.4 (10-30%)
	P0810	1	9.5 ± 2.9, N = 4 (18%)	54 (118 ± 13%, N = 4)	15.4 ± 0.7, N = 6 (6%)	4.9 ± 0.4, N = 2 (0.11)	46 ± 7, N = 4	137.9 ± 20.6, N = 4 (300%)	14 (21%)	9 – 14 (20-30%)	4.6	10.9 – 16.3	0.3 – 0.8 (10-30%)
	P0810	3	7.2 ± 0.3, N = 3 (17%)	44 (59 ± 13%, N = 3)	32.3 ± 1.8, N = 4 (14%)	9.5 ± 0.8, N = 2 (0.13)	74 ± 4, N = 3	140.5 ± 3.4, N = 3 (190%)	22 (42%)	15 – 22 (20-30%)	7.4	8.7 – 13.1	1.0 – 3.0 (10-30%)
	P0810	4	18.8 ± 0.0, N = 2 (53%)	35 (63 ± 14%, N = 2)	12.6 ± 4.1, N = 2 (8%)	18.6 ± 0.6, N = 2 (0.33)	56 ± 5, N = 2	178.5 ± 21.9, N = 2 (319%)	58 (107%)	11 – 17 (20-30%)	5.6	7.1 – 10.6	0.4 – 1.3 (10-30%)
	P1408	1	6.2 ± 0.8, N = 3 (12%)	52 (164 ± 26%, N = 3)	50.5 ± 4.8, N = 6 (66%)	16.4 ± 2.1, N = 2 (0.51)	32 ± 5, N = 3	117.7 ± 11.8, N = 3 (368%)	33 (57%)	6 – 10 (20-30%)	3.2	10.5 – 15.7	2.1 – 6.4 (10-30%)
	P1408	2	5.6 ± 0.0, N = 3 (17%)	32 (120 ± 23%, N = 3)	50.8 ± 3.1, N = 6 (82%)	9.3 ± 0.5, N = 3 (0.34)	27 ± 0, N = 3	139.6 ± 6.5, N = 3 (517%)	9 (23%)	5 – 8 (20-30%)	2.7	6.5 – 9.7	2.2 – 6.6 (10-30%)
	P1408	3	3.4 ± 0.3, N = 3 (18%)	19 (82 ± 15%, N = 3)	39.4 ± 1.0, N = 3 (32%)	6.5 ± 1.2, N = 3 (0.28)	23 ± 1, N = 3	97.7 ± 4.1, N = 3 (425%)	14 (64%)	5 – 7 (20-30%)	2.3	3.8 – 5.7	0.7 – 2.2 (10-30%)
	P1604	3	8.6 ± 2.5, N = 3 (23%)	37 (52 ± 6%, N = 3)	45.8 ± 3.0, N = 3 (30%)	7.5 ± 0.4, N = 3 (0.10)	72 ± 11, N = 3	161.8 ± 9.5, N = 3 (225%)	3 (8%)	14 – 22 (20-30%)	7.2	7.5 – 11.2	2.2 – 6.5 (10-30%)
	P1706	3	6.5 ± 2.6, N = 3 (10%)	66 (71 ± 17%, N = 3)	48.7 ± 3.6, N = 6 (15%)	24.3 ± 10.5, N = 3 (0.26)	93 ± 16, N = 7	147.4 ± 25.7, N = 3 (158%)	67 (92%)	19 – 28 (20-30%)	9.3	13.2 – 19.8	1.4 – 4.2 (10-30%)
	P1706	4	10.1 ± 2.2, N = 2 (33%)	31 (72 ± 5%, N = 2)	50.6 ± 0.9, N = 4 (52%)	34.3 ± 3.5, N = 3 (0.80)	43 ± 4, N = 5	201.7 ± 24.2, N = 2 (469%)	92 (224%)	9 – 13 (20-30%)	4.3	6.2 – 9.3	2.2 – 6.7 (10-30%)

[a]From this study (see Section 2.2 Methods for details)

[b]Calculated from calculated BGE (BGE calculated as described by del Giorgio and Cole (1998), see Section 2.2 Methods for details)

[c]Export assumed to be 30% of total mesozooplankton grazing, calculated as ("D"/0.3 – "C")

[d]Offshore (5%), transition (20-30%), and nearshore (12%) from Stephens et al. (2018)

[e]Nearshore (20%) from Halewood et al. (2012)

[f]From Nagata (2000)

[g]Steinberg and Landry (2017)

Table S2.2: Average EZ integrated values for the CCE food web with microbial loop by Lagrangian cruise-cycle (continued, 3/3)

Average EZ depth integrated values integrated and averaged per Lagrangian cycle, by CCE region. The percentages within parenthesis for columns A-G are the value within the column of interest as a percentage of the columns designated within the parentheses. The percentages within parenthesis for columns H-K were derived from the literature as cited.

			A[a]	B[a]	C[a]	D[a]	E[a]	F[b]	G[c]	H[d,e]	I[f]	J[f]	K[g]
Region	Cruise	Cycle	BP ("A":"B" as %)	Microzoo grazing on phyto ("B":"E" as %)	Mesozoo grazing on phyto ("C":"E" as %)	Export (e-ratio)	NPP	BCD ("F":"E" as %)	Mesozoo grazing on microzoo ("G":("A"+"B") as %)	Extracellular release of DOC by phyto ("H":"E" as %)	Release of DOC from phytoby viral lysis ("I":"E" = 10%)	Release of DOC by microzoo ("I":"B" = 20-30%)	Release of DOC by mesozoo ("K": ("D"/0.3 – "C") = 10-30%)
			mmol Carbon m^{-2} d^{-1}										
Nearshore	P0605	1	n.d. (n.d.)	165 (58 ± 16%, N = 4)	40.5 ± 11.6, N = 8 (14%)	n.d. (n.d.)	285 ± 63, N = 4	n.d. (n.d.)	n.d. (n.d.)	34 – 57 (12-20%)	28.5	33.1 – 49.6	4.0 – 12.1 (10-30%)
	P0605	3	n.d. (n.d.)	297 (88 ± 15%, N = 3)	22.5 ± 7.3, N = 7 (7%)	n.d. (n.d.)	337 ± 6, N = 3	n.d. (n.d.)	n.d. (n.d.)	40 – 67 (12-20%)	33.7	59.3 – 89.0	2.2 – 6.7 (10-30%)
	P0704	3	4.1 ± NA, N = 1. (2%)	198 (34 ± NA%, N = 1)	n.d. (n.d.)	n.d. (n.d.)	581 ± NA, N = 1	130.9 ± NA, N = 1 (23%)	n.d. (n.d.)	70 – 116 (12-20%)	58.1	39.5 – 59.3	n.d. (10-30%)
	P0810	5	17.1 ± 4.4, N = 2 (32%)	53 (38 ± NA%, N = 1)	n.d. (n.d.)	13.4 ± 1.7, N = 2 (0.10)	139 ± 18, N = 2	150.0 ± 22.9, N = 2 (108%)	n.d. (n.d.)	17 – 28 (12-20%)	13.9	10.6 – 15.8	n.d. (10-30%)
	P1604	4	29.0 ± 1.7, N = 3 (n.d.)	n.d. (n.d.)	27.4 ± 4.7, N = 2 (20%)	30.5 ± 3.6, N = 3 (0.22)	138 ± 16, N = 3	150.0 ± 7.1, N = 3 (109%)	n.d. (n.d.)	17 – 28 (12-20%)	13.8	n.d.	2.7 – 8.2 (10-30%)
	P1706	1	10.9 ± 3.1, N = 3 (3%)	335 (64 ± 7%, N = 3)	58.1 ± 5.7, N = 6 (11%)	33.5 ± 4.6, N = 3 (0.02)	524 ± 92[i], N = 7	97.0 ± 27.1, N = 3 (19%)	54 (15%)	63 – 105 (12-20%)	52.4	67.1 – 100.6	5.8 – 17.4 (10-30%)
	P1706	2	12.4 ± 1.3, N = 4 (8%)	164 (75 ± 9%, N = 4)	20.1 ± 2.6, N = 8 (9%)	32.1 ± 5.8, N = 3 (0.06)	218 ± 35[i], N = 8	148.4 ± 14.3, N = 4 (68%)	87 (49%)	26 – 44 (12-20%)	21.8	32.7 – 49.1	2.0 – 6.0 (10-30%)

[a]From this study (see Section 2.2 Methods for details)
[b]Calculated from calculated BGE (BGE calculated as described by del Giorgio and Cole (1998), see Section 2.2 Methods for details)
[c]Export assumed to be 30% of total mesozooplankton grazing, calculated as ("D"/0.3 – "C")
[d]Offshore (5%), transition (20-30%), and nearshore (12%) from Stephens et al. (2018)
[e]Nearshore (20%) from Halewood et al. (2012)
[f]From Nagata (2000)
[g]Steinberg and Landry (2017)

Table S2.3: Calculated NPP and DOC remaining

Values for each Lagrangian cycle were calculated using values (designated by letters) from Appendix Table S2.2.

Region	Cruise	Cycle	$NPP_{remaining}$ (%NPP utilized)	DOC released	$DOC_{remaining}$ (%DOC utilized)
			= E - B - C	= H + I + J + K	= F - H - I - J - K
			mmol Carbon m^{-2} d^{-1}		
Offshore	P0605	2	5 (78%)	8.8	n.d. (n.d.)
	P0605	5	-16 (158%)	17.4	n.d. (n.d.)
	P0704	2	-16 (133%)	26.4	-55 (308%)
	P0810	2	-1 (102%)	18.2	-150 (926%)
	P0810	6	n.d. (n.d.)	9.0	-140 (1,649%)
	P1408	4	-2 (117%)	5.0	-107 (2,235%)
	P1408	5	-3 (126%)	5.8	-153 (2,738%)
	P1604	1	3 (83%)	7.2	-172 (2,486%)
	P1604	2	-1 (105%)	10.2	-193 (1,979%)
Transition	P0605	4	33 (72%)	74.0	n.d. (n.d.)
	P0704	1	-15 (115%)	75.3	-41 (154%)
	P0704	4	70 (63%)	112.7	-22 (119%)
	P0810	1	-11 (124%)	35.5	-102 (388%)
	P0810	3	20 (73%)	45.7	-95 (307%)
	P0810	4	16 (71%)	34.3	-144 (521%)
	P1408	1	-42 (230%)	34.9	-83 (337%)
	P1408	2	-28 (202%)	27.2	-112 (514%)
	P1408	3	-3 (114%)	17.1	-81 (572%)
	P1604	3	13 (82%)	46.5	-115 (384%)
	P1706	3	13 (86%)	61.2	-86 (241%)
	P1706	4	-10 (124%)	33.2	-168 (607%)
Nearshore	P0605	1	79 (72%)	147.2	n.d. (n.d.)
	P0605	3	18 (95%)	196.8	n.d. (n.d.)
	P0704	3	n.d. (n.d.)	233.6	103 (56%)
	P0810	5	n.d. (n.d.)	57.5	-92 (261%)
	P1604	4	n.d. (n.d.)	49.6	-100 (302%)
	P1706	1	131 (75%)	275.2	178 (35%)
	P1706	2	34 (84%)	120.5	-28 (123%)

2.9 REFERENCES

Alvarez-Salgado XA, Aristegui J, Barton ED, Hansell DA (2007) Contribution of upwelling filaments to offshore carbon export in the subtropical Northeast Atlantic Ocean. Limnology and Oceanography 52:1287-1292

Alvarez-Salgado XA, Doval MD, Borges AV, Joint I, Frankignoulle M, Woodward EMS, Figueiras FG (2001) Off-shelf fluxes of labile materials by an upwelling filament in the NW Iberian Upwelling System. Progress in Oceanography 51:321-337

Aristegui J, Barton ED, Tett P, Montero MF, Garcia-Munoz M, Basterretxea G, Cussatlegras AS, Ojeda A, de Armas D (2004) Variability in plankton community structure, metabolism, and vertical carbon fluxes along an upwelling filament (Cape Juby, NW Africa). Progress in Oceanography 62:95-113

Azam F, Fenchel T, Field JG, Gray JS, Meyer-Reil LA, Thingstad F (1983) THE ECOLOGICAL ROLE OF WATER COLUMN MICROBES IN THE SEA. Marine Ecology Progress Series 10:257-264

Azam F, Malfatti F (2007) Microbial structuring of marine ecosystems (vol 5, pg 782-791, 2007). Nature Reviews Microbiology 5:966-923

Barbosa AB, Galvao HM, Mendes PA, Alvarez-Salgado XA, Figueiras FG, Joint I (2001) Short-term variability of heterotrophic bacterioplankton during upwelling off the NW Iberian margin. Progress in Oceanography 51:339-359

Bender M, Ducklow H, Kiddon J, Marra J, Martin J (1992) THE CARBON BALANCE DURING THE 1989 SPRING BLOOM IN THE NORTH-ATLANTIC OCEAN, 47-DEGREES-N, 20-DEGREES-W. Deep-Sea Research Part a-Oceanographic Research Papers 39:1707-1725

Biddanda B, Ogdahl M, Cotner J (2001) Dominance of bacterial metabolism in oligotrophic relative to eutrophic waters. Limnology and Oceanography 46:730-739

Billen G, Fontigny A (1987) DYNAMICS OF A PHAEOCYSTIS-DOMINATED SPRING BLOOM IN BELGIAN COASTAL WATERS .2. BACTERIOPLANKTON DYNAMICS. Marine Ecology Progress Series 37:249-257

Bond NA, Cronin MF, Freeland H, Mantua N (2015) Causes and impacts of the 2014 warm anomaly in the NE Pacific. Geophysical Research Letters 42:3414-3420

Burrell TJ, Maas EW, Hulston DA, Law CS (2017) Variable response to warming and ocean acidification by bacterial processes in different plankton communities. Aquatic Microbial Ecology 79:49-62

Carlson CA, Del Giorgio PA, Herndl GJ (2007) Microbes and the Dissipation of Energy and Respiration: From Cells to Ecosystems. Oceanography 20:89-100

Chavez FP, Messie M (2009) A comparison of Eastern Boundary Upwelling Ecosystems. Progress in Oceanography 83:80-96

Cho BC, Azam F (1990) BIOGEOCHEMICAL SIGNIFICANCE OF BACTERIAL BIOMASS IN THE OCEANS EUPHOTIC ZONE. Marine Ecology Progress Series 63:253-259

Coffin RB, Connolly JP, Harris PS (1993) AVAILABILITY OF DISSOLVED ORGANIC-CARBON TO BACTERIOPLANKTON EXAMINED BY OXYGEN UTILIZATION. Marine Ecology Progress Series 101:9-22

Cole JJ (1999) Aquatic microbiology for ecosystem scientists: New and recycled paradigms in ecological microbiology. Ecosystems 2:215-225

Cole JJ, Findlay S, Pace ML (1988) BACTERIAL PRODUCTION IN FRESH AND SALTWATER ECOSYSTEMS - A CROSS-SYSTEM OVERVIEW. Marine Ecology Progress Series 43:1-10

Conover RJ (1966) ASSIMILATION OF ORGANIC MATTER BY ZOOPLANKTON. Limnology and Oceanography 11:338-345

Cuevasa LA, Daneri G, Jacob B, Montero P (2004) Microbial abundance and activity in the seasonal upwelling area off Concepcion (similar to 36 degrees S), central Chile: a comparison of upwelling and non-upwelling conditions. Deep-Sea Research Part Ii-Topical Studies in Oceanography 51:2427-2440

Davis A, Di Lorenzo E (2015) Interannual forcing mechanisms of California Current transports I: Meridional Currents. Deep-Sea Research Part Ii-Topical Studies in Oceanography 112:18-30

del Giorgio PA, Cole JJ (1998) Bacterial growth efficiency in natural aquatic systems. Annual Review of Ecology and Systematics 29:503-541

del Giorgio PA, Condon R, Bouvier T, Longnecker K, Bouvier C, Sherr E, Gasol JM (2011) Coherent patterns in bacterial growth, growth efficiency, and leucine metabolism along a northeastern Pacific inshore-offshore transect. Limnology and Oceanography 56:1-16

del Giorgio PA, Duarte CM (2002) Respiration in the open ocean. Nature 420:379-384

Di Lorenzo E, Mantua N (2016) Multi-year persistence of the 2014/15 North Pacific marine heatwave. Nature Climate Change 6:1042-1047

Duarte CM, Agusti S (1998) The CO2 balance of unproductive aquatic ecosystems. Science 281:234-236

Duarte CM, Cebrian J (1996) The fate of marine autotrophic production. Limnology and Oceanography 41:1758-1766

Duarte CM, Regaudie-de-Gioux A, Arrieta JM, Delgado-Huertas A, Agusti S (2013) The Oligotrophic Ocean Is Heterotrophic. In: Carlson CA, Giovannoni SJ (eds) Annual Review of Marine Science, Vol 5, Book 5. Annual Reviews, Palo Alto

Ducklow HW (1999) The bacterial component of the oceanic euphotic zone. Fems Microbiology Ecology 30:1-10

Ducklow HW, Doney SC (2013) What Is the Metabolic State of the Oligotrophic Ocean? A Debate. In: Carlson CA, Giovannoni SJ (eds) Annual Review of Marine Science, Vol 5, Book 5. Annual Reviews, Palo Alto

Ducklow HW, Kirchman DL, Quinby HL, Carlson CA, Dam HG (1993) STOCKS AND DYNAMICS OF BACTERIOPLANKTON CARBON DURING THE SPRING BLOOM IN THE EASTERN NORTH-ATLANTIC OCEAN. Deep-Sea Research Part Ii-Topical Studies in Oceanography 40:245-263

Eiler A, Langenheder S, Bertilsson S, Tranvik LJ (2003) Heterotrophic bacterial growth efficiency and community structure at different natural organic carbon concentrations. Applied and Environmental Microbiology 69:3701-3709

Eppley RW, Holm-Hansen O (1986) Primary Production in the Southern California Bight, Vol 15. Springer-Verlag

Fasham MJR, Boyd PW, Savidge G (1999) Modeling the relative contributions of autotrophs and heterotrophs to carbon flow at a Lagrangian JGOFS station in the Northeast Atlantic: The importance of DOC. Limnology and Oceanography 44:80-94

Fenchel T (2008) The microbial loop-25 years later. Journal of Experimental Marine Biology and Ecology 366:99-103

Frolicher TL, Laufkotter C (2018) Emerging risks from marine heat waves. Nature Communications 9:650

Fuhrman JA, Azam F (1980) BACTERIOPLANKTON SECONDARY PRODUCTION ESTIMATES FOR COASTAL WATERS OF BRITISH-COLUMBIA, ANTARCTICA, AND CALIFORNIA. Applied and Environmental Microbiology 39:1085-1095

Fuhrman JA, Sleeter TD, Carlson CA, Proctor LM (1989) DOMINANCE OF BACTERIAL BIOMASS IN THE SARGASSO SEA AND ITS ECOLOGICAL IMPLICATIONS. Marine Ecology Progress Series 57:207-217

Garrison DL, Gowing MM, Hughes MP, Campbell L, Caron DA, Dennett MR, Shalapyonok A, Olson RJ, Landry MR, Brown SL, Liu HB, Azam F, Steward GF, Ducklow HW, Smith DC (2000) Microbial food web structure in the Arabian Sea: a US JGOFS study. Deep-Sea Research Part Ii-Topical Studies in Oceanography 47:1387-1422

Gasol JM, del Giorgio PA, Duarte CM (1997) Biomass distribution in marine planktonic communities. Limnology and Oceanography 42:1353-1363

Gentemann CL, Fewings MR, Garcia-Reyes M (2017) Satellite sea surface temperatures along the West Coast of the United States during the 2014-2016 northeast Pacific marine heat wave. Geophysical Research Letters 44:312-319

Goericke R (2011) The structure of marine phytoplankton communities--patterns, rules, and mechanisms. In, Book 52, California Cooperative Oceanic Fisheries Investigations Report

Goericke R, Ohman MD (2015) Introduction to CCE-LTER: Responses of the California Current Ecosystem to climate forcing. Deep-Sea Research Part Ii-Topical Studies in Oceanography 112:1-5

Gruber N, Lachkar Z, Frenzel H, Marchesiello P, Munnich M, McWilliams JC, Nagai T, Plattner GK (2011) Eddy-induced reduction of biological production in eastern boundary upwelling systems. Nature Geoscience 4:787-792

Halewood ER, Carlson CA, Brzezinski MA, Reed DC, Goodman J (2012) Annual cycle of organic matter partitioning and its availability to bacteria across the Santa Barbara Channel continental shelf. Aquatic Microbial Ecology 67:189-209

Haskell WZ, Prokopenko MG, Hammond DE, Stanley RHR, Berelson WM, Baronas JJ, Fleming JC, Aluwihare L (2016) An organic carbon budget for coastal Southern California determined by estimates of vertical nutrient flux, net community production and export. Deep-Sea Research Part I-Oceanographic Research Papers 116:49-76

Haskell WZ, Prokopenko MG, Hammond DE, Stanley RHR, Sandwith ZO (2017) Annual cyclicity in export efficiency in the inner Southern California Bight. Global Biogeochemical Cycles 31:357-376

Hendricks MB, Bender ML, Barnett BA, Strutton P, Chavez FP (2005) Triple oxygen isotope composition of dissolved O-2 in the equatorial Pacific: A tracer of mixing, production, and respiration. Journal of Geophysical Research-Oceans 110

Hill PG, Warwick PE, Zubkov MV (2013) Low microbial respiration of leucine at ambient oceanic concentration in the mixed layer of the central Atlantic Ocean. Limnology and Oceanography 58:1597-1604

Hoppe HG, Gocke K, Koppe R, Begler C (2002) Bacterial growth and primary production along a north-south transect of the Atlantic Ocean. Nature 416:168-171

Jacox MG, Hazen EL, Zaba KD, Rudnick DL, Edwards CA, Moore AM, Bograd SJ (2016) Impacts of the 2015-2016 El Nino on the California Current System: Early assessment and comparison to past events. Geophysical Research Letters 43:7072-7080

Karl DM, Church MJ (2017) Ecosystem Structure and Dynamics in the North Pacific Subtropical Gyre: New Views of an Old Ocean. Ecosystems 20:433-457

Kelly TB, Goericke R, Kahru M, Song H, Stukel MR (2018) CCE II: Spatial and interannual variability in export efficiency and the biological pump in an eastern boundary current upwelling system with substantial lateral advection. Deep-Sea Research Part I-Oceanographic Research Papers 140:14-25

Kirchman D, Ducklow H, Mitchell R (1982) ESTIMATES OF BACTERIAL GROWTH FROM CHANGES IN UPTAKE RATES AND BIOMASS. Applied and Environmental Microbiology 44:1296-1307

Kirchman D, Knees E, Hodson R (1985) LEUCINE INCORPORATION AND ITS POTENTIAL AS A MEASURE OF PROTEIN-SYNTHESIS BY BACTERIA IN NATURAL AQUATIC SYSTEMS. Applied and Environmental Microbiology 49:599-607

Kranz SA, Wang S, Kelly TB, Stukel MR, Goericke R, Landry MR, Cassar N (2020) Lagrangian studies of marine production: a multi-method assessment of productivity relationships in the California Current Ecosystem upwelling region. J Geophys Res Oceans

Lancelot C, Billen G (1984) ACTIVITY OF HETEROTROPHIC BACTERIA AND ITS COUPLING TO PRIMARY PRODUCTION DURING THE SPRING PHYTOPLANKTON BLOOM IN THE SOUTHERN BIGHT OF THE NORTH-SEA. Limnology and Oceanography 29:721-730

Landry MR, Ohman MD, Goericke R, Stukel MR, Tsyrklevich K (2009) Lagrangian studies of phytoplankton growth and grazing relationships in a coastal upwelling ecosystem off Southern California. Progress in Oceanography 83:208-216

Lee CW, Bong CW (2008) Bacterial abundance and production, and their relation to primary production in tropical coastal waters of Peninsular Malaysia. Marine and Freshwater Research 59:10-21

Legendre L, Lefevre J (1995) MICROBIAL FOOD WEBS AND THE EXPORT OF BIOGENIC CARBON IN OCEANS. Aquatic Microbial Ecology 9:69-77

Li QP, Franks PJS, Landry MR, Goericke R, Taylor AG (2010) Modeling phytoplankton growth rates and chlorophyll to carbon ratios in California coastal and pelagic ecosystems. Journal of Geophysical Research-Biogeosciences 115

Lopez-Urrutia A, Moran XAG (2007) Resource limitation of bacterial production distorts the temperature dependence of oceanic carbon cycling. Ecology 88:817-822

Lovecchio E, Gruber N, Mnnich M, Lachkar Z (2017) On the long-range offshore transport of organic carbon from the Canary Upwelling System to the open North Atlantic. Biogeosciences 14:3337-3369

Manning CC, Stanley RHR, Nicholson DP, Smith JM, Pennington JT, Fewings MR, Squibb ME, Chavez FP (2017) Impact of recently upwelled water on productivity investigated using in situ and incubation-based methods in Monterey Bay. Journal of Geophysical Research-Oceans 122:1901-1926

Marra J (2002) Approaches to the Measurement of Plankton Production, Vol. Blackwell Publishing Ltd.

Martinez-Garcia S, Karl DM (2015) Microbial respiration in the euphotic zone at Station ALOHA. Limnology and Oceanography 60:1039-1050

Monger BC, Landry MR (1993) FLOW CYTOMETRIC ANALYSIS OF MARINE-BACTERIA WITH HOECHST 33342. Applied and Environmental Microbiology 59:905-911

Moran XAG, Alonso-Saez L, Nogueira E, Ducklow HW, Gonzalez N, Lopez-Urrutia A, Diaz-Perez L, Calvo-Diaz A, Arandia-Gorostidi N, Huete-Stauffer TM (2015) More, smaller bacteria in response to ocean's warming? Proceedings of the Royal Society B-Biological Sciences 282:9

Morrow RM, Ohman MD, Goericke R, Kelly TB, Stephens BM, Stukel MR (2018) CCE V: Primary production, mesozooplankton grazing, and the biological pump in the California Current Ecosystem: Variability and response to El Nino. Deep-Sea Research Part I-Oceanographic Research Papers 140:52-62

Munro DR, Quay PD, Juranek LW, Goericke R (2013) Biological production rates off the Southern California coast estimated from triple O-2 isotopes and O-2 : Ar gas ratios. Limnology and Oceanography 58:1312-1328

Nagai T, Gruber N, Frenzel H, Lachkar Z, McWilliams JC, Plattner GK (2015) Dominant role of eddies and filaments in the offshore transport of carbon and nutrients in the California Current System. Journal of Geophysical Research-Oceans 120:5318-5341

Nagata T (2000) Production Mechanisms of Dissolved Organic Matter, Vol. Wiley-Liss, New York

Ohman MD, Barbeau K, Franks PJS, Goericke R, Landry MR, Miller AJ (2013) Ecological Transitions in a Coastal Upwelling Ecosystem. Oceanography 26:210-219

Ohman MD, Powell JR, Picheral M, Jensen DW (2012) Mesozooplankton and particulate matter responses to a deep-water frontal system in the southern California Current System. Journal of Plankton Research 34:815-827

Pedler BE, Aluwihare LI, Azam F (2014) Single bacterial strain capable of significant contribution to carbon cycling in the surface ocean. Proceedings of the National Academy of Sciences of the United States of America 111:7202-7207

Polovina JJ, Howell EA, Abecassis M (2008) Ocean's least productive waters are expanding. Geophysical Research Letters 35:5

Samo TJ, Pedler BE, Ball GI, Pasulka AL, Taylor AG, Aluwihare LI, Azam F, Goericke R, Landry MR (2012) Microbial distribution and activity across a water mass frontal zone in the California Current Ecosystem. Journal of Plankton Research 34:802-814

Sarmiento JL, Slater R, Barber R, Bopp L, Doney SC, Hirst AC, Kleypas J, Matear R, Mikolajewicz U, Monfray P, Soldatov V, Spall SA, Stouffer R (2004) Response of ocean ecosystems to climate warming. Global Biogeochemical Cycles 18:35

Simon M, Azam F (1989) PROTEIN-CONTENT AND PROTEIN-SYNTHESIS RATES OF PLANKTONIC MARINE-BACTERIA. Marine Ecology Progress Series 51:201-213

Smith DC, Azam F (1992) A simple, economical method for measuring bacterial protein synthesis in seawater using 3H-leucine. In, Book 6, Mar. Microb. Food Webs

Smith DC, Simon M, Alldredge AL, Azam F (1992) INTENSE HYDROLYTIC ENZYME-ACTIVITY ON MARINE AGGREGATES AND IMPLICATIONS FOR RAPID PARTICLE DISSOLUTION. Nature 359:139-142

Steinberg DK, Landry MR, Annual R (2017) Zooplankton and the Ocean Carbon Cycle. Annual Review of Marine Science, Vol 9 9:413-444

Stephens BM, Porrachia M, Dovel S, Roadman M, Goericke R, Aluwihare LI (2018) Nonsinking Organic Matter Production in the California Current. Global Biogeochemical Cycles 32:1386-1405

Strickland JDH, Parsons TR (1972) A Practical Handbook of Seawater Analysis. In, Book 157. Fisheries Research Board of Canada Bulletin

Stukel, Michael, Goericke R, Landry M (2019a) Predicting primary production in the southern California Current Ecosystem from chlorophyll, nutrient concentrations, and irradiance. bioRxiv 590240

Stukel MR, Barbeau KA (2020) Investigating the Nutrient Landscape in a Coastal Upwelling Region and Its Relationship to the Biological Carbon Pump. Geophysical Research Letters 47

Stukel MR, Kelly TB, Aluwihare LI, Barbeau KA, Goericke R, Krause JW, Landry MR, Ohman MD (2019b) The Carbon:(234)Thorium ratios of sinking particles in the California current ecosystem 1: relationships with plankton ecosystem dynamics. Marine Chemistry 212:1-15

Stukel MR, Landry MR, Benitez-Nelson CR, Goericke R (2011) Trophic cycling and carbon export relationships in the California Current Ecosystem. Limnology and Oceanography 56:1866-1878

Stukel MR, Ohman MD, Benitez-Nelson CR, Landry MR (2013) Contributions of mesozooplankton to vertical carbon export in a coastal upwelling system. Marine Ecology Progress Series 491:47-65

Taylor AG, Landry MR (2018) Phytoplankton biomass and size structure across trophic gradients in the southern California Current and adjacent ocean ecosystems. Marine Ecology Progress Series 592:1-17

Viviani DA, Church MJ (2017) Decoupling between bacterial production and primary production over multiple time scales in the North Pacific Subtropical Gyre. Deep-Sea Research Part I-Oceanographic Research Papers 121:132-142

Wear EK, Carlson CA, James AK, Brzezinski MA, Windecker LA, Nelson CE (2015) Synchronous shifts in dissolved organic carbon bioavailability and bacterial community responses over the course of an upwelling-driven phytoplankton bloom. Limnology and Oceanography 60:657-677

Williams PJL, Quay PD, Westberry TK, Behrenfeld MJ (2013) The Oligotrophic Ocean Is Autotrophic. In: Carlson CA, Giovannoni SJ (eds) Annual Review of Marine Science, Vol 5, Book 5. Annual Reviews, Palo Alto

Chapter 3: Control of heterotrophic bacterial production in the southern California Current System

Sara R. Rivera, Brandon M. Stephens, Ty J. Samo, Brooke Rasina, Michael R. Stukel, Michael R. Landry, Farooq Azam, Lihini I. Aluwihare

ABSTRACT

In the nearshore southern California Current System (sCCS) between 2006-2017, we observed strong correlations between bacterial production (BP) and particulate organic carbon (POC), chlorophyll, and autotrophic biomass. Furthermore, POC concentrations, particularly at the lower end, exhibited robust correlations with BP across all sCCS regions from nearshore to offshore. Such bottom up controls on microbial activity did not show a consistent relationship between years because of the interannual variability in oceanographic conditions within each region. We also observed an inverse relationship between temperature control and bottom-up control; however, because surface ocean temperatures in the sCCS during upwelling are inversely correlated with nutrient concentrations and therefore net primary production, BP can be strongly inversely correlated with temperature in the region. Finally, this study provides the necessary framework for future attempting to disentangle natural variability from new climate-related changes by identifying interannual variability in controls and examining temperature controls as a function of productivity. This will be particularly instructive to assess microbial food web consequences of marine heat waves that increase stratification and decrease nutrient availability, as observed during the 2014 warm anomaly.

3.1. INTRODUCTION

The California Current Ecosystem Long Term Ecological Research (CCE-LTER) program is placed within the Eastern Boundary Upwelling Ecosystem off the western coast of North America (Chavez & Messie 2009) and complements the co-located program, the California Cooperative Oceanic Fisheries Investigation (CalCOFI) survey grid, using short Lagrangian cycles to examine mesoscale variability and conduct biological process experiments in the southern California Current System (sCCS).

Both the CalCOFI timeseries, started in 1949, and the CCE-LTER program, started in 2004, have robustly demonstrated the role of interannual and decadal climate variability in altering ecosystems and biogeochemical fluxes in the region (Hayward & Venrick 1998, Goericke 2011, Ohman et al. 2013, Goericke & Ohman 2015) , but these initiatives have not synthesized the CCE-LTER reports of heterotrophic bacterial activity within the context of concomitant measurements across the sCCS domain.

The high abundance, fast growth rates, and biogeochemical importance of heterotrophic bacteria (Azam et al. 1983, Fenchel 2008, Burrell et al. 2017), make them an attractive and accessible component of ecosystems to study and monitor in the context of global change. For example, heterotrophic bacterial production (BP) may show enhanced sensitivity to the predicted decrease in nutrient supply and associated net primary production (NPP) that results from a warmer surface ocean (Sarmiento et al. 2004, Polovina et al. 2008) Additionally, bacterial size may decrease from increased water temperatures and impact food webs and the biological pump (Moran et al. 2015). Furthermore, the sCCS had a shift towards higher bacterial abundances and compression of bacteria to the nearshore region synchronously to a shift to the positive PDO phase (see Sections 1.3.2.2 and 1.4.1.2). These

examples highlight a few ways that heterotrophic bacteria can be used to study the impacts of climate forcing to the marine ecosystem.

Overall, the impact of heterotrophic bacteria on carbon turnover (i.e., bacterial productivity) can be constrained by both bottom-up and top-down controls. Evidence for bottom-up controls, which are driven by the availability of resources, such as dissolved organic carbon (DOC), is primarily found in the relationship of bacterial abundance (BA) and BP to indices of primary production (Billen et al. 1990, Ducklow 1992, Kim & Ducklow 2016). The availability or "quality" of DOC also impacts BP (Cherrier et al. 1996), but was not assessed in this study. In addition, warmer ocean temperatures can impact BP by increasing metabolic rates (White et al. 1991, Herrmann et al. 2014) throughout the microbial loop, which could enhance both bottom-up and top down controls. Top down controls such as grazing and viral lysis can reduce diversity, decrease BP, and remove bacterial cells based on size (Gonzalez et al. 1990, Monger & Landry 1991, Epstein & Shiaris 1992, Jurgens & Gude 1994, Hahn & Hofle 1999, Pasulka et al. 2015, Taylor & Landry 2018, Weinbauer et al. 2019). Previous studies have examined controls on BP in particular regions of the ocean and a few studies have provided a time series context (Cole et al. 1988, Barbosa et al. 2001, Karl & Church 2014, Kim & Ducklow 2016, Viviani & Church 2017).

Within the CCE-LTER, long term observations of both bottom-up and top down controls is possible. Sampling across different biomes that are hydrographically connected and influenced by similar climate forcing occur within a single cruise. Furthermore, the gradient from coastal upwelling driven regimes, through the California Current region (which includes areas of curl driven upwelling), out to the eastern edge of the North Pacific Subtropical Gyre expresses in a spatial gradient the expected temporal trajectory of surface

ocean conditions as the atmosphere continues to warm. Moreover, the CCE-LTER program has captured a warm anomaly event (Bond et al. 2015, Gentemann et al. 2017) and El Niño event (Jacox et al. 2016), in addition to years with more "normal" conditions. The long term structure of the CCE-LTER program, combined with the goals of elucidating mechanist understanding of ecosystem dynamics across the sCCS allows for examination of bottom-up and top down controls of BP across time and space.

Here, we examine heterotrophic bacterial properties across three biogeographic regimes within the sCCS. We find that the variability across biogeographic boundaries in heterotrophic bacterial parameters is much larger than the interannual variability encountered within a region over the course of this study- including during the 2015/2016 El Niño event (Jacox et al. 2016). Such a finding suggests that carbon fluxes and the microbial communities that control those fluxes within the coastal or wind curl driven upwelling biomes will be significantly altered if there is an expansion of warmer, more stratified environments within the sCCS. However, the interannual variability within a region was strong enough to scramble the detection of consistent bottom-up control mechanisms, as revealed by the bottom-up control index. An inverse relationship between temperature control and bottom-up control in this region was consistent with previous studies (Calvo-Diaz et al. 2014, Moran et al. 2017), but temperature was an indicator of upwelling and thus nutrient delivery within the sCCS rather than metabolic rate (Lopez-Urrutia & Moran 2007, Kelly et al. 2018). Finally, this study provides a baseline assessment against which future microbial biogeochemistry studies can make comparisons to disentangle natural variability anthropogenic perturbations, such as the marine heat waves observed in the 2014 warm anomaly (Bond et al. 2015, Gentemann et al. 2017, Smale et al. 2019).

3.2. METHODS

3.2.1 Study region and sampling periods

This study focuses on the southern California Current System (sCCS), encompassing typical springtime upwelling dominated waters nearshore of Point Conception out to the edge of the oligotrophic gyre, up to 500 km offshore. Samples for this study were collected on CCE-LTER cruises from May 8- June 7 2006 (P0605), April 2-21, 2007 (P0704), September 30 - October 29 2008 (P0810), August 6 -September 4 (P1408), April 19 – May 12 2016 (P1604), and June 1 - July 2 2017 (P1706) (see Sections 1.3.1 and 1.4.1, Kelly et al. 2018, Morrow et al. 2018 for details). Ecosystems conditions during 2004-2013 and 2017 were El Niño-neutral ("normal") and 2014-2016 were warm, with a warm anomaly encountered during P1408 (Bond et al. 2015, Gentemann et al. 2017) and the tail of end of El Niño conditions encountered during P1604 (Di Lorenzo & Mantua 2016, Jacox et al. 2016). The sampling framework for the CCE-LTER is well described (Landry et al. 2009, Ohman et al. 2012, Stukel et al. 2013). During CCE-LTER cruises, water masses with the appropriate characteristics for the planned sampling design were pre-identified using surveys collected by a Moving Vessel Profiler or a SeaSoar (Ohman et al. 2012). Water parcels were chosen to represent various water masses and system dynamics including, California Current waters, upwelling conditions, oligotrophic gyre regions, frontal zones, and filaments. Regional groupings of cruise cycles as nearshore, transition, and offshore, were delineated according to water column properties such as nitracline depth, chlorophyll maximum depth, and euphotic zone depth (see Sections 1.3.1 and 1.4.1).

3.2.2 Hydrographic conditions

In this study, the euphotic zone (EZ) depth is defined as the 0.1% surface irradiance depth instead of the more common 1% to most accurately approximate the depth of the light compensation point, or the point where net photosynthesis is zero (Eppley & Holm-Hansen 1986). Photosynthetically active radiation (PAR) was measured using a 4-π Licor PAC sensor in the water column and a 2-π Licor PAC sensor for surface measurements. The percent surface irradiance was calculated from *in situ* PAR recorded by the CTD downcast and surface PAR. Where possible, daily, cast by cast data were used and then averaged.

3.2.3 Chlorophyll and Primary Production measurements

Chlorophyll *a* (Chl) concentrations were measured at 6-8 depths after Strickland and Parsons (1972) and converted to autotrophic biomass (AB) using a carbon (mg):Chl (mg) of 51.5 (Taylor et al. 2015). NPP was measured at 6-8 depths using the ^{14}C method after Strickland and Parsons (1972) and as detailed in Morrow et al. (2018). For P1706, the ^{14}C-NPP samples were compromised, and so, NPP was computed from a model that assimilated data from previous CCE-LTER cruises (Stukel et al. 2019).

3.2.4 Supporting chemical measurements

Oxidized nitrogen species were analyzed following a modification of Armstrong et al. (1967). Approximately 40 mL of seawater (SW) was collected from at least 6 depths for TOC (P0704, P1408, P1604) and/or DOC (P1408, P1604, P1706) analysis following Stephens et al. (2018). Two (P0605, P0704, P0810) or four (P1408, P1604, P1706) L of SW were filtered and processed for suspended POC measurements following Stephens et al. (2018).

3.2.5 Heterotrophic BA and BB by Flow Cytometry (FCM, FCM*)

BA and BB were determined from preserved samples (2 ml SW + paraformaldehyde, 0.5% final or 3 ml SW + 25% glutaraldehyde, 1.0% final) that had been frozen in liquid N_2, stored at -80°C, and sent to the University of Hawaii's School of Ocean and Earth Science and Technology (SOEST) Flow Cytometry Facility. Prior to analysis, samples were thawed and stained with Hoechst 33342 in the dark at room temperature for 1 hour (Monger & Landry 1993) and analyzed with a Beckman-Coulter EPICS Altra flow cytometer with dual lasers (tuned to UV [200 mW] and 488 nm [1 W] excitation) to estimate abundances of heterotrophic bacteria. All samples were spiked with fluorescent beads to normalize fluorescence and scattering properties. Raw data were processed using the software FlowJo (Treestar Inc., www.flowjo.com) with correction factors of 0.95 for preservative, 0.10 for run volume and 0.82 for coincidence. Heterotrophic BA were converted to carbon biomass equivalents using a constant factor of 11 fg C $cell^{-1}$ (Garrison et al. 2000). In the text, FCM is used to refer to samples fixed with paraformaldehyde (2 a.m. local time cast) and FCM* refers to samples fixed with glutaraldehyde (11 a.m. local time cast, which was when BP measurements were made). Originally, 11 a.m. glutaraldehyde-fixed samples were collected for microscopy (counts, size determination etc.), but microscopy was only performed on a few CCE-LTER cruises, whereas FCM data were available for all cruises considered here. However, we did not want to directly compare BP from the 11 a.m. cast to FCM counts from the 2 a.m. cast without ensuring that BA had not changed significantly between 2 a.m. and 11 a.m. For that reason, we also analyzed 11 a.m. BA samples originally collected for microscopy and preserved in glutaraldehyde, by flow cytometry (designated FCM*).

Comparison of 2 a.m. and 11 a.m. casts, preserved differently enabled continuity over the timeseries and among the various datasets. The influence of different preservative methods has been discussed elsewhere (Monger & Landry 1993, Troussellier et al. 1995).

3.2.5.1 Heterotrophic BA and BB by Epifluorescence Microscopy (EFM)

For P0704, P1408, P1604, and P1706 microscopic cell counts were also performed. Preserved samples were frozen in liquid N_2 and stored at -80°C until analysis (<3 months). Samples (3 mL SW) from P0704 were preserved with 0.2 µm filtered formaldehyde (2-4% final), while samples (3 mL SW) from P1408, P1604, and P1706 were preserved with 25% glutaraldehyde (1% final). Aliquots from defrosted samples were filtered on polycarbonate 0.22 µm pore size, 25-mm diameter filters mounted on 0.45 µm backing filters, dried at room temperature, stained using VECTASHIELD with DAPI (4', 6-diamidino-2-phenylindole), and imaged at 100X magnification using a Nikon C1 upright microscope. Slides were imaged at 1000X magnification on a Nikon TE2000-U inverted epifluorescence microscope for P0704.

Stained slides were stored at -20°C until microscopy (<1 week for original processing, up to 1 year for additional processing as needed). Images were analyzed using Nikon Advanced Research 3.2 software. Either 20 image fields or at least 200 cells per filter, whichever was smaller, was processed to measure cell abundance, line length, and width using the signal thresholding. Bacterial counts were manually corrected by removing auto fluorescent cells identified in the TRITC channel. The line length cutoff of 0.20-2.0 µm was used to exclude non-bacterial cells. The average cell number per field was converted to abundance based on the surface area of the filter, the field of view and the volume filtered, after Samo et al. (2012). Biovolumes were calculated from the line length and width based on

the equation $V = (\pi/4) \times W^2 \times (L - W/3)$ (Bratbak 1985). The cell-specific carbon was calculated as described by Simon and Azam (1989) using the equation $Cell\ specific\ carbon\ = 0.86 \times 88.6 \times V^{0.59}$. The bacterial carbon content (BCC) is the mean of the cell-specific carbon values from a single sample.

3.2.6 Bacterial Production (BP)

Seawater samples were also taken from 6 depths from each mid-day CTD cast, typically at 11 a.m., to estimate rates of bacterial protein synthesis (Kirchman et al. 1982, Kirchman et al. 1985, Simon & Azam 1989, Smith & Azam 1992). These measurements were made by different investigators over the course of the CCE-LTER program, which resulted in some discrepancies in the method between cruises.

For each sample, 1.7 mL seawater, or 1.8 mL seawater during P1408, were incubated with approximately 20 nM 3H-Leucine for one hour. Incubation temperatures varied depending on the cruise: 10°C (samples collected from 75 to 200 m) and 12°C (samples collected from surface to 70 m) during P0704; *in situ* temperature during P0810; 12°C during P1408; room temperature during P1604; and 9°C during P1706. Incubation temperature in the offshore and transition regions had no significant impact on BP values (linear regression, p = 0.15 and 0.45, respectively), but was statistically significant in the nearshore ($p<0.05$); however, the nearshore was the most data limited and the resulting slope (m=0.052) suggests there was minimal impact of incubation temperature on BP. Samples from P0704 and P0810 were done in triplicate with duplicate TCA-killed controls. Samples from P1408 were done in quadruplicate with duplicate TCA-killed controls. Samples from P1604, and P1706 were done in triplicate with single TCA-killed controls. The standard errors of all methods were

comparable. After the incubation was complete, all samples were killed with an addition of 100% TCA for a final concentration of 5% TCA. The P0704 and P0810 samples were filtered on 0.2 µm pore size polycarbonate filters and three additions of 1 mL 5% TCA were made. The filters were dried in individual scintillation vials at room temperature before scintillation cocktail was added and analyzed. The P1408, P1604, and P1706 samples were processed using the centrifugation method as described in Smith et al. (1992). Samples were frozen and stored at -20°C as needed. All samples were analyzed for disintegrations per minute on a Beckan LS8000A liquid scintillation counter. Disintegrations per minute were converted to protein synthesis rates assuming 3.1 kg C mol^{-1} leucine and 24 h day^{-1} (Simon & Azam 1989).

3.2.7 Statistical comparison

Using the "MASS" package within R, a generalized linear model (GLM) for Poisson distributions was used to assess the effect of different sampling methods (FCM, FCM*, and EFM) on BA. FCM and EFM were available for each of P0704, P1408, P1604, and P1706 but were collected at different times of day and should not be considered as replicates. Because of differences in sampling depth, the comparison of the datasets was restricted to depths between the surface and 96 m in P0704, 134 m in P1408, 101 m in P1604, and 76 m in P1706 to minimize the influences of deeper samples. Samples were compared using a Tukey HSD for multiple comparisons of means test with a 95% confidence interval. A direct comparison of FCM* to EFM was done for P1604 and P1706 (both collected from the same casts) using linear regression and Kruskal–Wallis one-way analysis of variance with 95% confidence interval. FCM and FCM* for P1604 and P1706 were also conducted using a Kruskal–Wallis one-way analysis of variance with 95% confidence interval.

Depth profiles were generated using non-parametric least squares regression for Chl, BA, NPP, BP, and nitrate concentration in R using the the “geom_smooth” function within the “ggplot2” package. Correlations were also generated using the “geom_smooth” function within the “ggplot2” package. Displayed equations and R^2 values were determined using the “stat_poly_eq” function within the “ggpmisc” package, while the “stat_cor” function within the “ggpubr” package was used to determine the p-values.

3.2.8 Bottom-up and temperature control indices and bacterial-phytoplankton coupling

The relevance of bottom-up controls was assessed as described in Billen et al. (1990) using ordinary least square (OLS) linear regression between log-transformed BP and BB, and using the Ducklow (1992) categories of weak (slope: 0.2-0.4), moderate (0.4-0.6), and strong (>0.6) bottom-up control strength. Similarly, the degree of bacterial-phytoplankton coupling was evaluated using OLS linear regressions between log-transformed BP and Chl concentration and between log-transformed 10 m binned BP and NPP. Different depths were sampled for BP and NPP because samples were taken from different casts on the same day, and so, binning allowed us to compare them more accurately. Finally, the degree of temperature sensitivity was assessed using an OLS linear regression between log-transformed BP and temperature.

3.2.9 Microzooplankton grazing rates on phytoplankton

Grazing rates were assessed from rates of phytoplankton community growth in dilution experiments as described in Landry et al. (2009). Grazing rates were interpolated within a cruise-cycle to match the cruise-Cycle depths sampled for BP.

3.3. RESULTS

3.3.1 Method comparison of EFM, FCM, FCM* for heterotrophic BA

The CCE-LTER divides major sampling between the 2 a.m. and 11 a.m. CTD casts. In order to compare daily parameters measured on these different casts, we took advantage of the fact that samples were taken for FCM cell counts during both casts, albeit using different preservation methods. Although it was a limited comparison, overall, no significant difference between the FCM, taken from the 2 a.m. CTD cast and fixed with paraformaldehyde, and FCM*, taken from the 11 a.m. CTD cast and fixed with glutaraldehyde was observed (Appendix Table S3.1). Significant differences in FCM compared to FCM* were only observed for two cycles of the nearshore (Appendix Table S3.2), but even in this case, further analysis suggested that the discrepancy was not due to systematic differences between methods but a result of natural variability within the water parcel. The similarity between FCM and FCM* samples was unexpected because the samples were taken approximately nine hours apart and fixed using different methods that had previously been reported to yield different counts (Troussellier et al. 1995).

For CCE-LTER cruises P1604 and P1706, all three methods, EFM, FCM, and FCM*, were used to determine BA. This provided us with an opportunity to assess the similarity between these methods for our region of interest (Appendix Table S3.1). A direct comparison of FCM* to EFM estimated BA was possible for each Cycle for P1604 and P1706 (Figure 3.1). There were significant differences between FCM* and EFM across the sCCS and in all regions for both P1604 and P1706. Slopes of the relationship between FCM* and EFM were similar but not identical for three of the four cycles in P1604. Slopes from P1706 were closer

to 1, indicating that the methods were in closer agreement. In fact, a slope of 0.9 was observed for one nearshore cycle in P1706 (Figure 3.1). Using all data for P1604 and P1706, the relationship was EFM = 0.5 x FCM*, $R^2 = 0.76$. From a direct comparison of FCM* to EFM, EFM underestimated BA in nearly every case (Monger & Landry 1993), despite prior reports of close agreement in the sCCS (EFM = 0.850 x FCM in a frontal zone; Samo et al. 2012). Other studies have also reported variable relationships of FCM to EFM (e.g., from 1.47 to 0.75 in the Arabian Sea; Ducklow et al. 2001). In this study, the relationship between FCM* and EFM was not related to bacterial size (Figure 3.2).

The average bacterial carbon content per cell (BCC) for P1604 and P1706 as estimated by EFM was 12.6 ± 0.3 fg C $cell^{-1}$ and ranged from 6.44 to 21.61 fg C $cell^{-1}$ across the sCCS (Figure 3.2). Overall, this average value is comparable to the 11 fg C $cell^{-1}$ assumed when converting FCM BA to BB (Garrison et al. 2000), so we continued to use an assumed 11 fg C $cell^{-1}$ for calculated BB from FCM and FCM*. However, we did observe interannual and regional differences in this value as determined by EFM. For example, the highest individual BCC was calculated for P1706 nearshore and transition cycles (up to 21.61 fg C $cell^{-1}$) and for P1604 offshore (15.74 fg C $cell^{-1}$). The nearshore region had the highest variability, but its mean value adhered most closely to the assumed 11 fg C $cell^{-1}$. No clear trend of BCC with depth was apparent for any cycle but this was likely biased by the relatively shallow depths sampled and the decreasing coverage with depth.

3.3.2 Depth Profiles of Heterotrophic BA and BP in the sCCS

Depth profiles of BA and BP peaked in the EZ and decreased below that, generally reflecting trends in Chl and NPP (Figure 3.3a-d). Nitrate concentration increased below the

EZ and exhibited a deepening nitracline going from nearshore to offshore consistent with a deepening mixed layer and increasing stratification (Figure 3.3e). BA depth profiles revealed the highest abundance in the EZ of the nearshore region, decreasing with depth and "distance offshore" (i.e., transition to the offshore regions; Figure 3.3b). The BA was between 0.17 to 5.12 x 10^9 cells L^{-1} in the nearshore, 0.01 to 2.59 x 10^9 cells L^{-1} in the transition, and 0.06 to 1.85 x 10^9 cells L^{-1} in the offshore. In general, day to day variations in BA within a cycle were modest (Appendix Figure S3.1). The highest BA encountered on any cruise and cycle was found during 2016 in nearshore P1604-C4 at 5.6 ± 1.7 m. In the transition, the highest BA was observed during 2014 (P1408-C1) and reached its peak at 25 m, while offshore, BA peaked during 2006 (P0605-C2) at 71 m.

Unexpected subsurface maxima in BA were observed in the offshore region that aligned with deep maxima in Chl concentration (Figure 3.3a, b, panels I), but it is also possible that these subsurface anomalies were associated with lateral advection of subducted inshore water masses that maintained high BA (Figure 3.3b, and when available, BP in Figure 3.3d) and also high NPP (Figure 3.3c). These features were particularly prominent for the offshore sites sampled by P0605-C5 and P1604-C2 (at 71 m and 80 m, respectively). During 2008, a strongly stratified BA profile was present even in the offshore and likely reflected the sampling design for that cruise, which attempted to constrain the biogeochemistry of an offshore propagating frontal feature.

Bacterial production ranged from 0.0 to 25.74 µg C L^{-1} d^{-1} in the nearshore, 0.0 to 9.78 µg C L^{-1} d^{-1} in the transition, and 0.0 to 1.99 µg C L^{-1} d^{-1} in the offshore (Figure 3.3d). In all regions, BP was elevated in the EZ and decreased below it, reflecting the depth distribution of Chl concentration more closely than NPP (Appendix Figure S3.2). Limited sampling during

2008 in the nearshore and transition resulted in ill-fitting trend lines (Figure 3.3d). As with BA, BP was relatively stable across the days of an individual cycle (Appendix Figure S3.3).

3.3.3 Relationships between Bacterial Abundance (BA) and Bacterial Production (BP)

There was a significant ($p<0.05$) positive relationship between FCM* based BA, sampled during P1604 and P1076, and BP across all regions (Appendix Figure S3.4). The slope increased from 0.19 in the nearshore and transition to 0.39 in the offshore region indicating that on per cell basis, BP was much higher in the nearshore and transition compared to the offshore. The similar relationship of BA to BP in the nearshore and transition may identify some connectivity between those two regions. Overall, the variability in BP tracked BA most closely in the nearshore. The offshore region also had a high percentage of variance explained, but unlike other regions, BP data were limited to a single cruise (P1604) for that analysis.

3.3.4 Controls on heterotrophic bacteria

At steady state, the supply rate of organic carbon to bacteria should approximate bacterial carbon production. The bottom-up control index modeled by Billen et al. (1990), which examines the extent to which heterotrophic bacteria are limited by substrate availability, is estimated from the slope of log-transformed BP (the supply rate of the substrate) *vs* log-transformed BB (bacterial biomass). BB was calculated from EFM BA with an assumed BCC of 11 fgC cell^{-1} for cruises that lacked EFM derived BCC. An assumption of 11 fgC cell^{-1} for the BCC noticeably decreases the slope in the transition region, but not in the nearshore region (Appendix Figure S3.5).

Bottom-up control index was lowest in the offshore and highest in the transition (Figure 3.4a). The overall value when considering the entire dataset was 0.28 in the sCCS (Appendix Figure S3.6c), signifying weak control as described in Ducklow (1992). However, the average, when generating the index individually, from cruise-cycle data (0.51 ± 0.10) indicated moderate control. Since the overall index was calculated using an assumed BCC, it is more similar to log BP *vs* log BA. Billen et al. (1990) showed that log BP *vs* log BA does not result in as reliable a relationship as log BP *vs* log BB. As such, the average of the cruise-cycle slopes may be a better predictor because EFM based BB, as opposed to an assumed BCC, features more prominently in the cruise-cycle data and captures possible differences in BCC across the CCE region. Furthermore, because the bottom-up control index is based on the slope of a log-log relationship, multiplying by constant (assumed or average BCC) would result in the same slope but a different y-intercept. However, if the BCC is not a constant, such as when it is determined per individual sample, the slope would change. Overall, the bottom-up control reflected the dependency off BB on BP, i.e., the dependence of BB on organic carbon supplied to heterotrophic bacteria.

There was a considerable range in bottom-up control among individual cruises (Figure 3.4a, Appendix Figure S3.7). The nearshore region often had values that indicated moderate bottom-up control, except P1706-C2, which had weak control. This weak control was driven by high BP but low BB and may have resulted from a difference in bacterial growth efficiency (BGE) during this time. The transition was often characterized by moderate or strong bottom-up control, with 2014 indicating the strongest controls. Bottom-up controls in the transition from 2007 was an exception to this pattern, when unusually low BP led to a low

bottom-up control index. The offshore region was highly variable with some weak and some moderate bottom-up controls.

The temperature control index (Temperature vs log-transformed BP; Kim & Ducklow 2016) across the sCCS was 0.12 (Figure 3.4d), with a higher average when examined as cruise-cycle slopes (0.47 ± 0.06). The range by cruise-cycle was large, between 0.01-1.01, with highest values in the nearshore and lowest values offshore (Figure 3.4b, Appendix Figure S3.8). Using the same ranges for no, weak, moderate, and strong controls as were previously used for the bottom-up control index, results of temperature control from individual cruises showed that the nearshore region often had values that indicated moderate or strong temperature control. The transition region was highly variable with some strong, some moderate, one weak (P1706-C4) cycles, and those from 2014 exhibited no temperature control. The offshore region was also variable with mostly weak control, except for one moderate (P0810-C2), one strong (P0704-C2) cruise-cycle. Cycles from 2014 exhibited no temperature control.

For both bottom-up control and temperature control indices, most of the non-significant relationships were observed during 2014 when the sCCS was influenced by the North Pacific warm anomaly, where offshore and transition region waters in particular were more stratified, with little connection to the nearshore region. Overall, the low temperature control observed in 2014 is consistent with resource limitation controlling BP during this cruise (Figure 3.4c). Examination of microzooplankton grazing rates in 2014 suggested those were typical of other cruises in the same region and exhibited no strong relationship with BP (Figure 3.4d).

The relationship between bottom-up control and temperature control indices (Figure 3.4c), excluding P1408-C4, which had a negative index for bottom-up control, was fitted to the exponential line $Temperautre\ control\ index = 0.95e^{-1.69 \times Bottom-up\ Control\ index}$ (R^2 = 0.54, n = 16) and was primarily driven by the transition region that had its own trend of $Temperautre\ control\ index = 1.05e^{-1.76 \times Bottom-up\ Control\ index}$ (R^2 = 0.91, n = 8).

Top down control, or mortality, was examined for cruises where we had access to microzooplankton grazing rates calculated from phytoplankton dilution experiments (Landry et al. 2009). We found no linear relationship between microzooplankton grazing rates and BA in the offshore or transition, and only a weak negative relationship was observed in the nearshore (Appendix Figure S3.9a). However, significant, weakly positive linear relationships were found in all regions between microzooplankton grazing rates and BP, where grazing rates were interpolated to match the depths sampled for BP. The relationship in the nearshore region was strongest (Appendix Figure S3.9c). Previous work by Taylor and Landry (2018) reasoned that increased heterotrophic bacterial activity in the nearshore, due to the release of labile organic matter, would stimulate microzooplankton grazing. Therefore, a positive correlation may signify such a process, where both bottom-up and top-down controls are active (del Giorgio et al. 1996, Goericke 2011, Taylor & Landry 2018).

If we compare the bottom-up control index with microzooplankton grazing rates integrated over the euphotic zone for the limited number of cruises where we have BP, a negative relationship is apparent, and is primarily driven by the transition region (Figure 3.4d). The integrated microzooplankton grazing rate was higher offshore, where weak bottom-up controls dominated, than nearshore, which had more moderate bottom-up controls.

3.3.5 Relationships between BP and phytoplankton processes

Mean bottom-up control indices showed regional differences, however the cruise to cruise variability within each region was large. To further examine substrate limitation on BP, we assessed the relationships between BP and phytoplankton processes in two other ways, following an approach used by the Palmer LTER (PAL-LTER) site (Kim & Ducklow 2016). First, the relationship between Chl concentration or NPP and BP for all available data. Second, the same analysis was conducted using log transformed data.

First, the slope of the relationship between untransformed BP and Chl concentration or NPP data, though significant ($p<0.05$) in all regions, varied noticeably between years (Appendix Figure S3.2). The variability was most obvious in the nearshore. The relationships between BP and Chl concentration was closer to unity than the relationships between BP and NPP, suggesting a more direct link between BP and Chl concentration (Appendix Figure S3.2). This was further supported with higher explanatory powers in the nearshore and transition for BP *vs* Chl concentration compared to BP *vs* NPP, although neither parameter exceeded an R^2 value of 0.23.

Second, slope values derived from log-log regressions were examined (Appendix Figures S3.10 and S3.11). For the sCCS overall (Appendix Figure S3.6a, b), the log-log slope for Chl concentration vs BP ($m = 0.78$, $R^2 = 0.62$, $p<0.001$) was significant and similar to that calculated by Gasol and Duarte (2000) ($m = 0.71$), but the sCCS log-log slope of NPP vs BP ($m = 0.20$, $R^2 = 0.25$, $p<0.001$) was much lower than previously calculated by Gasol and Duarte (2000) ($m = 0.20$ vs $m = 0.67$). By cruise-cycle, slope values were not significant indicating weak coupling between heterotrophic BP and phytoplankton parameters in any region (Appendix Figure S3.12). Two outliers in the dataset in this respect were 2016 and

2017, which had significant coupling of Chl concentration with BP. 2017 also had significant coupling of NPP with BP, however, the NPP was estimated using a modelling approach and as such, was a 'predicted' value. In 2016 and 2017, particularly in nearshore stations, the tight coupling may have identified a greater amount of labile, autotrophic organic matter present.

3.3.6 Relationships between BP and Organic Carbon

As reported above, the relationships between BP and phytoplankton processes did not have high explanatory power, suggesting that they may not be the best indicators of strong bottom-up control. Instead, we hypothesized that the organic carbon pools, as the intermediaries between phytoplankton and heterotrophic bacteria, would have higher explanatory power. Indeed, organic carbon concentrations are good predictors of bacterial dynamics (Eiler et al. 2003). Furthermore, organic matter reservoirs have a long enough residence time in the upper ocean that they may be able to buffer any time lag between substrate production (NPP) and substrate consumption (BP).

TOC, suspended POC, and DOC concentrations exhibited significant ($p<0.05$) positive correlations with BP (Figure 3.5). The correlations with TOC concentrations had the highest explanatory power in the nearshore and offshore regions, but DOC concentrations had the highest explanatory power in the transition. In the offshore, TOC is primarily DOC (compare Figures 3.5b and 3.5c; see Stephens et al. 2018), and so, the correlation with TOC concentrations (Figure 3.5a) is essentially a correlation with DOC concentrations. Therefore, the weaker correlation with measured DOC concentrations in the offshore (Figure 3.5c) is most likely driven by the limited number of DOC samples available for that region. During P1604, the strong correlation of BP with TOC concentrations in the nearshore is reflected in

both the POC and DOC data. Here, the elevated POC concentrations indicate the production of fresh organic matter. Therefore, we propose that DOC in this region is also fresh, despite being lower in concentration than DOC in the offshore, where accumulation of less labile DOC may limit bacterial activity (Cho & Azam 1988, Cherrier et al. 1996).

For 2017, DOC and POC concentration data were available, and in the nearshore, it appeared that a greater fraction of the carbon was partitioned into DOC than POC (at least as determined from measuring the standing stocks of each) compared to observations during 2016. Despite the higher DOC concentrations encountered in the nearshore region during 2017, BP did not reach the high values observed during P1604. During 2017 the lower BP in the nearshore may signify repression of bacterial activity, perhaps due to top down controls such as grazers preferentially consuming active cells (Gasol et al. 1995), leading to greater accumulation of DOC during this cruise. Overall, comparing across all these data, the much higher BP values in the nearshore during 2016 appear to be a result of the uniquely elevated POC concentrations encountered in this region during that cruise.

The DOC data in the nearshore, and to a lesser extent the transition, also identify a 'threshold' DOC concentration that needs to be exceeded prior to observing a rapid increase in BP. This threshold appears to lie between 50-55 μM C (Appendix Figure S3.13) in the nearshore and is consistent with DOC concentrations in waters upwelling into this region (Stephens et al. 2018). The limited data in the offshore may indicate that the threshold concentration is slightly higher in oligotrophic environments. Overall, the threshold DOC concentration demonstrates that either most substrates in the "background" pool are present at too low a concentration for the affinities of relevant transporters and/or enzymes or that the

compounds that stimulate enzymatic activity (and thus BP) are not present in the background, upwelling pool.

The slope of BP *vs* POC concentration had the smallest range of organic carbon parameters, potentially indicating that POC concentration could be used as a consistent predictor of BP across the sCCS (Figure 3.5b). Examining the cruise-specific slope of this relationship by region, we found that the BP *vs* POC concentration relationship across regions was very similar at low BP (<4 μg C L^{-1} day^{-1}) and POC concentrations <10 μM C (Figure 3.6). However, the slopes began to deviate significantly at higher BP and POC (Figure, 3.6, Appendix Figure S3.13b). Despite the similarity across regions during each cruise, BP *vs* POC concentration relationships varied interannually. Thus, sCCS climatology may play a bigger role in controlling the mechanisms underlying the BP *vs* POC relationships in all regions. This contrasted with some of our other observations that showed greater inter-regional differences than interannual intra-regional differences.

3.3.7 Temperature in the sCCS

Finally, we proposed that the temperature control index was not reflecting the response of metabolic rates to water temperature, but was instead a proxy for nutrient concentrations (i.e., time since upwelling) (Lopez-Urrutia & Moran 2007, Kelly et al. 2018). Overall, log-transformed BP had a strong positive correlation with temperature (Appendix Figure S3.7d), or a strong negative correlation with inverse temperature (Appendix Figure S3.14), indicating that BP was more elevated in shallower (warmer), near surface waters. However, this relationship peaked at approximately 14°C nearshore, 15°C in the transition, and 17°C offshore, after which increasing temperature led to a decrease in BP (Figure 3.7a).

The relationship of temperature to log-transformed BP is separated into warm and normal years in the nearshore and offshore regions. In the offshore region, the peak in BP during normal years occurs at higher temperatures (17.4 vs 15.0 °C), which could reflect higher nitrate concentrations in upwelling waters during normal years. In this scenario, the higher upwelling nitrate concentrations enable sustained BP and NPP at the surface for a longer period of time (assuming temperature is a proxy for upwelled water-mass age).

Often, highest BP was associated with EZ waters that still contained some residual nitrate (Figure 3.7b) suggesting that at higher temperatures, where nitrate concentrations were low, heterotrophic bacteria were likely resource limited (bottom-controls began to dominate) (Figure 3.4c). A similar result was found for NPP (Figure 3.7c). These data confirmed that temperature gradients in the sCCS, in the nearshore and transition, accurately reflect the age of the water mass from the time of upwelling and thus its fresh organic matter load. A few cycles in the offshore region may have also experienced other limitation of BP including top down controls (Figure 3.4d).

3.4. DISCUSSION

3.4.1 Lessons learned from cross-dataset analyses

The CCE-LTER provides us with the opportunity to examine controls on bacterial dynamics across a range of environmental conditions. We quantified BA and compared three methods to determine whether FCM counts available for every cruise were comparable to the limited EFM and FCM* counts (Appendix Table S3.1). Our results provide a reliable basis to rely on FCM data in order to continue future assessment of long term bacterial dynamics without losing the time invested in EFM. The daily sampling time for FCM based BA

appeared to be flexible for the transition and offshore regions, but in the nearshore, where hydrography and biology can be more dynamic, we recommend that BA and BP be sampled simultaneously. Furthermore, our results suggest that it is crucial to continue limited EFM because, although our limited data don't show that the average cell size deviates strongly from 11 fg C $cell^{-1}$, previous work in the sCCS by Pedler et al. (2014) reported mean values between 2.60 to 16.2 fg C $cell^{-1}$, while Samo et al. (2012) had BCC values from individual samples across a front that ranged from 13.85 to 31.07 fg C $cell^{-1}$. BP was sampled for a subset of the cruises using a similar method; although incubation temperatures and some sample processing parameters varied from cruise to cruise, there was no indication that a cruise-specific bias strongly influenced our results.

In this overall context, we examined relationships between BP and a variety of datasets including BA, NPP, Chl concentration, and organic matter concentrations. While these latter datasets represented standing stocks and not fluxes, they should more closely approximate the substrates available to support bacterial activity. We also tested the importance of bottom-up controls, based on the relationship between BB and BP, as well as the potential importance of enhanced metabolic rates (i.e. the temperature control) and microzooplankton grazing rates.

Unlike many previous studies that have compared heterotrophic bacterial parameters from different oceanographic biomes collected at different times, each CCE-LTER study examines several biogeographic provinces that are connected through hydrography and climatology. Furthermore, the different oceanographic conditions that were encountered in each subregion and across the study area, during the various CCE-LTER cruises included in this analysis, enabled us to examine responses to interannual variability. The limited number

of normal and warm years examined precluded the identification of robust climate related changes. Yet the overall dataset provided evidence of possible future changes and enabled us to establish baseline relationships that can serve as a foundation for future work in the region.

3.4.2 Bottom-up and top down controls of Heterotrophic Bacteria

Bottom-up control has been assessed from the slope of the log-log relationships between BB and BP. In this case, BB was calculated from microscopy (EFM) based BA and BCC, and when carbon content was not determined, a per cell carbon content of 11 fgC cell^{-1} was assumed. The supply of substrate, which is expected to control bacterial biomass, was represented by BP, where it is assumed that the steady-state bacterial utilization of DOC (as represented by BP) is coupled to its supply rate (Billen et al. 1990). Overall, using slopes from each cycle, the average for the entire sCCS was 0.51 ± 0.10, indicating moderate control, and was similar to the global average (0.47) calculated for the subtropics and tropics (Moran et al. 2017). When examined by region, the average, regional bottom-up control indices in the sCCS indicated weak bottom-up control in the offshore similar to that found in the open ocean; moderate control in the nearshore similar to measurements from a North Atlantic bloom and an upwelling region in the Indian Ocean, and strong control in the transition region similar to Billen's global relation (Figure 3.4a) (Billen et al. 1990, Ducklow 1992). As such, the current study, where these distinct biomes were sampled during the same month within the same oceanographic region, followed the trends reported for companion biomes around the globe.

The substrate supply to maintain BP should be enhanced in the nearshore, given that NPP is highest in this region. However, as reported previously, the relationship between BP

and NPP is not straightforward. Both NPP and BP are determined independently from bottle incubations, and so, small discrepancies between these experiments and natural rates could arise and obscure the expected relationship between BP and NPP. Furthermore, when sampling newly upwelled water masses in the nearshore, there may be a lag expected between BP and NPP (McManus & Peterson 1988). Top-down controls, such as increased grazing pressure, could also play a role in decoupling BP from NPP (Figure 3.4d) (del Giorgio et al. 1996). Bottom-up control of BP is expected to be related to organic substrate availability, but (micro and macro) nutrient supply (Kirchman et al. 2000, King & Barbeau 2007, Hogle et al. 2018) may exert a stronger control in certain regions. For example, iron limitation has been demonstrated in the transition region of the sCCS (King & Barbeau 2007). In this dataset, the bottom-up control index did not scale with NPP as might be expected.

Top down control, or mortality, was examined for cruises where we had access to microzooplankton grazing rates calculated from phytoplankton dilution experiments (Landry et al. 2009). It is unclear whether these dilution experiments are an adequate predictor of grazing pressure on heterotrophic bacteria (Agis et al. 2007, Garzio et al. 2013, Pasulka et al. 2015). If we were to take these results at face value, it would appear that top down pressure from microzooplankton grazing had a smaller impact on BA in the transition or offshore but may have played a more dominant role in the nearshore where increased grazing correlated with a decrease in BA. Utilizing the BB calculated from EFM derived BCC and BA, we found significant, albeit weak, positive linear relationships between BB and interpolated microzooplankton grazing rates in the nearshore and transition regions, but a nonsignificant, weak positive linear relationship in the offshore (AppendiFigure S3.9b). Grazing is commonly size specific (Gonzalez et al. 1990, Monger & Landry 1991, Epstein & Shiaris 1992, Jurgens

& Gude 1994, Hahn & Hofle 1999, Pernthaler 2005) and can preferentially skew the population toward increased bacterial cell size (Weinbauer et al. 2019) and thus, BB, and we may be observing such a trend here. However, significant relationships between grazing and BP across all three regions may signify the presence of the enhanced microbial loop, where both bottom-up and top-down controls are active (del Giorgio et al. 1996, Goericke 2011, Taylor & Landry 2018).

3.4.3 Organic carbon concentrations as predictors of heterotrophic bacterial production

Evidence for bottom-up controls on bacterial dynamics have been previously examined by comparing BA and BP to indices of primary production (Bird & Kalff 1984, Cole et al. 1988, Gasol & Duarte 2000, Kim & Ducklow 2016, also see Sections 1.3.4 and 1.4.3).

Depth profiles of BA and BP generally followed the profiles of Chl concentration and NPP (Figure 3.3a-d) but these relationships, using untransformed data, did not result in high explanatory power (Appendix Figure S3.2). Further exploration of the relationships between BP and Chl concentration or NPP using log-transformed data showed mostly non-significant relationships, suggesting that there is a decoupling of primary and secondary production regionally (Appendix Figure S3.12). Though it was anticipated that BP and NPP would be related (Gasol & Duarte 2000), neither Chl concentration nor NPP appeared to be effective predictors of regional BP (i.e., the flux of carbon through heterotrophic bacteria). It is possible that extracellular carbon release by phytoplankton and/or the composition of the exudate, which we expect to be directly coupled to BP, may not be adequately represented by NPP or Chl concentration. For example, Halewood et al. (2012) measured both extracellular DOC

release and NPP and found that they were poorly correlated in the Santa Barbara Channel. They further reported that the lability of that extracellular DOC was also variable.

We did not directly determine extracellular DOC release in our study, but we did quantify different carbon reservoirs as either TOC, POC or DOC to test the hypothesis that these parameters may more closely track BP. We collected suspended POC on all cruises and either TOC and/or DOC. In fact, BP showed a stronger relationships with organic matter stocks (Figure 3.5), confirming that organic matter bioavailability is a key driver of BP (Cherrier et al. 1996). This was additionally consistent for BA, where the explanatory power was higher for DOC and POC concentrations than for Chl concentration or NPP (see Sections 1.3.4 and 1.4.3). The nearshore relationships with organic carbon parameters and both BA and BP were strongest, suggesting that bottom-up controls may be more easily detected in the nearshore region. Overall, the organic matter reservoirs may have a long enough residence time in the water column to more effectively serve as a link between NPP and BP.

The observed correlation of nearshore BP with suspended POC concentration, and to a lesser extent, DOC concentration, is consistent with findings reported for the Santa Barbara Channel (Wear et al. 2015). Stronger correlations of BP and BA with suspended POC concentration in the nearshore, may indicate that particle-colonization is an important mode of carbon acquisition for nearshore bacteria. For example, marine snow colonization and subsequent remineralization has been shown to be an important process driving BP (Paerl 1975, Ploug & Grossart 1999, Ploug et al. 1999, Grossart & Ploug 2001). Furthermore, suspended POC concentration is a reliable indicator of new organic matter production in marine environments and may be an even stronger predictor of BP than DOC concentration. In the nearshore, detectable new DOC accumulation can lag NPP because upwelling

contributes a high background of refractory DOC to the upper ocean (Halewood et al. 2012, Stephens et al. 2018), whereas in the offshore, high concentrations of accumulating DOC are not accompanied by high BP. As such, high DOC concentration is not necessarily an indicator of bioavailability and labile DOC can be present even when DOC concentrations are low. We also found that at low BP and POC concentration, the relationship between these two parameters was uniform across the three regions for each cruise (Figure 3.6). This was surprising since the regions separated prominently for other parameters including if you examined individual POC concentrations and BP. The observed relationships to BP indicated that POC concentration, which is more commonly measured, may serve as an effective predictor of BP in models that wish to parameterize BP.

We observed that DOC concentration was more strongly correlated with BP in the transition and offshore regions, where it may serve as a more direct conduit of carbon flow to heterotrophic bacteria (Figure 3.5c). When the data were separated by cruise and cycle, it was possible to recognize a threshold concentration in the nearshore in particular, but also in the transition, where DOC concentration in excess of 50-55 μM C would result in rapid increases in BP (Appendix Figure S3.13).

3.4.4 Increasing stratification in the sCCS may decrease bacterial production and abundance

Climate models predict and direct measurements show that the surface ocean is warming and stratifying. Our study sampled a warm anomaly in 2014 with strongly stratified, warm waters in the upper 100 m that may be indicative of future conditions in the sCCS (Bond et al. 2015, Gentemann et al. 2017). Results from 2014 CCE-LTER and CalCOFI

cruises showed decreased nutrient concentrations and NPP in the region at this time (Gomez-Ocampo et al. 2018, Kelly et al. 2018, Morrow et al. 2018), which could significantly impact bottom-up controls on BP by reducing photosynthetically derived organic matter.

The strongest bottom-up control was observed during the warm anomaly captured in 2014. These high values resulted from the fact that the change in BP was anomalously low relative to the change in BB during this time period (Appendix Figure S3.7). While the high significance of the relationship for two of the transition cycles confirms that BB was tied to substrate supply rate, as tracked by BP, we recognize that our methods could have overestimated BB because we used a constant carbon conversion factor when we did not estimate BCC directly with EFM. We found that BA during 2014 was not unusually high, which means that our use of a constant bacterial carbon content of 11 fgC $cell^{-1}$ may have represented an overestimate for the region at this time. For example, BGE may have been elevated during this time compared to other years, which would have shifted BCC toward higher values. However, other studies have reported that under stratified conditions, like those prevalent in 2014, more metabolic energy is partitioned to maintenance rather than biomass production (lowering BGE) (e.g., Kim et al. 2017). Additionally, we would expect lower BGEs during 2014 due to the increased environmental "hostility" imposed by the warm anomaly (Carlson et al. 2007, Gomez-Ocampo et al. 2018).

If the offshore environment is considered a good analog for the warmer conditions encountered in the CCE during 2014, then we can turn to EFM derived BCC from the offshore during 2016 and 2017, the two cruises for which we have robust data. We encountered values higher than 11 fgC $cell^{-1}$ in the offshore and transition region (Figure 3.2) during these two cruises, which would further increase our calculated BB. The unusual

conditions encountered in the system during 2014 could have also resulted in a larger number of inactive/dormant bacterial cells with low bacterial carbon content. Starvation of heterotrophic bacterial cells, perhaps driven by low NPP (Figure 3.3c), can induce dormancy and reduced cell size (Kjelleberg et al. 1987, Lennon & Jones 2011). Others have also shown that dormant heterotrophic bacterial cells are often some of the smallest cells (known as 'dwarf' cells) with low BCC (Stevenson 1978, Kjelleberg et al. 1987, Gasol et al. 1995, Lennon & Jones 2011). Moreover, Moran et al. (2015) found a shift towards smaller heterotrophic bacterial cells in warmer waters. Unfortunately, without direct determination of BCC or an estimate of the nucleic acid content of cells (Lebaron et al. 2001, Moran et al. 2007) during 2014, we are unable to determine what portion of the heterotrophic bacterial cells encountered in the region were inactive and/or unusually small during the warm anomaly.

In contrast, significant but moderate bottom-up controls were sampled in 2016, where we expected to see the impact of El Niño have similar impacts at the warm anomaly due to warmer temperatures and increased stratification (Jacox et al. 2016). However, the temperature and nutrient data (Figures 3.6 and 3.7b, Appendix Figure S3.6d) confirmed that our sampling coincided with the return of more typical upwelling conditions. This may be the reason that we did not observe the high bottom-up control indices of P1604. Furthermore, the influence of upwelling on the strength of the temperature control index is exemplified in the nearshore cycle P1604-C4, where BP exhibited a strong and significant, positive relationship with temperature (Figure 3.4b, Appendix Figure S3.8). However, examination of the entire dataset showed that this relationship breaks down when waters warm further and nitrate is drawn down, because temperature is a proxy for nutrient availability (Figure 3.7b).

In conclusion, although the relationship between upwelling and BP was sustained throughout the stratified warm anomaly in 2014, unique bottom-up and temperature forcing for 2014 compared to other years, including the warm 2016 El Niño, indicated an anomalous heterotrophic bacterial response. This response may be linked to starvation induced dormancy of heterotrophic bacteria. Previous work has suggested the growing importance of the microbial loop to nutrient cycling in areas of rising ocean temperatures and strengthened stratification (Kim et al. 2017), and so, future work in the sCCS should continue to monitor the bottom-up and temperature control indices for heterotrophic bacterial metabolism as shifts in microbial food web responses to increased stratification of shallow surface waters is anticipated (Polovina et al. 2008, Danovaro et al. 2011, Chen et al. 2012, Flombaum et al. 2013, Moran et al. 2015).

3.4.5 Temperature control related to upwelling and nutrient conditions, not metabolic rates

The inverse relationship between bottom-up and temperature control indices observed in this study (Figure 3.4c) has been previously shown for other regions (Calvo-Diaz et al. 2014, Moran et al. 2017). Although a significant component of our dataset conformed to this expectation, including data from 2014, where temperature control was highest at lowest bottom-up control indices (Figure 3.4c), the results from the offshore region, where temperature control should have been high, exhibited both low temperature control and low bottom-up control. In the offshore region, both resource limitation, which would prevent significant temperature control of bacterial activity, and top-down control as proposed by Gasol et al. (2002), may be more relevant. This aligns with the grazing rate analysis, where

higher EZ integrated microzooplankton grazing rates were detected in the offshore region (Figure 3.4d). However, the slope and fit of non-integrated microzooplankton grazing rate to BA were low (Appendix Figure S3.9). This may be because the experimental set up that is used to calculate microzooplankton grazing rate (using changes in autotrophic biomass) may not effectively capture the influence on heterotrophic bacteria (Agis et al. 2007, Garzio et al. 2013, Pasulka et al. 2015). Comparison of interpolated, non-integrated microzooplankton grazing rates with BB or BP had strong, positive relationships in the nearshore region, as would expected in an area with an enhanced microbial loop and where both bottom-up and top-down controls are present (Taylor & Landry 2018). Another possible explanation for the poor fit between grazing rates and BA comes from Billen et al. (1990) who discussed that grazing rates would be expected to be proportional to BB, not BA (or BB calculated from BA using a constant). Furthermore, viral controls are completely unconstrained in our study and may have had a strong influence on BP in the offshore region and elsewhere.

As discussed previously, to deconvolute the impact of temperature on BP, we used the temperature-nitrate relationship in the sCCS because previous studies have shown a strong dependence of nitrate (which influences NPP) on temperature (e.g., Lucas et al. 2011, Palacios et al. 2013) (Figure 3.7b,c). We found that maximum BP values decreased from the nearshore to the transition to the offshore, whereas the temperature at which BP reached its maximum value, increased from nearshore through the transition to the offshore. The latter trend is consistent with the hypothesis that maximum BP corresponds with water mass conditions that support high labile organic matter production either because of the interplay between available nutrients and light (offshore) and/or because nutrient rich waters are being upwelled to the surface (nearshore) and then transported offshore, and during this offshore

transit water temperature will rise and nutrient concentrations and NPP will decrease (Kelly et al. 2018).

3.5. CONCLUSIONS

This study expands on recent, localized findings (e.g., Halewood et al. 2012, Samo et al. 2012, Wear et al. 2015) to provide a comprehensive analysis of heterotrophic bacterial dynamics within the sCCS. We provide a baseline of heterotrophic bacterial properties alongside relevant phytoplankton and organic carbon parameters across three defined biogeographic regimes to identify controls on bacterial production. Average, regional bottom-up controls are in line with previously reported global trends assessed from combining studies. The warm anomaly from 2014 showed that although temperature control is often associated with organism metabolic rates, in the sCCS it is indicative of nutrient concentrations. Classified as a marine heatwave, the anomaly was associated with the highest bottom-up controls with depressed NPP and BP, setting the stage for what we might expect to observe in the future as stratification increases due to surface water warming. Overall, BP in the nearshore correlated most strongly with POC concentrations, whereas in the transition and offshore regions BP correlated better with DOC concentrations, reflective of the lag between POC production from enhanced phytoplankton growth in a productive upwelling region and DOC production from enzymatic breakdown of POC by heterotrophic bacteria. Future sampling of sCCS regions featuring low POC concentrations and low BP would further constrain the reported relationship for potential use in modeling studies. To this end, and as revealed by the stronger correlations of BP with organic carbon pools compared to NPP or Chl, there is a need to more carefully quantify DOC production from phytoplankton

exudation. Climate forcings within the sCCS have distinct signatures that impact heterotrophic bacterial activity, likely generating currently unknown consequences and feedbacks as a function of microbial community composition, substrate processing rate, and growth efficiency.

3.6 ACKNOWLEDGEMENTS

Chapter 3, in part, is currently being prepared for submission for publication of the material. Rivera, S. R.; Stephens, B. M.; Samo, T. J.; Rasina, B.; Stukel, M. R.; Landry, M. R.; Farooq, A.; Aluwihare, L. I.. The dissertation author was the primary investigator and author of this material.

3.7 FIGURES AND TABLES

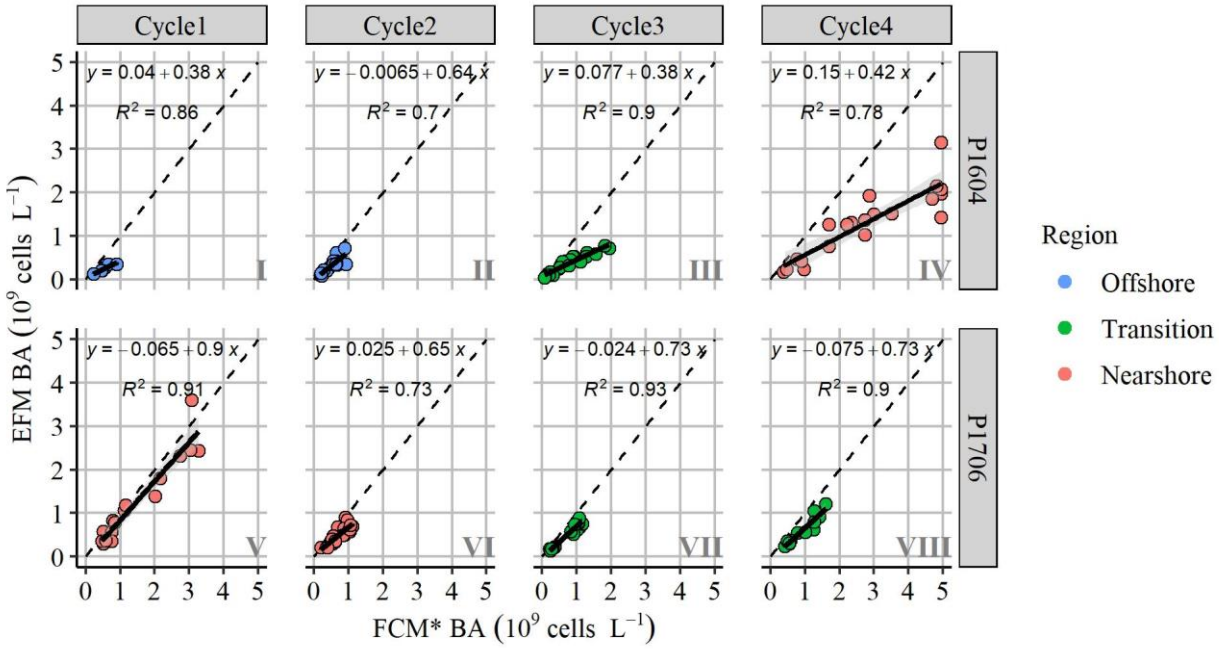

Figure 3.1: BA method comparison of epifluorescent microscopy (EFM) and flow cytometry (FCM*)

Relationships between EFM and FCM* determinations of heterotrophic BA examined using linear regression on replicate samples (solid line) in comparison to the 1:1 line (dashed line), colors by oceanic region.

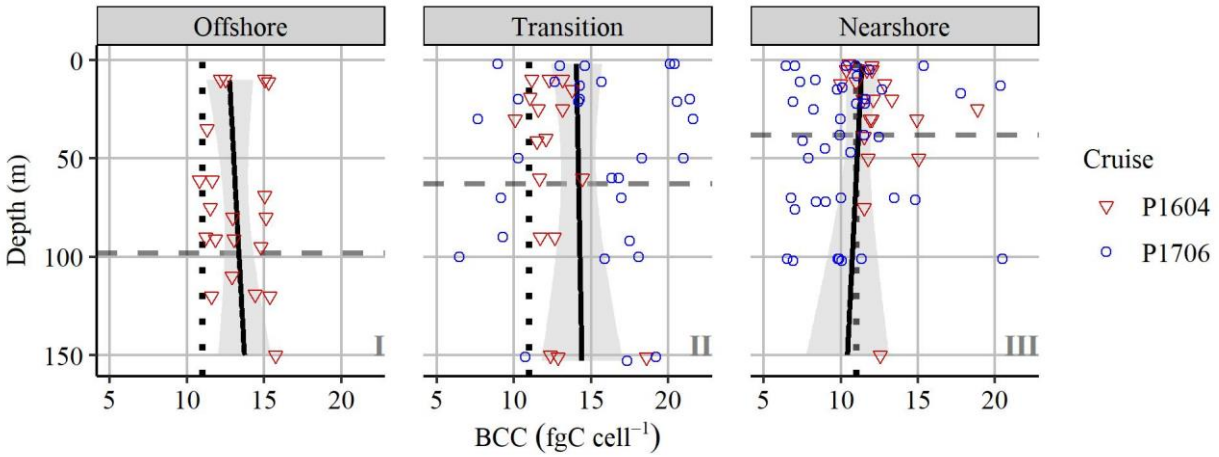

Figure 3.2: Bacterial carbon content per cell from EFM

Depth profile of mean bacterial carbon content per cell (BCC), or cell specific carbon, calculated using cell biovolumes determined from the line length and width as measured by EFM (see Methods). The mean euphotic zone by region (grey dashed line), overall trend (black solid line with grey-shaded 95% CI), and 11 fgC cell^{-1} (black dotted line) are designated.

Figure 3.3: Depth profiles of Chl concentration, BA, NPP, BP, and NO_3 concentration

Depth profiles of Chl concentration (a), BA (b), NPP (c), BP (d), and NO_3 concentration (e) with colors designating normal (blue) or warm (red) years with all data points to 150m depth displayed. Colored trend lines per year (see legend). The euphotic zone depth (black dashed line) and overall trend per region (black solid line with grey-shaded 95% CI) are also shown.

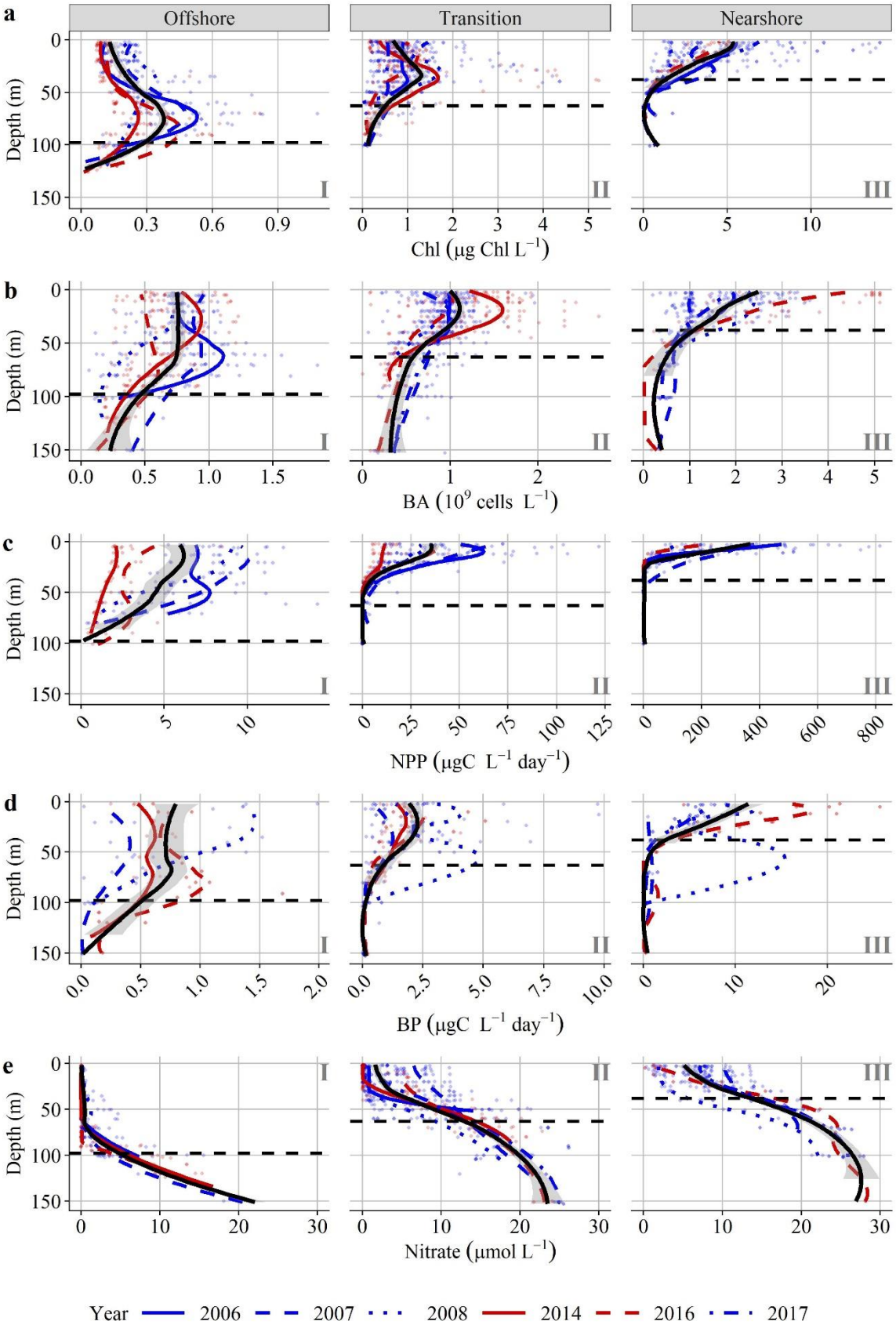
a
Offshore
Transition
Nearshore
Depth (m)
0
50
100
150
I
II
III
0.0
0.3
0.6
0.9
0
1
2
3
4
5
0
5
10
Chl (µg Chl L^{-1})
b
0.0
0.5
1.0
1.5
0
1
2
0
1
2
3
4
5
BA (10^9 cells L^{-1})
c
0
5
10
0
25
50
75
100
125
0
200
400
600
800
NPP (µgC L^{-1} day^{-1})
d
0.0
0.5
1.0
1.5
2.0
0.0
2.5
5.0
7.5
10.0
0
10
20
BP (µgC L^{-1} day^{-1})
e
0
10
20
30
Nitrate (µmol L^{-1})
Year
2006
2007
2008
2014
2016
2017

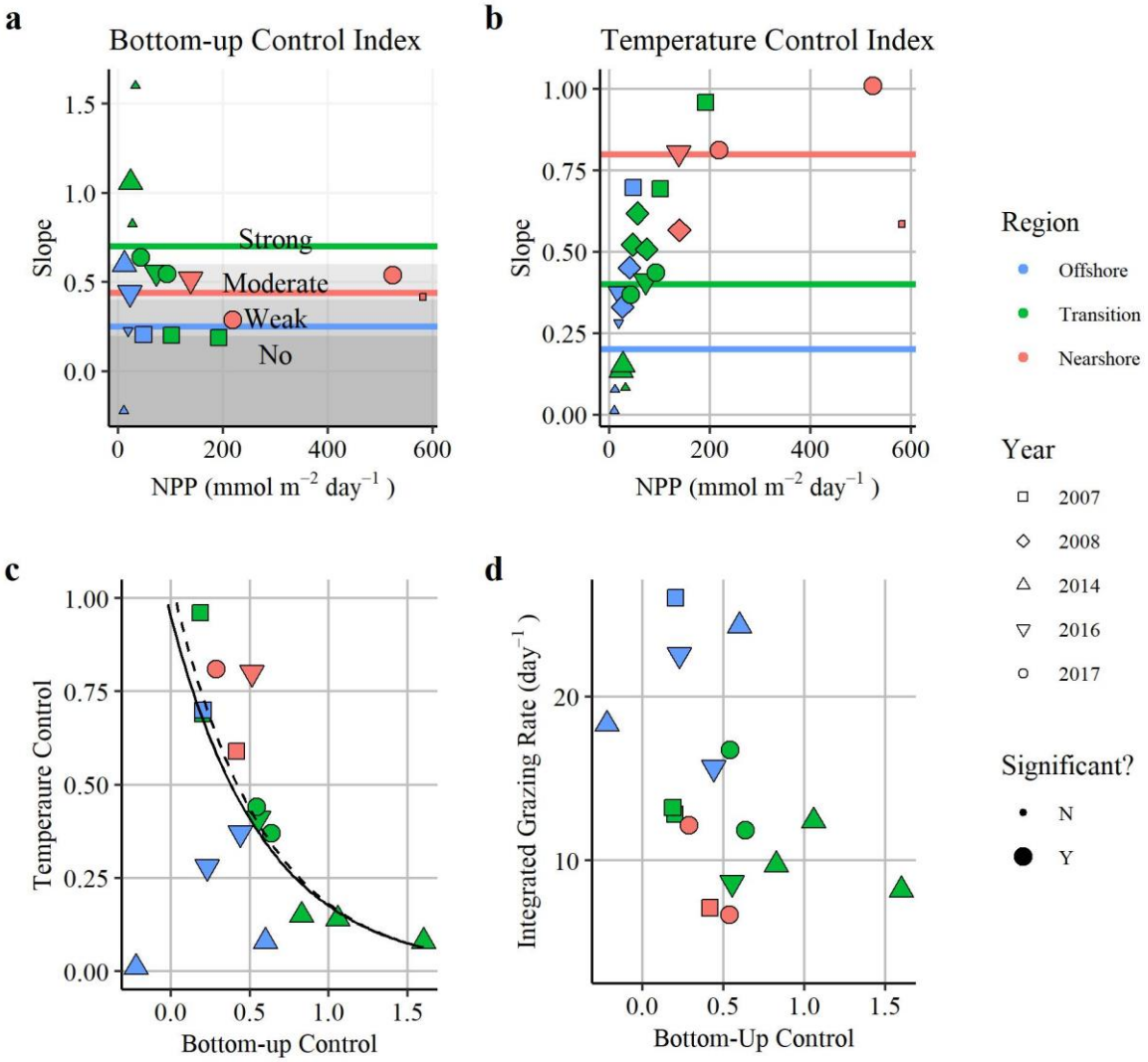

Figure 3.4: Bottom-up and top-down controls on heterotrophic bacteria

The degree of bottom-up control (a) on bacterial biomass was examined from log(BP) *vs* log(BB) regression slope values with slopes indicating no to strong control as described by Ducklow (1992). (b) Temperature control on BP examined from T *vs* logBP regression slope values. Mean per region (horizontal colored lines) are shown (a,b). Larger shapes indicate significant regressions at $p<0.05$ (a,b). (c) Relationship between the bottom-up control and temperature control indices with fitted regression for all data (solid black line) and for only transition region data (dashed black line) (d) The relationship between the EZ integrated microzooplankton grazing rate on phytoplankton and the bottom-up control index.

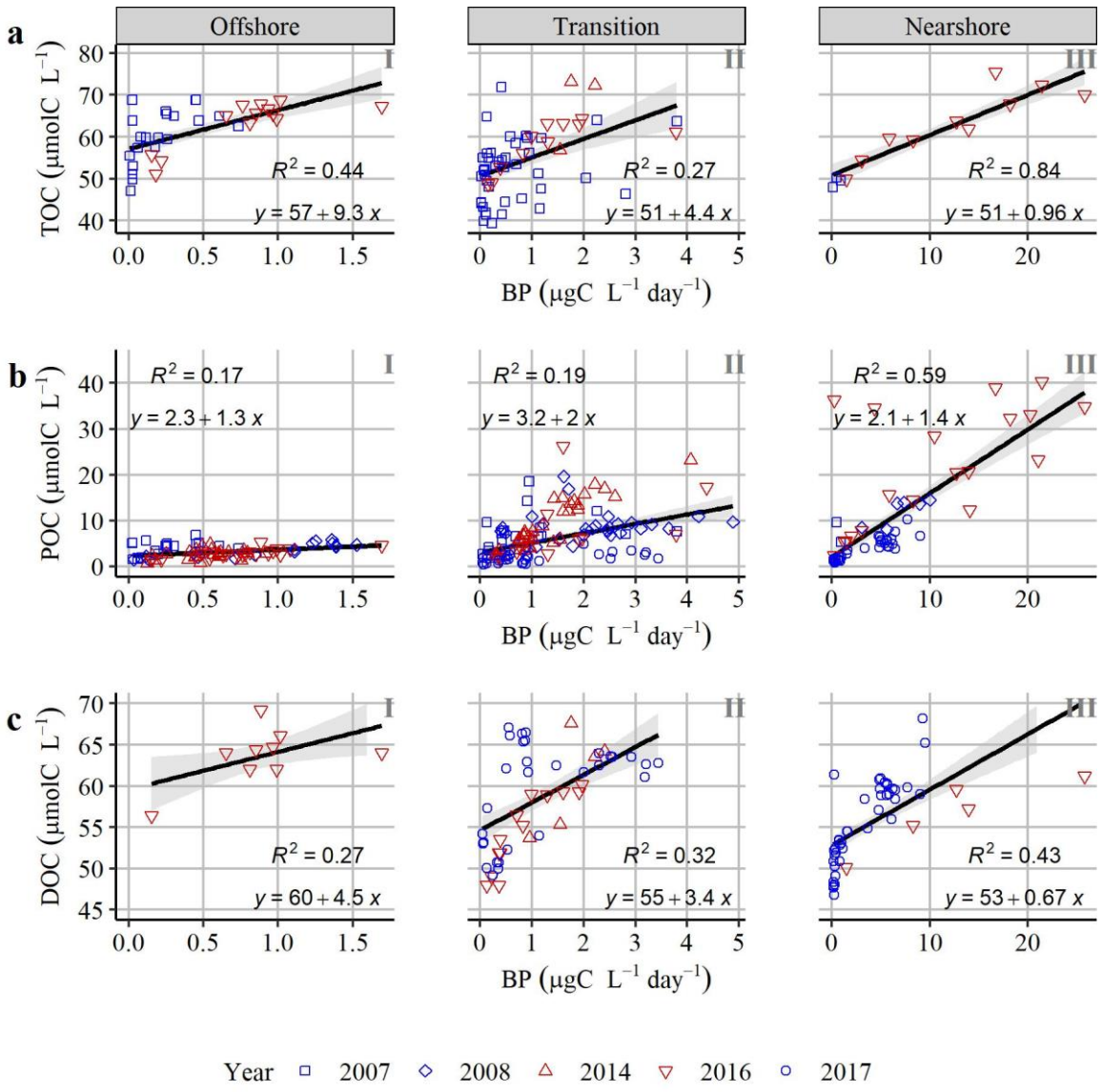

Figure 3.5: Relationships between BP and TOC, POC, and DOC

Data plotted in cruise colored by condition (blue- normal years or red- warm years). The linear relationships between BP and organic carbon pools, TOC (a), POC (b), and DOC (c). All linear relationships are significant ($p<0.05$).

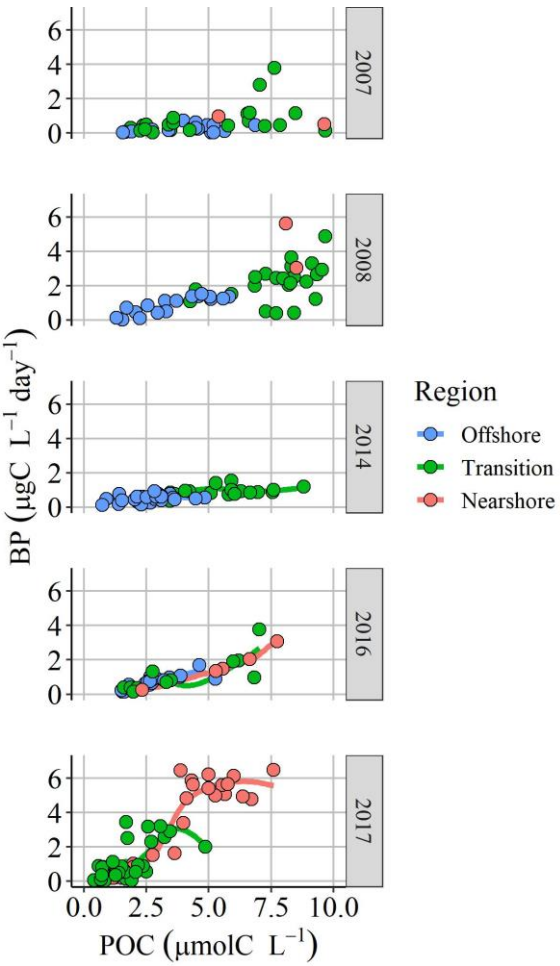

Figure 3.6 Relationship between BP and low POC concentration

A robust, consistent slope between BP and low POC concentrations was observed across all three oceanic regions, but the slope varied by year. Data plotted by year and colored by region. A best fit line for each region was also plotted.

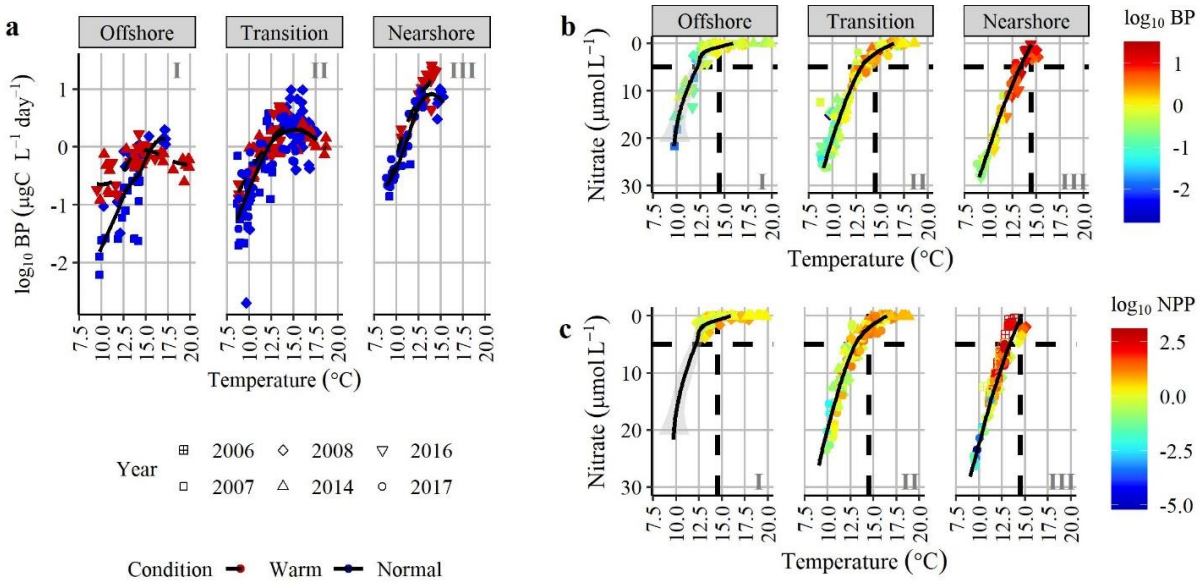

Figure 3.7 Temperature and nitrate relationship to production

Log-transformed BP had a strong positive correlation with temperature (a) until approximately 17°C offshore (I), 15°C in the transition (II), and 14°C nearshore (III) when increasing temperature led to a decrease in BP. (b) Relationship between nitrate and temperature with dashed lines at 14.5°C and 5 µM nitrate. Points colored by logBP (b) and logNPP (c) increased with increasing temperature and decreasing nitrate.

3.8 APPENDIX

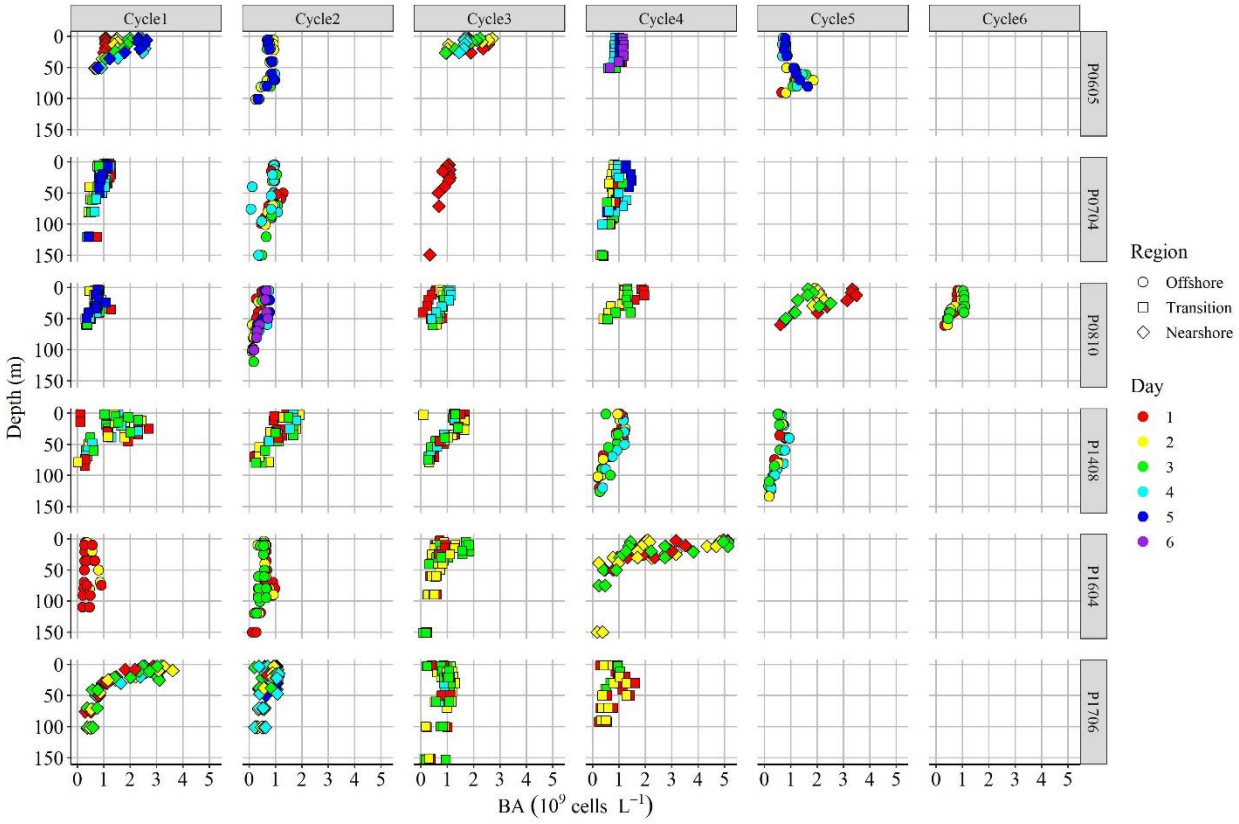

Figure S3.1 Daily variation of bacterial abundance (BA) within a cycle

Data plotted by cruise and cycle with color signifying cycle day.

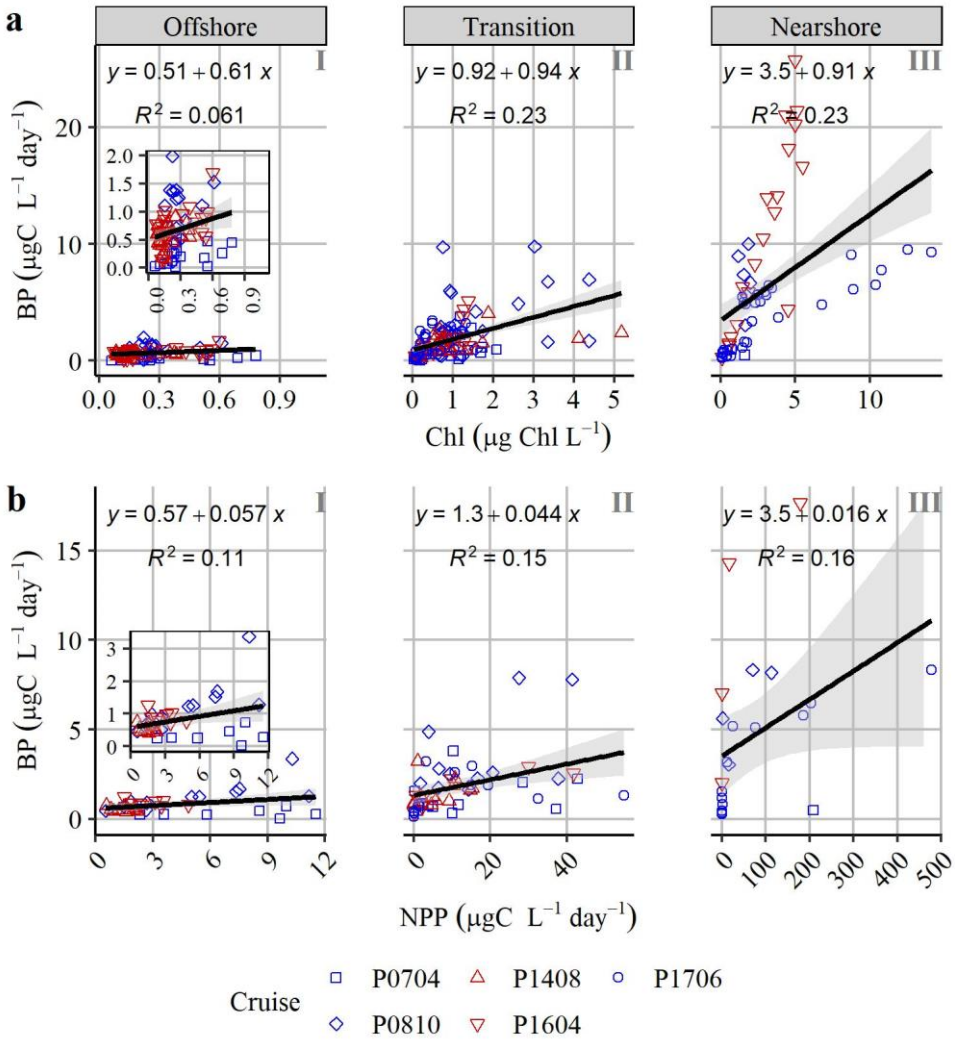

Figure S3.2: Relationships between bacterial production and phytoplankton properties for the sCCS

Data plotted in cruise colored by condition (blue- normal years or red- warm years). Linear relationships of phytoplankton properties, Chl (a) and NPP (b), to bacterial production (BP) for each region of the sCCS. All are significant ($p<0.05$) except the relationships between BP and NPP in the offshore (b,IV, $p=0.05$) and nearshore (b,VI, $p=0.06$).

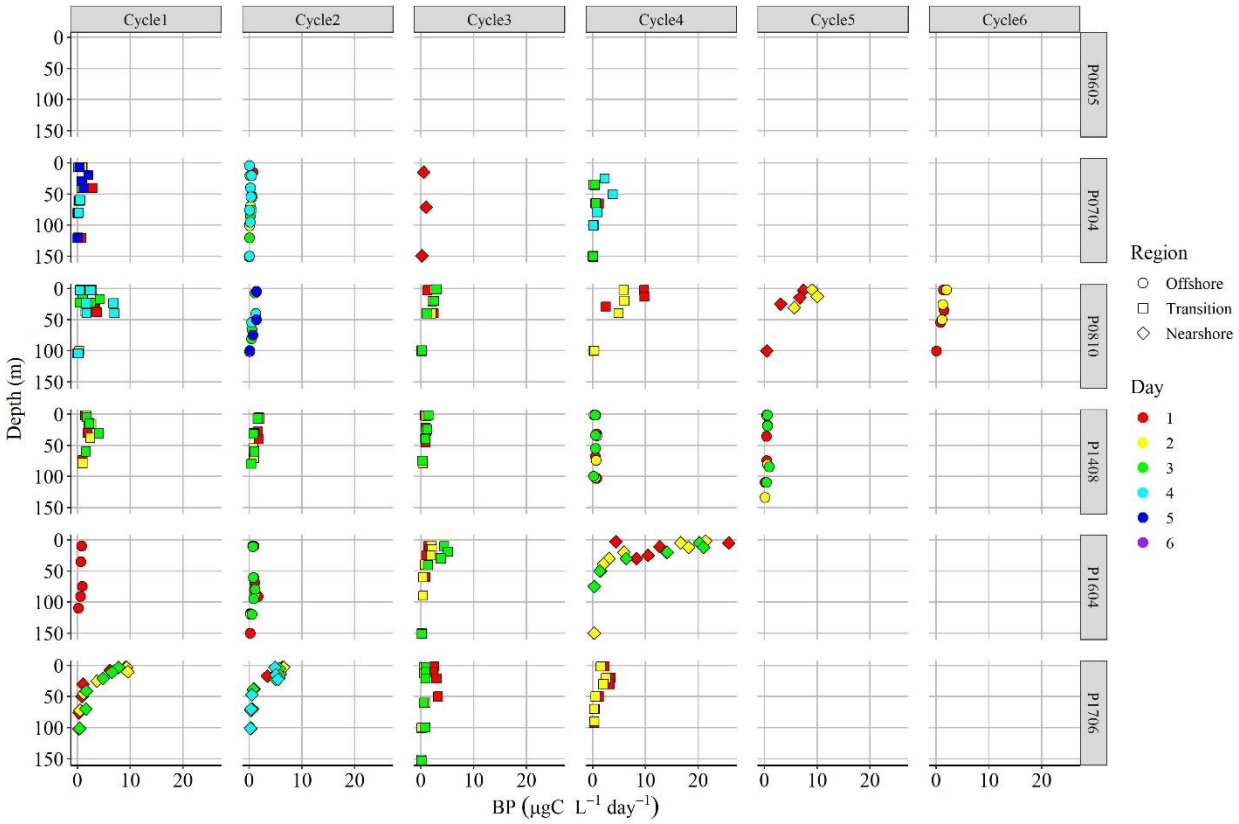

Figure S3.3: Daily variation of bacterial production (BP) within a cycle

Data plotted by cruise and cycle with color signifying cycle day.

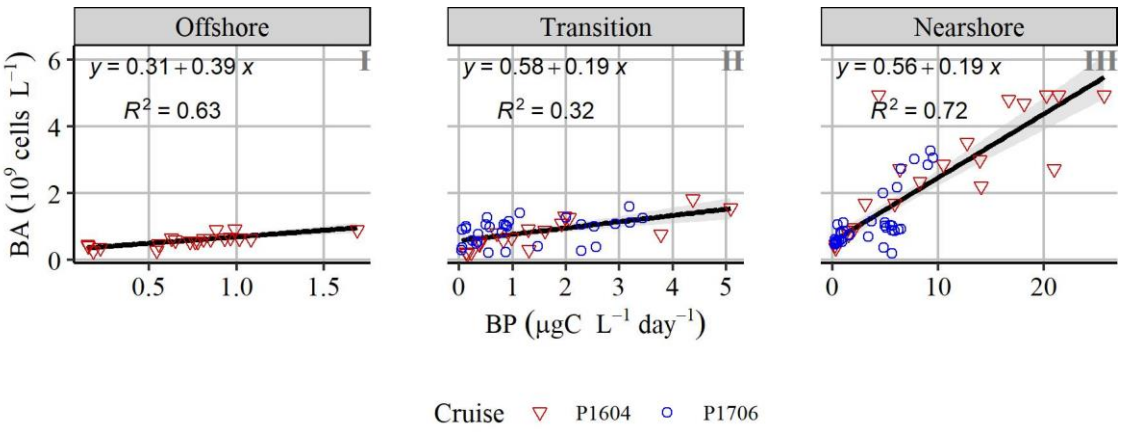

Figure S3.4: Relationship between FCM* BA and BP by region

Data plotted in cruise colored by condition (blue- normal years or red- warm years). The linear relationship between bacterial abundance (BA) and bacterial production (BP) across sCCS oceanic regions.

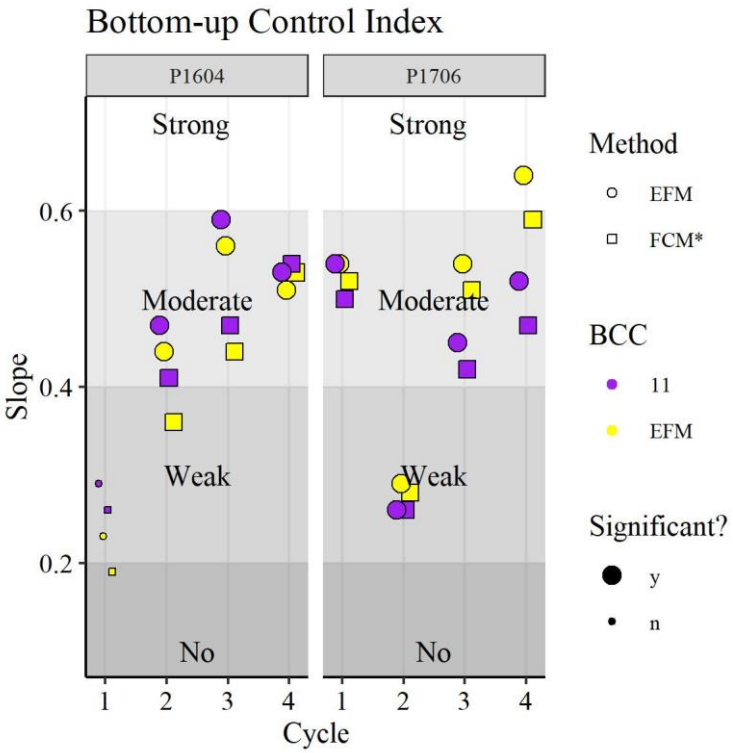

Figure S3.5: Impact of BCC choice on the bottom-up control index

Slope of the log BP vs log BB relationship when BB is calculated using EFM BA (circles) or FCM* BA (squares) and BCC derived from EFM cell sizing (yellow) or an assumed 11 fgC cell^{-1} (purple) for cruises P1604 and P1706 shown by cycle.

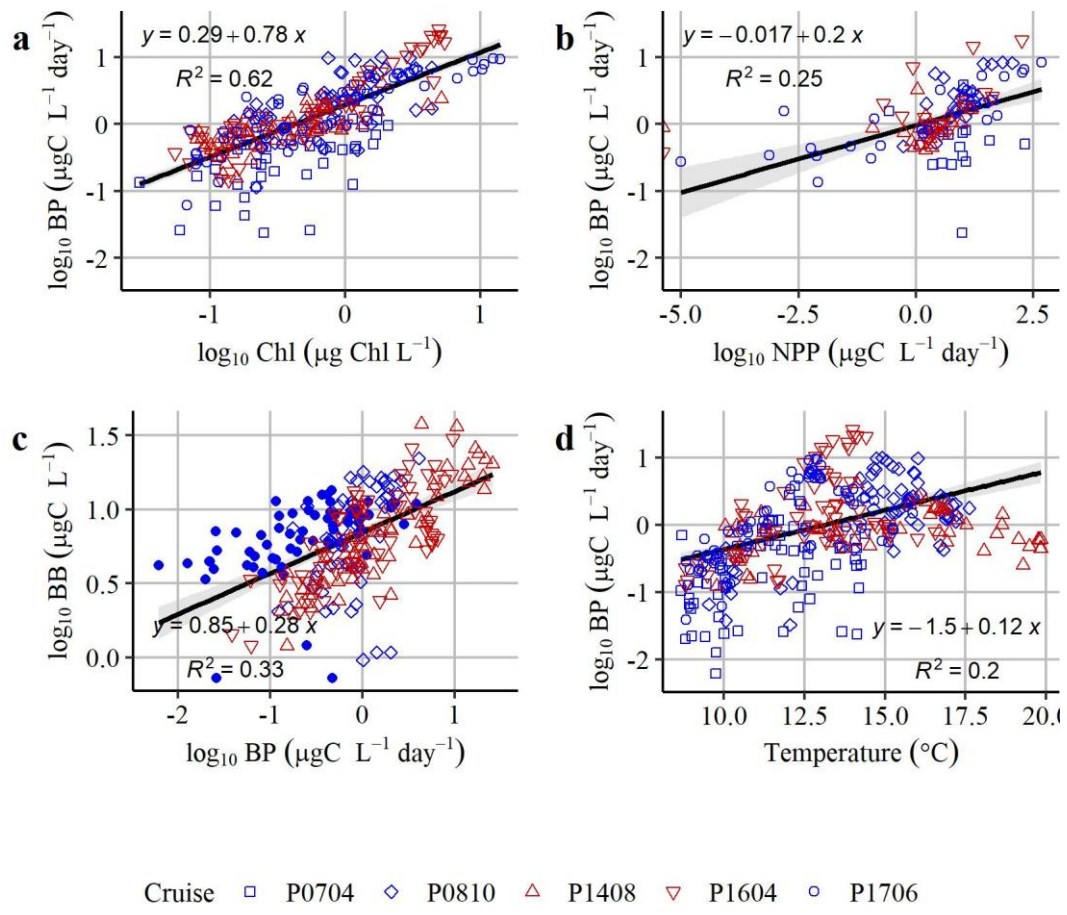

Figure S3.6: Log transformations and linear regressions

Linear regressions for BP~Chl coupling (a), BP~NPP coupling (b), bottom-up control (c), and temperature control (d) for all available data. All regressions are significant ($p<0.001$).

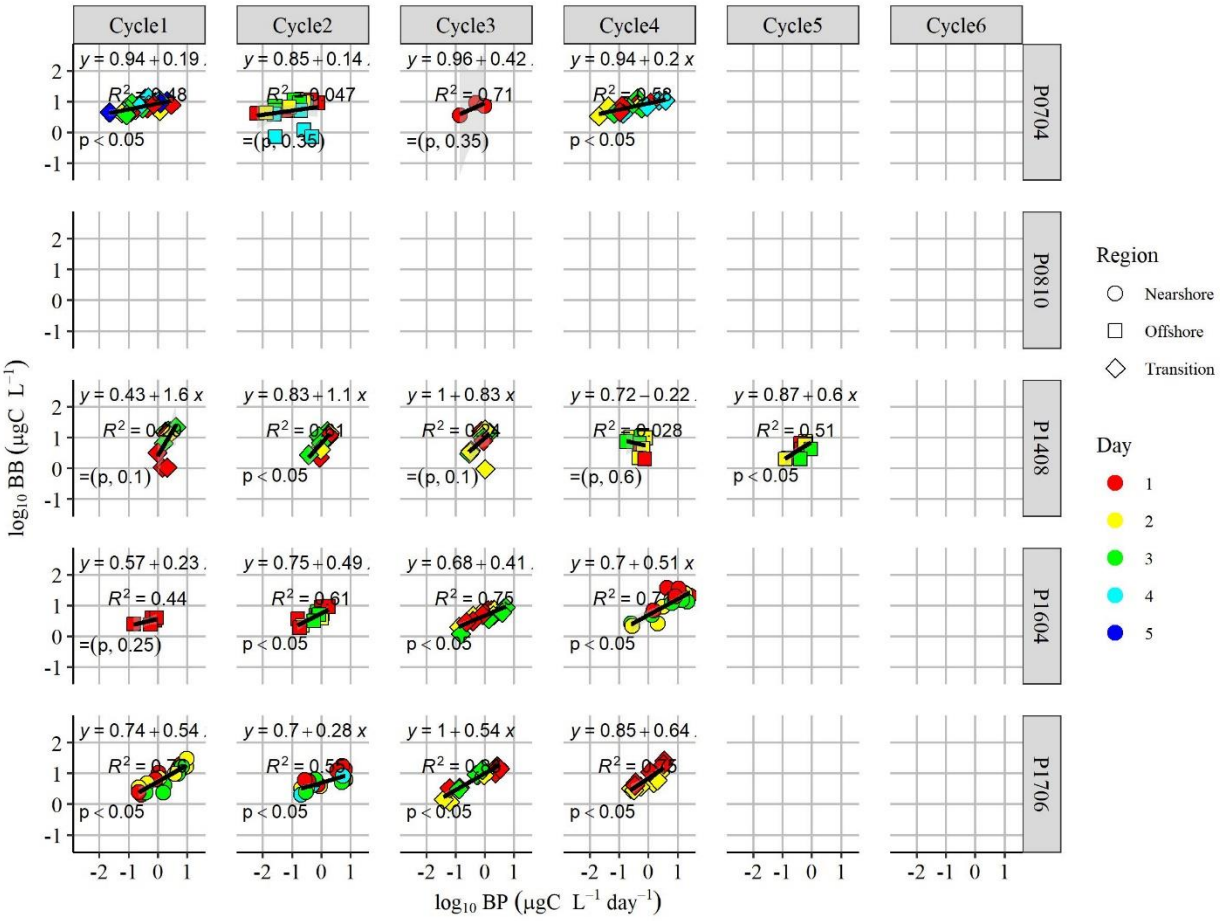

Figure S3.7: Bottom-up control index calculations

Data plotted by cruise and cycle with color signifying cycle day.

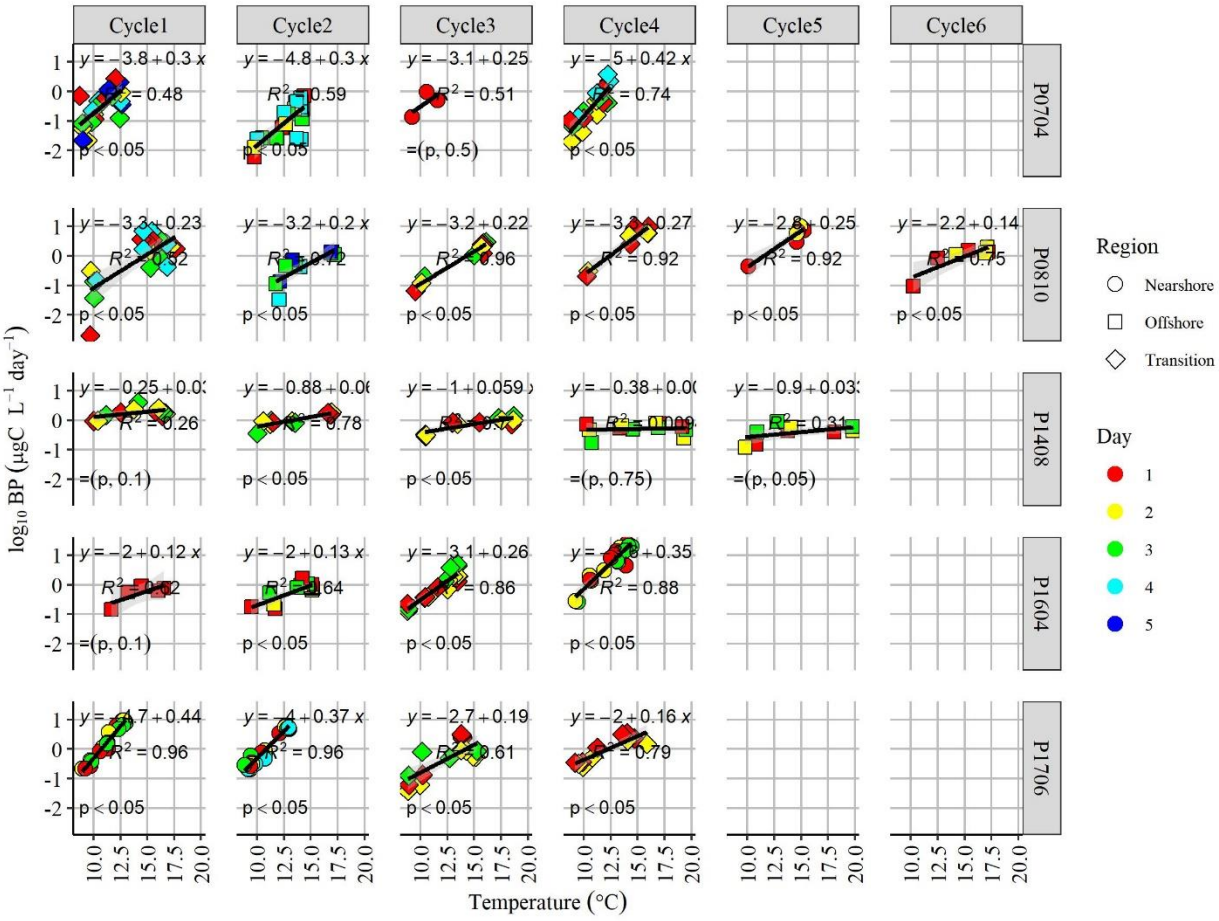

Figure S3.8: Temperature control index calculations

Data plotted by cruise and cycle with color signifying cycle day.

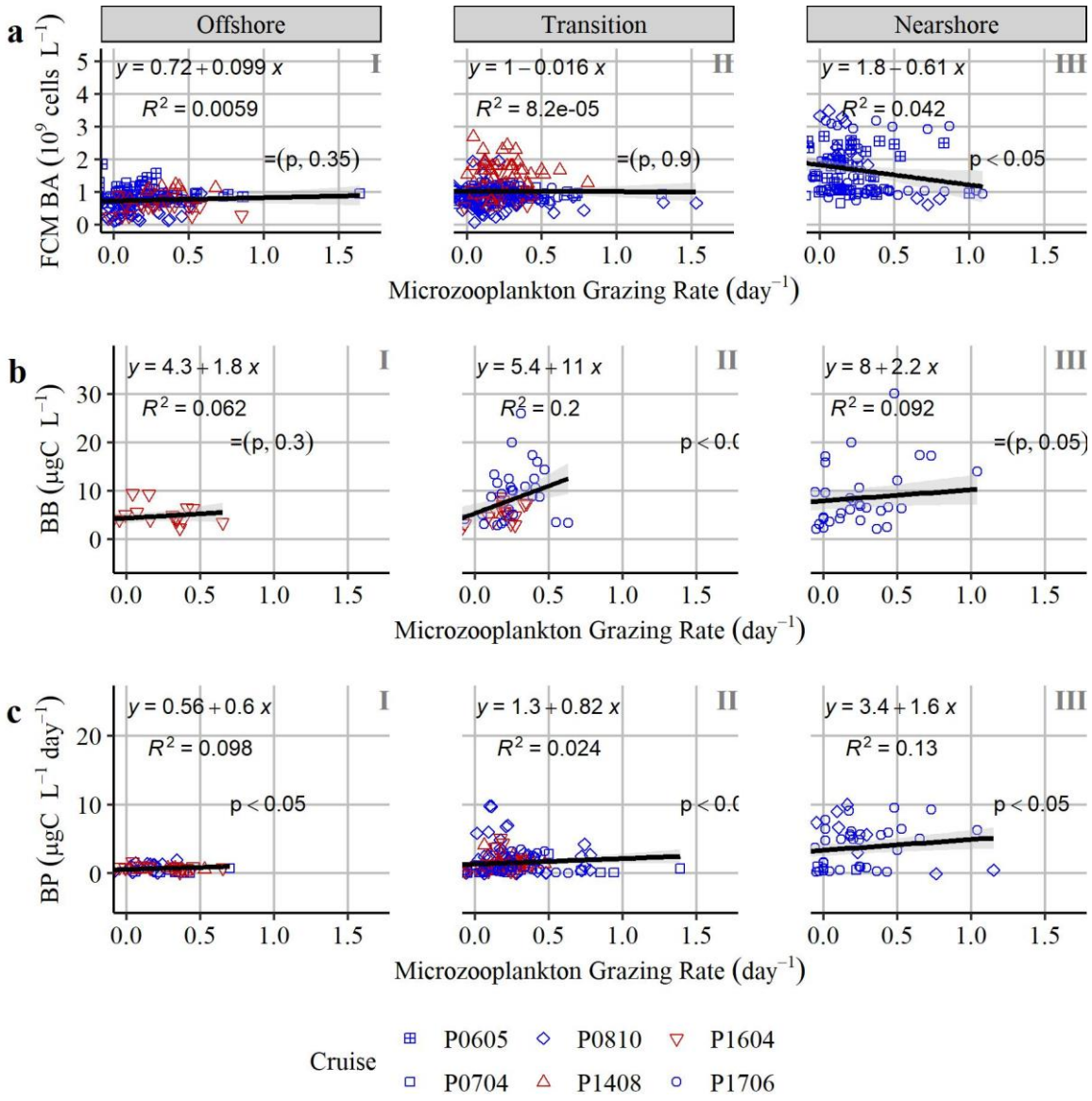

Figure S3.9: Relationships of microzooplankton grazing rates and heterotrophic bacterial abundance

Linear relationships between microzooplankton grazing rate on phytoplankton and heterotrophic FCM BA (a) by oceanic region. Linear relationships between microzooplankton grazing rate on phytoplankton interpolated to match the depths sampled for BB (b), calculated from EFM BA and EFM derived BCC, and BP (c) by oceanic region.

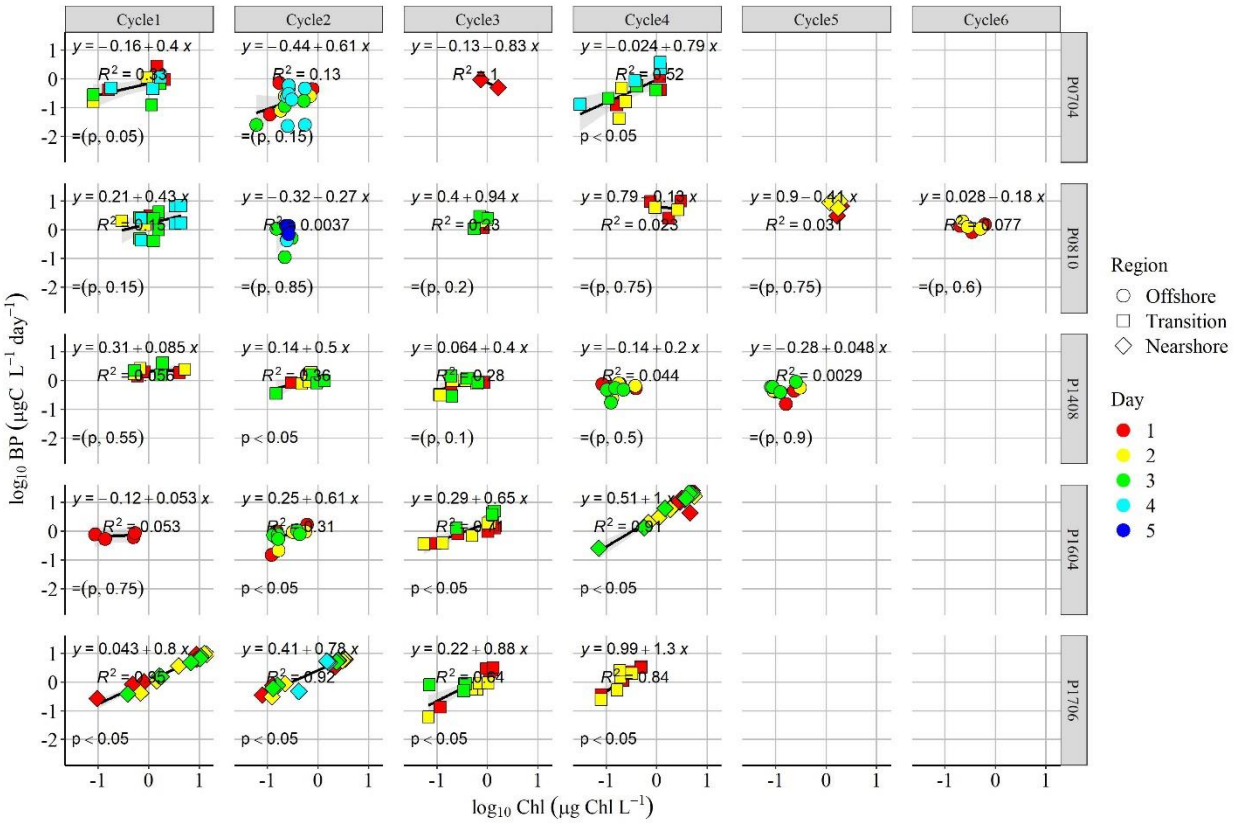

Figure S3.10: Chl and BP coupling calculations

Data plotted by cruise and cycle with color signifying cycle day.

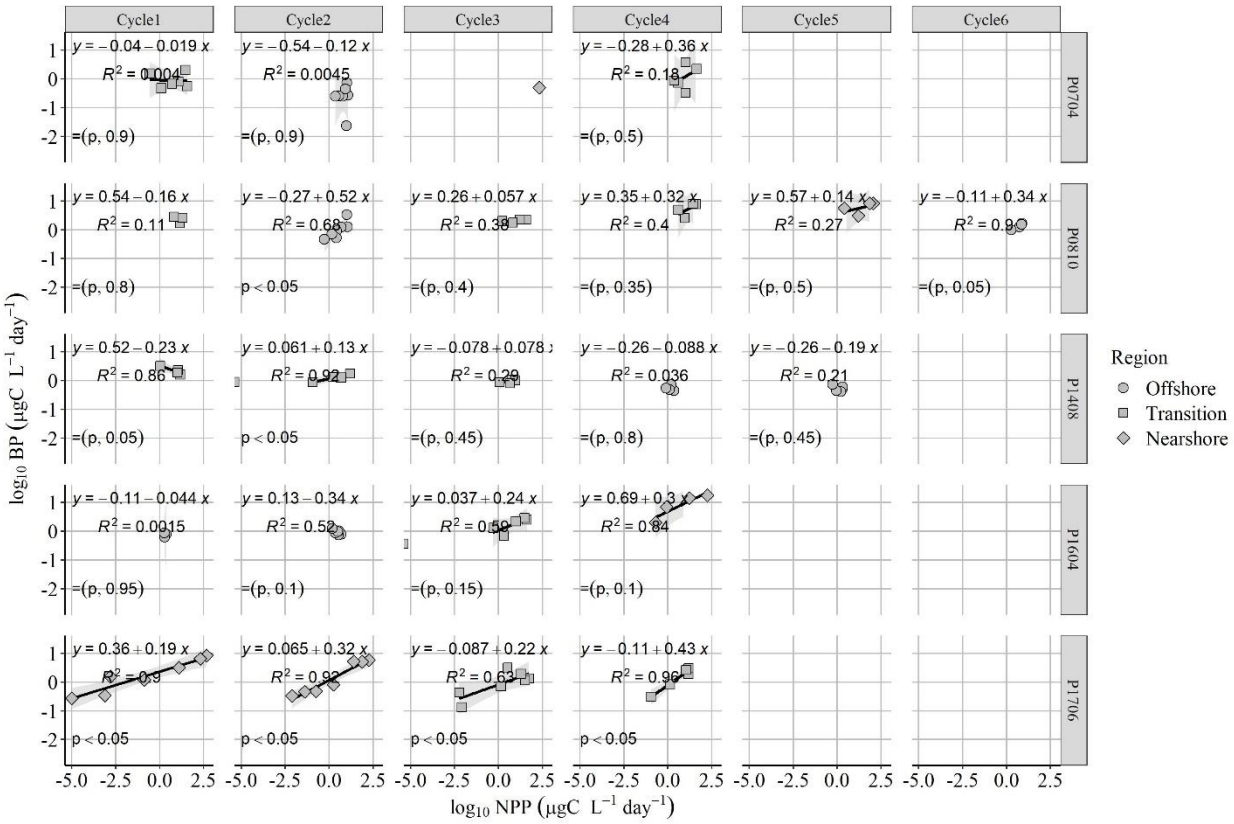

Figure S3.11: NPP and BP coupling calculations

Binned (5m) data plotted by cruise and cycle.

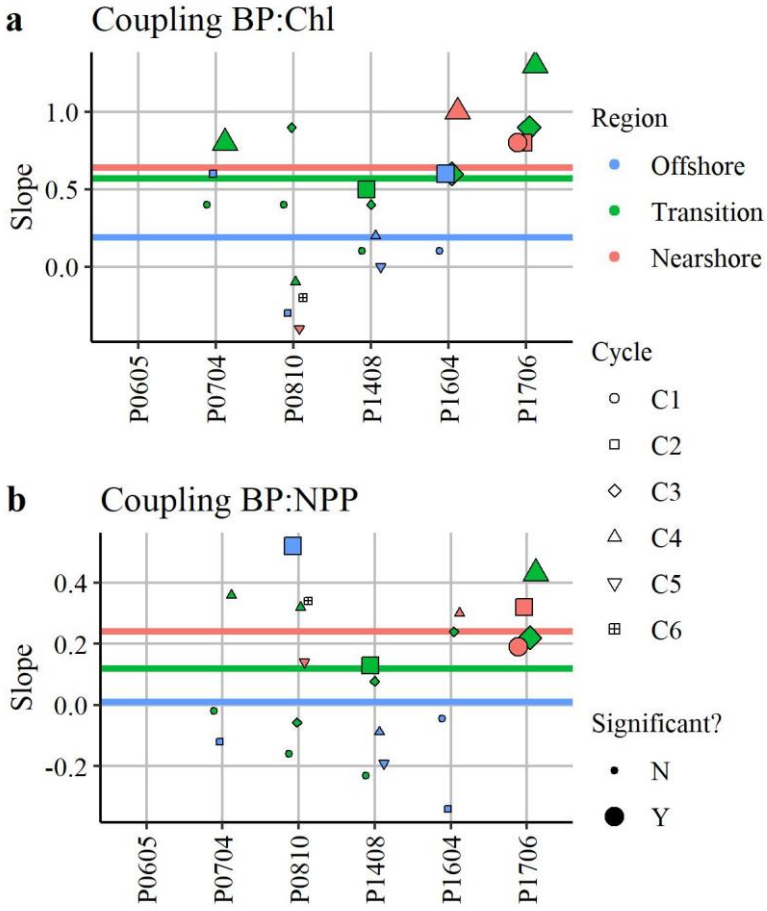

Figure S3.12: Coupling between bacterial production and phytoplankton properties by cruise-cycle

The degree of BP coupling with Chl (a) and NPP (b) were examined from log-log regression slope values with mean slope (horizontal colored lines). Mean slope was calculated as the average of the slopes. Larger shapes indicate significant regressions at $p<0.05$.

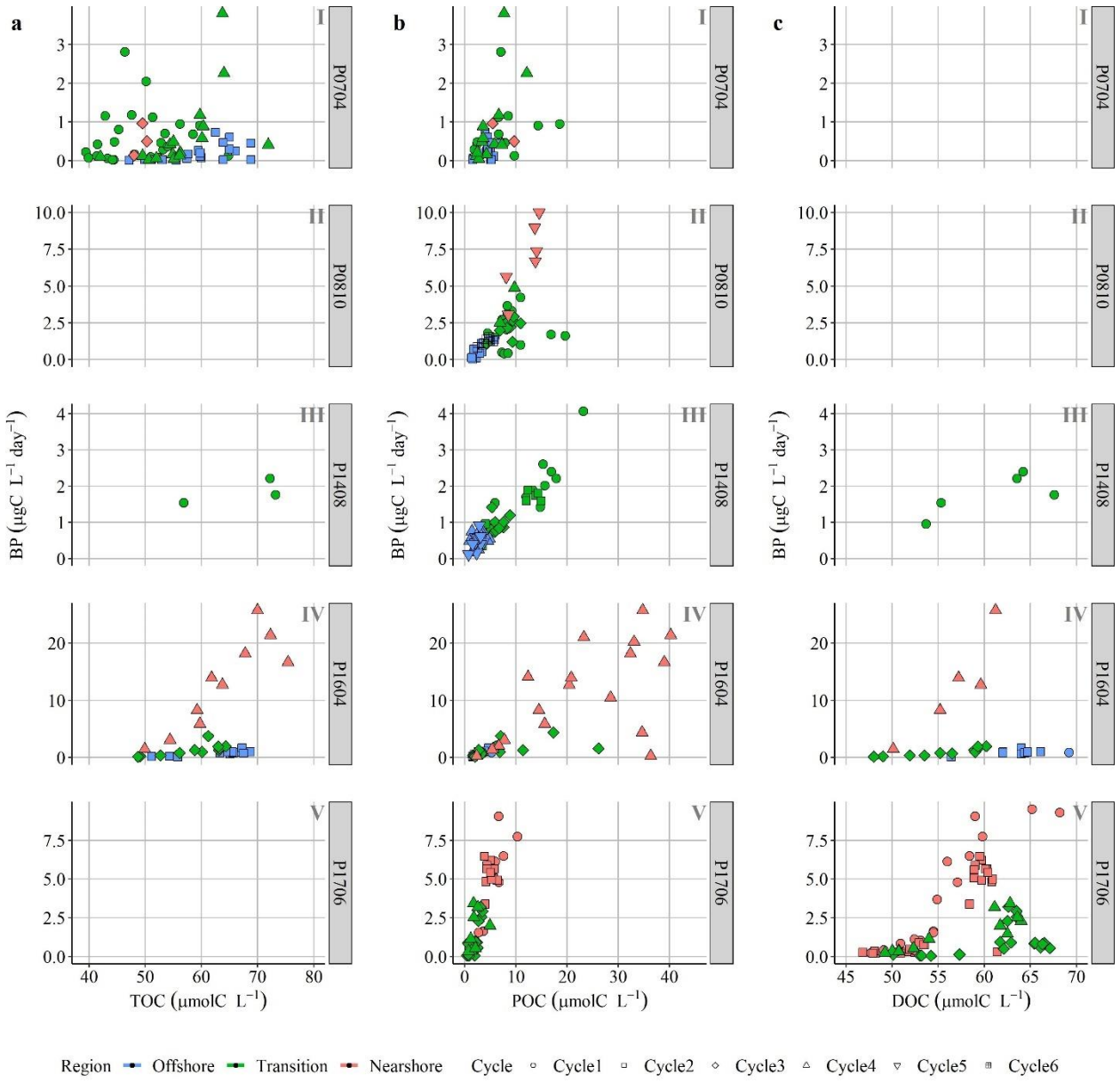

Figure S3.13: Relationships between BP and organic carbon pools by cruise

Data plotted by cruise and colored by region between BP and organic carbon pools, TOC (a), POC (b), and DOC (c). A best fit line for each region of each cruise was also plotted.

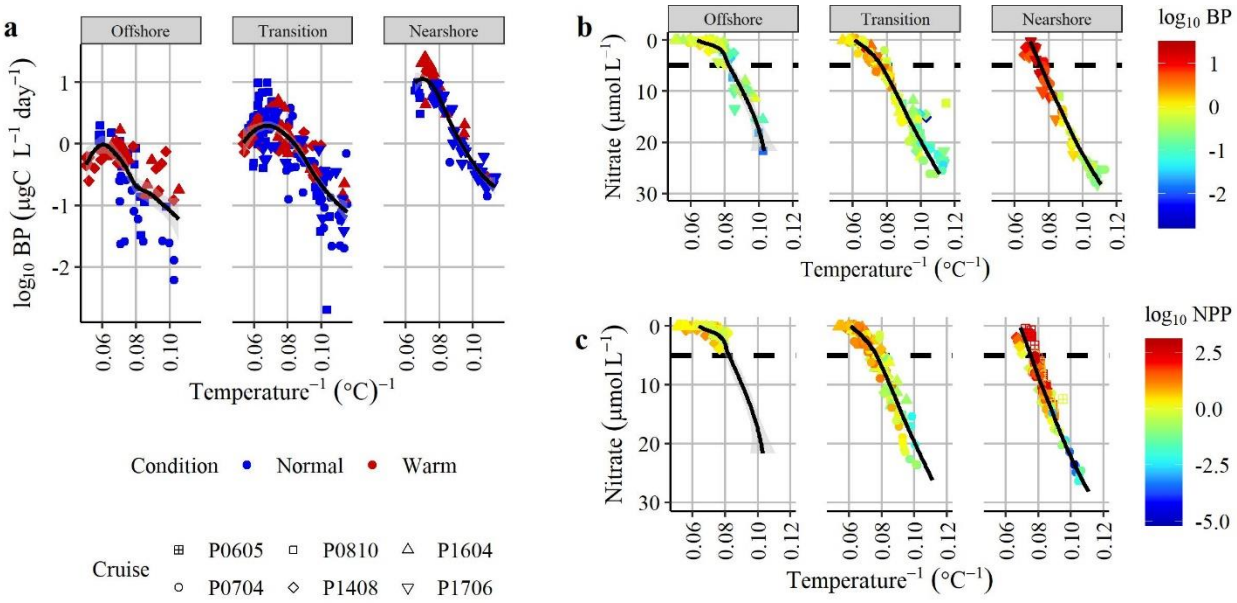

Figure S3.14: Inverse temperature and nitrate relationship to production

Log-transformed BP had a strong positive correlation with inverse temperature (a) until approximately 0.06 °C^{-1} offshore, 0.07 °C^{-1} in the transition and nearshore when increasing temperature led to a decrease in BP. (b) Relationship between nitrate and temperature with dashed lines at 0.08 °C^{-1} and 5 mM nitrate. Points colored by logBP (b) and logNPP (c) increased with increasing temperature and decreasing nitrate.

Table S3.1: BA method comparison using Kruskal-Wallis

Kruskal-Wallis one-way analysis of variance with 95% confidence interval comparing FCM and FCM* methods using data from P1604 and P1706. No significance means that there was no significant difference between the methods. Significantly different comparisons ($p<0.05$) are **bold**.

	P0704	P1408	P1604	P1706
EFM vs FCM				
All	**Chi-sq: 39.525** **p-value: 3.239E-10**	**Chi-sq: 9.1609** **p-value: 0.002472**	**Chi-sq: 27.348** **p-value: 1.699E-07**	**Chi-sq: 38.335** **p-value: 5.958E-10**
Offshore	**Chi-sq: 13.599** **p-value: 0.0002263**	**Chi-sq: 4.2998** **p-value: 0.03812**	**Chi-sq: 16.878** **p-value: 3.987E-5**	n.d.
Transition	**Chi-sq: 28.741** **p-value: 8.275E-08**	**Chi-sq: 7.3665** **p-value: 0.006645**	**Chi-sq: 24.756** **p-value: 6.506E-07**	**Chi-sq: 13.611** **p-value: 0.0002249**
Nearshore	Chi-sq: 0.47339 p-value: 0.4914	n.d.	**Chi-sq: 17.778** **p-value: 2.483E-5**	**Chi-sq: 24.79** **p-value: 6.394E-07**
EFM vs FCM*				
Overall	n.d.	n.d.	**Chi-sq: 13.894** **p-value: 0.0001934**	**Chi-sq: 13.496** **p-value: 0.0002391**
Offshore	n.d.	n.d.	**Chi-sq: 11.575** **p-value: 0.0006684**	n.d.
Transition	n.d.	n.d.	**Chi-sq: 5.9596** **p-value: 0.001464**	**Chi-sq: 9.2759** **p-value: 0.002322**
Nearshore	n.d.	n.d.	**Chi-sq: 8.5451** **p-value: 0.003465**	**Chi-sq: 7.3294** **p-value: 0.006784**
FCM vs FCM*				
Overall	n.d.	n.d.	Chi-sq: 2.055 p-value: 0.1517	Chi-sq: 2.4172 p-value: 0.12
Offshore	n.d.	n.d.	Chi-sq: 0.25485 p-value: 0.6137	n.d.
Transition	n.d.	n.d.	Chi-sq: 2.9338 p-value: 0.08675	**Chi-sq: 3.9722** **p-value: 0.04626**
Nearshore	n.d.	n.d.	**Chi-sq: 3.8519** **p-value: 0.04969**	**Chi-sq: 10.403** **p-value: 0.001258**

Table S3.2. Flow cytometry method comparison by cruise-cycle

Kruskal-Wallis one-way analysis of variance with 95% confidence interval comparing FCM and FCM* methods using data from P1604 and P1706. No significance means that there was no significant difference between the methods.

Cruise	Cycle	Chi-sq	df	p-value	Significant?
P1604	All	2.0555	1	0.1517	No
	C1	1.0614	1	0.3029	No
	C2	1.9379	1	0.1639	No
	C3	2.9338	1	0.08675	No
	C4	3.8519	1	0.04969	Yes
P1706	All	2.4172	1	0.12	No
	C1	2.7075	1	0.09988	No
	C2	11.2	1	0.000818	Yes
	C3	1.0822	1	0.2982	No
	C4	2.5034	1	0.1136	No

3.9 REFERENCES

Agis M, Granda A, Dolan JR (2007) A cautionary note: Examples of possible microbial community dynamics in dilution grazing experiments. Journal of Experimental Marine Biology and Ecology 341:176-183

Armstrong FAJ, Stearns CR, Strickland JDH (1967) Author links open overlay panel The measurement of upwelling and subsequent biological process by means of the Technicon Autoanalyzer® and associated equipment. Deep Sea Research and Oceanographic Abrstracts 14:381-389

Azam F, Fenchel T, Field JG, Gray JS, Meyer-Reil LA, Thingstad F (1983) THE ECOLOGICAL ROLE OF WATER COLUMN MICROBES IN THE SEA. Marine Ecology Progress Series 10:257-264

Barbosa AB, Galvao HM, Mendes PA, Alvarez-Salgado XA, Figueiras FG, Joint I (2001) Short-term variability of heterotrophic bacterioplankton during upwelling off the NW Iberian margin. Progress in Oceanography 51:339-359

Billen G, Servais P, Becquevort S (1990) Dynamics of bacterioplankton in oligotrophic and eutrophic aquatic environments: bottom-up or top-down control?. Hydrobiologia:37-42

Bird DF, Kalff J (1984) EMPIRICAL RELATIONSHIPS BETWEEN BACTERIAL ABUNDANCE AND CHLOROPHYLL CONCENTRATION IN FRESH AND MARINE WATERS. Canadian Journal of Fisheries and Aquatic Sciences 41:1015-1023

Bond NA, Cronin MF, Freeland H, Mantua N (2015) Causes and impacts of the 2014 warm anomaly in the NE Pacific. Geophysical Research Letters 42:3414-3420

Bratbak G (1985) BACTERIAL BIOVOLUME AND BIOMASS ESTIMATIONS. Applied and Environmental Microbiology 49:1488-1493

Burrell TJ, Maas EW, Hulston DA, Law CS (2017) Variable response to warming and ocean acidification by bacterial processes in different plankton communities. Aquatic Microbial Ecology 79:49-62

Calvo-Diaz A, Franco-Vidal L, Moran XAG (2014) Annual cycles of bacterioplankton biomass and production suggest a general switch between temperature and resource control in temperate coastal ecosystems. Journal of Plankton Research 36:859-865

Carlson CA, Del Giorgio PA, Herndl GJ (2007) Microbes and the Dissipation of Energy and Respiration: From Cells to Ecosystems. Oceanography 20:89-100

Chavez FP, Messie M (2009) A comparison of Eastern Boundary Upwelling Ecosystems. Progress in Oceanography 83:80-96

Chen BZ, Landry MR, Huang BQ, Liu HB (2012) Does warming enhance the effect of microzooplankton grazing on marine phytoplankton in the ocean? Limnology and Oceanography 57:519-526

Cherrier J, Bauer JE, Druffel ERM (1996) Utilization and turnover of labile dissolved organic matter by bacterial heterotrophs in eastern north Pacific surface waters. Marine Ecology Progress Series 139:267-279

Cho BC, Azam F (1988) MAJOR ROLE OF BACTERIA IN BIOGEOCHEMICAL FLUXES IN THE OCEANS INTERIOR. Nature 332:441-443

Cole JJ, Findlay S, Pace ML (1988) BACTERIAL PRODUCTION IN FRESH AND SALTWATER ECOSYSTEMS - A CROSS-SYSTEM OVERVIEW. Marine Ecology Progress Series 43:1-10

Danovaro R, Corinaldesi C, Dell'Anno A, Fuhrman JA, Middelburg JJ, Noble RT, Suttle CA (2011) Marine viruses and global climate change. Fems Microbiology Reviews 35:993-1034

del Giorgio PA, Gasol JM, Vaque D, Mura P, Agusti S, Duarte CM (1996) Bacterioplankton community structure: Protists control net production and the proportion of active bacteria in a coastal marine community. Limnology and Oceanography 41:1169-1179

Di Lorenzo E, Mantua N (2016) Multi-year persistence of the 2014/15 North Pacific marine heatwave. Nature Climate Change 6:1042-1047

Ducklow HW (1992) Factors regulating bottom-up control of bacteria biomass in open ocean plankton communities. Arch Hydrobiol Beih Ergebn Limnol:207–217

Ducklow HW, Smith DC, Campbell L, Landry MR, Quinby HL, Steward GF, Azam F (2001) Heterotrophic bacterioplankton in the Arabian Sea: Basinwide response to year-round high primary productivity. Deep-Sea Research Part Ii-Topical Studies in Oceanography 48:1303-1323

Eiler A, Langenheder S, Bertilsson S, Tranvik LJ (2003) Heterotrophic bacterial growth efficiency and community structure at different natural organic carbon concentrations. Applied and Environmental Microbiology 69:3701-3709

Eppley RW, Holm-Hansen O (1986) Primary Production in the Southern California Bight, Vol 15. Springer-Verlag

Epstein SS, Shiaris MP (1992) SIZE-SELECTIVE GRAZING OF COASTAL BACTERIOPLANKTON BY NATURAL ASSEMBLAGES OF PIGMENTED FLAGELLATES, COLORLESS FLAGELLATES, AND CILIATES. Microbial Ecology 23:211-225

Fenchel T (2008) The microbial loop-25 years later. Journal of Experimental Marine Biology and Ecology 366:99-103

Flombaum P, Gallegos JL, Gordillo RA, Rincon J, Zabala LL, Jiao NAZ, Karl DM, Li WKW, Lomas MW, Veneziano D, Vera CS, Vrugt JA, Martiny AC (2013) Present and future global distributions of the marine Cyanobacteria Prochlorococcus and Synechococcus. Proceedings of the National Academy of Sciences of the United States of America 110:9824-9829

Garrison DL, Gowing MM, Hughes MP, Campbell L, Caron DA, Dennett MR, Shalapyonok A, Olson RJ, Landry MR, Brown SL, Liu HB, Azam F, Steward GF, Ducklow HW, Smith DC (2000) Microbial food web structure in the Arabian Sea: a US JGOFS study. Deep-Sea Research Part Ii-Topical Studies in Oceanography 47:1387-1422

Garzio LM, Steinberg DK, Erickson M, Ducklow HW (2013) Microzooplankton grazing along the Western Antarctic Peninsula. Aquatic Microbial Ecology 70:215-232

Gasol JM, delGiorgio PA, Massana R, Duarte CM (1995) Active versus inactive bacteria: Size-dependence in a coastal marine plankton community. Marine Ecology Progress Series 128:91-97

Gasol JM, Duarte CM (2000) Comparative analyses in aquatic microbial ecology: how far do they go? Fems Microbiology Ecology 31:99-106

Gasol JM, Pedros-Alio C, Vaque D (2002) Regulation of bacterial assemblages in oligotrophic plankton systems: results from experimental and empirical approaches. Antonie Van Leeuwenhoek International Journal of General and Molecular Microbiology 81:435-452

Gentemann CL, Fewings MR, Garcia-Reyes M (2017) Satellite sea surface temperatures along the West Coast of the United States during the 2014-2016 northeast Pacific marine heat wave. Geophysical Research Letters 44:312-319

Goericke R (2011) The structure of marine phytoplankton communities--patterns, rules, and mechanisms. In, Book 52, California Cooperative Oceanic Fisheries Investigations Report

Goericke R, Ohman MD (2015) Introduction to CCE-LTER: Responses of the California Current Ecosystem to climate forcing. Deep-Sea Research Part Ii-Topical Studies in Oceanography 112:1-5

Gomez-Ocampo E, Gaxiola-Castro G, Burazo R, Beier E (2018) Effects of the 2013-2016 warm anomalies on the California Current phytoplankton. Deep-Sea Research Part Ii-Topical Studies in Oceanography 151:64-76

Gonzalez JM, Sherr EB, Sherr BF (1990) SIZE-SELECTIVE GRAZING ON BACTERIA BY NATURAL ASSEMBLAGES OF ESTUARINE FLAGELLATES AND CILIATES. Applied and Environmental Microbiology 56:583-589

Grossart HP, Ploug H (2001) Microbial degradation of organic carbon and nitrogen on diatom aggregates. Limnology and Oceanography 46:267-277

Hahn MW, Hofle MG (1999) Flagellate predation on a bacterial model community: Interplay of size-selective grazing, specific bacterial cell size, and bacterial community composition. Applied and Environmental Microbiology 65:4863-4872

Halewood ER, Carlson CA, Brzezinski MA, Reed DC, Goodman J (2012) Annual cycle of organic matter partitioning and its availability to bacteria across the Santa Barbara Channel continental shelf. Aquatic Microbial Ecology 67:189-209

Hayward TL, Venrick EL (1998) Nearsurface pattern in the California Current: coupling between physical and biological structure. Deep-Sea Research Part Ii-Topical Studies in Oceanography 45:1617-1638

Herrmann M, Estournel C, Adloff F, Diaz F (2014) Impact of climate change on the northwestern Mediterranean Sea pelagic planktonic ecosystem and associated carbon cycle. Journal of Geophysical Research-Oceans 119:5815-5836

Hogle SL, Dupont CL, Hopkinson BM, King AL, Buck KN, Roe KL, Stuart RK, Allen AE, Mann EL, Johnson ZI, Barbeau KA (2018) Pervasive iron limitation at subsurface chlorophyll maxima of the California Current. Proceedings of the National Academy of Sciences of the United States of America 115:13300-13305

Jacox MG, Hazen EL, Zaba KD, Rudnick DL, Edwards CA, Moore AM, Bograd SJ (2016) Impacts of the 2015-2016 El Nino on the California Current System: Early assessment and comparison to past events. Geophysical Research Letters 43:7072-7080

Jurgens K, Gude H (1994) THE POTENTIAL IMPORTANCE OF GRAZING-RESISTANT BACTERIA IN PLANKTONIC SYSTEMS. Marine Ecology Progress Series 112:169-188

Karl DM, Church MJ (2014) Microbial oceanography and the Hawaii Ocean Time-series programme. Nature Reviews Microbiology 12:699-713

Kelly TB, Goericke R, Kahru M, Song H, Stukel MR (2018) CCE II: Spatial and interannual variability in export efficiency and the biological pump in an eastern boundary current upwelling system with substantial lateral advection. Deep-Sea Research Part I-Oceanographic Research Papers 140:14-25

Kim B, Kim SH, Kwak JH, Kang CK, Lee SH, Hyun JH (2017) Heterotrophic bacterial production, respiration, and growth efficiency associated with upwelling intensity in the Ulleung Basin, East Sea. Deep-Sea Research Part Ii-Topical Studies in Oceanography 143:24-35

Kim H, Ducklow HW (2016) A Decadal (2002-2014) Analysis for Dynamics of Heterotrophic Bacteria in an Antarctic Coastal Ecosystem: Variability and Physical and Biogeochemical Forcings. Frontiers in Marine Science 3

King AL, Barbeau K (2007) Evidence for phytoplankton iron limitation in the southern California Current System. Marine Ecology Progress Series 342:91-103

Kirchman D, Ducklow H, Mitchell R (1982) ESTIMATES OF BACTERIAL GROWTH FROM CHANGES IN UPTAKE RATES AND BIOMASS. Applied and Environmental Microbiology 44:1296-1307

Kirchman D, Knees E, Hodson R (1985) LEUCINE INCORPORATION AND ITS POTENTIAL AS A MEASURE OF PROTEIN-SYNTHESIS BY BACTERIA IN NATURAL AQUATIC SYSTEMS. Applied and Environmental Microbiology 49:599-607

Kirchman DL, Meon B, Cottrell MT, Hutchins DA, Weeks D, Bruland KW (2000) Carbon versus iron limitation of bacterial growth in the California upwelling regime. Limnology and Oceanography 45:1681-1688

Kjelleberg S, Hermansson M, Marden P (1987) THE TRANSIENT PHASE BETWEEN GROWTH AND NONGROWTH OF HETEROTROPHIC BACTERIA, WITH EMPHASIS ON THE MARINE-ENVIRONMENT. Annual Review of Microbiology 41:25-49

Landry MR, Ohman MD, Goericke R, Stukel MR, Tsyrklevich K (2009) Lagrangian studies of phytoplankton growth and grazing relationships in a coastal upwelling ecosystem off Southern California. Progress in Oceanography 83:208-216

Lebaron P, Servais P, Agogue H, Courties C, Joux F (2001) Does the high nucleic acid content of individual bacterial cells allow us to discriminate between active cells and inactive cells in aquatic systems? Applied and Environmental Microbiology 67:1775-1782

Lennon JT, Jones SE (2011) Microbial seed banks: the ecological and evolutionary implications of dormancy. Nature Reviews Microbiology 9:119-130

Lopez-Urrutia A, Moran XAG (2007) Resource limitation of bacterial production distorts the temperature dependence of oceanic carbon cycling. Ecology 88:817-822

Lucas AJ, Dupont CL, Tai V, Largier JL, Palenik B, Franks PJS (2011) The green ribbon: Multiscale physical control of phytoplankton productivity and community structure over a narrow continental shelf. Limnology and Oceanography 56:611-626

McManus GB, Peterson WT (1988) BACTERIOPLANKTON PRODUCTION IN THE NEARSHORE ZONE DURING UPWELLING OFF CENTRAL CHILE. Marine Ecology Progress Series 43:11-17

Monger BC, Landry MR (1991) PREY-SIZE DEPENDENCY OF GRAZING BY FREE-LIVING MARINE FLAGELLATES. Marine Ecology Progress Series 74:239-248

Monger BC, Landry MR (1993) FLOW CYTOMETRIC ANALYSIS OF MARINE-BACTERIA WITH HOECHST 33342. Applied and Environmental Microbiology 59:905-911

Moran XAG, Alonso-Saez L, Nogueira E, Ducklow HW, Gonzalez N, Lopez-Urrutia A, Diaz-Perez L, Calvo-Diaz A, Arandia-Gorostidi N, Huete-Stauffer TM (2015) More, smaller bacteria in response to ocean's warming? Proceedings of the Royal Society B-Biological Sciences 282:9

Moran XAG, Bode A, Suarez LA, Nogueira E (2007) Assessing the relevance of nucleic acid content as an indicator of marine bacterial activity. Aquatic Microbial Ecology 46:141-152

Moran XAG, Gasol JM, Pernice MC, Mangot JF, Massana R, Lara E, Vaque D, Duarte CM (2017) Temperature regulation of marine heterotrophic prokaryotes increases latitudinally as a breach between bottom-up and top-down controls. Global Change Biology 23:3956-3964

Morrow RM, Ohman MD, Goericke R, Kelly TB, Stephens BM, Stukel MR (2018) CCE V: Primary production, mesozooplankton grazing, and the biological pump in the California Current Ecosystem: Variability and response to El Nino. Deep-Sea Research Part I-Oceanographic Research Papers 140:52-62

Ohman MD, Barbeau K, Franks PJS, Goericke R, Landry MR, Miller AJ (2013) Ecological Transitions in a Coastal Upwelling Ecosystem. Oceanography 26:210-219

Ohman MD, Powell JR, Picheral M, Jensen DW (2012) Mesozooplankton and particulate matter responses to a deep-water frontal system in the southern California Current System. Journal of Plankton Research 34:815-827

Paerl HW (1975) Microbial Attachment to Particles in Marine and Freshwater Ecosystems. Microbial Ecology 2:73-83

Palacios DM, Hazen EL, Schroeder ID, Bograd SJ (2013) Modeling the temperature-nitrate relationship in the coastal upwelling domain of the California Current. Journal of Geophysical Research-Oceans 118:3223-3239

Pasulka AL, Samo TJ, Landry MR (2015) Grazer and viral impacts on microbial growth and mortality in the southern California Current Ecosystem. Journal of Plankton Research 37:320-336

Pedler BE, Aluwihare LI, Azam F (2014) Single bacterial strain capable of significant contribution to carbon cycling in the surface ocean. Proceedings of the National Academy of Sciences of the United States of America 111:7202-7207

Pernthaler J (2005) Predation on prokaryotes in the water column and its ecological implications (vol 3, pg 537, 2005). Nature Reviews Microbiology 3:1

Ploug H, Grossart HP (1999) Bacterial production and respiration in suspended aggregates - a matter of the incubation method. Aquatic Microbial Ecology 20:21-29

Ploug H, Grossart HP, Azam F, Jorgensen BB (1999) Photosynthesis, respiration, and carbon turnover in sinking marine snow from surface waters of Southern California Bight: implications for the carbon cycle in the ocean. Marine Ecology Progress Series 179:1-11

Polovina JJ, Howell EA, Abecassis M (2008) Ocean's least productive waters are expanding. Geophysical Research Letters 35:5

Samo TJ, Pedler BE, Ball GI, Pasulka AL, Taylor AG, Aluwihare LI, Azam F, Goericke R, Landry MR (2012) Microbial distribution and activity across a water mass frontal zone in the California Current Ecosystem. Journal of Plankton Research 34:802-814

Sarmiento JL, Slater R, Barber R, Bopp L, Doney SC, Hirst AC, Kleypas J, Matear R, Mikolajewicz U, Monfray P, Soldatov V, Spall SA, Stouffer R (2004) Response of ocean ecosystems to climate warming. Global Biogeochemical Cycles 18:35

Simon M, Azam F (1989) PROTEIN-CONTENT AND PROTEIN-SYNTHESIS RATES OF PLANKTONIC MARINE-BACTERIA. Marine Ecology Progress Series 51:201-213

Smale DA, Wernberg T, Oliver ECJ, Thomsen M, Harvey BP, Straub SC, Burrows MT, Alexander LV, Benthuysen JA, Donat MG, Feng M, Hobday AJ, Holbrook NJ, Perkins-Kirkpatrick SE, Scannell HA, Sen Gupta A, Payne BL, Moore PJ (2019) Marine heatwaves threaten global biodiversity and the provision of ecosystem services. Nature Climate Change 9:306-312

Smith DC, Azam F (1992) A simple, economical method for measuring bacterial protein synthesis in seawater using 3H-leucine. In, Book 6, Mar. Microb. Food Webs

Stephens BM, Porrachia M, Dovel S, Roadman M, Goericke R, Aluwihare LI (2018) Nonsinking Organic Matter Production in the California Current. Global Biogeochemical Cycles 32:1386-1405

Stevenson LH (1978) CASE FOR BACTERIAL DORMANCY IN AQUATIC SYSTEMS. Microbial Ecology 4:127-133

Strickland JDH, Parsons TR (1972) A Practical Handbook of Seawater Analysis. In, Book 157. Fisheries Research Board of Canada Bulletin

Stukel, Michael, Goericke R, Landry M (2019) Predicting primary production in the southern California Current Ecosystem from chlorophyll, nutrient concentrations, and irradiance. bioRxiv 590240

Stukel MR, Ohman MD, Benitez-Nelson CR, Landry MR (2013) Contributions of mesozooplankton to vertical carbon export in a coastal upwelling system. Marine Ecology Progress Series 491:47-65

Taylor AG, Landry MR (2018) Phytoplankton biomass and size structure across trophic gradients in the southern California Current and adjacent ocean ecosystems. Marine Ecology Progress Series 592:1-17

Taylor AG, Landry MR, Selph KE, Wokuluk JJ (2015) Temporal and spatial patterns of microbial community biomass and composition in the Southern California Current Ecosystem. Deep-Sea Research Part Ii-Topical Studies in Oceanography 112:117-128

Troussellier M, Courties C, Zettelmaier S (1995) FLOW CYTOMETRIC ANALYSIS OF COASTAL LAGOON BACTERIOPLANKTON AND PICOPHYTOPLANKTON - FIXATION AND STORAGE EFFECTS. Estuarine Coastal and Shelf Science 40:621-633

Viviani DA, Church MJ (2017) Decoupling between bacterial production and primary production over multiple time scales in the North Pacific Subtropical Gyre. Deep-Sea Research Part I-Oceanographic Research Papers 121:132-142

Wear EK, Carlson CA, James AK, Brzezinski MA, Windecker LA, Nelson CE (2015) Synchronous shifts in dissolved organic carbon bioavailability and bacterial community responses over the course of an upwelling-driven phytoplankton bloom. Limnology and Oceanography 60:657-677

Weinbauer MG, Suominen S, Jezbera J, Kerros ME, Marro S, Dolan JR, Simek K (2019) Shifts in cell size and community composition of bacterioplankton due to grazing by heterotrophic flagellates: evidence from a marine system. Aquatic Microbial Ecology 83:295-308

White PA, Kalff J, Rasmussen JB, Gasol JM (1991) THE EFFECT OF TEMPERATURE AND ALGAL BIOMASS ON BACTERIAL PRODUCTION AND SPECIFIC GROWTH-RATE IN FRESH-WATER AND MARINE HABITATS. Microbial Ecology 21:99-118

CONCLUSIONS

The goals of this thesis were to 1, examine heterotrophic bacterial production and distribution in the sCCS and 2, examine the role of bacteria in the CCE carbon cycle. To accomplish this, data from both the CalCOFI and CCE-LTER were utilized. In Chapter 1, using the long-term observations conducted by CalCOFI, significant shift in abundance and spatial distribution of picoplankton, including heterotrophic bacteria, was identified following the switch to a positive PDO at the end of 2013 that persisted through the 2014 warm anomaly and 2015/2016 El Nino event to the end of my study period (November 2017).

Also in Chapter 1, CalCOFI stations along Line 80 were designated as nearshore (stations 51 and 55), transition (stations 60, 70, and 80), and offshore (stations 90 and 100). Biogeochemical parameters (nitracline, chlorophyll max, and euphotic zone depths) were then assessed and used to separate CCE-LTER datasets into these same designated regions. Variability of picoplankton populations (heterotrophic bacteria, *Prochlorococcus*, *Synechococcus*, and picoeukaryotes) was also assessed within each region and between programs. Obvious mismatches between programs resulted from the CCE-LTER targeting specific features for Lagrangian cycles, compared to the CalCOFI surveys sampling along a predetermined grid. “Binning” findings from CCE-LTER cruises into the relevant CalCOFI climatology and hydrography allowed the discoveries enabled by the CCE-LTER program to be interpreted in the long-term observations made by the CalCOFI program. For example, data (from both CalCOFI and CCE-LTER programs) support previous studies in the region that invoked the importance of microzooplankton grazing, triggered by increases in heterotrophic bacteria, for controlling picoplankton populations, particularly in the nearshore (coined the enhanced microbial loop). Using bacterial production data from CCE-LTER

cruises, the underlying mechanism was tested and found support for the enhanced microbial loop hypothesis in 2017; however, it appeared that different processes dominated during the tail end of the 2015/2016 El Nino. Until now, the microbial loop hypothesis had only hypothesized that increased bacterial production would lead to decreased picoplankton abundance or biomass. Placing the bacterial component with the larger ecosystem food web is critical to understanding carbon fluxes through the system.

Adding the bacterial component to the traditional (grazing) food web in Chapter 2 strengthened previous conclusions that the nearshore is net autotrophic. Net heterotrophy offshore was much more prominent when the bacterial component was included. Previous work focused on the traditional (grazing) food web independently of the microbial food web but this work exposed that the estimated trophic state determined from the traditional food web can be opposite that determined from the microbial food web. This mismatch highlights the need to include the microbial food web within discussions of organic carbon cycling and trophic state. In fact, a close examination of the westward propagating Morro Bay filament in 2017 showed how the traditional (grazing) food web estimated a trophic state in a nearshore Lagrangian cycle (P1706-C2) that was different from the net heterotrophic ecosystem state estimated when the microbial food web was included. The excess carbon available in the nearshore regions of this filament, if laterally transported, would be sufficient to support heterotrophic communities offshore. Chapter 2 not only exemplified the need to consider bacterial processes within food webs, but also supported that lateral transport of organic material in mesoscale features such as filaments could support offshore communities.

Finally, in Chapter 3, controls on bacterial production were assessed to better understand how environmental conditions were linked to measured bacterial production.

Strong correlations between bacterial production and organic carbon pools, chlorophyll *a*, and net primary production were observed. Particulate organic carbon (POC) concentrations had robust correlations with bacterial production, and at low POC concentrations the relationship with BP was the same across the three regions, nearshore, transition, and offshore, for any given year. The correlation between BP and POC concentration may be useful for parameterizing BP in models or in a retrospective analysis. The bottom-up control index, which related bacterial production (i.e., the rate of substrate supply) to bacterial biomass (calculated from bacterial abundance), encompassed a range that was comparable to global trends. Bottom-up controls reflect nutrient availability and were hypothesized to scale with net primary production, however, no such scaling was found. The lower bottom-up control index for the productive nearshore could be the result of tight grazing controls associated with the enhanced microbial loop acting on bacterial populations in the nearshore region more so than in the transition and offshore regions.

An inverse relationship between bottom-up and temperature controls was observed, but further exploration revealed that temperature control reflected nutrient concentration and not metabolic rate in the CCE. Utilizing the 2014 warm anomaly to observe the response of the bacterial community to a marine heat wave, strong bottom-up and low temperature controls were identified. The strong bottom-up controls were the result of depressed bacterial production compared to the bacterial biomass, which could have resulted from grazing or bacterial dormancy. Ultimately, the response in 2014 may reflect the ecosystem state under future warm and stratified conditions within the CCE.

In summary, this work highlights the need for continued examination of the bacterial community, especially bacterial production in the CCE, to better understand carbon fluxes

through bacteria. Future work should better constrain bacterial carbon demand by measuring both bacterial production and bacterial respiration. Additionally, better constraints are needed for dissolved organic carbon released by extracellular release, viral lysis of both phytoplankton and bacteria, and both micro- and mesozooplankton processes. Furthermore, the microbial community showed rapid responses to environmental changes, both expected (PDO change, El Nino) and unexpected (2014 warm anomaly), stressing the importance of both long-term time series and mechanistic studies to understanding community dynamics. The microbial food web plays an essential role in carbon flow within the CCE and cannot be ignored.